

Co(salen)-mediated enantioselective radiofluorination of epoxides. Synthesis and biological evaluation of both enantiomers of [18F]FMISO

Revunov, Evgeny V.; Zhuravlev, Fedor

Publication date:
2014

Document Version
Peer reviewed version

[Link back to DTU Orbit](#)

Citation (APA):

Revunov, E. V., & Zhuravlev, F. (2014). Co(salen)-mediated enantioselective radiofluorination of epoxides. Synthesis and biological evaluation of both enantiomers of [18F]FMISO. Technical University of Denmark (DTU).

DTU Library

Technical Information Center of Denmark

General rights

Copyright and moral rights for the publications made accessible in the public portal are retained by the authors and/or other copyright owners and it is a condition of accessing publications that users recognise and abide by the legal requirements associated with these rights.

- Users may download and print one copy of any publication from the public portal for the purpose of private study or research.
- You may not further distribute the material or use it for any profit-making activity or commercial gain
- You may freely distribute the URL identifying the publication in the public portal

If you believe that this document breaches copyright please contact us providing details, and we will remove access to the work immediately and investigate your claim.

DTU Nutech (Center for Nuclear Technologies) is Denmark's national competency center for nuclear technology. With roots in research in the peaceful use of nuclear power, DTU Nutech works with the applications of ionizing radiation and radioactive substances for the benefit of society. The Hevesy Laboratory develops radiotracers for the diagnosing of particularly cancer.

The center's expertise in radiation dosimetry is used both for radiation sterilization, for medical purposes and for dating. A third field of application is the studies and analysis of radioactive isotopes in the environment, in food and in materials. The center also monitors radioactive substances and radiation levels in the Danish environment, contributing to the national nuclear emergency.

Center for Nuclear Technologies - The Hevesy Laboratory
Technical University of Denmark

PO Box 49
Frederiksborgvej 399
4000 Roskilde
Tel. +45 4677 4677
Fax +45 4677 5688
<http://www.nutech.dtu.dk/>



Evgeny Revunov

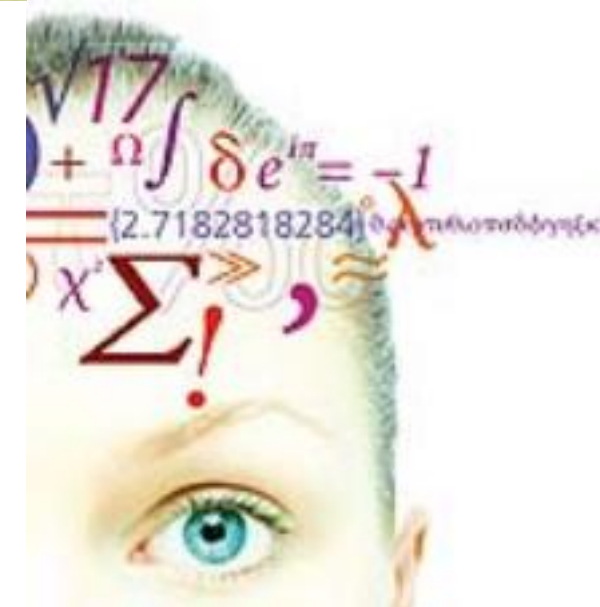
Co(salen)-mediated enantioselective radiofluorination of epoxides. Synthesis and biological evaluation of both enantiomers of [18F]FMISO

2014

PhD 2014



Evgeny Revunov



DTU Nutech
Center for Nuclear Technologies

In much wisdom is much grief, and increase of knowledge is increase of sorrow.

King Solomon

Preface

This thesis is a result of three years of graduate work performed at the Hevesy Laboratory, Center for Nuclear Technology, DTU Risø Campus, The Technical University of Denmark, under the supervision of Dr. Fedor Zhuravlev, senior scientist at the Hevesy Lab. The work has been funded by a scholarship “Mobility” (The Council for Research and innovation, DTU, project number 59510).

The main parts of the work presented here are Chapter 1 (introduction to PET), Chapter 2 (Co(salen)-mediated enantioselective radiofluorination of epoxides) and Chapter 3 (synthesis and biological evaluation of both enantiomers of [^{18}F]FMISO).

The purpose of the 1st Chapter is to provide background information about PET, PET isotopes and ^{18}F -radiopharmaceuticals in general.

The background about cold ^{19}F fluorination of epoxides and the development of Co(salen)-mediated enantioselective radiofluorination of epoxides methodology is presented in the 2nd Chapter and the Appendix.

And the 3rd Chapter provides the overview of [^{18}F]FMISO radiosynthesis methods, the development of our method, automated radiosynthesis and *in vivo* studies of both the *R* and the *S* enantiomers of [^{18}F]FMISO.

Acknowledgement

I would like to thank all the people who have inspired me and helped along the way in the Hevesy lab. I am very grateful for all that you have done for me.

I would like to highlight the enormous input from my supervisor F. Zhuravlev.

I would like to thank our collaborators from the Panum Institute Dr. Jesper Tranekjær Jørgensen and Prof. Andreas Kjær.

I need to express my gratitude to Prof. Mikael Jensen and Dennis Ringkjøbing Elema for support and trust to my capabilities. I would like to acknowledge Sorin Aburel for discussions and sharing his experience.

Furthermore I would like to say my gratitude to our laboratory technicians Henrik Prip and Henrik Dennis Nielsen for their help. To my present and ex office and lab mates Alex Givskov, Bente Mathiessen, Anders Frellsen, Pil Federicia and Martin H.F. Pedersen.

Thank you all!

Publications

Co(salen)-mediated enantioselective radiofluorination of epoxides. Radiosynthesis of enantiomerically enriched [^{18}F]F-MISO via kinetic resolution.

Revunov E., Zhuravlev F.

Journal of Fluorin Chemistry, v. 156, 130-135, 2013.

Manuscripts in preparation

Synthesis and biological evaluation of both enantiomers of [^{18}F]F-MISO

Evgeny Revunov, Jesper Tranekær Jørgensen, Andreas Tue Ingeman Jensen, Gregory Severin, Andreas Kjær and Fedor Zhuravlev

Selected oral presentations

Enantioselective radiofluorination of epoxides.

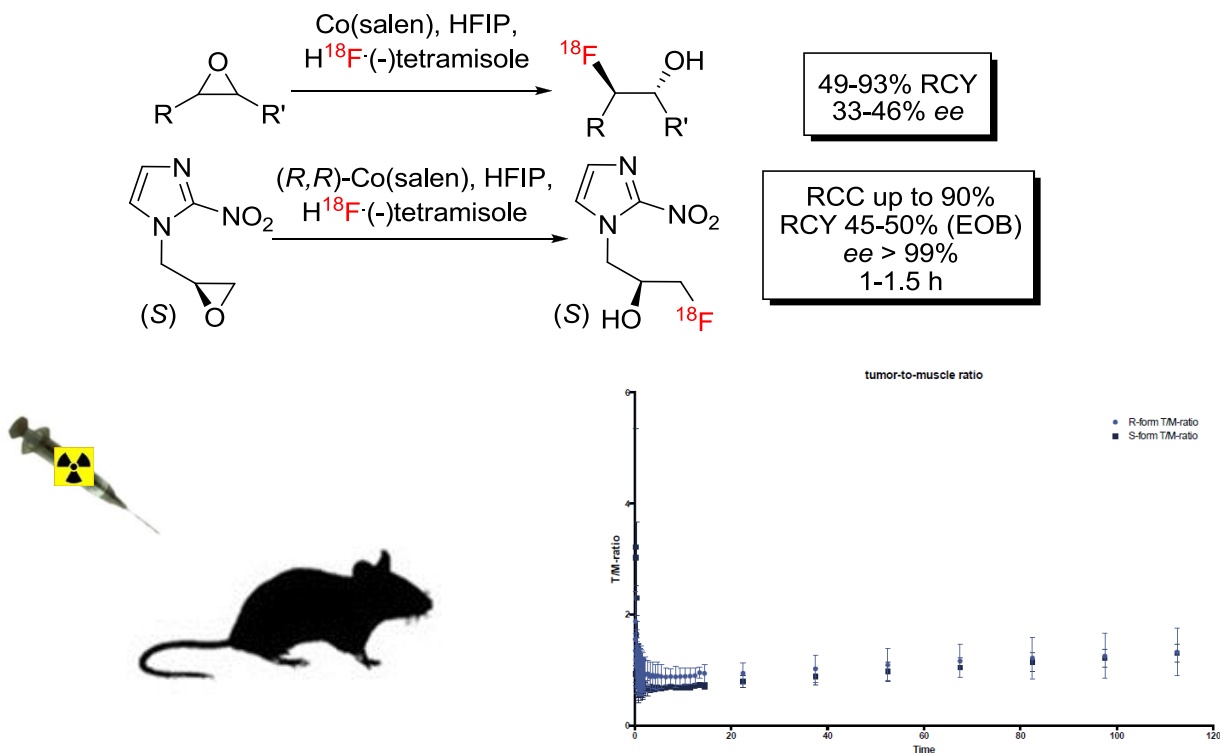
At the Danish Radiochemical Meeting, 2012.

Revunov E.

Abstract

The purpose of this PhD project was to develop an enantioselective cobalt-mediated radiofluorination of epoxides and apply this methodology for radiosynthesis of the PET radiopharmaceutical [^{18}F]FMISO. The developed procedure utilizes [^{18}F]HF-gas (as an efficient source of nucleophilic ^{18}F -fluoride) in a combination with chiral base ((-)-tetramisole), chiral Lewis acid ((*R,R*)-Co(salen)) and hexafluoroisopropanol, providing the corresponding (*S*)-[^{18}F]fluoroalcohols enantioselectively (20-46% enantiomeric excess) with high yields (78-93 % radiochemical yield). The enantioselective Co(salen)-mediated no-carrier-added radiofluorination of epoxides has been achieved for the first time. A number of model *meso*-epoxides were successfully radiofluorinated producing ^{18}F -fluoroalcohols in high RCC and RCY, and modest enantioselectivity. The developed procedure is simple, rapid and lends itself to easy automation. This methodology was adopted for the first automated enantioselective single step radiosynthesis of PET hypoxia radiotracer [^{18}F]FMISO in 81% RCY and 55% enantioselectivity. The use of enantiopure substrates for the synthesis of both enantiomers allowed us to obtain the (*S*) and (*R*)-[^{18}F]FMISO enantiomers with > 99% enantiopurity. *In vivo* quantitative and pharmacokinetic data were obtained for the first time for the both enantiomers of [^{18}F]FMISO. The *R*-form showed higher uptake in tumor as well as in muscle tissues, thus displaying nearly identical tumor-to muscle ratios and showing very similar imaging profiles of both the (*S*) and the (*R*)-[^{18}F]FMISO enantiomers.

Graphical abstract



Resume

(på Dansk)

Formålet med dette Ph.D. projekt var at undersøge overgangsmetal medieret radiofluorinerings. Hovedmålet for arbejdet var at udvikle en effektiv procedure for radiosyntese af PET (positronemissionstomografi) radiolægemidlet [^{18}F]FMISO.

Denne afhandling beskriver det første eksempel på en 'non-carrier added' overgangsmetal medieret enantioselektiv radiofluorinerings af epoxider. Tidligere udviklede metoder til effektiv syntese af [^{18}F]HF (gas) og [^{18}F]HF base (vandfri opløsning) foranledigede os til at undersøge omfanget af enantioselektiv radiofluorinerings af epoxider. Den nyudviklede procedure anvender [^{18}F]HF-gas kombineret med en kiral base ((-)-teramisole), kiral Lewisyre ((*R,R*)-Co(salen)) og hexafluorisopropanol til at give (*S*)-[^{18}F]fluorohydriner enantioselektivt (20-46% enantiomerisk overskud) med høje udbytter (78-93% radiokemisk udbytte).

PET radiolægemidler med alifatiske ^{18}F -C fragmenter fremstilles typisk ved nukleofil substitution af alkoholderivater med [^{18}F]KF/Kryptofix 2.2.2, hvilket kan føre til epimerisering. Vores metode tillod os at udvikle en direkte et-trins radiosyntese af den vigtige PET hypoxi tracer [^{18}F]FMISO via kinetisk adskillelse af det korresponderende epoxid. Vi udviklede en effektiv solid-phase-ekstraktionsbaseret oprensningsmetode, som tillod os at undgå HPLC oprensning og minimere den samlede radiosyntesetid (1.5 t, 45% RCY end of bombardment).

Eftersom alle nuværende tilgængelige metoder for syntese af [^{18}F]FMISO giver en racemisk blanding af isomerer, involverede vi os i dyreforsøg for at opklare om de to enantiomerer af [^{18}F]FMISO viser forskellige biologiske aktiviteter og/eller billeddannelsesegenskaber.

Dette arbejde gjorde det klart, at der er minimal forskel på *R* og *S* isomererne: (*R*)-isomerer viser højere tumoroptag i forhold til (*S*)-formen af FMISO. Muskeloptaget var også højere for (*R*)-[^{18}F]FMISO, men tumor-til-muskel forholdet var det samme for begge isomerer.

Resultaterne fra in vivo musestudierne viste den samme adfærd for *R* og *S* formerne af [^{18}F]FMISO, hvilket betyder at stereokemien ikke har nogen indflydelse på PET billedkvaliteten af hypoxiske tumorer.

Table of content

Chapter 1	9
1.1 Multidisciplinary nature of Positron Emission Tomography	10
1.2 PET imaging	10
1.3 Principles of PET	15
1.4 PET isotopes	20
1.5 PET isotopes production	21
1.5.1 Production of fluorine-18	23
1.6 PET radiopharmaceuticals.....	26
1.7 Challenges and directions of modern radiofluorination.....	28
1.7.1 Fluoride recovery and processing	28
1.7.3 Expanding the substrate scope and selectivity with transition metals.....	32
Chapter 2	37
2.1 Transition metal mediated fluorination of epoxides	38
2.2 Results and discussions	42
2.2.1 Preparation of [¹⁸ F]HF	42
2.2.2 Preliminary studies.....	43
2.2.3 Screening of alcohol additives	46
2.2.4 Screening of bases and solvents	47
2.2.5 Screening of substrates	47
2.2.6 Stereochemistry studies	48
2.3 Experimental part	56
Chapter 3	66
3.1.1 Hypoxia	68
3.1.2 [¹⁸ F]FMISO as a hypoxia tracer and its mechanism of action	69
3.1.3 [¹⁸ F]FMISO labelling strategies	71
3.2 Results and discussion	75
3.2.1 Discussions of [¹⁸ F]FMISO synthesis.....	75
3.2.2 [¹⁸ F]FMISO stereochemistry	76
3.2.3 New strategy.....	78
3.2.4 Purification	81

3.2.5 QC control.....	84
3.3 Experimental part.....	86
3.4 <i>In vivo</i> studies.....	97
Conclusions.....	102
Refernces.....	103
Appendix.....	111

Chapter 1
Short introduction to PET

1.1 Multidisciplinary nature of Positron Emission Tomography

Over the years positron emission tomography (PET) has become an essential research and medical imaging modality. PET is one of the most specific and sensitive imaging modalities for studying molecular pathways and molecular interactions in the living human body.

PET is essential imaging modality that combines imaging, cyclotron production of radionuclides, radiosynthesis and radiopharmacology. The multidisciplinary nature of radioimaging and PET include the collaboration and proficiency of chemists and radiochemists, medical staff, physicists and medical physicists, radio-pharmacologists, radio-physicists, biologists, and engineers.

However, the key to the PET research program will be the development and synthesis of novel innovative radiopharmaceuticals with appropriate pharmacokinetics and pharmacodynamics that can follow the aspects of physiological and pathophysiological processes.

1.2 PET imaging

PET is a type of a non-invasive medical imaging modality that produces functional rather than anatomical images, thereby providing greater insight to the patient's condition. PET is non-invasive, sensitive, quantitative method with application in cardiology¹, oncology², metabolic imaging³, neurology⁴, neuro-oncology and neurological diseases⁵.

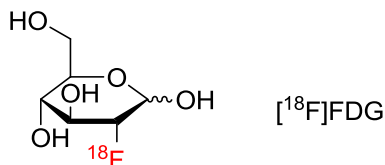
Why PET is so attractive? Nuclear medicine imaging with PET offers valuable functional/physiological information, whereas computer tomography (CT) or magnetic resonance imaging (MRI) demonstrates exquisite anatomic detail. With PET-CT or PET-MRI, function and structure can be viewed together, providing impressive insight into human disease.

Entry	Imaging modality	Form of energy used	Spatial resolution, mm		Acquisition time, frames	Probe mass required, ng	Sensitivity of detection, mol/L	Depth of penetration, mm
			Clinical	Animal				
1	PET	Annihilation photons	3-8	1-3	1-300	1-100	10^{-11} - 10^{-12}	>300
2	SPECT	γ -photons	5-12	1-4	60-2000	1-1000	10^{-10} - 10^{-11}	>300
3	CT	X-rays	0.5-1	0.03-0.4	1-300			>300
4	MRI	RF waves	0.1-0.2	0.025-0.1	50-3000	10^3 - 10^6	10^{-3} - 10^{-5}	>300
5	Ultrasound	High frequency sound	0.1-1.0	0.05-0.1	0.1-100	10^3 - 10^6		1-200

Table 1. *In vivo* imaging modalities⁶.

In cardiology, PET offers unique possibilities in cardiovascular imaging⁷, in particular accurate and quantitative assessment of myocardial blood flow and the identification of myocardial viability. The most important clinical applications in cardiology are the assessment of myocardial perfusion and metabolism⁸. The measurement of the myocardial blood flow under rest and stress conditions⁹ with [¹³N]ammonia and

$[^{15}\text{O}]\text{H}_2\text{O}$ and the energy consumption with 2-deoxy-2- $[^{18}\text{F}]\text{fluoro-D-glucose}$ ($[^{18}\text{F}]\text{FDG}$, Scheme 1) is a standard examination in order to discriminate between ischemic and infarcted tissue¹⁰.



Scheme 1. 2-Deoxy-2- $[^{18}\text{F}]\text{fluoro-D-glucose}$.

PET cardiology viability imaging determines how much heart muscle has been damaged by heart disease or a heart attack¹¹. Cardiac imaging with PET provides a high degree of diagnostic accuracy, a higher temporal and spatial resolution, and a well-established methodology for attenuation correction¹¹. PET images can be analyzed qualitatively or semi-quantitatively¹². Unlike conventional cardiac imaging, PET studies can also provide absolute quantification of myocardial blood flow in absolute terms (mL/g per minute), which cannot be determined by other nuclear imaging methods (SPECT, MRI imaging etc.).

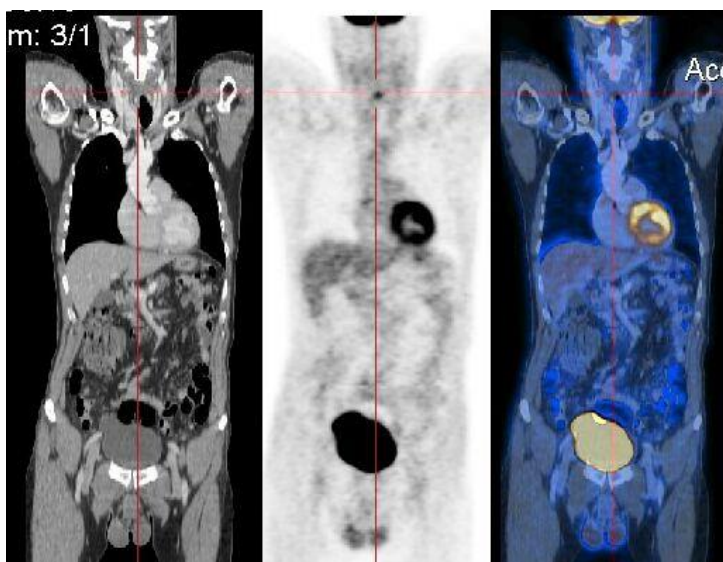


Figure 1. Combined PET-CT whole-body images (CT scan, PET image and their superposition PET-CT).

From the beginning of 1990s, PET imaging of brain tumors has become a standard treatment at many medical centers^{13,14}. PET is being increasingly used in clinical neurology to improve understanding of disease pathogenesis, to complement the diagnosis, and to monitor disease progression and response to treatment¹⁵.

PET is an extremely powerful method allowing early diagnosis of brain metastasis, distinguishing local recurrences from radiotherapy induced changes and detecting malignant transformation of low grade tumors, early and presymptomatic diagnosis of individuals at risk for neurodegenerative disorders such as Alzheimer's disease and Parkinson's disease^{16,17}.

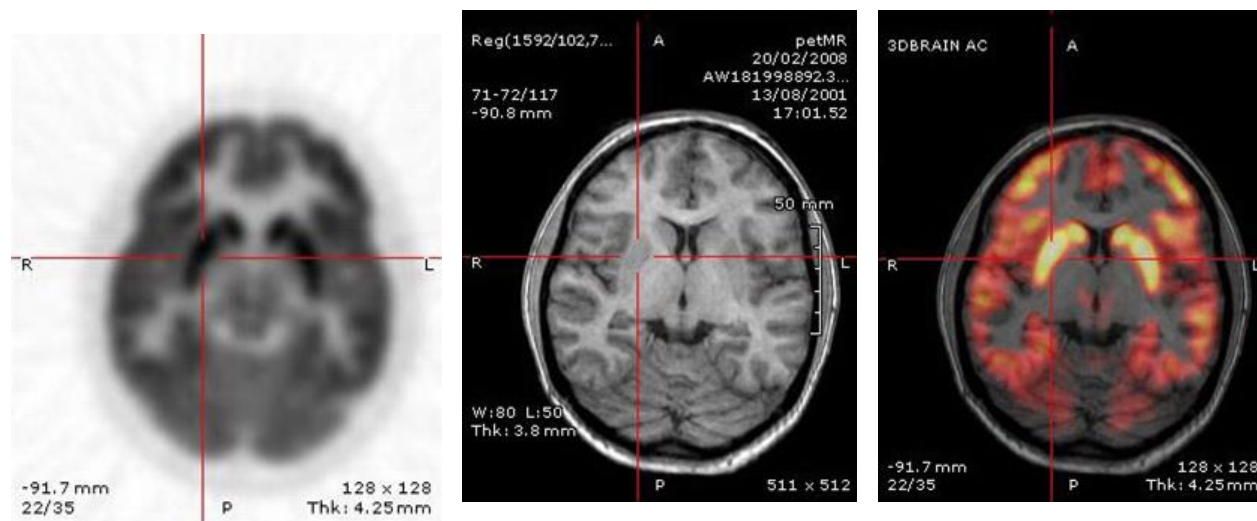
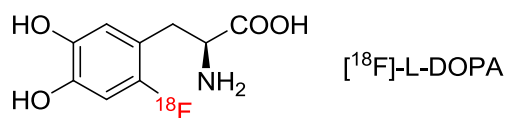


Figure 2. PET-MRI head image.

As well as a standard radio tracer for everyday clinical use (e.g. [^{18}F]FDG showing glucose metabolism, and H_2^{15}O for examining cerebral blood flow), specific tracers were made to illustrate the particular brain functions – [^{18}F]-6-fluorodopa (or [^{18}F]-L-DOPA, Scheme 2).



Scheme 2. [^{18}F]-6-fluorodopa.

PET is essential for oncological application because it visualizes molecular events in living human tissue, gives an understanding of the biological characteristics of tumor tissue. Its diagnostic accuracy is generally higher than that of the conventional imaging technique of magnetic resonance imaging (MRI), and PET result may facilitate more appropriate therapeutic planning for cancer patients. For example, [^{18}F]FDG-PET scanning of lung cancer had a sensitivity of 96.8% and a specificity of 77.8% (compiled data from 4 years of work, and selected 40 studies for inclusion, based on the analysis of almost 1500 total focal pulmonary lesions)¹⁸.

[^{18}F]FDG PET has become routine in evaluating patients with lymphoma¹⁹ (Figure 3).



Figure 3. [^{18}F]FDG PET-CT whole-body images showing widespread hypermetabolic lymphadenopathy.

[^{18}F]FDG PET scans are more sensitive in assessing for viable tumor in both nodal and extranodal sites, with sensitivities ranging from 72% to 100% as opposed to 63–83% for gallium^{20,21}. SPECT (single-photon emission computed tomography) is less sensitive than [^{18}F]FDG PET when disease is small or involves extranodal sites such as the skeleton or the spleen. From a practical standpoint, [^{18}F]FDG PET scanning can be done in 1 day instead of the 2–7 days required for gallium imaging. Radiation dose is also significantly less – roughly one fourth compared to gallium studies²².

Multiple studies have demonstrated that [^{18}F]FDG PET imaging is more accurate than conventional anatomic imaging (CT or MRI) for staging melanoma²³ and breast cancer imaging²⁴.

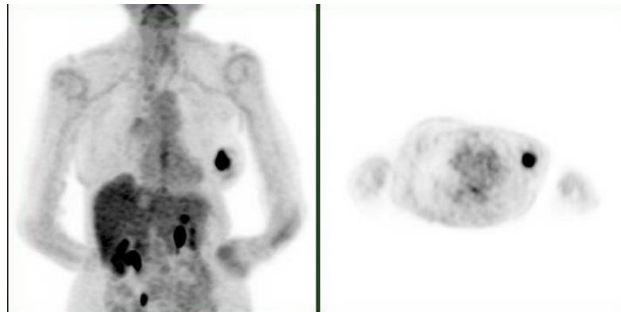


Figure 4. [^{18}F]FDG PET study of breast cancer.

PET and PET-CT imaging has been found particularly helpful at the time of diagnosis of head and neck cancer - results can provide biopsy and surgical guidance, which may result in fewer false-negative findings and more accurate surgical staging. Several studies have compared PET to CT and MRI for the non-invasive staging of regional nodes, with surgical neck dissection as the gold standard^{25,26}.

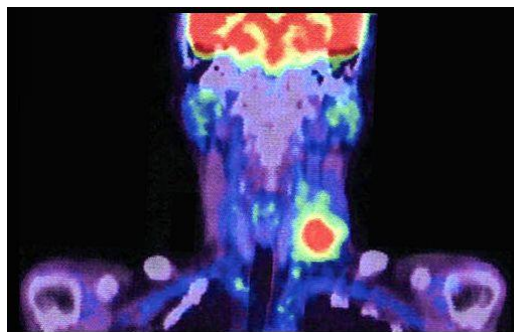
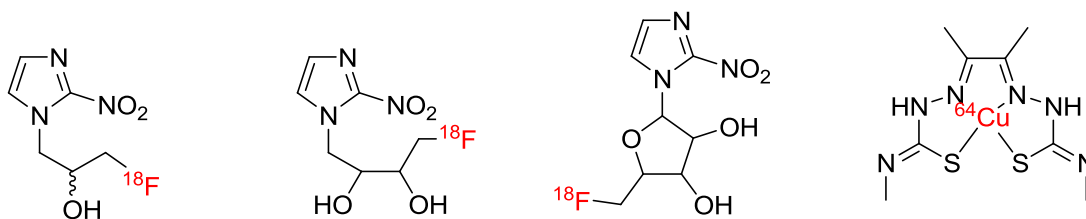


Figure 5. PET-CT [^{18}F]FDG scanning of a male patient, with left inferior internal jugular node metastases. Warm colors (red) correspond to intense radiotracer uptake.

The accuracy and effectiveness of PET imaging in colorectal cancer has been well studied. The information provided by PET-CT is likely to combine the best imaging features of both modalities and become the gold standard for staging in colorectal carcinoma²⁷.

[^{18}F]FDG PET does have superior sensitivity in detecting of thyroid cancer relative to other nuclear medicine techniques²⁸.

Hypoxia in tumors is a serious problem in developing feasible treatment methods. Hypoxic cancer cells are known to be more resistant than aerobic cells to ionizing radiation and chemotherapy. The ability for noninvasive PET imaging to examine the hypoxia status in tumors with radiolabeled hypoxic tracers (Scheme 3) seems to be really challenging compared to old invasive techniques. Its high spatial resolution, high sensitivity, and advantages for visualizing molecular events in living tissue made this tool very useful²⁹.



Scheme 3. PET hypoxia radiopharmaceuticals [^{18}F]FMISO, [^{18}F]FETNIM, [^{18}F]FAZA, and ^{64}Cu -ATSM.

In summary, PET has many advantages over existing imaging techniques for the diagnosis – it is a very high sensitivity and a high negative predictive value for lesion detection as compared to classical modalities like computed tomography (CT), ultrasonography (USG) and magnetic resonance imaging (MRI). PET – is the most specific and sensitive functional diagnostic imaging device for cancers (tumors and metastasis) and brain diseases. Image information, obtained from PET, helps to establish the treatment plan (surgery, chemotherapy, radiation/proton/ion therapy). Prospects of PET are only limited by the development of tracers with adequate specificity to characterize pathology.

1.3 Principles of PET

PET is an imaging technique in which a radionuclide is synthetically introduced into a molecule of potential biological relevance and administered to a patient. Depending on the nature of the so-called radiopharmaceutical, it may be inhaled, ingested, or, most commonly, injected intravenously. The subsequent uptake of the radiotracer is measured over time and used to obtain information about the physiological process of interest³⁰.

Because of the high-energy (γ -ray) emissions of the specific isotopes employed and the sensitivity and sophistication of the instruments used to detect them, the two-dimensional distribution of radioactivity within an organ slice may be inferred from outside of the body. Thus, PET is both emission and tomographic (Greek *tomos* - cut) technique.

PET uses proton-rich radionuclides with a deficiency of neutrons. Unstable nuclides with an excess number of protons may reduce their net nuclear positivity by two approaches. The first one occurs when certain proton-rich radionuclides may capture an orbiting electron, transforming a proton to a neutron³¹. The resulting daughter nucleus often remains residually excited. This metastable arrangement subsequently dissipates, thereby achieving a ground state and producing a single γ -photon in the process. Isotopes that decay by electron capture and/or γ -emission are used in SPECT, and include, among others 123-iodine (^{123}I) and the long-lived metastable nuclide 99m-technetium ($^{99\text{m}}\text{Tc}$)³².

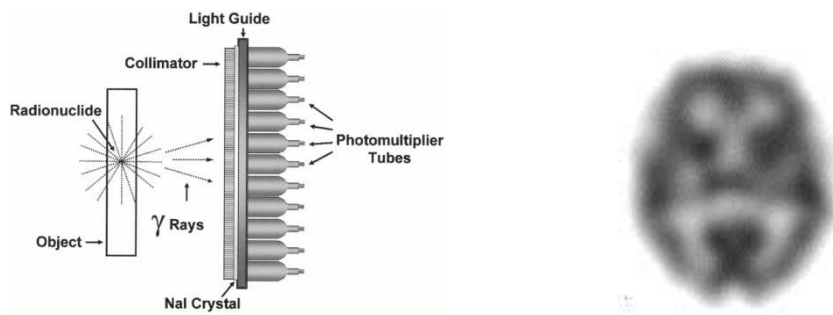


Figure 6. Basic principles and components of a gamma camera³³ (left). SPECT slice of the distribution of $^{99\text{m}}\text{Tc}$ within a patient's brain (right).

The many advantages of SPECT imaging (standardized protocols, large evidence base for diagnostic accuracy, risk stratification, guiding patient management) made it widely available. Nonetheless, the disadvantages of traditional rest/stress SPECT (the typical protocol is inefficient, often taking 3 to 5 hours to complete) limit this method^{34,35}.

An alternative to γ -emission is a situation when a proton is converted to a neutron and a particle called a positron (e^+), which is the event utilized in PET. With identical mass but opposite charge, positrons are the antimatter equivalent of electrons. When ejected from the nucleus, a positron collides with an electron, resulting in the annihilation of both particles and the release of energy. The principles of conservation of mass and momentum dictate that two γ -photons are produced, each of equivalent energy

of 511 keV and in directions at approximately 180° from each other. For this reason, PET is sometimes referred to as dual photon emission tomography³⁶.

The positron travels a short distance in tissue before the annihilation reaction occurs. This results in some degree of uncertainty about the exact location of its origin. In addition, the annihilation photons may actually be emitted at angles slightly different than the theoretical 180° - up to 0.25°. These limitations contribute to the inherent degradation of spatial resolution in all PET detector systems. However, even given these limitations, the spatial resolution in PET imaging is still superior to that seen in imaging with a gamma camera for other nuclear medicine examinations³⁷.

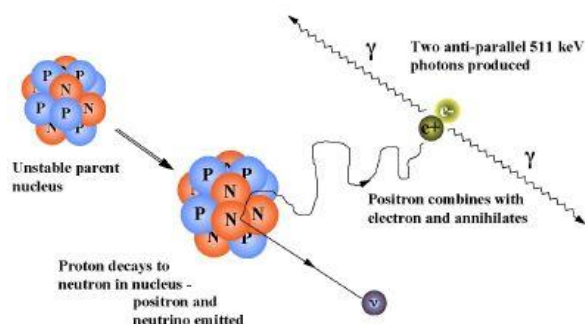


Figure 7. Positron emission and annihilation.

PET imaging offers many advantages compared to SPECT such as image quality, diagnostic accuracy, interpretative certainty, lower dose, and shorter protocol (for example, a rest-stress PET study using ⁸²Rb can be completed in 20 to 30 minutes).

The spatial signature of back-to-back photon paths is used by PET scanners in locating the source of an annihilation event, a method known as coincidence detection. A PET scanner may be conceptualized as a ring-like camera that surrounds the patient. PET scanners employ highly sensitive scintillation detectors made of dense crystalline materials (bismuth-germanium oxide, sodium iodide, cesium fluoride) which capture the invisible, high-energy γ-rays and convert them into visible light. This flash of light is converted into an electrical pulse by a photomultiplier tube (PMT). The crystal and PMT together make up a radiation detector. Rather than using individual detectors in isolation, a PET camera is constructed such that opposing detectors are electronically connected. Thus, when separate scintillation events in paired detectors coincide (3- 10 ns), an annihilation event is presumed to have occurred at some point along an imaginary line between the two. This information is registered by a computer and later used to reconstruct images using the principles of computed tomography. Conversely, single events are ignored. Although it is conceivable that two unrelated photons from spatially separate annihilation events might reach opposing detectors in unison, these accidental coincidences are much less frequent than true ones. In fact, coincidence detection is a very efficient technique that gives greater sampling rates and sensitivity^{38,39}.

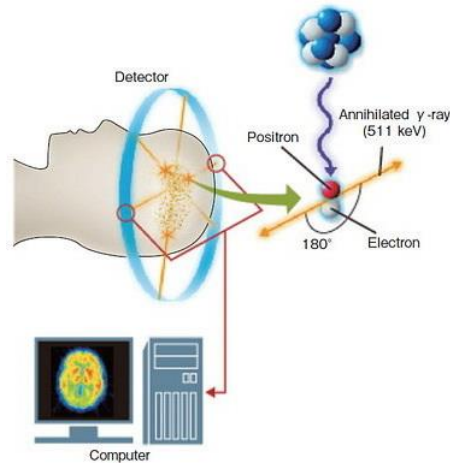


Figure 8. Scheme of positron decay in PET.

One limitation derives from the nature of positron decay - PET recognizes a place of positron annihilation but not the site of radioactive decay. Since a positron must generally come to rest in tissues before being able to collide with an electron, annihilation often occurs some distance away from the positron's origin. The distance separating these two events, decay and annihilation, depends on the energy of the positron as it leaves the nucleus, and varies according to the specific isotope involved. For ^{18}F decay, this range is 2.4 mm. In addition, if the positron is not entirely at rest at annihilation, photons will be emitted at an angle slightly different than 180° . Taken together, remote positron annihilation and photon noncolinearity place a theoretical limit on PET's achievable spatial resolution, which is estimated at 2–3 mm⁴⁰. Typical clinical scanners have a resolution of approximately 4-7 mm⁴⁰.

PET isotope	Mean range, mm	Max range, mm
^{11}C	1.03	3.9
^{13}N	1.32	5.1
^{15}O	2.01	8.0
^{18}F	0.64	2.4
^{68}Ga	2.24	8.9
^{82}Rb	4.29	16.5

Table 2. Mean and maximal range of positrons in water.

Before this resolution was achieved, PET scanners technique passed a long way from 1950, when the whole concept of PET imaging was developed and first setups were built.

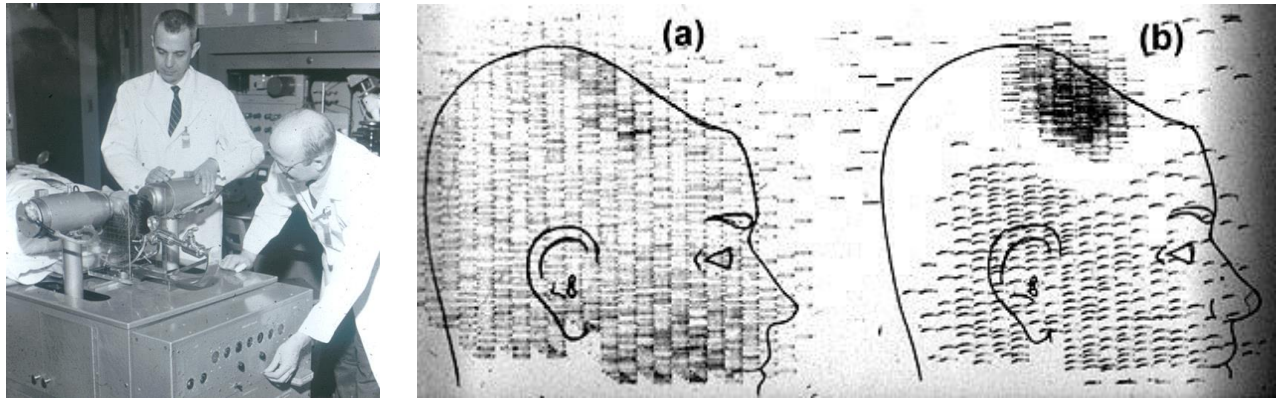


Figure 9. The first PET scanner for brain imaging (1952). 2D-images were obtained by moving opposed sodium iodide crystal detectors. Scans of patient with recurring brain tumor. Coincidence scan (a) of a patient showing recurrence of tumor under previous operation site, and unbalance scan (b) showing asymmetry to the left⁴¹.

The first commercial PET scanner was introduced in 1978; during the 1970s and 1980s PET was mainly used for research. First approval (FDA, US Food and Drug Administration) was done in 1998. To increase the resolution and the sensitivity, new types of detectors have been attempted. To get 3D images, rings of detectors surrounding the patient, were advanced. Usually detectors are 18-40 rings of crystals forming a cylindrical field of view about 15 cm long that can acquire many slices of coincidence data. A progress in personal computers and information storage devices resulted in improved attenuation correction and image reconstruction with newer detectors.

Figure 10 shows the evolution of image quality from the first Siemens manufactured PET scanner PET III, commercially available in 1975, to the quite sophisticated model from 1995, ECAT Exact HR+. The finer details of internal brain structures can be visualized much better in the latest model. This improvement has been achieved with a larger number and better radiation sensors, better software and the possibility of getting several slices at the same time using many rings of sensors.

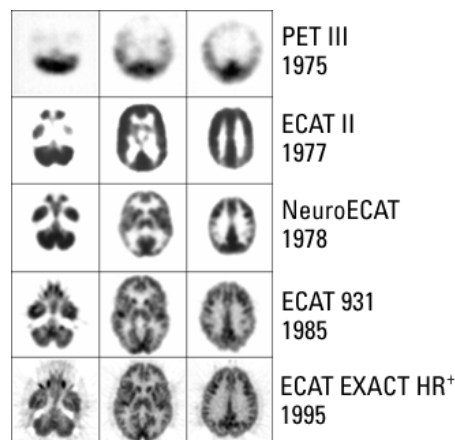


Figure 11. Increasing of resolution and sensitivity made in PET imaging of brain for the period from 1975 to 1995, the Siemens biomedical equipment manufacturer (www.siemens.com).

As a result, nowadays hospitals and research centers possessing unique instruments with more slices in CT, short time of flight, list mode acquisition, gating etc.

Currently almost all PET scanners are joint with CT scanners because the resolution of PET is relatively low and precise anatomical information could be provided well by CT. The useful PET information can be accurately localized inside of the body by using the CT scans. But CT gives an additional radiation exposure. The use of Magnetic Resonance (MRI) instead of CT eludes this additional radiation exposure. For the first time MRI/PET scanners were presented in 2010. MRI is a more flexible imaging modality and could provide additional information that is not available with CT.



Figure 12. Siemens Healthcare Biograph mCT/PET scanner – the last generation of PET-CT scanners from Siemens, 2008, and PET-CT image obtained from Siemens Biograph mCT, www.siemens.com.

1.4 PET isotopes

Isotopes used for PET have decay half time short enough to not to irradiate the patients, and long enough to provide sufficient freedom for the chemists to perform radiolabeling/purification/certification/ delivering procedures. In fact, a choice is not so broad – only limited amount of positron decaying nuclei found their application in radiopharmacy.

Table 3. PET isotopes with medical applications, based on Dr. Robert E. Schenter publications⁴².

Isotope	Half-life time	Cyclotron energy, MeV	$E_{\max}(\beta^+)$, MeV	Diagnostic applications*
Carbon-11	20.3 min	3-16	0.96	Cancers: chest, chronic lymphocytic, glioblastoma, liver, multiple myeloma, prostate, urinary tract; diseases: Alzheimer's, brain, epilepsy, heart, Parkinson's alcohol addiction, amphetamine release, drug addiction, neuropsychiatric, nicotine dependence, pain processing, schizophrenia, small animal imaging, tobacco addiction
Nitrogen-13	9.97 min	7-16	1.19	Ammonia dog studies, coronary artery disease, diabetes, gamma camera, heart disease, imaging of heart, pancreas and liver, lupus erythematosus, myocardial perfusion, pulmonary ventilation
Oxygen-15	122 s	0-10	1.72	Acute brain injury, arterial blood flow, brain cancer, oxygen utilization, brain studies, cerebral blood volume, cerebral responses, coronary artery vasospasm, coronary reserve, heart disease, ischemic stroke disease, kinetics of oxygen, liver cancer, myocardial viability, oxygen metabolism, pain control, venous ulceration
Fluorine-18	1.83 h	3-16	0.635	Cancers: adrenal gland, anal, bone, bone marrow transplants, bowel, breast, cervical, chest, colorectal, esophageal, gastric, head and neck, Hodgkin's disease, laryngeal, leukemia, liver, lung (NSCLC), lung (SCLC), melanoma, multiple myeloma, non-Hodgkin's lymphoma, osseous, ovarian, pancreatic, prostate, rectal, Rhabdomyosarcoma, squamous cell, thyroid, urinary, vocal cord; diseases: alcohol addiction, Alzheimer's, anorexia, atherosclerosis, brain, depression, diabetes, heart, herpes, HIV, hypoxia, infection, liver, muscle, narcolepsy, lung inflammation, osteomyelitis, Parkinson's, pneumonia, ulcerative colitis, schizophrenia, Tourette's syndrome infection: pen-prosthetic, hip-prosthetic, joint-prosthetic small animal imaging, chemotherapy research
Iron-52	8.28 h	192	0.8	Anemia, human bone marrow
Copper-62	9.74 min	21-26	2.93	Cerebral and myocardial perfusion, colorectal cancer, biodistribution, liver cancer, renal blood flow, renal injury
Copper-64	12.70 h	5-18	0.65	Cancers: cervical, colon, colorectal, lymphoma, melanoma, pancreatic, prostate; diseases: angiogenesis, brain, hypoxia, Parkinson's, Wilson's stem cell research
Gallium-68	1.13 h	13-22	1.89	Breast cancer, heart imaging, immunoscintigraphy, molecular imaging, neuroendocrine tumors, pancreatic cancer
Bromine-76	16.0 h	10-16	3.4	Anti-carcinoembryonic antigens, anti-CEA antibodies, DNA studies, nerves of the heart, quantitative imaging
Rubidium-82	1.26 min	40-60	3.35	Heart disease, myocardial perfusion, sarcoidosis
Yttrium-86	14.74 h	10-15	1.54	Distribution of Y-90, lung cancer, melanoma, renal cell carcinoma
Zirconium-89	3.27 d	5-18	0.90	Brain tumors, head and neck cancers, non-Hodgkin's lymphoma
Iodine-124	4.18 d	13-16	2.10	Apoptosis, cancer biotherapy, glioma, heart disease, mediastinal micrometastases, scouting of therapeutic radioimmunoconjugates, thyroid cancer

First four isotopes in this list are the most common and the most important. The production energies required for these PET isotopes are low (usually around 5 to 20 MeV). A half-life is rather short, high

doses could be produced with short labelling processes. An external production and delivery to PET installations without a cyclotron are presently only established for ^{18}F -radiotracers⁴³.

1.5 PET isotopes production

Radiopharmaceuticals are used as radioactive tracers for the diagnosis and treatment of patients. George Charles de Hevesy published the first paper on the radioactive tracer concept in 1913. He coined the term radioindicator or radiotracer and introduced the tracer principle in biomedical sciences. An important characteristic of a tracer is that it can facilitate the study of components of a homeostatic system without disturbing their function. In 1924, the tracer concept paved the way for the use of radioisotopes as diagnostic tools. In 1927, the US physicians Hermann Blumgart and Soma Weiss injected solutions of bismuth-214 (^{214}Bi) into the veins of men to study the velocity of blood.

After the discoveries of the cyclotron by Ernest Lawrence in 1931 and artificial radioactivity by Irène Curie and Jean-Frédéric Joliot in 1934, it was possible to make practically every imaginable radioisotope for use in diagnostics or in therapy. Isotopes such as iodine-131 (^{131}I), phosphorus-32 (^{32}P) and cobalt-60 (^{60}Co) are already used in diagnostics and therapy since the mid-1930s⁴⁴.

Ernest Lawrence recognized the medical potential of radioisotopes. His brother, John Lawrence, a hematologist, helped research the field's potential and established and administered the therapeutic procedures. In 1936 he treated a leukemia patient using cyclotron produced ^{32}P . It was the first time that a radioisotope had been used in the treatment of a disease, marking the birth of nuclear medicine.

Of the many different radionuclides used in diagnostic procedures, only a few are valuable in diagnosing cancer. PET-CT is currently accepted to be the most accurate way to stage and monitor many types of cancer. It is used routinely in detecting tumors of thyroid and primary or metastatic tumors. Globally, the vast majority of these investigations are performed using the glucose analogue [^{18}F]FDG.

There are two methods to produce medical isotopes – irradiation of a target material in nuclear reactor and bombardment of target with beams of accelerated particles in a cyclotron. Cyclotrons have a number of advantages over nuclear reactors for radioisotope production, such as safety, cheaper operating and decommissioning costs. Because cyclotrons are powered by electricity rather than the uranium fission reaction of a nuclear reactor, they generate far less waste compared to research reactors.

Generally, medical isotopes are produced by cyclotrons - a particle accelerator which produces positron-emitting elements or short-lived radioisotopes. The cyclotron bombards non-radioactive elements in the target with accelerated particles, which converts these elements into positron-emitting radioactive isotopes. The production of radionuclides with an accelerator demands that particle beams be delivered with two specific characteristics. The beam must have sufficient energy to bring about the required nuclear reactions, and there must be sufficient beam current to give practical yields.

Accelerator production of radioisotopes reached its turning point with the construction of the first cyclotron by Lawrence, Edlfsen and Livingston in 1930. The first cyclotron dedicated to medical applications was installed at Washington University, St Louis, in 1941, where radioactive isotopes of phosphorus, iron, arsenic and sulfur were produced⁴⁵.

Cyclotrons are the most commonly used devices for acceleration of particles to energies sufficient for bringing about the required nuclear reactions. It was the remarkable idea of E. Lawrence to bend the path of the particles into a circle and therefore to use the same electrode system over and over again to accelerate the particles. This idea is the basis of all modern cyclotrons, and has made the cyclotron the most widely used type of particle accelerator. The first model was built in 1930, with proof of particle acceleration being provided by Livingston in 1931.

According to the theory of electrodynamics, the rotational frequency of a charged particle travelling in a magnetic field is independent of the radius of its orbit. The energy of the particle increases as the velocity of the particle increases. The cyclotron utilizes this fact to produce particles of reasonably high energy in a relatively confined space. The acceleration chamber of the cyclotron is placed between the poles of a homogeneous magnetic field (Figure 12).

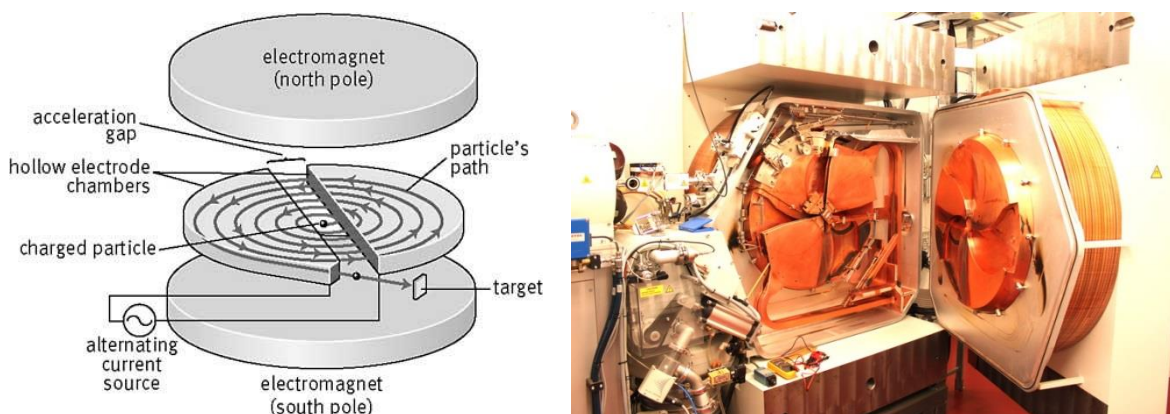


Figure 12. Principle of a cyclotron (left). GE PETtrace cyclotron installed in the Hevesy laboratory (right).

The cyclotron magnetic field causes particles to travel in circular orbits. Ions are produced in an ion source at the center of the machine and are accelerated out from the center. The ions are accelerated by a high frequency electric field through two or more hollow electrodes called 'dees'. The ions are accelerated as they pass from one dee to the next through a gap between the dees. Since the rotational frequency of the particles remains constant as the energy of the particles increases, the diameter of the orbit increases until the particle can be extracted from the outer edge of the machine. The limit on the energy of a particle is determined on a practical basis by the diameter of the magnet pole face⁴⁶.

Carbon-11, nitrogen-13, oxygen-15 and fluorine-18 – are the most common isotopes for PET clinical use.

Isotop	Cyclotron reaction, target material	Decay mode	Radiopharmaceuticals	References
Carbon-11	$^{14}\text{N}(\text{p},\alpha)^{11}\text{C}$ $^{14}\text{N}_2$ - gas	99.8% β^+ , 0.2% EC	$[^{11}\text{C}]$ acetate, $[^{11}\text{C}]$ methionine, N-methyl- $[^{11}\text{C}]$ flumazenil, $[^{\text{O-methyl-}}^{11}\text{C}]$ -raclopride	47
Nitrogen-13	$^{16}\text{O}(\text{p},\alpha)^{13}\text{N}$ ^{16}O -water	100% β^+	$[^{13}\text{N}]$ ammonia, $[^{13}\text{N}]\text{N}_2$	48, 49
Oxygen-15	$^{14}\text{N}(\text{d},\text{n})^{15}\text{O}$ $^{14}\text{N}_2$ - gas	99.9% β^+	H_2^{15}O -water, $[^{15}\text{O}]\text{O}_2$, $[^{15}\text{O}]\text{CO}$	50, 51, 52
Fluorine-18	$^{20}\text{Ne}(\text{d},\alpha)^{18}\text{F}$ Ne – gas or $^{18}\text{O}(\text{p},\text{n})^{18}\text{F}$ ^{18}O -water	96.9% β^+ , 3.1% EC	$[^{18}\text{F}]\text{FDG}$, $[^{18}\text{F}]\text{NaFe}$, $[^{18}\text{F}]\text{FDOPA}$, $[^{18}\text{F}]\text{FLT}$, $[^{18}\text{F}]\text{Flutemetamol}$, $[^{18}\text{F}]\text{FMISO}$	53, 54, 55
Copper-64	$^{64}\text{Ni}(\text{p},\text{n})^{64}\text{Cu}$ ^{64}Ni – solid metal, electroplated	17.9% β^+ , 39.0% β^- , 43.1% EC, 0.5% γ/IC	^{64}Cu -ATSM (diacetyl-bis(N4-methylthiosemicarbazone))	56, 57

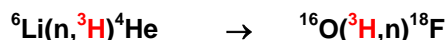
Table 4. Most important PET isotopes.

Sometimes long lived positron emitting radionuclides are commercially available or obtainable from research facilities with larger accelerators. Some examples of longer lived positron emitting radionuclides are ^{52}Fe ($t_{1/2} = 8.3$ h), ^{55}Co ($t_{1/2} = 17.5$ h) and ^{124}I ($t_{1/2} = 4.2$ d). Sometimes also positron emitting radionuclides can be obtained from a generator system. Examples are ^{82}Rb ($t_{1/2} = 76$ s) from ^{82}Sr ($t_{1/2} = 25.5$ d) and ^{68}Ga ($t_{1/2} = 68$ m) from ^{68}Ge ($t_{1/2} = 270$ d). Although all these radionuclides are used, the isotopes of the biological most important elements receive most attention.

1.5.1 Production of fluorine-18

Among different radioisotopes, biopharmaceutically and PET-friendly $[^{18}\text{F}]$ -fluorine is currently the most widely used. Radioactive ^{18}F has a half-life 109.8 min - long enough to ^{11}C , ^{13}N or ^{15}N . This fact allows for commercial distribution of ^{18}F -radiopharmaceuticals. ^{18}F is almost pure β^+ emitter (96.9% β^+ , 3.1% EC) with endpoint energy of 0.635 MeV and maximal positron range 2.4 mm in water. These properties make ^{18}F an ideal candidate for radiolabelling.

^{18}F -fluoride could be produced in nuclear reactors or in cyclotrons. An interesting example is the production of ^{18}F from nuclear reactor^{58,59} by starting with neutrons which induce a charged particle reaction in a nuclear reactor:



By the irradiation with neutrons, tritons are generated by the breaking up of the ^6Li into a tritium and a helium-3 nucleus. The triton is then able to produce ^{18}F from the ^{16}O -nucleus. Because of the incorporation of the oxygen inside the molecule, the range of the tritons is not essential. Since this is a two-stage process the yield is lower (30 mCi) than the yields achievable with direct reactions as can be

done with charge particle induced reaction. The practical difficulties are significant, not least because of the need to isolate the product from tritium and lithium.

Cyclotron production of ^{18}F has two main directions. A first method for the production of ^{18}F is carrier added (CA) reaction $^{20}\text{Ne}(\text{d},\alpha)^{18}\text{F}$. The ^{18}F becomes available as F_2 and the relative low specific activity depends on the amount of fluorine (0.1-0.2%) added before irradiation⁶⁰.

The bombardment of high pressure neon (up to 25 bar) containing a low percentage (0.1-0.2%) of molecular fluorine with moderate energy deuterons is now a common and well-established method for producing CA molecular ^{18}F -fluorine^{53,54}.

The most common modern way to produce NCA ^{18}F is the $^{18}\text{O}(\text{p},\text{n})^{18}\text{F}$ reaction with H_2^{18}O (oxygen-18 95% enriched water) as target material. The ^{18}F is available as fluoride ion in water. This is the most effective method for the non-carrier added ^{18}F -fluoride. After separation of the fluoride from the water, the fluoride is available for chemistry. The water can be reused after distillation to eliminate impurities. The enrichment grade will diminish of course by the distillation procedure. The specific activity of the fluorinated end product can easily be better than carbon-11 product because fluoride is less abundant than e.g. CO_2 .

The beam energy required for (p,xn) reaction follows a rule of thumb: $7 + 10 \cdot \text{xn}$ MeV with xn the number of neutrons to be knocked out. For an exact calculation one should calculate the mass difference and add roughly 7 MeV for the maximum cross section.

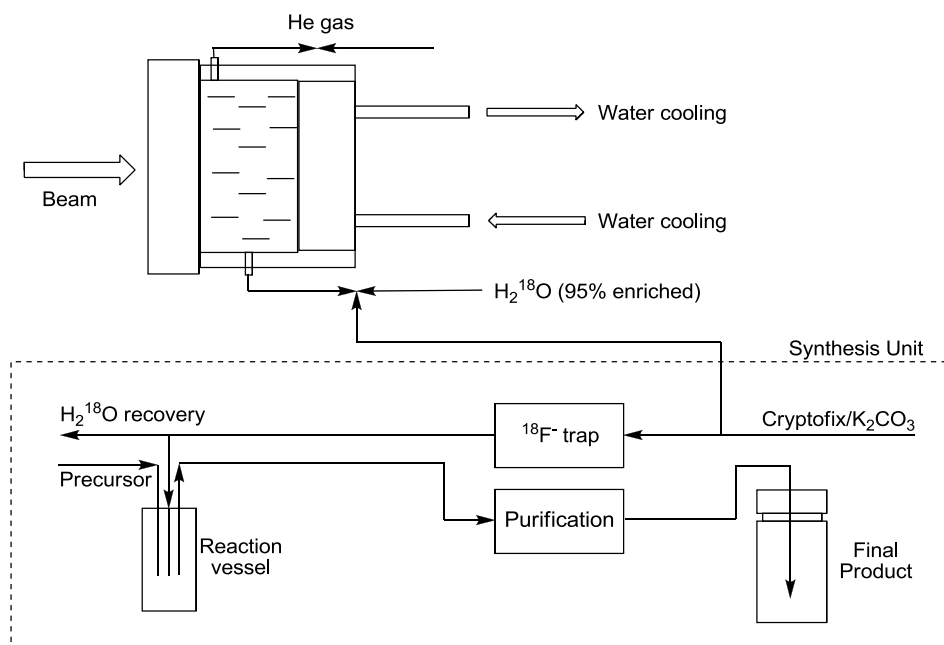


Figure 13. Schematic view of the NCA ^{18}F target and synthesis unit.

The targets may use approx. 1-2 mL of ^{18}O -enriched water. Target materials containing chromium, iron or cobalt are undesirable, as they possibly produce unreactive ^{18}F -fluorides, but nickel, titanium, niobium and silver are acceptable. ^{18}O -enriched water is expensive; it can be re-used after distillation or after recovery of ^{18}F -fluoride, for example, by adsorption on an anion exchange column or cartridge. The process is intrinsically high yielding. Very high specific activities can be achieved from fluoride-free water.

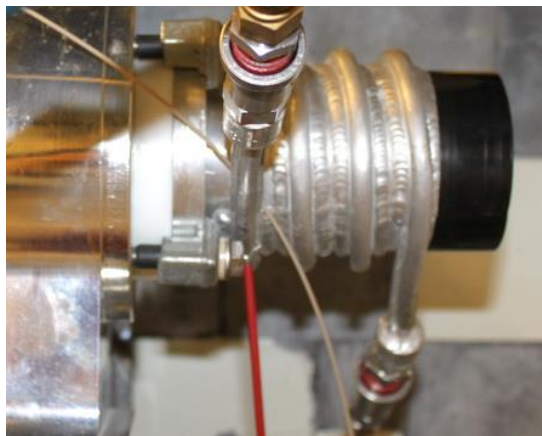


Figure 14. Cyclotron high beam current target for $^{18}\text{F}^-$ production.

For the nucleophilic processes the $^{18}\text{F}^-$ is required as 'naked' non-carrier added fluoride i.e. in the absence of water. Several procedures have been described for the recovery of NCA fluoride in a reactive form from ^{18}O -enriched water. The strategy for generation of reactive ^{18}F is generally dissolution of the ^{18}F -fluoride with a large counterion (Cs^+ , Rb^+ , Bu_4N^+ or K^+ /Kryptofix) in a polar aprotic solvent. Where required, water (or other solvent) is removed by distillation from an added base (e.g. KOH , K_2CO_3 , Rb_2CO_3 , $\text{Et}_4\text{N}^+\text{OH}^-$, $\text{Bu}_4\text{N}^+\text{OH}^-$ or K_2CO_3 -Kryptofix) by azeotropic distillation with acetonitrile or even by microwaves. This salt is then solubilized in the solvent containing the substrate for nucleophilic attack. Resolubilization efficiency is affected by the reaction vessel, solvent and other factors such as metal ion contamination. The intrinsic reactivity of the ^{18}F -fluoride is affected by several factors, including cation and anion contaminants whose level is largely determined by the materials of target construction and operation. Cations, especially Al^{3+} , and Ca^{2+} , are probably most detrimental to successful chemistry^{55,61}.

Among this variety of isotopes, currently, ^{18}F – is the most used isotope because of advantages listed below:

- the decay positrons are relatively of low energy and therefore have short ranges in the body,
- high specific activities can be produced,
- the labeled tracers are structurally very similar to their non-labeled counterparts.

Possessing these unique properties, ^{18}F chemistry has one disadvantage – introducing of ^{18}F into new molecules can be problematic.

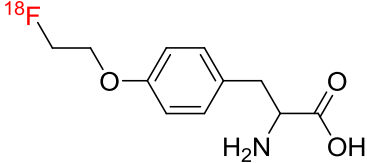
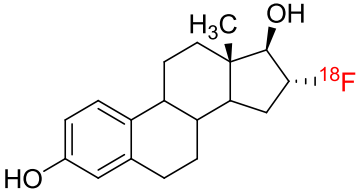
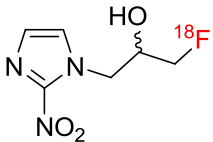
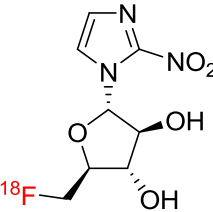
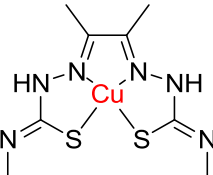
1.6 PET radiopharmaceuticals

The most important need for further utilization of PET imaging is the development of new radiopharmaceuticals. Molecular imaging with radiopharmaceuticals can be used for a wide ranging of applications, like drug development, pharmacokinetics studies, clinical investigations, and routine diagnostics.

Some of radiopharmaceuticals for molecular imaging of biochemical processes such as metabolism, specific receptors, blood flow, perfusion and hypoxia are listed below. Each radiopharmaceutical focuses on specific target of each biochemical or biological process⁶². For example, the most known and the most widely used PET radiopharmaceutical [¹⁸F]FDG - also called “the molecule of the millennium”. [¹⁸F]FDG can target the enzyme, hexokinase, and specifically measure the glucose metabolism *in vivo*. Many attempts of the [¹⁸F]FDG synthesis were tried before the major breakthrough was done in 1986 by Hammacher et al., who developed a method with high radiochemical yield (RCY) and short total time of synthesis.

Table 5. Main PET radiopharmaceuticals for clinical use.

Acronym / name	Structure	Biochemical process	Specific target	Ref.
[¹⁸ F]FDG ¹⁸F-fluorodeoxyglucose		Sugar metabolism	Hexokinase	63, 64, 65, 66, 67
[¹⁸ F]NaF ¹⁸F-Sodium Fluoride	Na ¹⁸ F	Fluoride metabolism		68
[¹⁸ F]FDOPA 3,4-dihydroxy-6-¹⁸F-fluoro-L-phenylalanine		Dopamine metabolism	Aromatic amino acid decarboxylase	69, 70
[¹⁸ F]FLT 3'-Deoxy-3'-(¹⁸F)-fluorothymidine		DNA synthesis	Thymidine kinase	71, 72, 73
[¹⁸ F]FLM ¹⁸F-Flumetamol or Vizamyl		Apoptosis	Phosphatidylserine	74
[¹⁸ F]FCH ¹⁸F-fluorocholine		Cellular ligand transport	Choline kinase	75

¹⁸ F]FET ¹⁸F-fluoroethyl-L-tyrosine		Amino acids metabolism	Protein synthesis	76
¹⁸ F]FES ¹⁸F-fluoro-β-estradiol		Tumor receptors	Estrogen receptor	61
¹⁸ F]FMISO 1H-1-(3-[¹⁸F]-fluoro-2-hydroxy-propyl)-2-nitroimidazole		Hypoxia	Acidic pH and reductive potential	77
¹⁸ F]FAZA ¹⁸F-fluoroazomycin arabinoside		Hypoxia	Acidic pH and reductive potential	78
⁶⁴ Cu-ATSM ⁶⁴Cu-diacetyl-bis N4-methylthiosemicarbazone		Hypoxia	Acidic pH and reductive potential	79

[¹⁸F]FDG, [¹⁸F]NaF, Amyvid™ and VizamyI™ are FDA (United States Food and Drug Administration) approved imaging radiopharmaceuticals. The first and the most important radiotracer from this list [¹⁸F]FDG - FDA announced to be safe and effective for certain indications when produced under conditions specified in approved applications (March 2000).

Synthesis, quality control and regulations of [¹⁸F]FDG became a model in the development of new radiopharmaceuticals. The conception of using robots or automatic synthesis modules is a standard in PET radiochemistry of modern time. Many others radiopharmaceuticals were developed using the same strategy - for example [¹⁸F]FET ([¹⁸F]fluoroethyl-L-tyrosine), [¹⁸F]FCH ([¹⁸F]fluorocholine), [¹⁸F]FMISO ([¹⁸F]fluoromisonidazole), [¹⁸F]FES ([¹⁸F]fluoro-β-estradiol).

The development of new tracers with even better properties, tracers labelling specific sites, evolving of new methods and procedures is therefore still a highly prioritized research area.

1.7 Challenges and directions of modern radiofluorination

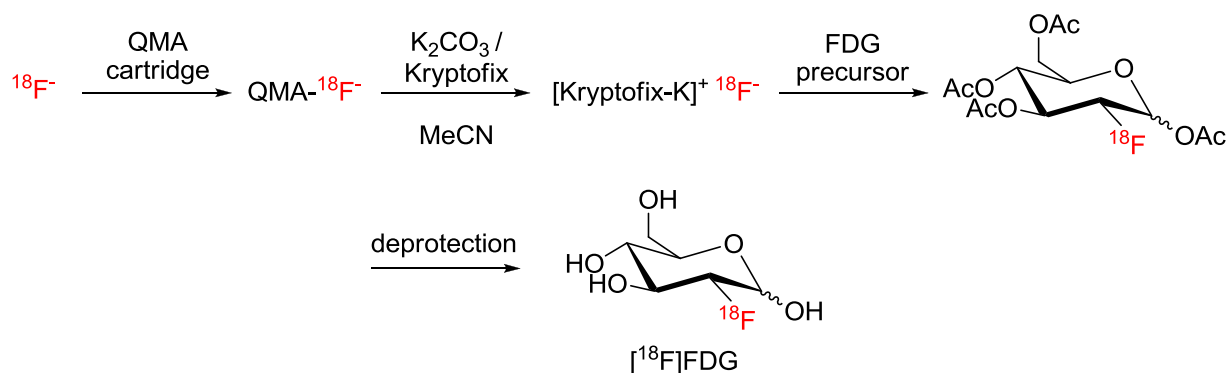
Elemento- and organometallic chemistry and improving of radiofluorination

PET has been always limited by chemistry. New methods for the synthesis of radiolabeled molecules have the prospective to impact clinical PET imaging only if they can be successfully translated. However, progression of modern reactions from the stage of synthetic chemistry development to the preparation of radiotracer doses ready for use in human PET imaging is challenging and rare.

Once chemistry with ^{18}F is feasible (i.e. a fluorination reaction can be accomplished with ^{18}F , and a RCY can be determined), the reaction still may not lead to a practical synthesis method for molecules useful for PET imaging experiments. Most importantly, radiochemistry techniques must allow for efficient purification due to time constraints. The formation of constitutional isomers that are difficult-to-separate must be minimized during synthesis, and starting materials as well as byproducts must be removable from the desired sample. Final samples must be radiochemically and chemically pure, sterile and endotoxin free. Additionally, a substantial quantity of radioactivity must be obtained at the end of synthesis.⁸⁰

1.7.1 Fluoride recovery and processing

Fluoride has high hydration energy, so water is not a suitable solvent for $\text{S}_\text{N}2$ radiofluorination. Polar aprotic solvent such as acetonitrile should be used in $\text{S}_\text{N}2$ nucleophilic substitution reaction. Since ^{18}F -fluoride is produced via a $^{18}\text{O}(\text{p},\text{n})^{18}\text{F}$ reaction, it is necessary to isolate the ^{18}F -ion from its aqueous environment.



Scheme 4. Synthesis of $[^{18}\text{F}]\text{FDG}$ by nucleophilic substitution

The most convenient way to separate is to use a light QMA (quaternary ammonium anion exchange) Sep-Pak column. The ^{18}F is retained by or via an ion-exchange reaction and allowed the ^{18}O -water to flow through. The retained ^{18}F is then eluted with an acetonitrile solution of Kryptofix and potassium carbonate. Evaporation of the acetonitrile in a nitrogen atmosphere will remove any residual $[^{18}\text{O}]\text{H}_2\text{O}$ escaped into the reaction vial together with the ^{18}F . The automatic synthesizers perform this step several times to ensure all residual water is removed.⁶⁴

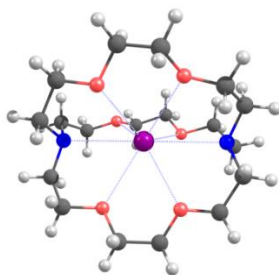


Figure 15. Potassium - Kryptofix complex $[N(CH_2CH_2OCH_2CH_2OCH_2CH_2)_3N]K$

The overall procedure of $^{18}F^-$ recovery and activation requires several liquid and gas transfers resulting in lengthening of synthesis, reduced yields, and complex automation. Significant efforts focused on eliminating the azeotropic evaporation step.

$[^{18}F]HF$ transfer

An alternative to a conventional ^{18}F -K/Kryptofix method is recovery and processing⁸¹ of ^{18}F -fluoride via gaseous $[^{18}F]HF$. This method was developed in our laboratory and successfully used in radiofluorination.

We found that the reaction of target water with H_2SO_4 (98-100%) allowed to recover of up to 82% of ^{18}F -fluoride as $[^{18}F]HF$ -gas or $[^{18}F]HF$ -amine/base solution in anhydrous organic solvent⁸². Home-made glassy carbon and PE devices for transfer were made to perform this experiment.

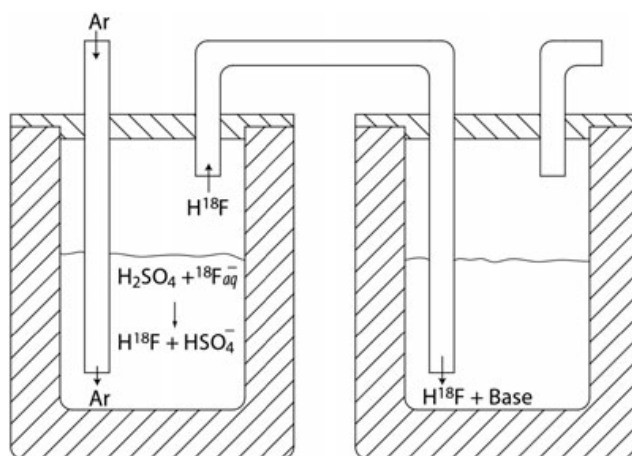
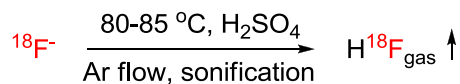


Figure 16. Schematic view of $[^{18}F]HF$ generator.



Scheme 5.

The $[^{18}F]HF$ distillate is acid-free but slightly moist (5180 ppm after 30 min of distillation) – even this moisture content is not crucial for most of experiments. High and reproducible transfer of $[^{18}F]HF$ could be achieved under vigorous argon flow (up to 400 ccm) and ultrasound irradiation⁸³.

This method was used for the synthesis of a series of phosphazanium hydrofluorides, $P_1^{tBu}[^{18}F]HF$, $P_1^{Oct}[^{18}F]HF$, $P_2^{Et}[^{18}F]HF$, and $P_4^{tBu}[^{18}F]HF$.

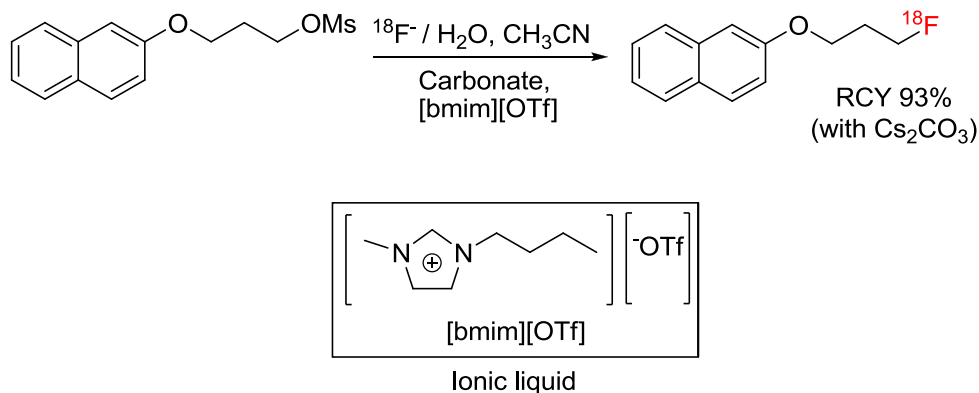
High specific activity and excellent radiochemical yields with various substrates (Table 6) suggest that the proposed radiofluorination methodology can complement the current $[^{18}F]KF/Kryptofix$ methods in the areas for which nonpolar reaction conditions are required⁸³.

Reagent	Substrate	RCY, %
$P_2^{Et}[^{18}F]HF$	2-(naphthalen-1-yl)ethyl methanesulfonate	91
$P_2^{Et}[^{18}F]HF$	2-(naphthalen-1-yl)ethyl 4-methylbenzenesulfonate	82
$P_4^{tBu}[^{18}F]H$	FDG precursor	82

Table 6. Radiofluorination with $[^{18}F]$ phosphazanium hydrofluorides.

Ionic liquids

Ionic liquids are novel promising materials that consist of very lipophilic cations and their counter anions having melting points below ambient temperature. This symbiosis of unique physical and chemical properties, made ionic liquids to be considered as alternative green chemistry reaction media, in contrast to the classical organic solvents. Ionic liquids as powerful media for organic reactions, because they can accelerate reaction rates, improve selectivity, and facilitate catalyst recovery.



Scheme 6.

Some model halo- and mesyloxyalkanes can be fluorinated to the corresponding fluoroderivatives via nucleophilic fluorination in the presence of KHCO_3 or Cs_2CO_3 in $[\text{bmim}][\text{OTf}]$. The main benefit from the use of ionic liquids is that $^{18}\text{F}^-$ in target irradiated $[^{18}\text{O}]\text{H}_2\text{O}$ can be added directly to the reaction mixture instead of following long protocol of dehydration procedures⁸⁴.

Polymer supported radiofluorination (PSRF)

Probably a more attractive approach involves radiofluorination performed directly on the solid phase extraction (SPE) media. One of the first examples of PSRF was described with 4-aminopyridinium salt on

a polymer support. This resin is a phase transfer catalyst, that eliminates the need of toxic Kryptofix, simplifies purification and remove the need for fluoride elution and azeotropic evaporation. The possibility of “polymer supported” radiofluorination was described before, but the aminopyridine-based resin gave poor stability and inconsistent $^{18}\text{F}^-$ - trapping and radiofluorination^{85,86}.

A new method was developed in our group – PSRF with the polymer supported phosphazene bases PS- P_2^{tBu} and the novel PS- P_2^{PEG} which allowed for efficient extraction of $[\text{}^{18}\text{F}]\text{F}^-$ from irradiated water and succeeding radiofluorination of a broad range of substrates directly on the resin. This method could be characterized by high radiochemical yields (up to 70% with aliphatic sulfonates and 42% with bromides) and a short time (30–45 min) of the total radiosynthesis. The resins could be reused several times with the same or different substrates.

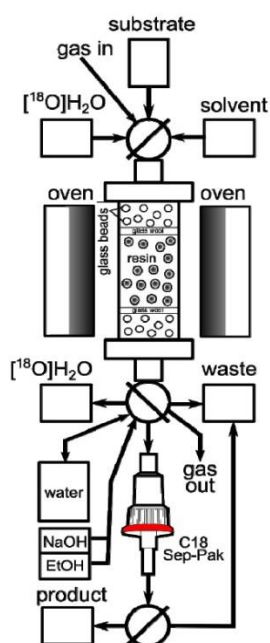
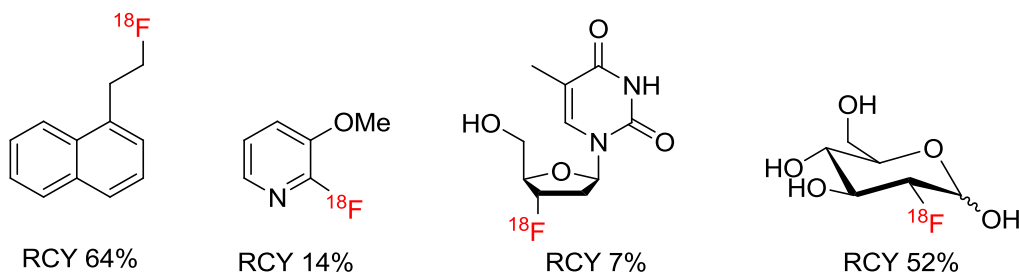


Figure 17. Scheme of automated radiosynthesis module for on-column radiofluorination and some ^{18}F -products obtained via this method⁸⁷.

The fully automated on-column radiofluorination methodology was applied to the radiosynthesis of the important PET radiotracers $[\text{}^{18}\text{F}]\text{FLT}$ and $[\text{}^{18}\text{F}]\text{FDG}$ (40% RCY on a 120 GBq scale, all GMP-regulated quality control tests, required for commercial production of $[\text{}^{18}\text{F}]\text{FDG}$, were passed).



Scheme 7. Selection of radiofluorinated products, obtained using PSRF.

The combination of compact form factor, simplicity of ^{18}F -fluoride recovery and processing, column reusability can make solid phase radiofluorination an attractive radiochemistry platform for the emerging dose-on-demand instruments for bedside production of PET radiotracers.⁸⁷

1.7.3 Expanding the substrate scope and selectivity with transition metals

The synthesis of ^{18}F -radiotracers used for PET imaging is different compared to the conventional ^{19}F -fluorination. Translation from ^{19}F to ^{18}F is challenging and significantly more complicated and unpredictable than would be anticipated from the synthesis of an ordinary isotopologue. Concentration and reaction conditions, most notably stoichiometry, dramatically change as a consequence of the nanomolar amount of ^{18}F -fluoride used in radiosyntheses. An excellent ^{19}F fluorination reaction may not necessarily be suitable for ^{18}F chemistry⁸⁸.

It is important to introduce the short half-life radioisotope ^{18}F as late and as rapidly as possible in the synthetic system to achieve maximal RCY. Moreover, ^{18}F -fluorination should ideally be performed using a ^{18}F -fluoride source in preference to $[^{18}\text{F}]\text{F}_2$ or other derivatives of electrophilic fluorine, as most PET centers are not equipped with gas targets and gaseous reagents. Also, the specific activity of $[^{18}\text{F}]\text{F}_2$ is low (440 GBq/mmol) compared to that achievable using $[^{18}\text{O}]\text{water}/[^{18}\text{F}]\text{fluoride}$ target technology ($3.7 \cdot 10^5$ GBq/mmol).

Fluoride is the most abundant form of fluorine. Extremely powerful nucleophile and base, fluoride completely loses its reactivity in water due to enormous free energy of hydration. This “hydration penalty” will influence both the kinetics and overall thermodynamics of nucleophilic fluorination. Can the transition metals (TM) alleviate this penalty by trading TM-fluorophilicity for fluoride hydrophilicity?

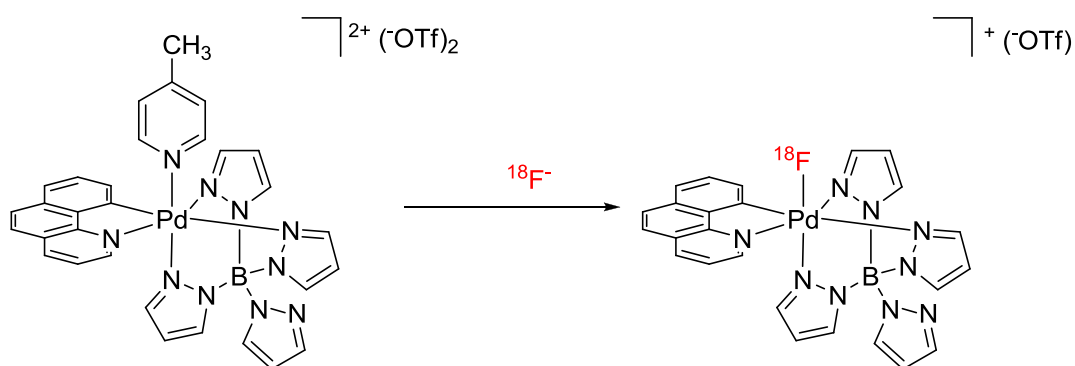
Fluorinations catalysed by transition metals have been extensively scrutinized and reviewed, especially reactions employing electrophilic fluorinating reagents ($[^{18}\text{F}]\text{DOPA}$ for example). On the other hand, transition metal catalysed fluorination with nucleophilic fluorinating reagents is an emerging area in catalysis. The successful development of transition metal catalysed fluorination is directly dependent on the availability of competent, soluble fluoride sources and a clear understanding of the parameters that control nucleophilicity vs basicity.

Recent developments in transition metal catalysed processes have enabled the nucleophilic fluorination of substrates that could not be fluorinated in the absence of catalysts.

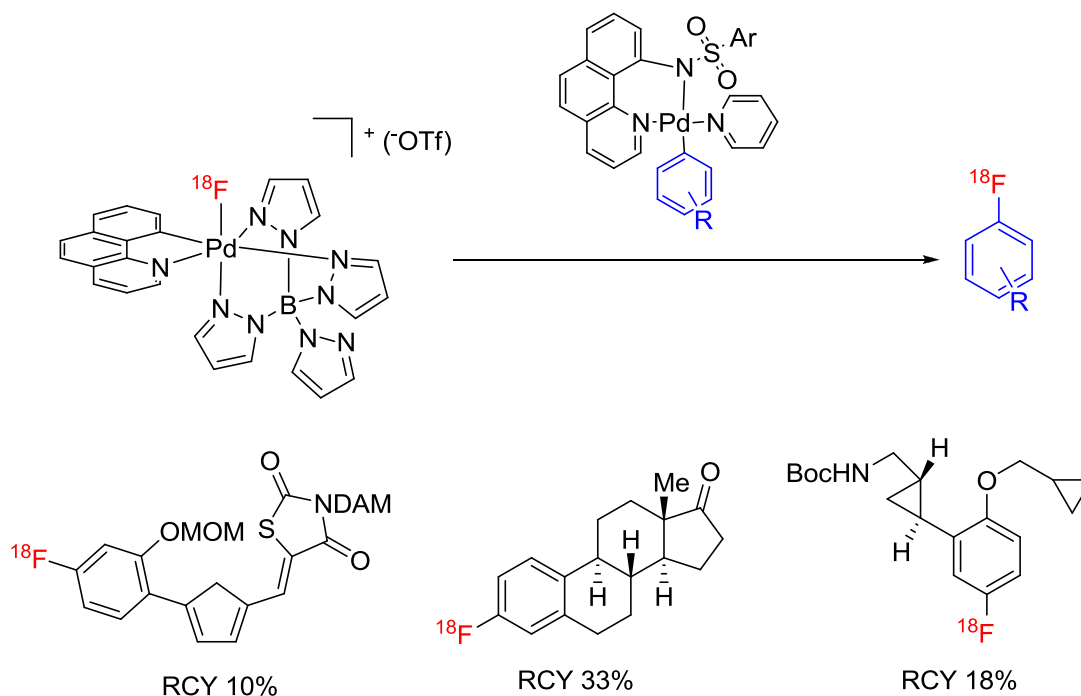
Pd-mediated radiofluorination of aryls

Transition metal mediated fluorination to the formation of ^{18}F -aryl bonds from ^{18}F -fluoride has recently been validated. Ritter et al. have established a synthesis of a Pd^{IV} [^{18}F]fluoride from [^{18}F]fluoride that can be used as an electrophilic fluorinating reagent of high specific activity. Potentially this could provide a route to previously unattainable PET tracers as the fluorination step is no longer limited to nucleophilic methodologies.⁸⁹

The synthesis is shown to give decay-corrected radiochemical yields (RCY) up to 33% in 10 min, with an overall reaction time of 60 minutes.



Scheme 8. Synthesis of an electrophilic fluorinating reagent from nucleophilic fluoride.



Scheme 9. Synthesis of ^{18}F aryl fluorides.

An electrophilic radiofluorination for the synthesis of aryl fluorides with high specific activity makes use of Pd^{IV} complex to incorporate ^{18}F -fluoride into arenes. The Pd^{IV} complex captures fluoride and then functions as an electrophilic ^{18}F -fluorination reagent. An advantage of this method is that [^{18}F]fluoride can be incorporated into functionalized arenes at a late stage. Moreover, the Pd^{IV} -[^{18}F] complex is thermally stable and insensitive to water⁹⁰.

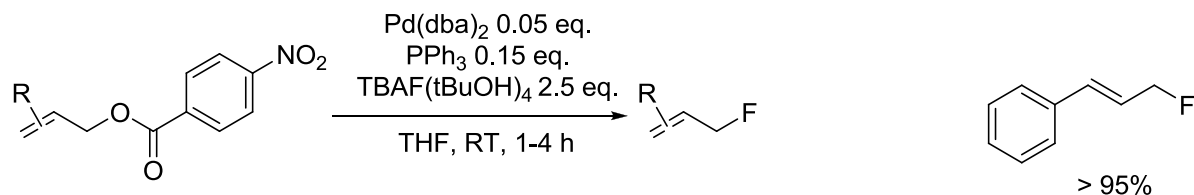
Nevertheless, this method has disadvantages. Pd-compounds are very expensive; making the end product more costly than it is already. Also a need to be separated at the end of the synthesis and too complicated synthetical route limit practical use of this method in routine radiopharmacy/radiochemistry practice.

Pd-mediated radiofluorination in allylic position

Another transition metal mediated synthesis of ^{18}F -radiolabelled compounds was described by Gouverneur et al⁸⁹. An attractive route to allylic fluorides is the Pd(0)-catalyzed Tsuji–Trost allylic alkylation with fluoride as the nucleophilic reactant^{91,92}. This reaction is a very powerful transformation for the attachment of a variety of carbo- and heteroatom nucleophiles to allylic electrophiles. Togni et al⁹³ investigated the feasibility of a Pd-catalyzed allylic nucleophilic fluorination in 2006. It was found that exposure of cationic Pd(II) allyl complexes to various fluoride sources at room temperature and showed no conversion to allylic fluoride.

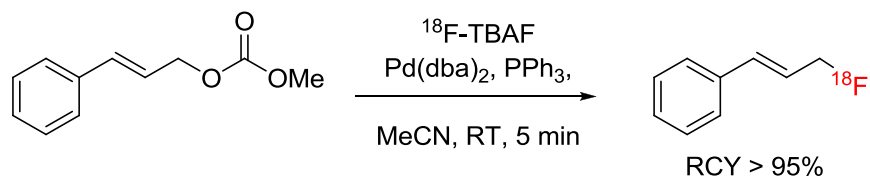
Further studies of this reaction in “cold” ^{19}F variant demonstrated that allylic fluorination of allyl carbonates with TBAF·4tBuOH is feasible⁸⁹. A p-nitrobenzoate was identified as a superior leaving group to

carbonate, an interesting observation since the use of this leaving group in classical palladium chemistry is sparse in the literature⁹⁴.



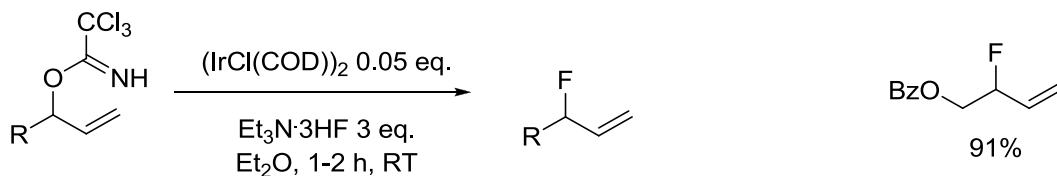
Scheme 10. Pd⁰-catalyzed fluorination of allylic *para*-nitrobenzoates.

For the radiochemistry work, the methyl carbonate was found to be the superior leaving group.



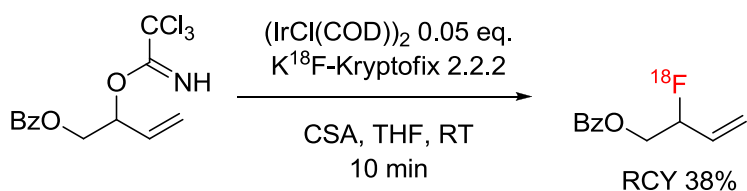
Scheme 11. Pd⁰-catalyzed radiofluorination of carbonates.

Iridium variant of this reaction was reported by Nguyen et al⁹⁵. Secondary and tertiary racemic allylic fluorides from allylic trichloroacetimidate under iridium catalysis (5 mol% (IrCl(COD))₂). Triethylamine trihydrofluoride (Et₃N·3HF or TREATHF) was found to be the optimized source of fluoride allowing moderate to good yields of secondary branched allylic fluorides to be obtained. Tertiary allylic fluorides though accessible by this route could not be isolated owing to polymerization or decomposition.



Scheme 12. Ir-catalyzed fluorination of allylic trichloroacetimidates.

This rapid and functionally tolerant reaction has also been extended to the preparation of a representative ¹⁸F-allylic fluoride in 38% RCY (decay-corrected).



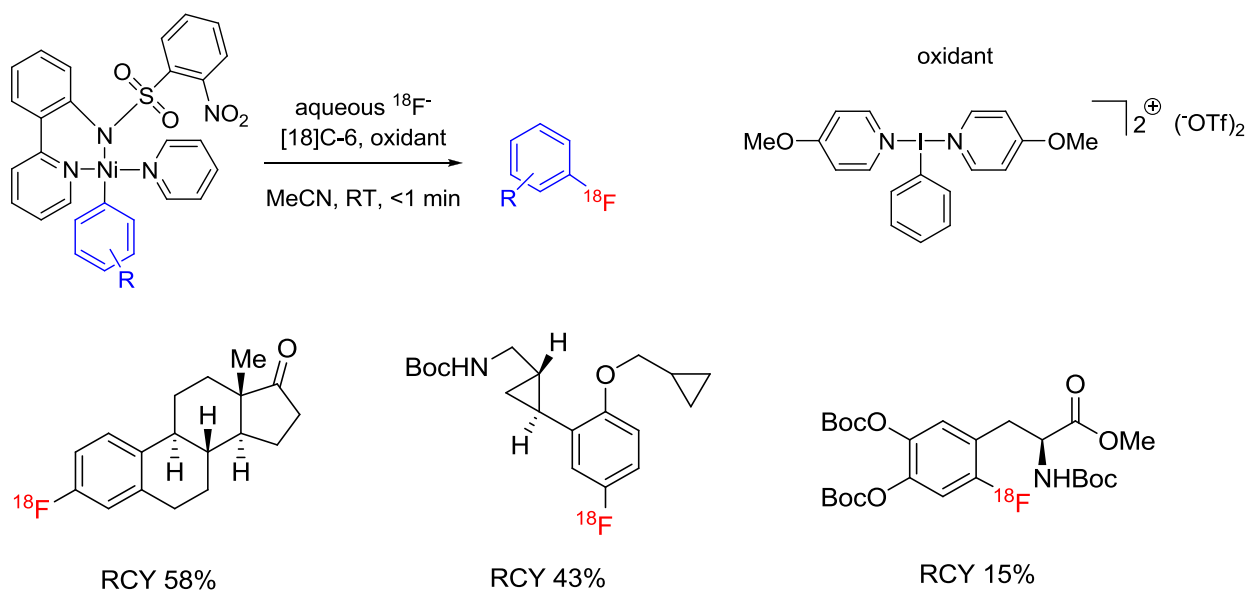
Scheme 13. Ir-catalyzed radiofluorination.

Ir or Pd catalysts are expensive, this adds to the overall cost of the synthesis. This method has almost no practical use in radiopharmacy. In fact, no relevant radiopharmaceuticals could be produced via this method.

Ni-mediated radiofluorination

The ability to use aqueous fluoride solutions makes extensive drying procedures, which are typical for radiochemistry with [^{18}F]fluoride, excessive. Drying procedures increase the time from ^{18}F -production to tracer purification; drying fluoride for the [^{18}F]FDG takes 20-30 min. The direct use of aqueous fluoride solution could avoid loss of activity and also increases the RCY because of drying fluoride absorption onto walls of glass reaction vessels.

The one-step oxidative fluorination of well-defined nickel complexes with oxidant and aqueous fluoride enables a straightforward and practical ^{18}F late-stage fluorination of complex small molecules. The ability to use aqueous solutions of ^{18}F -fluoride is remarkable⁹⁶.



Scheme 14. Ni^{II} complexes for the radiofluorination in aqueous media and ^{18}F -labelled aryl fluorides.

Radiofluorination takes place at room temperature and is complete within less than one minute. Ni^{II} aryl pyridylsulfonamide complexes can be oxidized with oxidant in the presence of aqueous [^{18}F]fluoride to afford complex ^{18}F -labeled arenes in 13–58% radiochemical yield. The use of an aqueous ^{18}F solution obviates the need for time-consuming anion-exchange and azeotropic drying steps during the synthesis of the PET tracer⁹⁶.

The disadvantage of this method is complicated multistep synthetic route, which also makes it expensive.

Chapter 2

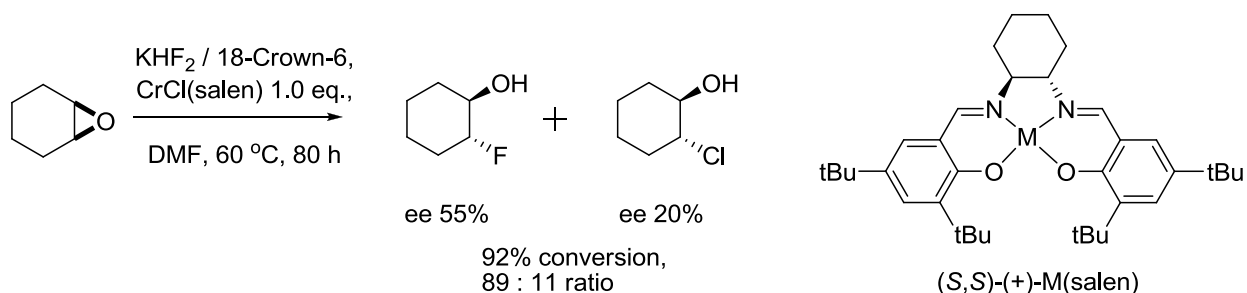
Co(salen)-mediated enantioselective radiofluorination of epoxides

2.1 Transition metal mediated fluorination of epoxides

Incorporated into organic molecules C-F bond modulate useful properties like lipophilicity, bioavailability, and oxidative stability. Introduction of fluorine into organic molecules is a challenging field of elementoorganic chemistry. New methods for the formation aliphatic C-F bonds have the potential to deliver chiral fluorinated structures inaccessible from commercial or biogenic sources⁹⁷.

Opening of epoxides with fluoride can provide access to fluorinated secondary or tertiary carbon centers. Stable solutions of HF with amines such as pyridine·nHF and Et₃N·3HF are suitable for the ring opening of epoxides, but usually gave poor yields of racemate. When used in combination with Lewis acids, problems arise due to competitive uncatalyzed pathways and catalyst inhibition.

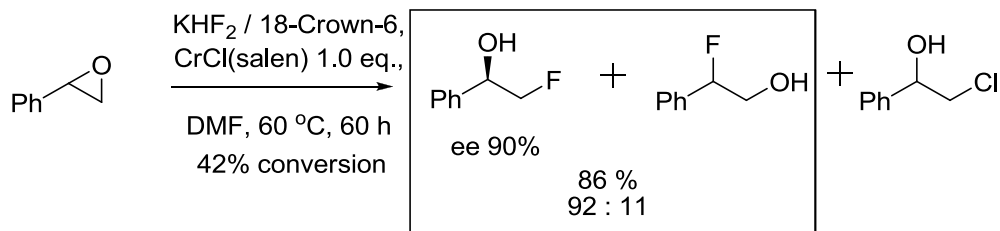
Historically, asymmetric opening of meso-epoxides with fluoride was first reported by Haufe et al^{98,99,100} with stoichiometric amounts of chiral Lewis acid complexes. Haufe desymmetrized cyclohexene oxide using KHF₂/18-crown-6 in the presence of 1 eq. of (*S,S*)-(+)-(salen) chromium chloride complex in DMF at 60 °C.

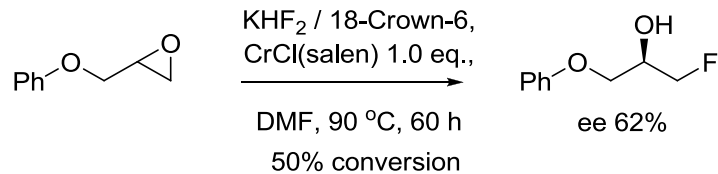


Scheme 15.

Trans-2-fluorocyclohexanol was formed in 55% ee in mixture with trans-2-chlorocyclohexanol (20% ee). Using 0.1 eq. of CrCl(salen), the ee of the fluorohydrin decreased to 11%. These reactions constitute the first enantioselective nucleophilic fluorination by desymmetrization of meso-epoxides⁹⁸.

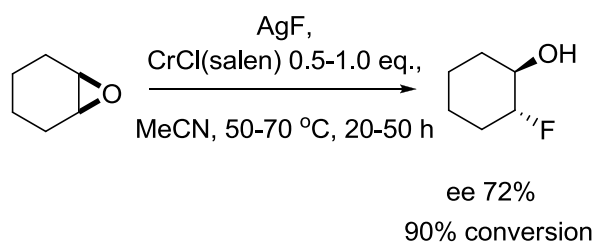
When subjected to fluorination, the racemic epoxide styrene oxide and phenyl glycidylether led to preferential attack of the fluoride at the less substituted carbon. The products of these reactions were formed in 90% and 62% ee respectively.





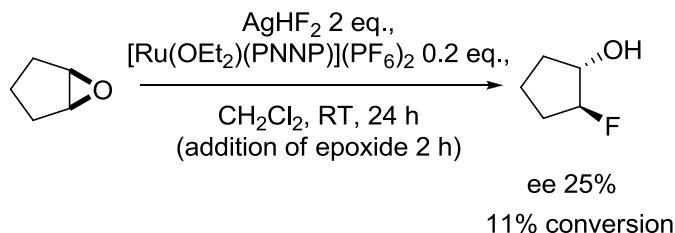
Scheme 16.

Different fluoride sources were investigated. Silver fluoride was found to be a superior reagent, preventing the formation of undesired chlorohydrin and delivering the fluorocyclohexanol, fluorocyclopentenol and fluorocycloheptanol with ee of 72%, 44% (75% conversion) and 65% (82% conversion) respectively. These reactions need to use 1 eq. or at best 0.5 eq. of the metal complex^{99,100}.



Scheme 17.

Mezzetti et al⁹¹ investigated the enantioselective desymmetrization of *meso* epoxides in 2009, trying to define a more efficient catalytic system. Cyclopentene oxide underwent ring opening with AgHF_2 in the presence of 0.2 eq. of either $([\text{RuCl}(\text{PNNP})_2]\text{PF}_6)$ or the dicationic complex $([\text{Ru}(\text{OEt}_2)_2(\text{PNNP})](\text{PF}_6)_2)$ ($\text{PNNP} = 3,5\text{-bis}(\text{diphenylphosphinomethyl})\text{pyrazol}$). The best results were obtained by slow addition of the epoxide to a solution of 0.2 eq. $([\text{Ru}(\text{OEt}_2)_2(\text{PNNP})](\text{PF}_6)_2)$ in CH_2Cl_2 and 2 eq. of AgHF_2 .

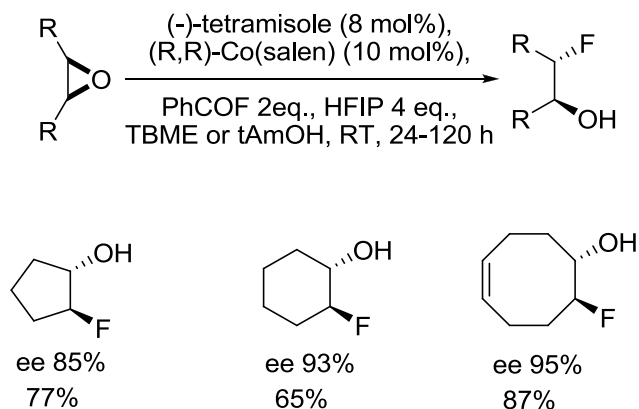


Scheme 18.

Under these conditions, the ring opened fluorinated product was isolated in 11% yield and 25% ee. Competing polymerization was responsible for the low isolated yield of this transformation. Alternative fluoride sources such as $\text{Et}_3\text{N}\cdot 3\text{HF}$, $(\text{Bu}_4\text{N})\text{H}_2\text{F}_3$, KHF_2 and PhCOF led only to epoxide polymerization or gave no conversion at all^{91,92}.

The most recent development in this area was done with a Co^{III} -salen catalyst by Kalow and Doyle^{101,97} for *meso*-epoxides and terminal epoxides. HF was generated *in situ* upon addition of 1,1,1,3,3,3-hexafluoroisopropanol (HFIP) to benzoyl fluoride in the presence of an amine catalyst. An asymmetric

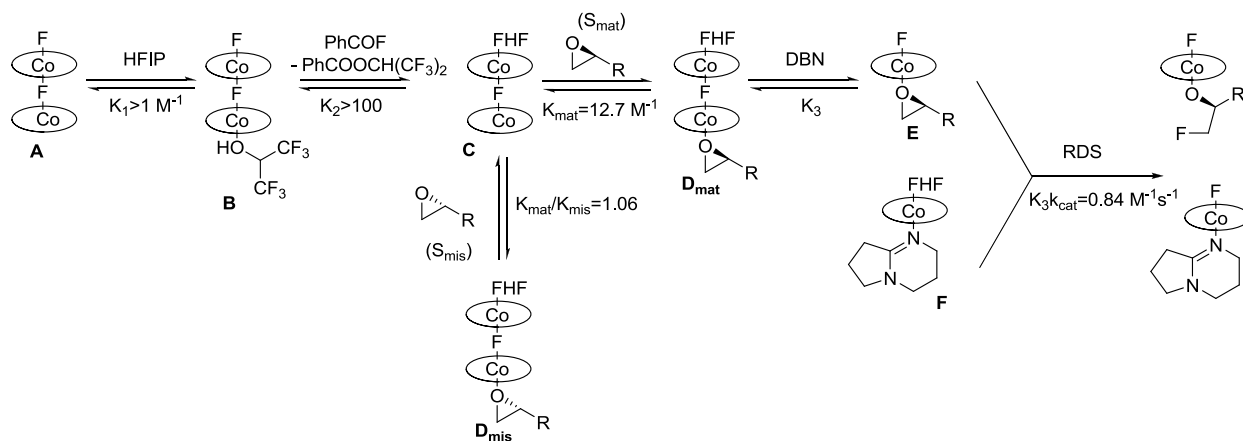
variant of this protocol was successfully implemented (yields up to 88% and ee ranging from 58% to 95%) performing the hydrofluorination of various *meso* epoxides in TBME using both the chiral isothioureia (-)-tetramisole (8 mol%) and the chiral Co(salen) complex (10 mol%) as a catalysts¹⁰¹.



Scheme 19. Assymmetric fluorination of meso epoxides by Doyle.

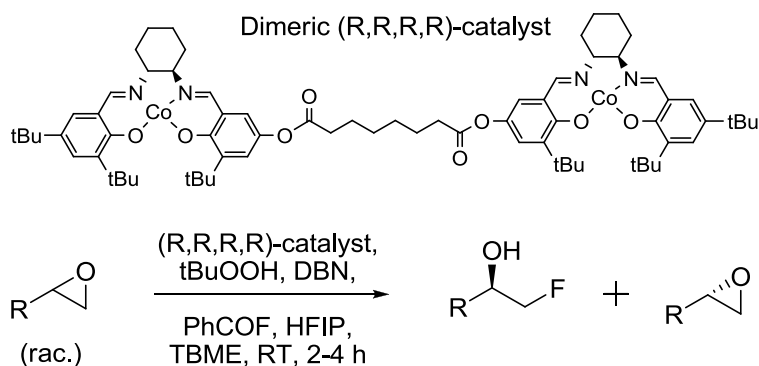
The limitation of this chemistry is the long reaction time (24–120 h). Control reactions with achiral amines or the use of a mismatched Lewis acid/amine pair had a detrimental impact both on yield and enantioselectivity, an observation supporting the synergic cooperative effect of the two chiral cocatalysts. Meso cyclic epoxides containing alkene, ester and protected amine functionalities were all amenable to hydrofluorination under the optimized reaction conditions or slightly readjusted variants (t-AmOH or diethylether as the solvent). When applied to racemic terminal epoxides, kinetic resolution took place delivering the fluorohydrins (regioselective opening at the terminal position) with ee 88 - 99%.

Further studies⁹⁷ shed light on the mechanism of this hydrofluorination. The rate limiting step, the fluoride ring opening event, is proposed to proceed via a bimetallic mechanism based on kinetics non-linear effect studies¹⁰² with monomeric Co(salen) catalysts and experiments using a linked catalyst:



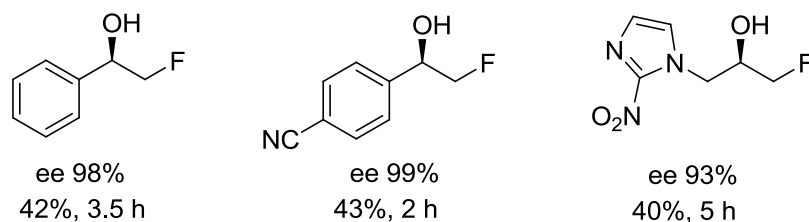
Scheme 20.

A kinetic profile with apparent first-order dependence on Co(salen) was observed. To account for these data, the authors propose a mechanism involving a cobalt fluoride as the active nucleophilic fluorine species that forms a resting state dimer. In this mechanistic scenario, axial ligation of the amine cocatalyst to Co(salen) can facilitate dimer dissociation and is accounting for the observed cooperativity. Taken together, these insights led to the strategy of a second generation dimeric catalyst displaying dramatically improved efficiency (shorter reaction time)⁹⁷.



Scheme 21. Improved protocol of enantioselective fluorination of epoxides via kinetic resolution by Doyle.

The nitroimidazole-substituted fluorohydrin represents the “cold” version of the PET hypoxia imaging radiotracer fluoromisonidazole FMISO.



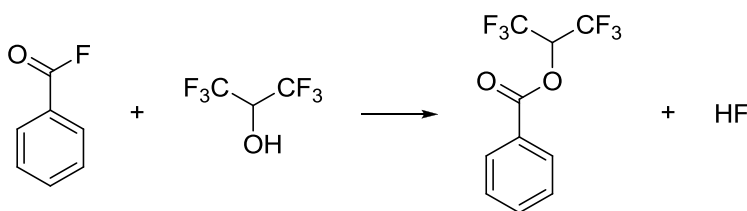
Scheme 22.

2.2 Results and discussions

Transition metal-mediated asymmetric hydrofluorination of epoxides, pioneered by Haufe⁹⁸ has been developed into a highly efficient catalytic system by Doyle and co-workers^{101, 97}. The translation of transition metal mediated ¹⁹F-chemistry into no carrier added (NCA) radiofluorination has so far been limited^{103,104}. Although the nucleophilic epoxide opening with ¹⁸F-fluoride has received attention over the years the efficient reaction remains challenging and the yields vary significantly.

2.2.1 Preparation of [¹⁸F]HF

Doyle et al used benzoyl fluoride as a latent source of HF. The combination of benzoyl fluoride and HFIP generates HF *in situ*:



Scheme 23.

Benzoyl fluoride is manufactured from benzoyl chloride and KF via Halex reaction. Similar methodology could be used for the synthesis of [¹⁸F]PhCOF, but will lead to low RCY, time extension of the radio synthesis and extra complication of setup (GC separation is needed)¹⁰⁵.

In our opinion, since the real fluorinating agent is HF but not PhCOF, there is no real need to synthesize [¹⁸F]PhCOF. Even in cold variant of this reaction, PhCOOCH(CF₃)₂ is produced in excess and makes the separation difficult.

Anhydrous hydrogen fluoride HF is one of the cheapest fluorinating reagents. But the low boiling point (19.6 °C) of this highly corrosive acid leads to logistic challenges, which highly limits its use in laboratory practice. Stable solutions of HF with amines have been reported. In the mid-seventies, Olah and coworkers demonstrated that pyridinium poly-hydrogen fluoride is a stabilized highly versatile reagent for the fluorination of a large range of functional groups¹⁰⁶. Various neutral reagents have been developed.

Previous research from our group has shown that ¹⁸F-fluoride can be efficiently recovered from irradiated target ¹⁸O-water as H¹⁸F gas^{82,83}. To obtain [¹⁸F]HF in a high yield and purity, efficient degassing of the reaction mixture is needed. This can be achieved using vigorous argon flow and ultrasound irradiation.

HF is known as an extremely corrosive and etching substance for many materials, common in laboratory practice - especially for glass and stainless steel. This fact resulted in a search for suitable material, compatible with automation module. In the preliminary experiments polyethylene (**PE**) vials/vessels and tubing were used for construction of kits for HF transfer. Later we found polypropylene (**PP**) vials and tubing could be used with similar success. Our final variant of setup was however performed from Teflon

(PTFE) and perfluoroalkoxy polymer (PFA). This setup showed robustness and excellent HF transfer (up to 95% in 15-30 min). Argon was more efficient for HF-transfer than helium.

In our experiments H^{18}F was generated by adding ^{18}O -enriched cyclotron-irradiated water to 98-99% sulfuric acid followed by ultra sound irradiation at 80-85 °C. The flow of argon carried the liberated hydrogen fluoride to a trapping vial charged with a solution of organic base.

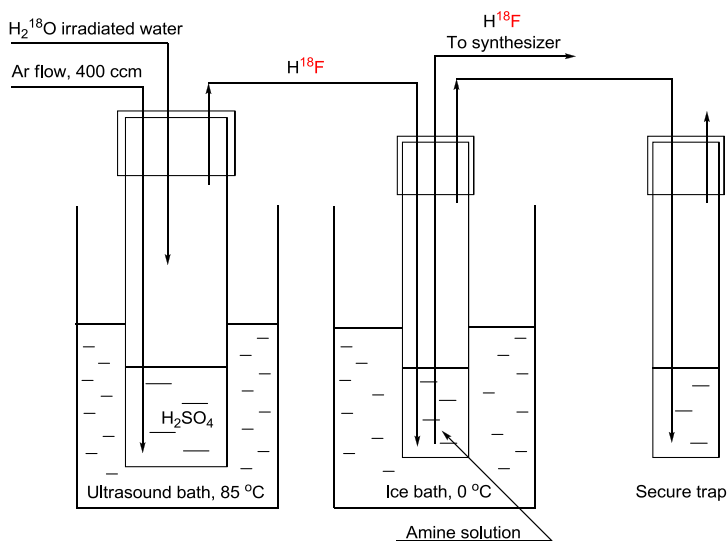
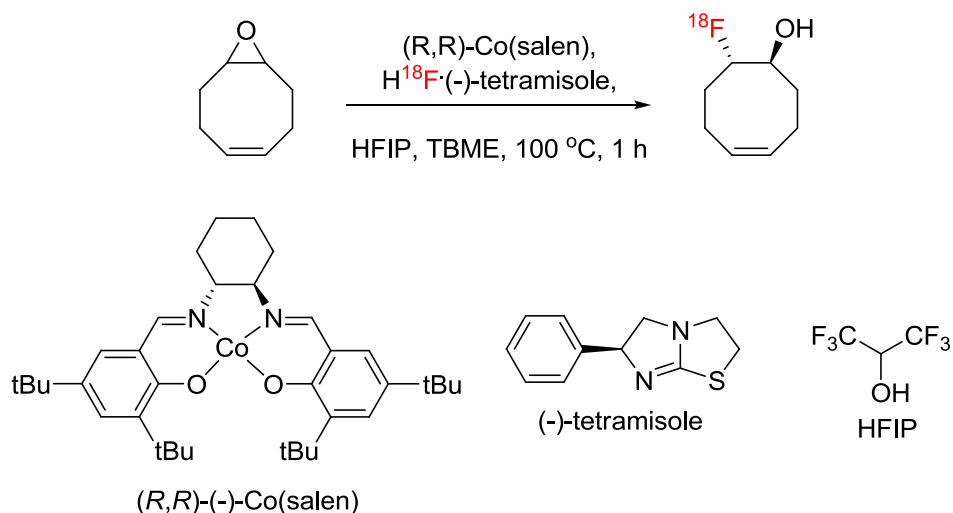


Figure 18. Scheme of ^{18}F HF generator.

After this step regular glassware and reaction vessels could be used for further reactions. Importantly, ^{18}F HF generator was integrated into remotely controlled robot, used later to produce ^{18}F FMISO from 60-70 GBq of cyclotron produced ^{18}F . With ^{18}F HF in hand we were ready for further studies.

2.2.2 Preliminary studies

In our preliminary experiment, ^{18}F HF (-)tetramisole (prepared as described above), was reacted with 9-oxabicyclo[6.1.0]non-4-ene in the presence of chiral (*R,R*)-Co(salen) and hexafluoroisopropanol (HFIP) in tert-butyl methyl ether (TBME):



Scheme 24. ^{18}F -hydrofluorination of 9-oxabicyclo[6.1.0]non-4-ene using [^{18}F]HF/(-)-tetramisol and (R,R)-Co(salen).

After 1 h at 100 °C radio-TLC analysis showed that the corresponding ^{18}F -fluorohydrin was obtained in 78% radiochemical conversion (RCC). The enantioselectivity was only 32%, as measured by the normal phase chiral radio-HPLC performed on a Chiralpak AD-3 column.

As expected, lowering the reaction temperature led to an increase in enantioselectivity and dropping of RCC. No reaction was observed at room temperature (Table 7).

Entry	^{18}F -fluorohydrine	t, °C	RCC, %	ee, %
1	8-fluorocyclooct-4-enol	100	78	33
2	8-fluorocyclooct-4-enol	75	25	48
3	8-fluorocyclooct-4-enol	50	5	-
4	8-fluorocyclooct-4-enol	25	0	-

Table 7.

The mismatched Lewis acid enantiomer (S,S)-Co(salen) under the same conditions gave the enfluorohydrine in only 36% RCY and 27% ee (Table 8). It seems to be a cooperative effect in catalysis.

Entry	Catalyst	RCC, %	ee, %
1	(R,R)-Co(salen)	78	33
2	(S,S)-Co(salen)	36	27
3	phenylene-Co(salen)	55	0
4	(R,R)-Co(salen)OTs	0	-

Table 8.

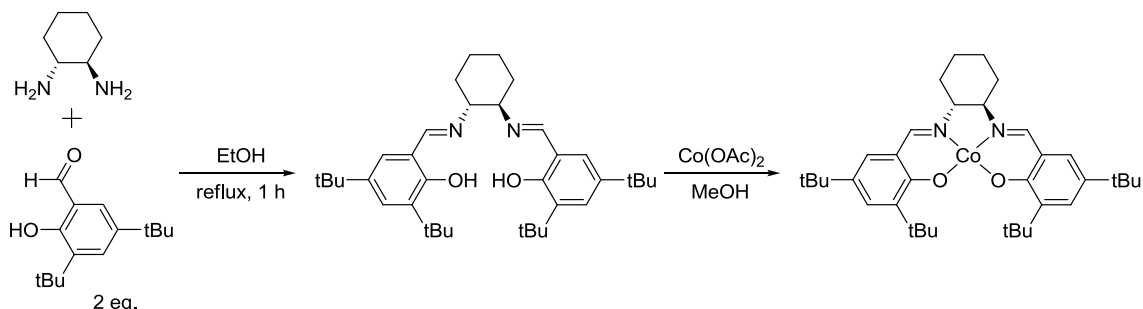
Non-chiral variant of phenylene-Co(salen) showed lower conversion compare to chiral (R,R)-Co(salen).

The pre-oxidized form of the catalyst like Co^{III} (salen)OTs was ineffective in the absence of HFIP.

Oxidation of Co(salen) with tBuOOH (similar system was described by Doyle et al) offered no radiofluorination as well.

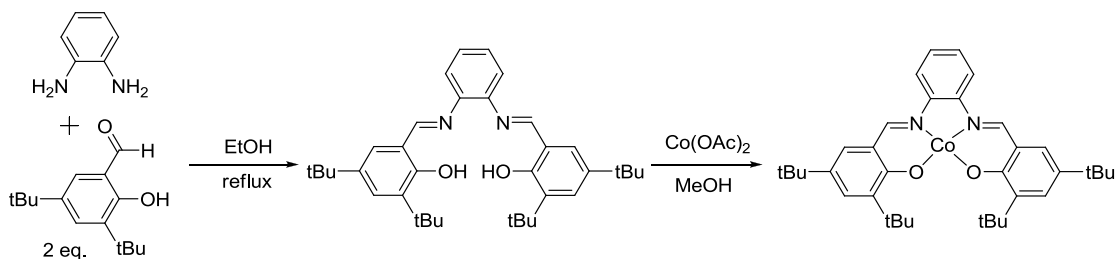
Synthesis of Co(salen) catalysts

We started our experiments with Co(salen) purchased from Strem Chemicals, but because we were not able to reproduce the yields of our experiments with commercially available Co(salen), we used Co(salen) that was synthesized according to the procedure described below. It seems like impurities of Co(OAc)₂ in the catalyst are most likely critical for the successful radiofluorination. We used a 5% excess of a chiral salen-ligand in our method instead of using excess of Co^{II}. The whole synthesis was performed as a one pot procedure (Scheme 25).



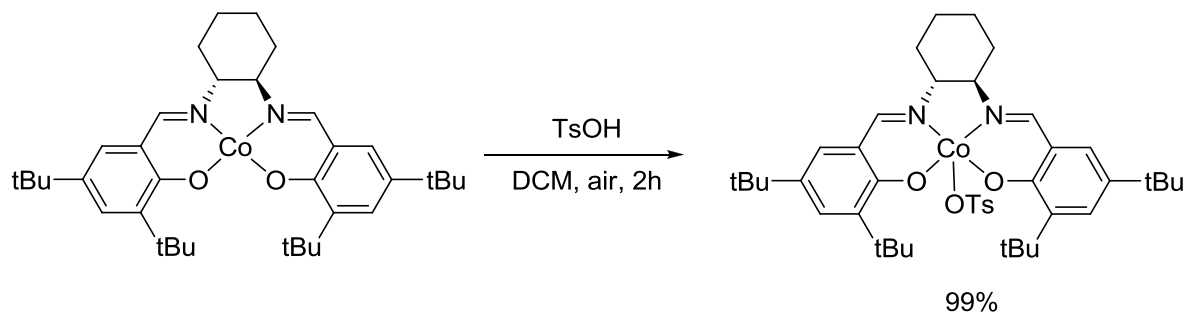
Scheme 25.

Non-chiral Co(salen) made from 1,2-phenylenediamine instead of chiral 1,2-cyclohexanediamine was synthesized by the same route (Scheme 26):



Scheme 26.

Co^{III}(salen)OTs was synthesized from the corresponding Co^{II}(salen) precursor according to the described procedure¹⁰⁷ (Scheme 27):



Scheme 27.

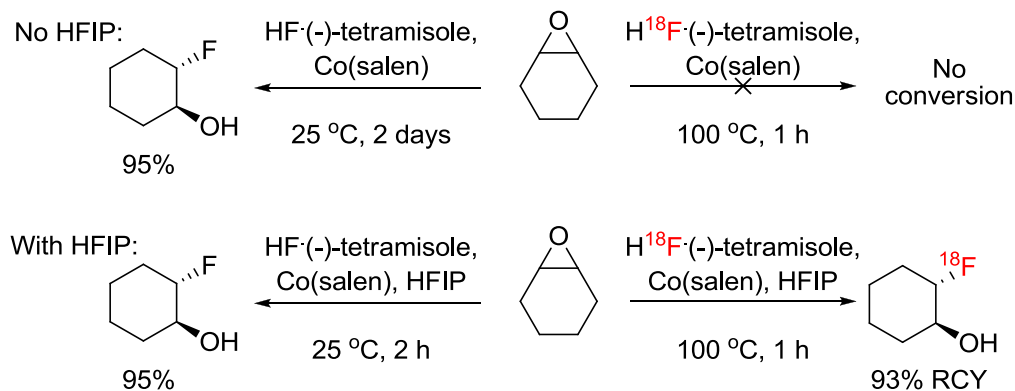
2.2.3 Screening of alcohol additives

We found that HFIP, used in the earlier work to facilitate the release of HF from benzoyl fluoride, was essential for successful radiofluorination. A control experiment where [^{18}F]HF was introduced into the reaction mixture without HFIP yielded no ^{18}F -fluorohydrin. Different alcohols were tried instead of HFIP. These alcohol additives, varying in acidity and steric bulk, were noticeably less effective than HFIP. While the role of hydroxylic additives is unclear at the moment, there seemed to be a pronounced “fluorous” effect, as the RCC increased when the fluorinated analogs were used (Table 9, entries 2 and 3, 4 and 5, 6 and 7). To prove the absence of carrier effect (due to possible traces of cold fluoride in HFIP), HFIP was purified by a sequential passing through basic alumina and silica, followed by vacuum distillation. This purification had no discernible effect on either the RCY or the specific activity of the product. The pKa of the protic additives did not seem to play a major role in the “fluorous” effect as phenol (pKa = 10) remained inferior to HFIP (pKa = 9.3).

Entry	R-OH	pKa	RCY, %
1	None		< 1
2	HFIP	9.3	78
3	iPrOH	16.5	3
4	tBuOH	17.0	5
5	(CF ₃) ₃ COH	5.2	26
6	PhOH	9.9	5
7	C ₆ F ₅ OH	5.5	16

Table 9.

The effect of HFIP was also prominent under the “cold” fluorination conditions. The freshly prepared cold HF (-)-tetramisole used in combination with Co(salen) gave the desired fluorocyclohexanol in 95% yield within 2 h. Without HFIP the reaction took two days to reach the same level of conversion. Based on these observations we believe that HFIP kinetically facilitates hydrofluorination by acting on one or more catalytic Co(salen) species.



Scheme 28.

2.2.4 Screening of bases and solvents

A few nitrogen bases were tested, but only (-)-tetramisol was effective. Other bases, such as DBU, DBN, Et₃N and pyridine, showed no conversion of [¹⁸F]F⁻ at all. The strong cooperative effect of Co(salen)/base on RCY and enantioselectivity was observed earlier^{101,97}. We have also confirmed that for radiofluorination. The mismatched enantiomer ent-(S,S)-2 gave the product in only 36% RCC and 27% ee.

Entry	Solvent	RCC, %	ee, %
1	CH ₃ CN, DMF, DMSO	<1	
2	THF, EtOH, (H ₃ C) ₂ CO	<1	
3	TBME	78	32
4	tAmOH	50	68

Table 10.

Aprotic solvents are usually preferred for this kind of reactions, because nucleophilicity and reactivity are severely inhibited by the influence of the hydrogen bonds of protic solvents. Other solvents used for Sn2 fluorination/radiofluorination like acetonitrile, DMF, DMSO resulted in no radiofluorinated products at all. THF, EtOH and acetone showed no conversion either.

On the other hand, our experimental systems with TBME showed high conversion of radioactive fluoride. Changing the solvent from TBME to tAmOH resulted in lower yield but higher enantioselectivity. A remarkable effect of using tertiary alcohols as a reaction medium for nucleophilic substitution was described previously for the fluorination and radiofluorination with alkali metal fluorides¹⁰⁸. Hindered protic solvents like tert-butanol and tert-amyl alcohol are more promising compared to the aprotic solvents. tBuOH could not be used in our experiments as a solvent (but was tried as an additive showing 5% RCC) because of the high melting point (25 °C) – and thus it was not possible to trap gaseous H¹⁸F at low temperatures. But tAmOH with a low melting point at -9 °C and a high boiling point of 101-103 °C seems to be an excellent solvent for our reaction. Almost no loss of alcohol was observed during the transfer of H¹⁸F.

2.2.5 Screening of substrates

The substrate scope of ¹⁸F-hydrofluorination was investigated by reacting a substrate with a mixture of [¹⁸F](-)-tetramisole hydrofluoride, (R,R)-Co(salen), and HFIP in TBME at 100 °C (Table 11). The RCYs for desymmetrization of the meso epoxides were uniformly high. However, the enantioselectivities were only moderate-to-low, most likely due to the high reaction temperatures required for opening of cyclic epoxides. This was consistent with the moderate 52% ee obtained after applying the cold protocol to cyclopentane oxide. Surprisingly, terminal polycyclic aromatic epoxides proved to be challenging substrates. The 1-naphthalenyloxirane was unreactive, and 9- anthryloxirane gave unidentified products. Our attempt to make “cold” fluorohydrine from these substrates also failed as no signals of desired

products were observed (^{19}F and ^1H NMR spectroscopy) (Table 11, entries 4 and 5). It looks like epoxides undergo polymerization as all NMR-signals were broadened.



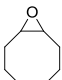
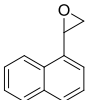
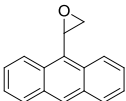
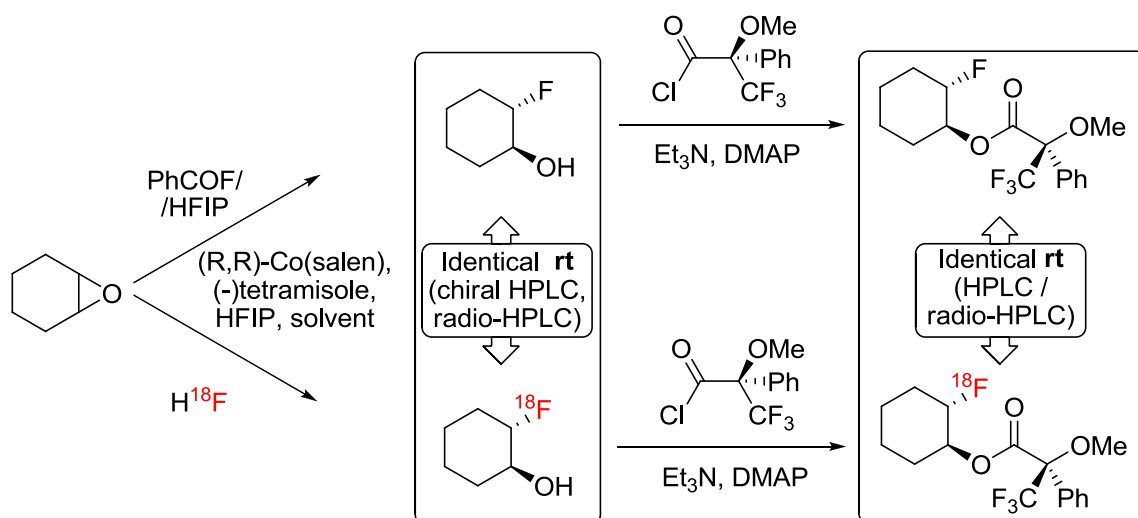
Entry	Epoxide	RCY, %	ee, %
1		73	20
2		93	45
3		78	33
4		<1	-
5		<1	-

Table 11.

2.2.6 Stereochemistry studies

An important question concerns the absolute configuration of radiofluorinated products. Due to nanomolar amounts of ^{18}F , this can lead to different stoichiometry and mechanism. Because of nanomolar concentrations of ^{18}F -fluorohydrines, any approaches to the direct determination of the absolute stereochemistry of radiolabeled substrates are not usable. An indirect method, based on comparison of chromatography parameters (R_f for thin layer chromatography and retention time t_r for HPLC methods) of ^{18}F -radiofluorohydrin derivatives with their ^{19}F -isotopomers, for which absolute configuration could be reliably established using classical methods, was applied. To determine the absolute configuration the following “hot” and “cold” experiments were made in parallel.

The (R,R)Co(salen)-mediated fluorination and radiofluorination of meso epoxides (cyclopentene oxide, cyclohexene oxide, cyclooctadiene oxide) yielded the corresponding isotopomeric fluorohydrins and ^{18}F -fluorohydrins. These had identical t_r values as measured by normal phase chiral HPLC/radioHPLC (Scheme 29). The reaction of “cold” and “hot” fluorohydrines with (*R*)-(-)- α -methoxy- α -(trifluoromethyl)phenylacetyl chloride was fast and complete within minutes giving the corresponding Mosher esters in high diastereoselectivity ($d_e > 95\%$).



Scheme 29.

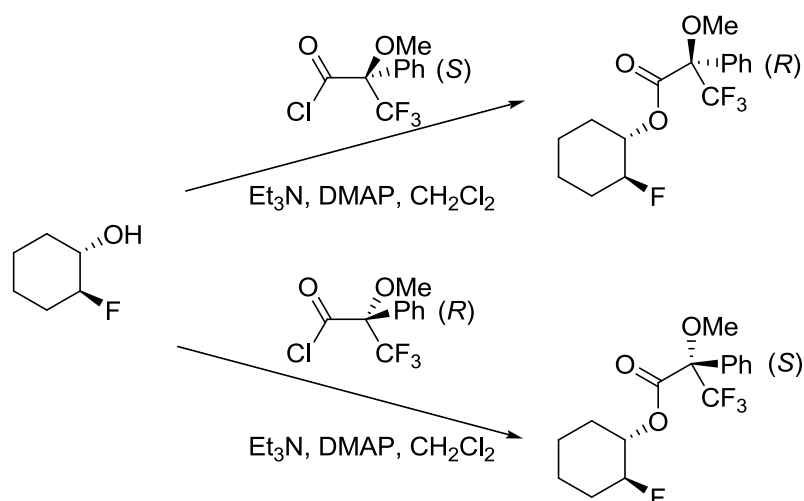
The “cold” diastereomers can be resolved by the standard reverse-phase HPLC. The Mosher derivatization of the corresponding “hot” fluorohydrins resulted in radio-HPLC-resolvable diastereomeric ^{18}F -isotopomers. “Cold” and “hot” Mosher esters had identical HPLC/radioHPLC retention times, thus establishing the same absolute configuration.

To determine the absolute configuration we performed Mosher ester and enzymatic resolution studies.

2.2.6.1 NMR Mosher esters experiments

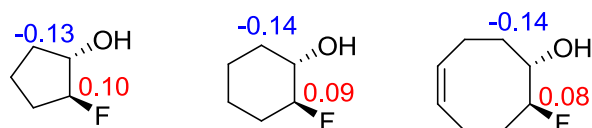
The absolute stereochemistry of 8-fluorocyclooct-4-enol, 2-fluorocyclohexanol and 2-fluorocyclopentanol was assigned using NMR spectroscopy methods via derivatization of fluorohydrines with two enantiomers of α -methoxy- α -trifluoromethylphenylacetyl chloride (MTPACl).

The esters of these fluorohydrines were prepared according to the described method^{109,110}.



Scheme 30.

The difference in shifts from ^{13}C and ^{19}F NMR spectra was insignificant. ^1H NMR method in combination with 2D ^1H - ^1H COSY and ^1H - ^{13}C HSQC was applied. Shifts of corresponding protons were distinguished and identified from ^1H NMR. When overlapping of signals was observed, the shifts were estimated from 2D NMR spectra.



Scheme 31.

Procedure of distinguishing and identifying of proton shifts:

- from HSCQ spectra -FCH- and =CHO- protons can be reliably assigned;
- from COSY spectra coupling between =CHO- proton and neighboring $\text{-CH}_2\text{-}$ can be found.

For both fluorohydrins the $\Delta\delta^{\text{SR}}$ values are clearly positive or negative.

Entry	Fluorohydrine	Proton	$\Delta\delta^{\text{SR}}$	Carbon configuration
1	2-fluorocyclopentanol	-FCH-	5.06-4.96 = 0.10 (pos.)	S
		$\text{-CH}_2\text{-HCO-}$	2.18-2.21 = -0.03 (neg.) 1.63-1.79 = -0.13 (neg.)	
2	2-fluorocyclohexanol	-FCH-	4.48-4.39=0.09 (pos.)	S
		$\text{-CH}_2\text{-HCO-}$	1.34-1.48= - 0.14 (neg.)	
3	8-fluorocyclooct-4-enol	-FCH-	4.78-4.70=0.08 (pos.)	S
		$\text{-CH}_2\text{-HCO-}$	2.10-2.17= - 0.07 (neg.) 1.72-1.86= - 0.14 (neg.)	

Table 12. Determination of absolute stereochemistry by ^1H NMR using Mosher esters.

^1H NMR of Mosher ester from 2-fluorocyclohexanol was also modeled^{*}. The computational model was in agreement with our experiment.

The conformational search on the Mosher ester structures was performed using MM2 force field. The top scoring poses were optimized at B3LYP/6-31G^{*} level as implemented in Jaguar 8.1. All structures were verified to be minima on the potential energy surfaces by vibrational analyses. The NMR shielding were calculated using DFT calculations with GIAO method at BLYP/cc-VTZ level using Gaussian 09 suite of programs.

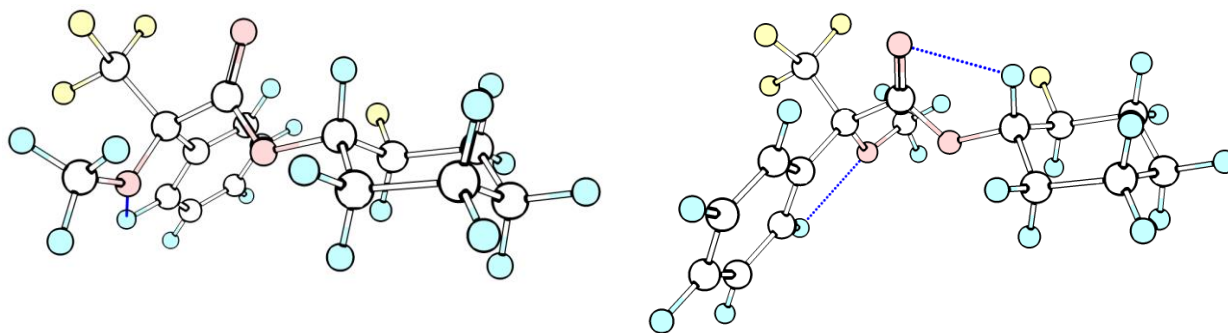


Figure 19. Models of *R* and *S* Mosher esters of (*S,S*)-2-fluorocyclohexanol.

Proton	$\Delta\delta^{\text{SR}}$	$\Delta\delta^{\text{SR}}$	Carbon configuration
	experimental	theoretical	
-FCH-	4.48-4.39=0.09 (pos.)	0.36 (pos.)	<i>S</i>
-CH ₂ -HCO-	1.34-1.48= - 0.14 (neg.)	-0.29 (neg.) -0.27 (neg.)	<i>S</i>

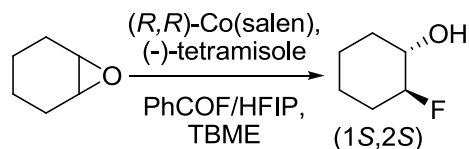
Table 13. Experimental and theoretical values of ^1H shifts for 2-fluorocyclohexanol Mosher esters.

^{*}The computational model was made by F. Zhuravlev

2.2.6.2 Lipase-catalyzed deracemization of 2-fluorocyclohexyl acetate

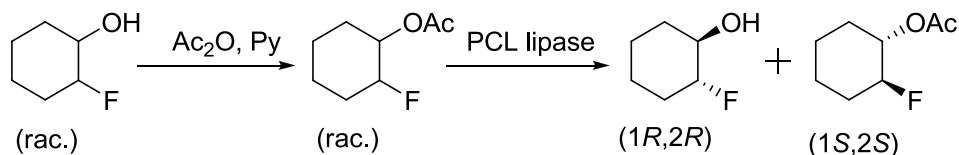
In addition to Mosher esters studies we performed enzymatic deracemization to prove independently the formation of (*S,S*)-stereoisomer of 2-fluorocyclohexanol from the reaction of *meso*-epoxide with (*R,R*)-Co(salen).¹¹¹

Enantiomerically enriched 2-fluorocyclohexanol was synthesized from *meso*-cyclohexene oxide according to the procedure described by Doyle¹⁰¹, applying (*R,R*)-Co(salen) as a chiral catalyst and (-)-tetramisole as a chiral base.



Scheme 32.

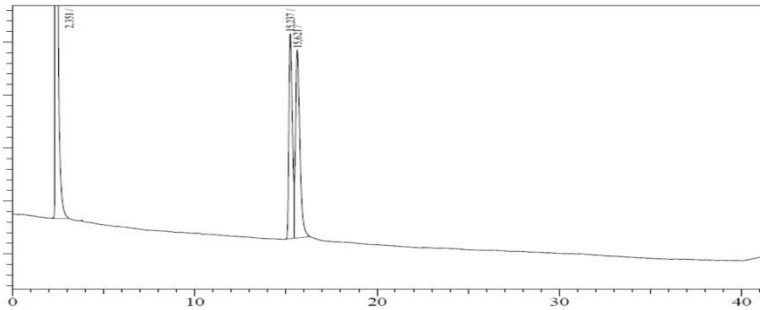
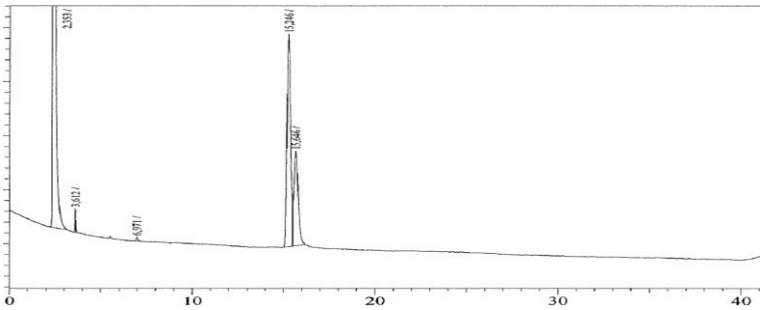
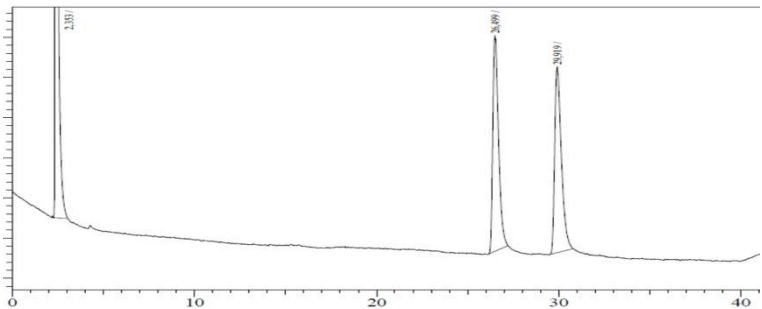
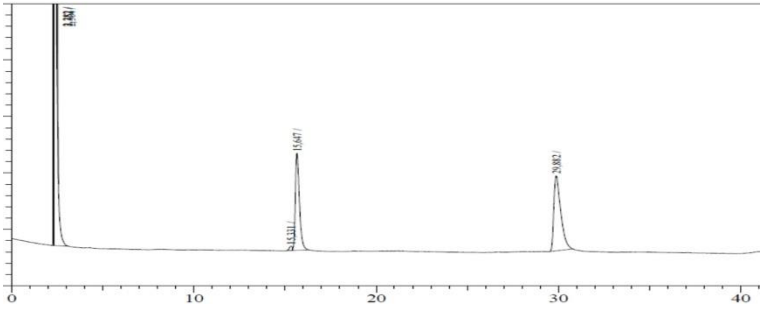
Racemic 2-fluorocyclohexyl acetate was prepared via acylation of corresponding fluorohydrine with acetic anhydride in pyridine. This ester was then involved into the reaction with PCL lipase¹¹¹ (water, phosphate buffer), providing us with material for GC analysis (chiral cyclodex-B column (30 m × 0.25 mm) was used).



Scheme 33.

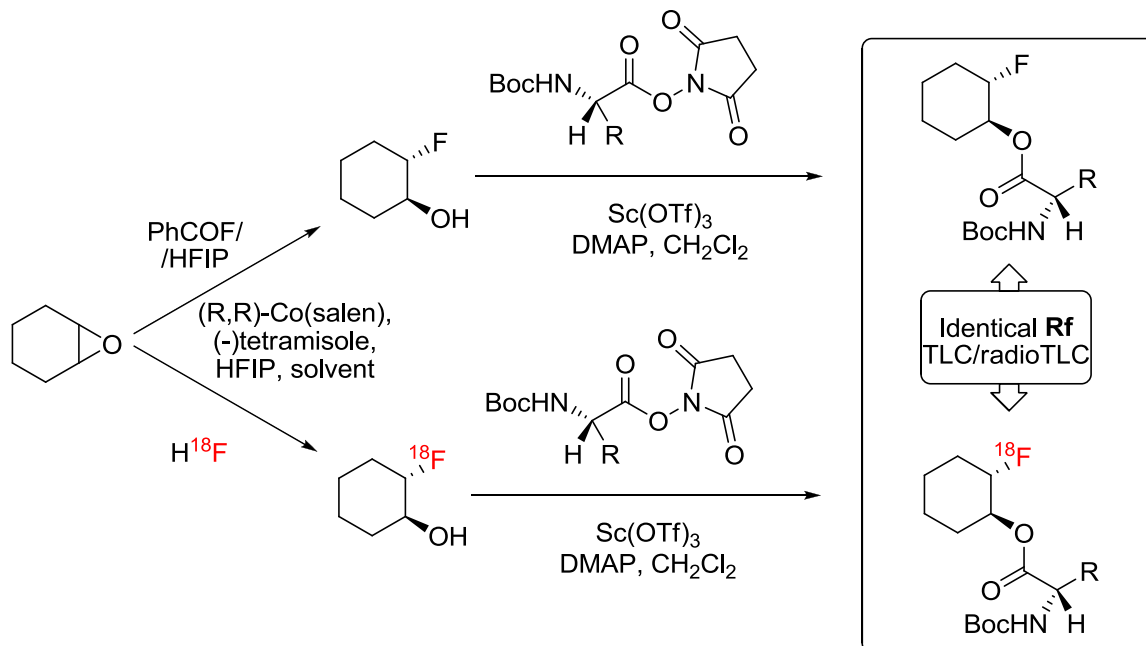
The GC traces of the two enantiomerically enriched samples were compared. From the fact that enzymatic hydrolysis of racemic acetate forms (*R,R*)-fluorohydrine while keeping (*S,S*)-acetate unreacted, the stereochemistry of (*R,R*)-Co(salen) catalyzed reaction was shown to be (*S,S*).

Table 14. Chiral GC traces from lipase-catalyzed deracemization of 2-fluorocyclohexyl acetate (conditions: cyclodex-B column (30 m x 0.25 mm), 80 °C, isotherm (40 min), FID detector).

Entry	Chiral GC trace	Description
1		Racemic 2-fluorocyclohexanol (0% ee)
2		(<i>S,S</i>)-2-fluorocyclohexanol (32% ee)
3		Racemic 2-fluorocyclohexyl acetate (0% ee)
4		Racemic 2-fluorocyclohexyl acetate after lipase: (<i>R,R</i>)-2-fluorocyclohexanol (94% ee) (<i>S,S</i>)-2-fluorocyclohexyl acetate (99% ee)

2.2.6.3 Resolution of fluorohydrines with chiral amino acids derivatives

With no access to chiral HPLC and GC at the beginning of our study, we have developed radio-TLC based methodology for resolution of enantiomeric fluorohydrines.



Scheme 34.

Fluorohydrins were derivatized with hydroxysuccinimide esters of Boc-protected amino acids according to the procedure described below, based on the published methods^{112,113}. The enantiomeric resolution of fluorohydrins has been achieved using C18-silica TLC plates (Analtech). These plates showed the best separation compared to the others. Chiral silica and normal silica plates were tried but showed lower separation than C18-plates or no separation. Sometimes decomposition of products of acylation was observed on normal and chiral silica. For these reasons experiments were made mostly with C18-silica. When the separation of enantiomers was poor, long plates (up to 190 mm) were used.

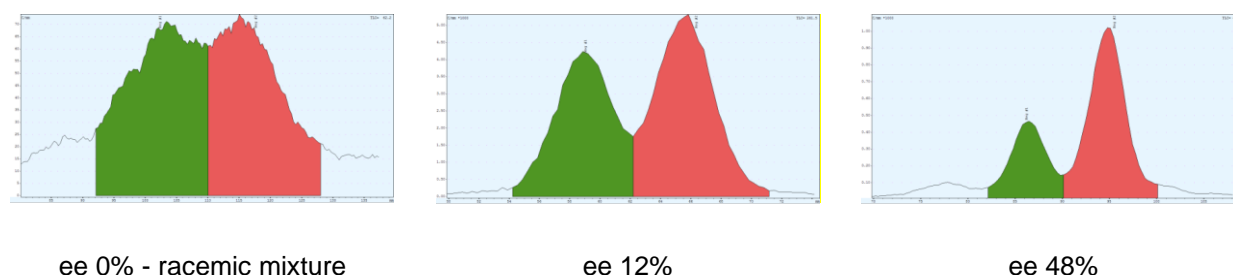


Figure 20. Radio TLC traces of the derivatives fluorohydrines.

It is important to make the starting spot not too large, since a larger spot makes it harder to see the diastereomers separation after running the plate. Various developing solvents can be used to develop the

plate. The completed TLC plates were then analyzed under UV lamp (cold standards) and radioTLC scanner (Table 15). Various developing components (e.g. solvent, TLC plate, amino acid derivative) can be used to define the optimal separation:

Entry	Fluorohydrine	Amino acid derivative	TLC plate	Solvent (v/v)	R _{F1}	R _{F2}	R _{F2} /R _{F1}
1	8-fluorocyclooct-4-enol	Boc-Ala-OSu	normal	40/60 EtOAc/Hept	0.60	0.66	1.10
2	8-fluorocyclooct-4-enol	Boc-Ala-OSu	chiral	40/60 EtOAc/Hept	0.70	0.72	1.03
3	8-fluorocyclooct-4-enol	Boc-Ala-OSu	C18	40/60 EtOAc/Hept	0.79	0.85	1.08
4	8-fluorocyclooct-4-enol	Boc-Ala-OSu	C18	20/80 EtOAc/Hept	0.53	0.60	1.13
5	8-fluorocyclooct-4-enol	Boc-Phe-OSu	normal	20/80 EtOAc/Hept	0.37	0.39	1.06
6	8-fluorocyclooct-4-enol	Boc-Phe-OSu	C18	20/80 EtOAc/Hept	0.50	0.55	1.09
7	2-fluorocyclohexanol	Boc-Ala-OSu	C18	10/1 Tol/EtOAc	0.569	0.639	1.12
8	2-fluorocyclopentanol	Boc-Ala-OSu	norm., C18 and chiral	10/1 Tol/EtOAc	no separation		
9	2-fluorocyclopentanol	Boc-Phe-OSu					
10	2-fluorocyclopentanol	Boc-Pro-OSu	C18	5/1 Tol/EtOAc	0.52	0.55	1.07
11	2-fluorocyclopentanol	Boc-Ala-OSu,	norm., C18 and chiral	Tol/EtOAc, CHCl ₃ /CH ₃ CN	no separation		
12	FMISO	Boc-Phe-OSu					
13	FMISO	Boc-Val-OSu	C18	1/1 Tol/EtOAc	0.41	0.46	1.12
14	FMISO	Boc-Val-OSu	C18	5/1 Tol/EtOAc	0.28	0.33	1.17

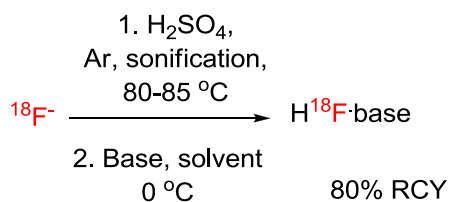
Table 15. R_F values for enantiomers, ratio of the R_F values, solvent and type of silica TLC plates.

2.3 Experimental part

¹⁸F-Fluoride radiochemistry

The aqueous solutions of ¹⁸F-fluoride were prepared by the ¹⁸O(p,n)¹⁸F reaction in a GE PET-trace cyclotron using a 1.8-mL target of 95% enriched ¹⁸O-water irradiated by a 14.1-MeV beam at 20–25mA for 60–90 min. The transfer was run in an ultrasound bath Sonorex DT52H, operating at 240 W / 35 kHz at 80 °C (Ar flow 200-400 cm³/min). The kit for transfer was constructed using PE, PP or PFA reaction vials and PTFE tubing (ID=3.0 mm).

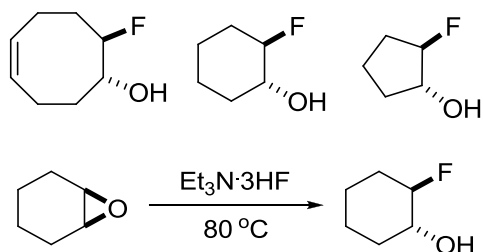
[¹⁸F]HF-Transfer procedure



Scheme35.

First vial of the kit was charged with 5 or 10 mL of conc. H₂SO₄. The second vial was charged with a solution of base ((-)-tetramisole, DBU, DBN, TREAT HF) in 3 or 5 mL of solvent (TBME or ¹AmOH) and cooled down to 0 °C (ice bath) A portion of irradiated ¹⁸O-water or target wash was injected into the first vial, followed by blowing with argon (350-400 mL/min), heating (80-85 °C) and ultrasound irradiation at 35kHz (Sonorex DT52H) for 15 to 30 min. Thereafter the second vial was disconnected from the kit and the activity of the produced solution was measured (80% RCY). An additional quantity of solvent was added. This solution of base/H¹⁸F was used for further experiments.

Reference racemic fluorohydrines synthesis

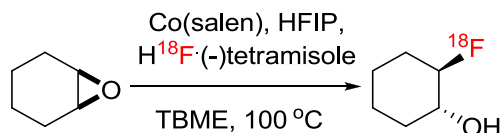


Scheme 36.

A glass ampule was charged with an epoxide (18.4 mmol, 1.0 eq.) and TREAT HF (3.0 mL, 18.4 mmol, 1.0 eq.), sealed and heated overnight at 80 °C. The resulting reaction mixture was crashed with a mixture of ice (10 g) and ammonia hydroxide solution (30%, 10 mL), then washed with Et₂O (3x20 mL). The organic phase was washed with an aqueous solution of HCl (1N, 10 mL) and dried over Na₂SO₄. The

solvent was removed in vacuo. Oil residues were passed through a short SiO₂ column (EtOAc/Hexane, 1/5 to 1/1), which usually gave 80-90% of fluorohydrine as a single product.

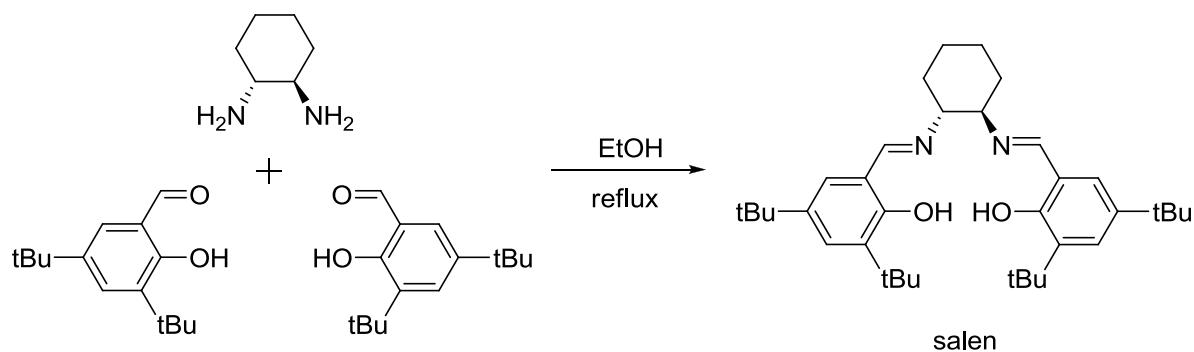
General procedure for radiofluorination of the epoxides



Scheme 37.

An oven-dried high pressure glass tube equipped with a stir bar was charged with Co(salen) (12.0 mg, 0.020 mmol) and HFIP (112 μ L, 0.80 mmol). The resulting slurry was then stirred for 5 min under air; an epoxide (0.20 mmol) was added neat followed by the solution of [¹⁸F]HF/(-)-tetramisole (4.1 mg, 0.020 mmol) in TBME (3 mL). The reaction mixture was then heated at 100 °C for 1 h. The reaction conversion was monitored by radio-TLC. No loss of activity due to volatilization was observed.

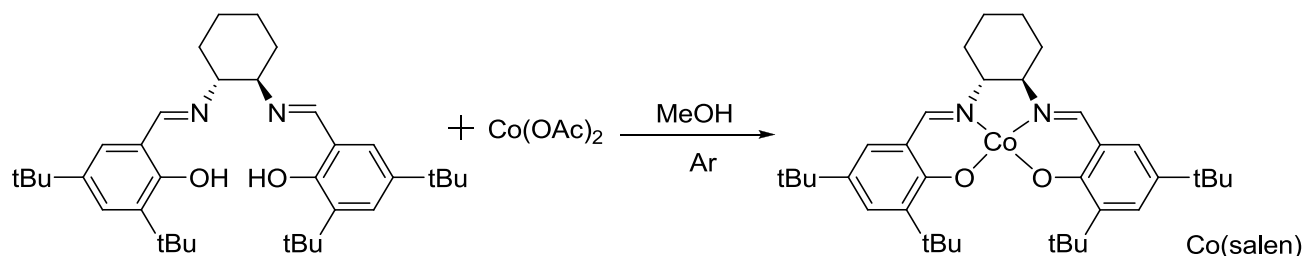
(Salen)-ligand



Scheme 38.

3,5-Di-tert-butyl-2-hydroxybenzaldehyde (4.10 g, 17.5 mmol, 2.0 eq.) was dissolved in 70 mL of dry EtOH, then was mixed with a solution of (1R,2R)-cyclohexane-1,2-diamine (1.00 g, 8.75 mmol, 1.0 eq.) in 40 mL of EtOH. The mixture was diluted with additional EtOH (50 mL) and refluxed for 1 h under argon. The solvent was removed in vacuo; solids (4.60 g, 8.41 mmol, 96%) were dried in deep vacuo overnight. No impurities were observed. This compound was used for the next step without further purification.

(1R,2R)-(-)-1,2-Cyclohexanediamino-N,N'-bis(3,5-di-*t*-butylsalicylidene)cobalt(II) (or Co(salen))

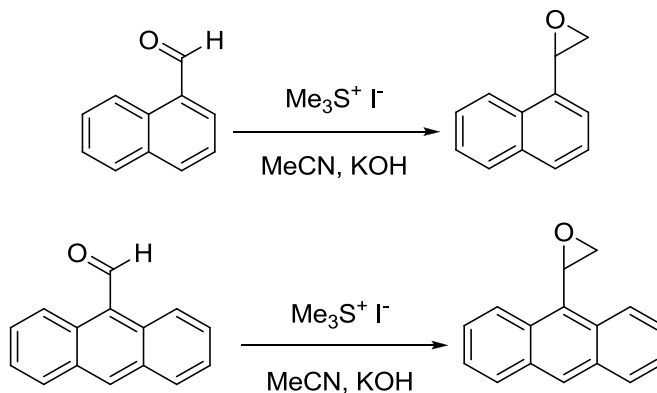


Scheme 39.

A solution of cobalt(II) acetate tetrahydrate ($\text{Co}(\text{OAc})_2 \cdot 4\text{H}_2\text{O}$) (1.94 g, 7.82 mmol, 1.0 eq.) was added via cannula to a solution of salen-ligand (4.50 g, 8.24 mmol, 1.05 eq., 5% excess) in CH_2Cl_2 (40 mL) at room temperature under argon. The mixture was stirred for 5 min, and then cooled to 0 °C. The red precipitate was filtered under argon, washed with cold MeOH (3x25 mL) and dried in vacuo (4.13 g, 6.84 mmol, 88%). This material was recrystallized from TBME under argon (thin dark red needles, m.p. > 400 °C), providing Co(salen)-catalyst for radiofluorination experiments.

2-(Naphthalen-1-yl)oxirane and 2-(anthracen-9-yl)oxirane

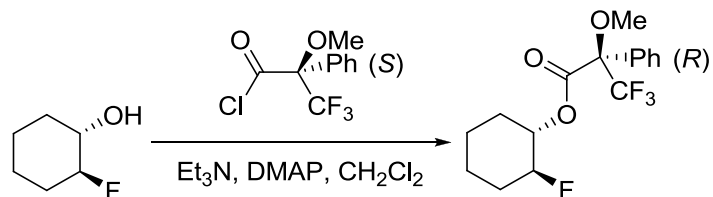
These two epoxides were synthesized via Corey–Chaykovsky reaction from the corresponding aromatic aldehydes and trimethylsulfonium iodide^{114,115}.



Scheme 40.

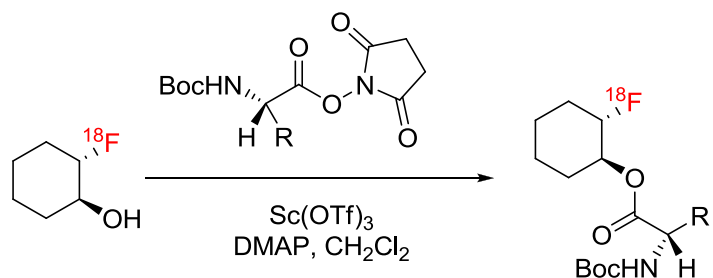
A suspension of aromatic aldehyde (13.8 mmol, 1.0 eq.), trimethylsulfonium iodide (3.47 g, 16.6 mmol, 1.2 eq.), KOH (1.55 g, 27.6 mmol, 2.0 eq.) and water (62 μl , 62.1 mg, 3.45 mmol, 0.25 eq.) in MeCN (50 mL) was stirred at 60 °C for 4 h. The suspension was cooled to rt and diluted with CH_2Cl_2 , filtered over celite and the solvent was removed in vacuo to give the product as a yellow solid.

Mosher esters procedure



Scheme 41.

A solution of DMAP (<0.1 mg, cat. amount), Et₃N (6.1 μ L, 0.0440 mmol, 10eq.) and fluorohydrin (0.0044 mmol, 1 eq.) in 0.5 mL of dry CH₂Cl₂ was prepared under argon and transferred into the NMR tubes. (*S*)-MTPACl (1.64 μ L, 0.0088 mmol, 2 eq.) was added. The NMR tubes were sealed and shaken vigorously for 15 min at room temperature. The solvent was frozen and removed in vacuo, CDCl₃ (0.6 ml) was added and the ampule was sealed under vacuo, providing a sample for NMR studies. The second sample with (*R*)-MTPACl was prepared in exactly the same way.

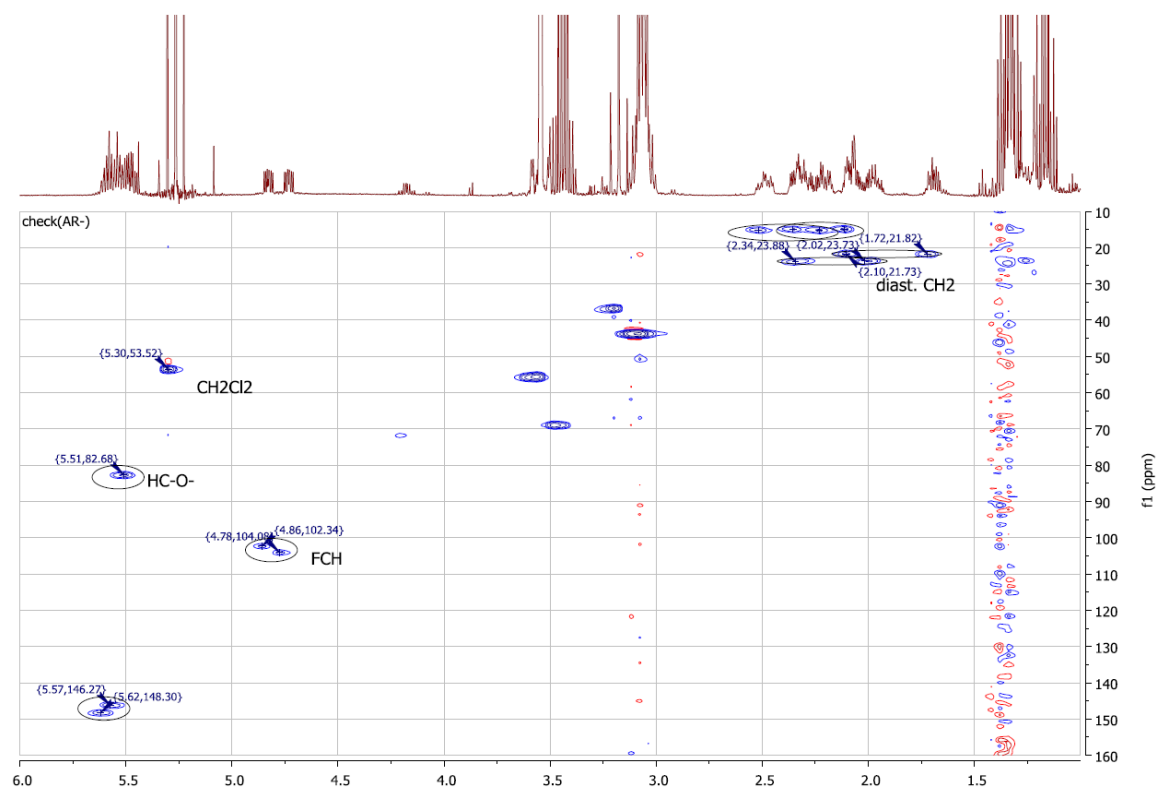


Scheme 42.

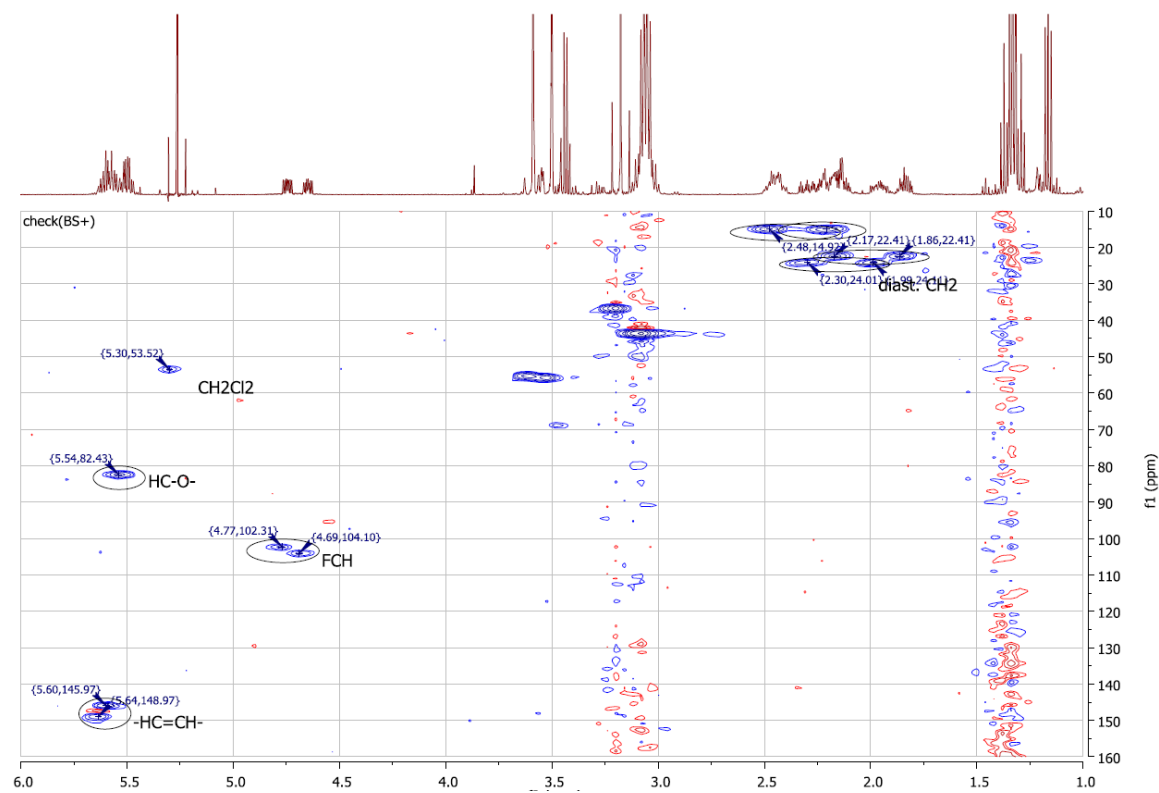
Acylation of ¹⁸F-fluorohydrins with hydroxysuccinimide esters of Boc-protected amino acids

1 mL of “hot” reaction mixture was placed into a vial (10 mL volume) and the solvent was evaporated with a flow of argon. 1 mL of CH₂Cl₂ was then added and blown again to remove the rests of the solvent. The resulting “hot” dry residues were dissolved in 1 mL of CH₂Cl₂. A second glass vial (4 mL vial with screwed top) was charged with Sc(OTf)₃ (1 eq., 0.04 mmol, 21 mg), DMAP (5 eq., 0.20 mmol, 26 mg) and 0.5 mL of CH₂Cl₂. This mixture was stirred for 5 min at rt. Thereafter “hot” solution from the first vial was added to the second. The resulting mixture was stirred for an additional 2 minutes at rt, followed by addition of Boc-Ala-OSu (5 eq., 0.21 mmol, 60 mg) in one portion. The mixture was stirred for 2 minutes, providing the diastereomeric material for radio-TLC.

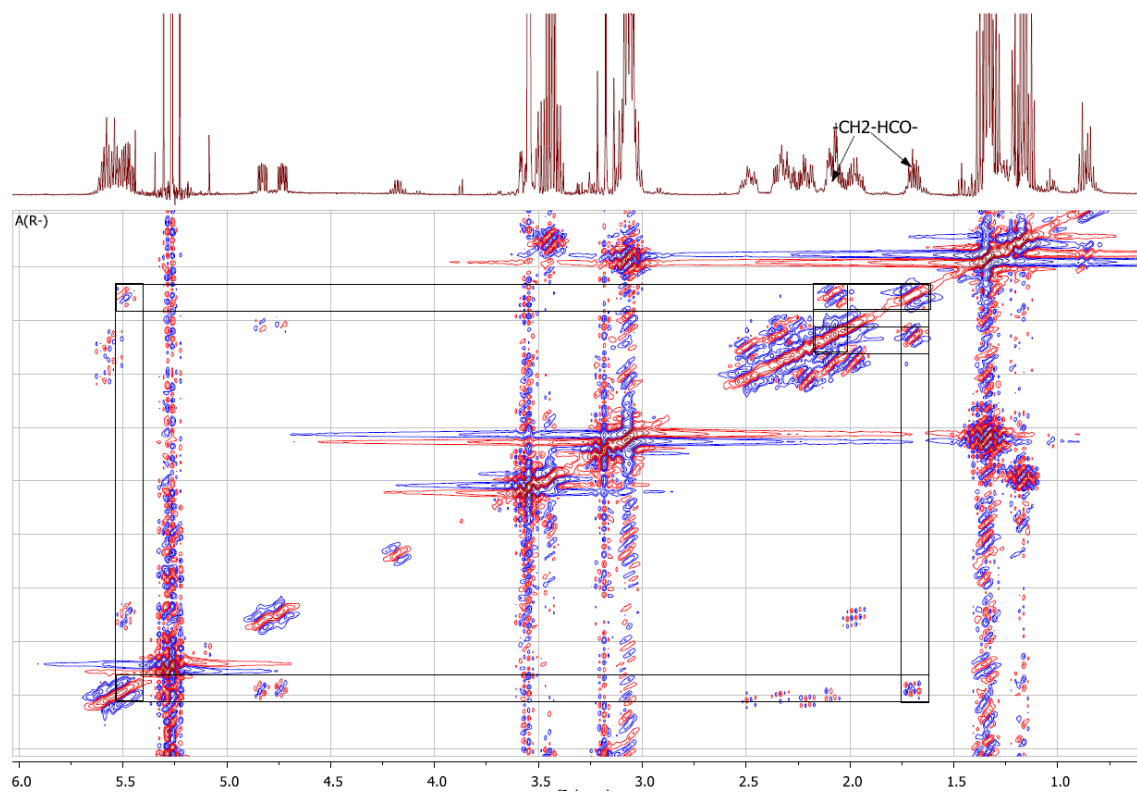
HSQC of (S)-MTPA ester of 8-fluorocyclooct-4-enol (from (R)-MTPACl)



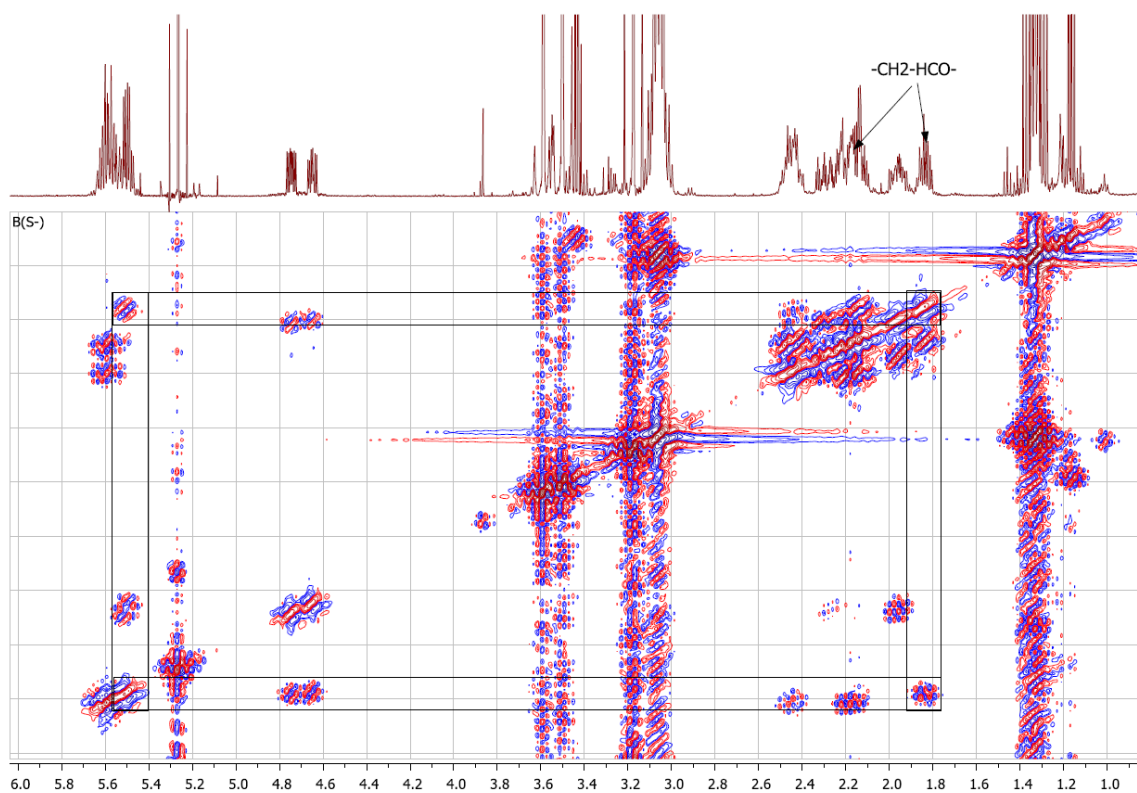
HSQC of (R)-MTPA ester of 8-fluorocyclooct-4-enol (from (S)-MTPACl)



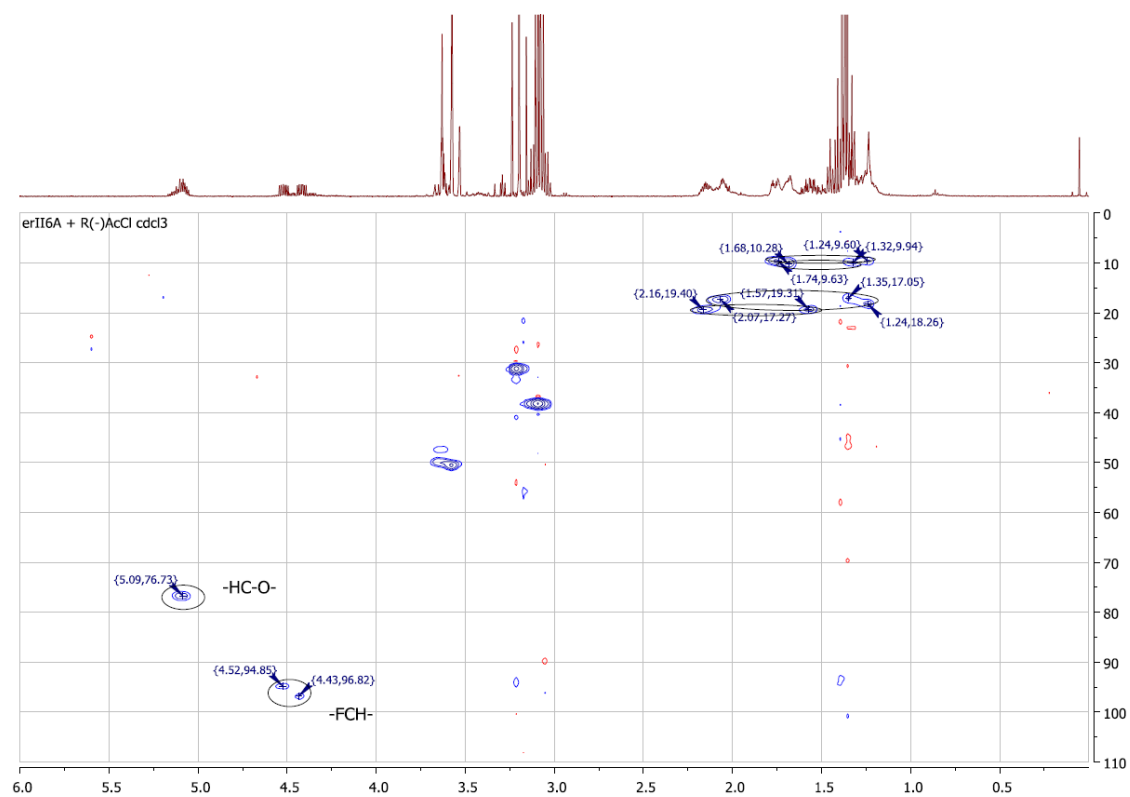
COSY of (*S*)-MTPA ester of 8-fluorocyclooct-4-enol (from (*R*)-MTPACl)



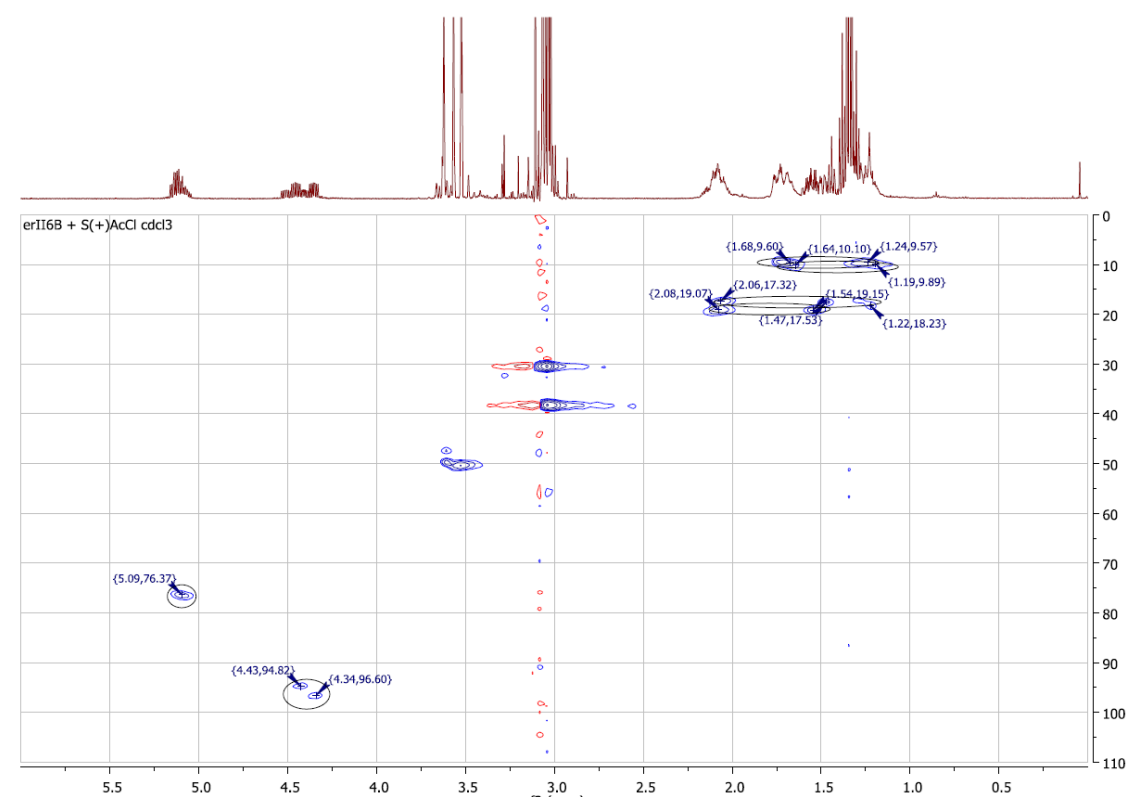
COSY of (*R*)-MTPA ester of 8-fluorocyclooct-4-enol (from (*S*)-MTPACl)



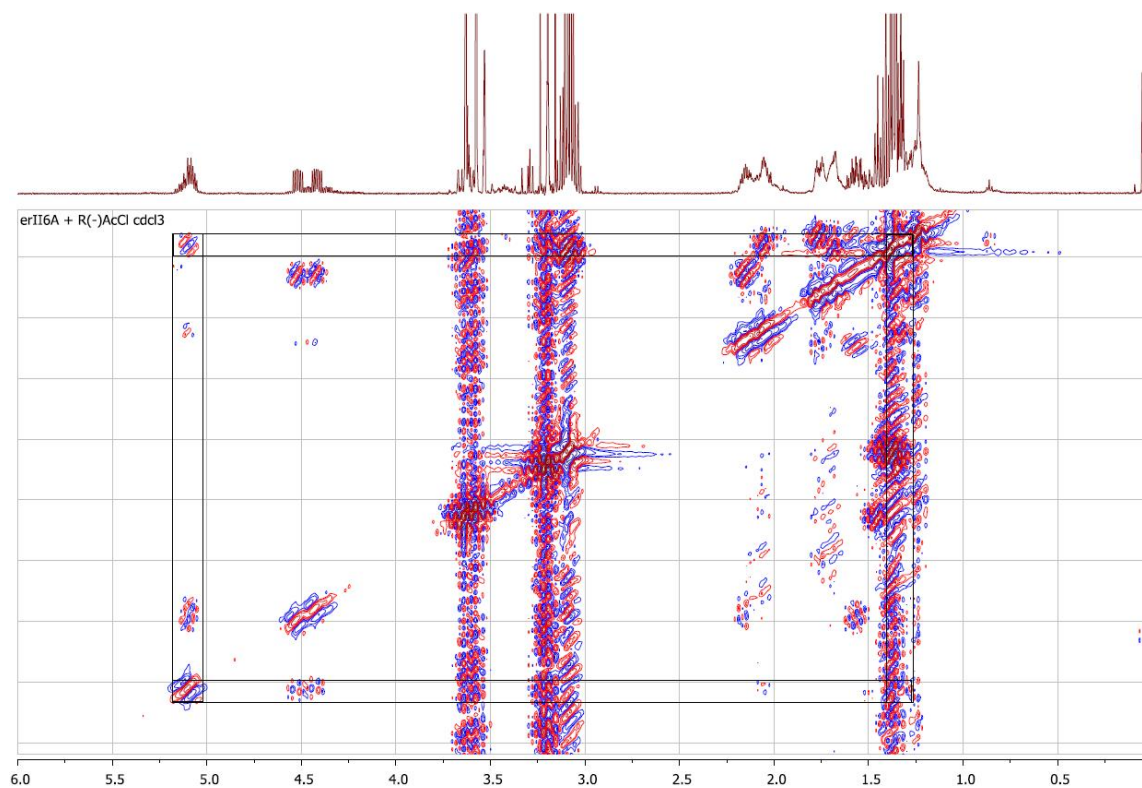
HSQC of (S)-MTPA ester of 2-fluorocyclohexanol (from (R)-MTPACI)



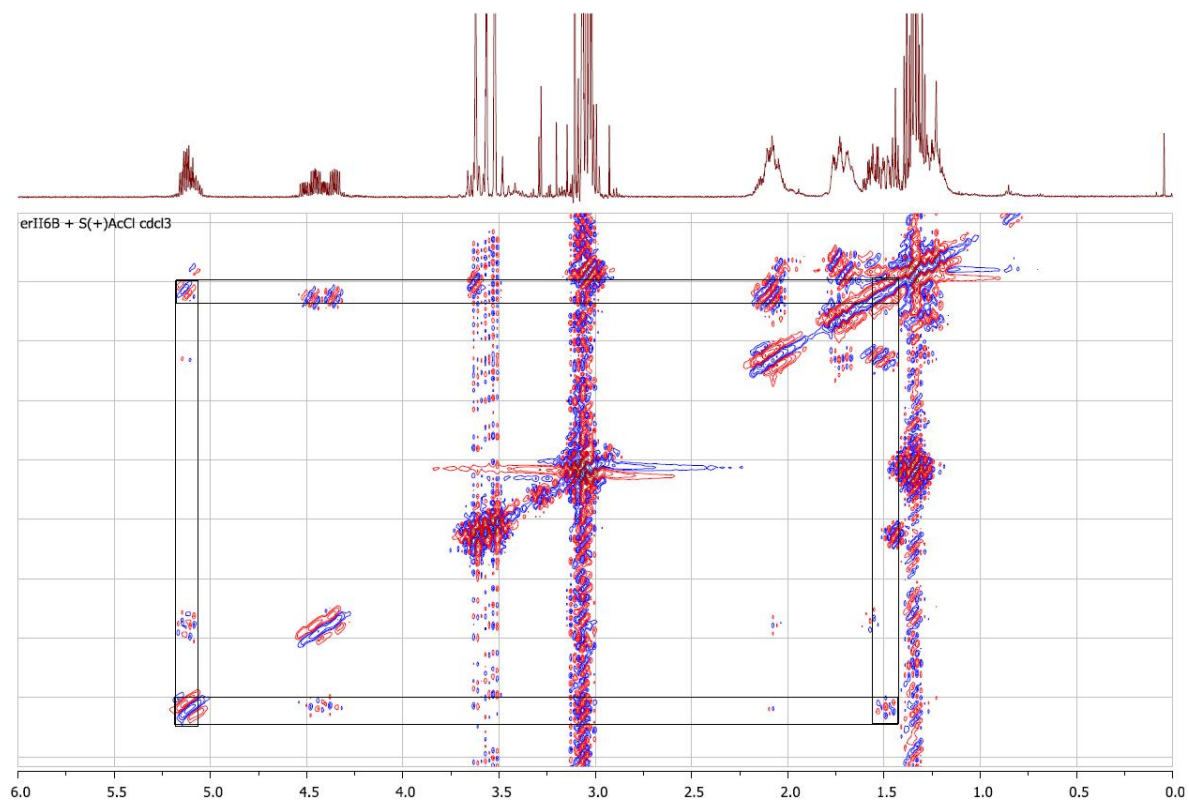
HSQC of (R)-MTPA ester of 2-fluorocyclohexanol (from (S)-MTPACI)



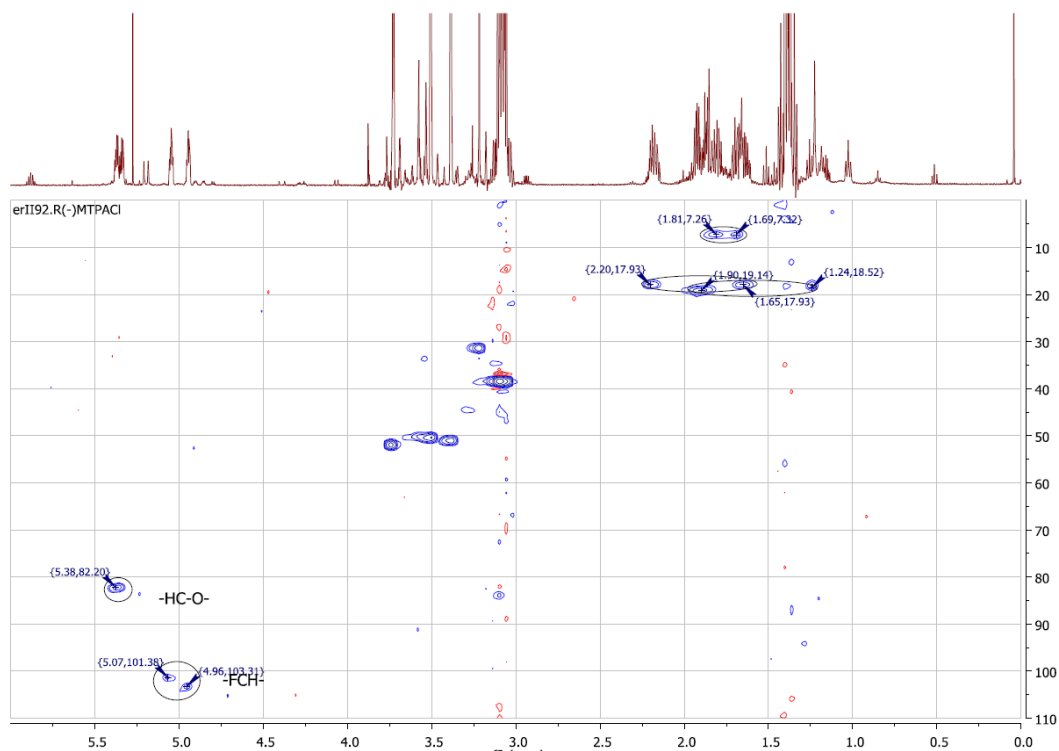
COSY of (S)-MTPA ester of 2-fluorocyclohexanol (from (R)-MTPACl)



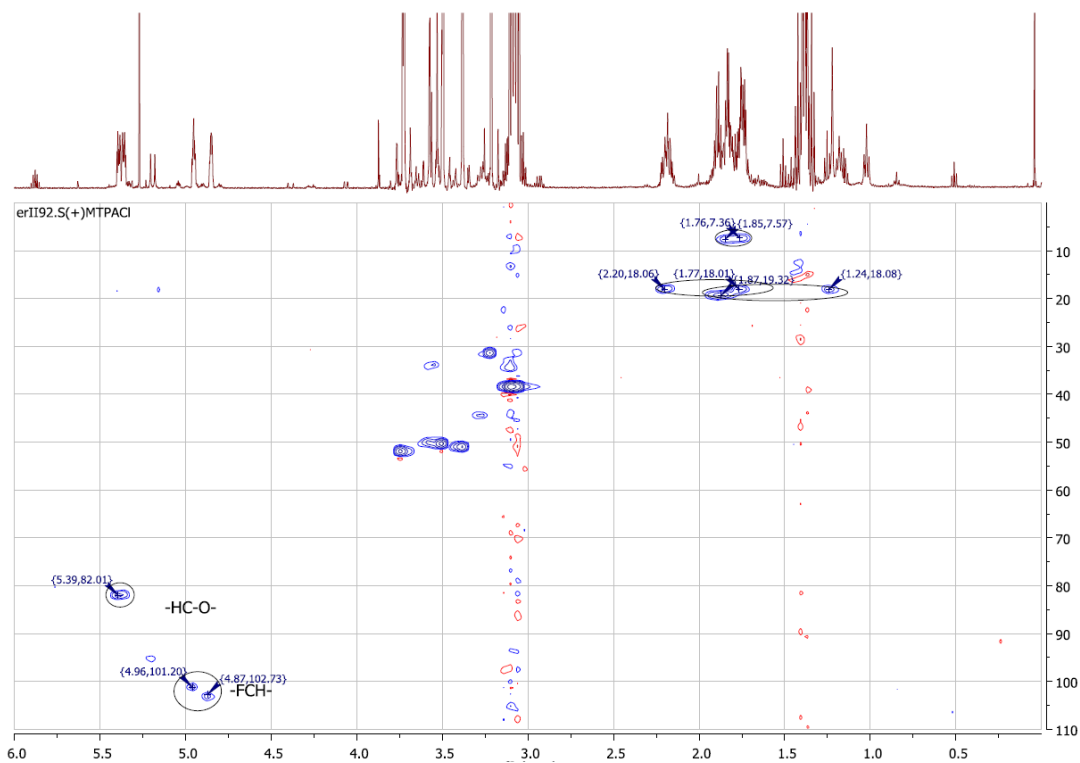
COSY of (R)-MTPA ester of 2-fluorocyclohexanol (from (S)-MTPACl)



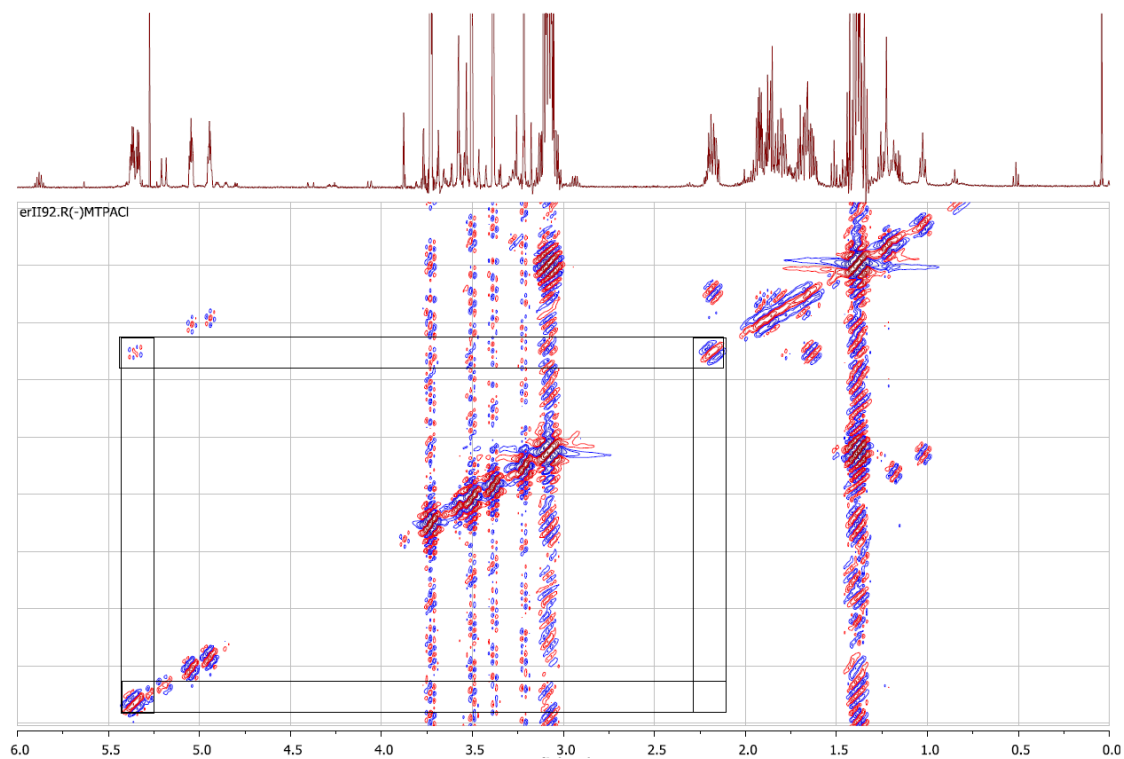
HSQC of (S)-MTPA ester of 2-fluorocyclopentanol (from (R)-MTPACI)



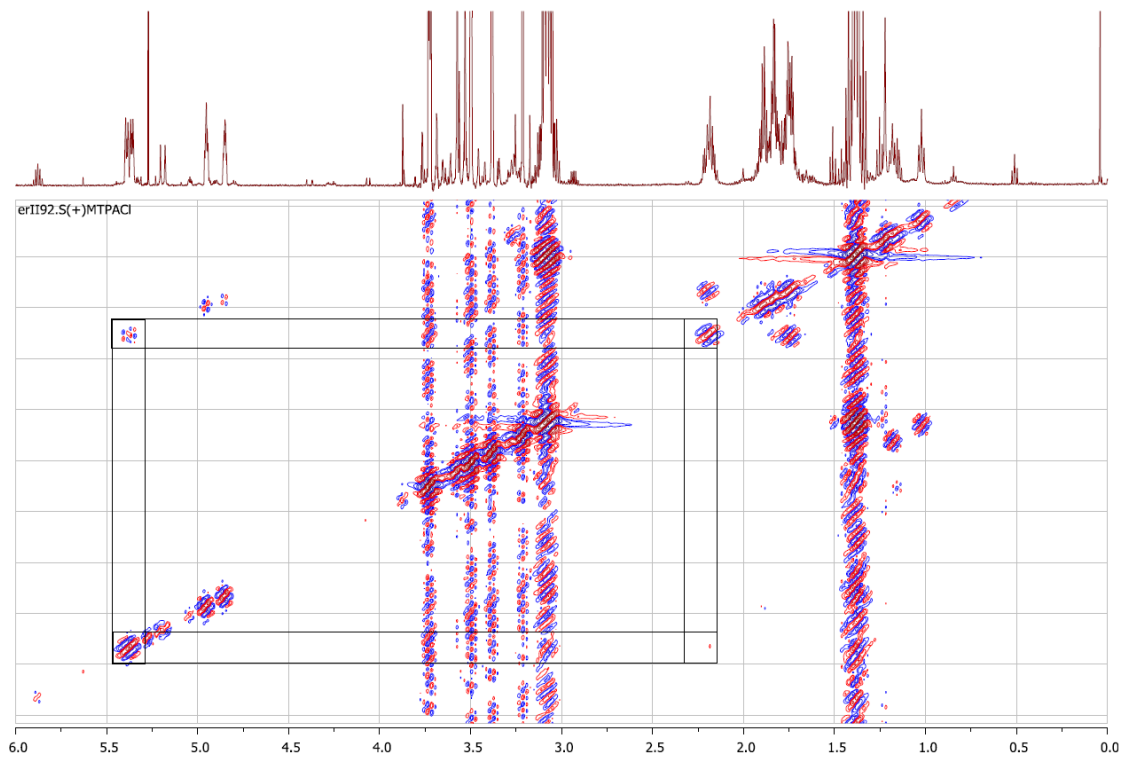
HSQC of (R)-MTPA ester of 2-fluorocyclopentanol (from (S)-MTPACI)



COSY of (S)-MTPA ester of 2-fluorocyclopentanol (from (R)-MTPACl)



COSY of (R)-MTPA ester of 2-fluorocyclopentanol (from (S)-MTPACl)

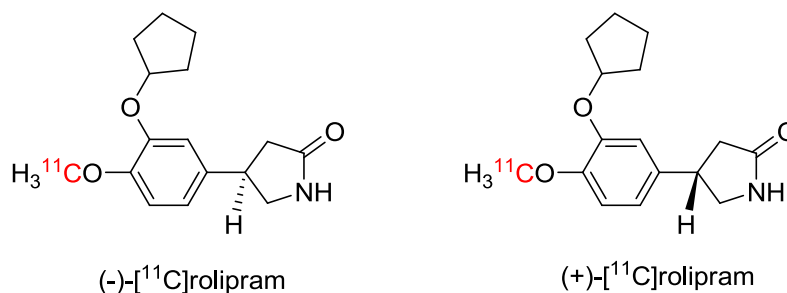


Chapter 3
Synthesis and biological evaluation of both enantiomers of [¹⁸F]FMISO

The most important need for further utilization of PET imaging is the development of new radiopharmaceuticals and more efficient synthetic routes to already known substances.

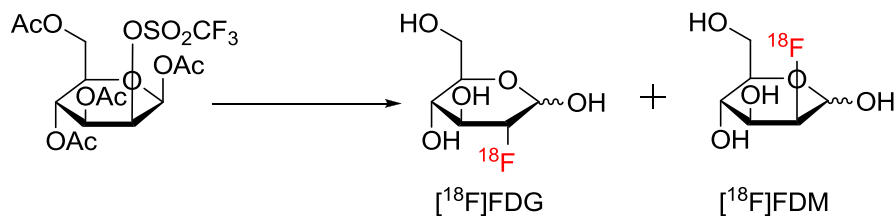
The use of enantiomerically pure compounds is a standard requirement in the pharmaceutical industry, and today - also for PET studies. Often pre-existing chirality can be built into a target molecule prior to the labeling step (chiral carbon atoms bound to OH and NH₂); a number of syntheses have been developed (for example, for amino acids) where asymmetric induction has been achieved using chiral handles, stereoselective enzymes or chiral resolution¹¹⁶.

A biological problem can sometimes be solved using PET-labeled enantiomers. For example, the specific binding of rolipram to the enzyme phosphodiesterase-4 in the central nervous system is almost exclusively observed using the [¹¹C]*R*(-)-rolipram enantiomer, while the [¹¹C]*S*(+)-rolipram enantiomer exhibits homogeneous binding in the brain. Since there is no discrete region in the brain which is devoid of this enzyme, *S*(+)-enantiomer be used to estimate the free and nonspecifically bound component of its biologically active antipode¹¹⁷.



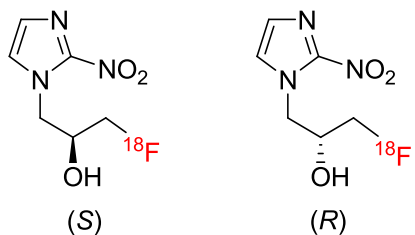
Scheme 43.

The synthesis of [¹⁸F]FDG can yield a product which is contaminated with a variable percentage of 2-fluoro-2-deoxy-D-mannose ([¹⁸F]FDM), an epimer of [¹⁸F]FDG. The level of such contamination is ranging from 0 to 50%. The presence of FDM as an impurity could result in a significant source of error in estimating glucose consumption using the [¹⁸F]FDG method.



Scheme 44.

[¹⁸F]FMISO or [¹⁸F]fluoromisonidazole is hypoxia PET tracer which is quite often used in preclinical and clinical studies. The molecule has a chiral center, but is used for injection as a racemic mixture.



Scheme 45.

To the best of our knowledge nobody tried to investigate the difference between the *R* and *S* enantiomers for the distributions in major tissues. In this chapter we try to give an answer to the question whether the biodistribution and imaging characteristics of [¹⁸F]FMISO as a PET tracer is connected to its enantiomeric purity.

3.1.1 Hypoxia

Appropriate radiotracers, especially [¹⁸F]FMISO, enable non-invasive assessment of hypoxia. Hypoxia is a state in which insufficient amount of oxygen is delivered to the tissue. This is a more serious problem than realized in clinical routine work. During incidence and progress of many types of diseases hypoxia may enhance development and progress of disease and, even more, decrease chances of efficient treatment of tumors.

Oxygen is an essential nutrient for mammalian cells because of its role as the terminal electron acceptor in oxidative phosphorylation. Supplied through breathing, O₂ dissolves in plasma and tissues and is carried throughout the body as oxyhemoglobin, O₂Hb, which releases O₂ when it is needed for mitochondrial respiration. It is so essential to the well-being of cells that intricate control mechanisms have evolved to maintain a sufficient supply of O₂ for the mitochondria. This control system can adjust blood flow, blood vessel dilation, or oxygen extraction fraction to maintain a life-sustaining level of O₂.

When cells are suddenly deprived of sufficient O₂ to maintain oxidative phosphorylation, the cells die either by necrosis or programmed cell death, apoptosis. This phenomenon is called hypoxia and it happens, for example, in stroke, myocardial infarction, or as a consequence of poor perfusion in diabetic limbs or arthritic joints. Cancer cells often respond to hypoxia in a different way – the fact that hypoxic tumors are up to three times more resistant towards radiation therapy than normoxic cells was observed by Gray over 50 years ago.

Most of oxygen-breathing species express the highly-conserved transcriptional complex HIF-1 (Hypoxia-inducible factor 1). The HIF signaling cascade mediates the effects of hypoxia on the cell. HIF-1, when stabilized by hypoxic conditions, regulates several genes to promote survival in low-oxygen conditions. These include glycolysis enzymes, which allow adenosine triphosphate (ATP) synthesis in an oxygen-independent manner. Hypoxia often keeps cells from differentiating. However, hypoxia promotes the

formation of blood vessels, and is important for the formation of a vascular system in embryos, and cancer tumors¹¹⁸.

Tumor cells are gradually exposed to chronic hypoxia as they outgrow their vascular supply, and this can lead to an adaptation that has a negative effect on their response to treatment. If the tumor is not well perfused, chemotherapeutic drugs do not have good access to each tumor cell. Furthermore, tumor cells rapidly adapt to hypoxia by slowing their growth rate, and conventional chemotherapy generally is toxic to cells at a level that is proportional to proliferation. Most chemotherapeutic drugs are essentially antiproliferation agents rather than specific anticancer agents so that when cells enter a resting phase in their cycle, they are not sensitive to these cytotoxic agents.

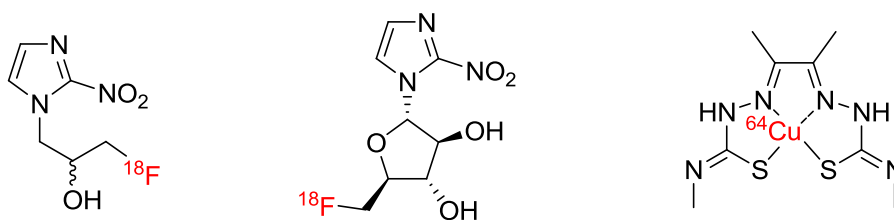
Tumor hypoxia is a key mechanism that leads to resistance of treatment. Different invasive and noninvasive approaches have been developed for measuring tumor oxygenation, from oxygen-sensitive electrodes to hypoxia marker techniques using various labels/markers. These labels can be detected by different methods - autoradiography and immunohistochemistry, MRI, SPECT and the most advanced - PET. PET method seems to be an excellent solution for imaging hypoxia because it is non-invasive, quantitative, has high spatial resolution, and high sensitivity^{119,120}.

3.1.2 [¹⁸F]FMISO as a hypoxia tracer and its mechanism of action

When chemists started developing hypoxia imaging strategies, the goal to identify three factors in cancer biology that were thought to limit response to treatment: decreased blood flow and hence delivery of drugs, decreased proliferation and hence fewer cycling cells, and absence of the oxygen enhancement ratio (OER) in these tumors¹²¹.

The ideal noninvasive hypoxic marker should be:

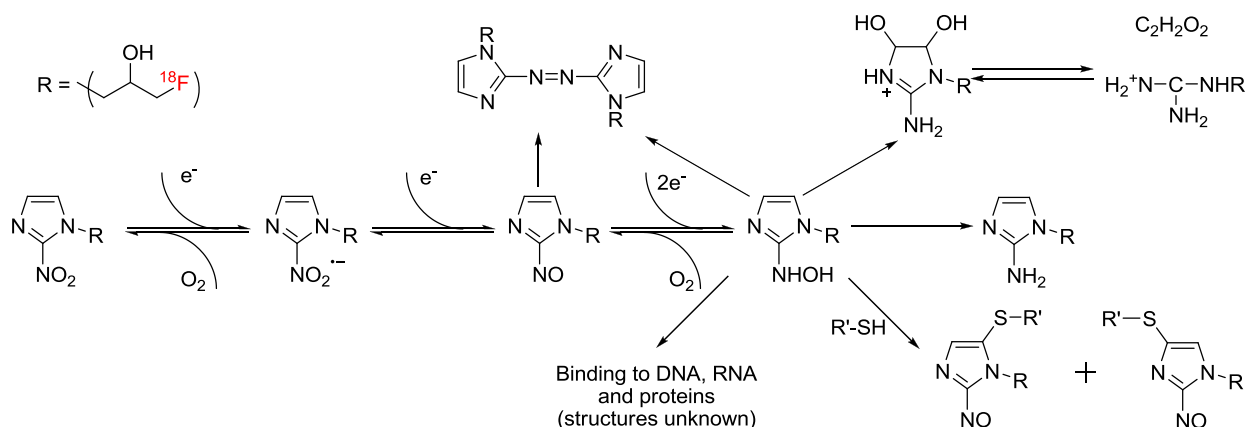
- specific for hypoxia
- be structurally simple, non-toxic, easy to synthesize and allow repeated measurements
- lipophilic to get an equal biodistribution in all tissues
- hydrophilic at the same time to have a faster elimination
- be sensitive at pO₂ levels relevant to tumor therapy
- offer the ability to quantify measurements and the difference between hypoxic and necrotic tissues



Scheme 46. Hypoxia imaging PET radiopharmaceuticals [¹⁸F]FMISO, [¹⁸F]FAZA and ⁶⁴Cu-ATSM.

^{18}F -labeled misonidazole, or [^{18}F]FMISO, was the first hypoxia radiotracer proposed and has been the most extensively investigated one to date. Today [^{18}F]FMISO is the most popular hypoxia marker for investigating tumor hypoxia with PET. Studies using [^{18}F]FMISO demonstrated variable, but significant levels of hypoxia in several tumor types. [^{18}F]FMISO PET imaging has been used as a prognostic indicator¹²². With a diagnostic tool as provided by hypoxia PET tracer [^{18}F]FMISO the particular tissue situation becomes detectable, and, thus treatable. Although the clinical importance of hypoxia is obviously great both the clinical and scientific community has not been focusing much research activities on the hypoxia problem.

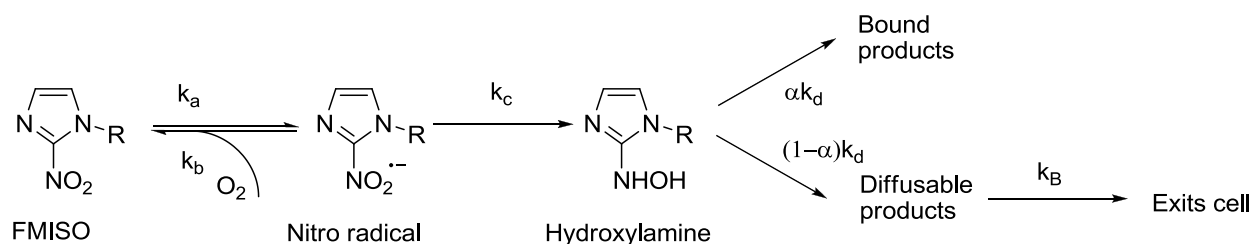
[^{18}F]FMISO is an azomycin-based hypoxic cell sensitizer that has a nearly ideal octanol:water partition coefficient (0.41) and, when reduced by hypoxia, binds covalently to cellular molecules at rates that are inversely proportional to intracellular oxygen concentration, rather than by any downstream biochemical interactions.



Scheme 47. A schematic model of the reductive metabolism of [^{18}F]FMISO in cells¹²³.

The covalent binding of nitroimidazoles is due to bioreductive alkylation based on reduction of the NO_2 -group through a series of one-electron steps in the absence of oxygen. The NO_2 -reduction is performed by nitroreductase enzymes, which are expected to show chiral specificity. It is conceivable that the reduction rates depend on chirality of the substrate.

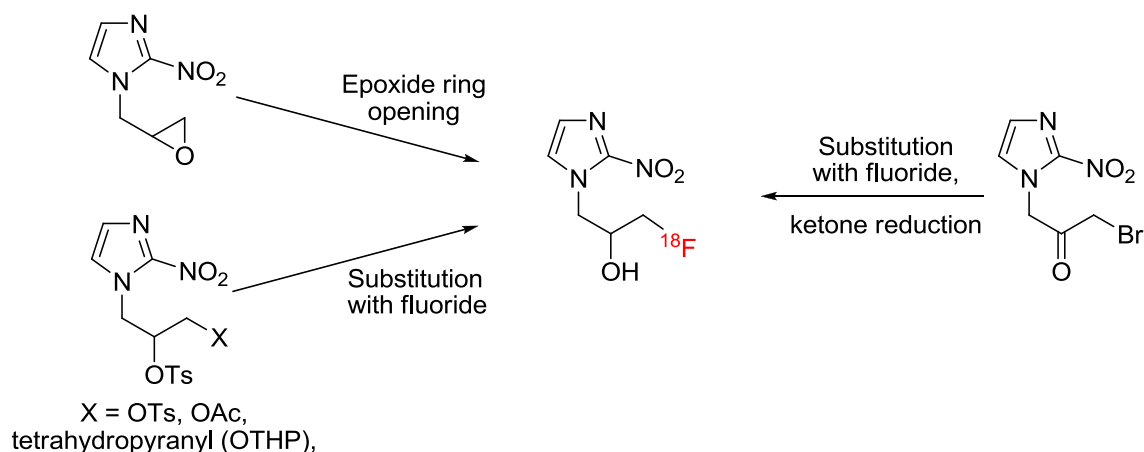
The 2-electron reduction product hydroxylamine, bind stably in cells to macromolecules such as DNA, RNA, and proteins. In the presence of oxygen, a futile cycle results in which the first 1-electron reduction product, the nitro radical anion, is re-oxidized to the parent nitroimidazole, with simultaneous production of an oxygen radical anion.



Scheme 48. A simplified kinetic model of FMISO cellular bio-reduction¹²³.

FMISO is not trapped in necrotic tissue because mitochondrial electron transport is absent. The normal route of elimination for FMISO is renal. A small fraction of [¹⁸F]FMISO is glucuronidated and excreted through the kidneys as the conjugate¹²⁴.

3.1.3 [¹⁸F]FMISO labelling strategies

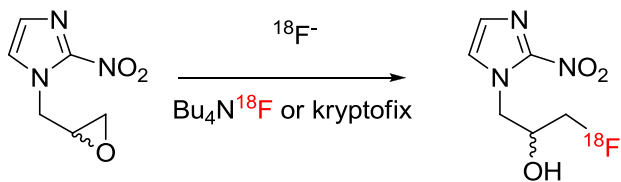


Scheme 49. Direct labelling strategies with nucleophilic fluoride¹²⁵.

A number of synthetic approaches were used for [¹⁸F]FMISO synthesis. The bis-tosylate was employed with the expectation that selective substitution of the primary OTs-group would be favored, with concomitant protection of the secondary alcohol function (Scheme 49). Labelled fluorine incorporation proceeded well (10-35%) within 30 minutes, but unfortunately the remaining OTs-group could not be cleaved to give [¹⁸F]FMISO. This work had, however, set the stage for the high yielding [¹⁸F]FMISO synthesis using tosylate-tetrahydropyranyl protection.

The bromo-ketone was also examined with a proposed fluoro for bromo exchange, followed by a fast ketone reduction (Scheme 49, right). The fact that the bromo-ketone decomposed on a contact with TBAF without fluorine incorporation, led to abandoning this route. This result may reflect the acidity (enolization) in basic media.

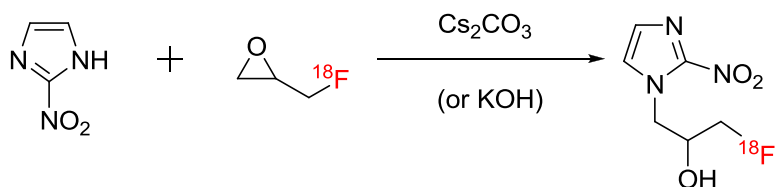
[¹⁸F]FMISO was first successfully prepared by Jerabek et al¹²⁶, this method was based on the nucleophilic ring opening of the strained ring of epoxide using [¹⁸F]TBAF.



Scheme 50.

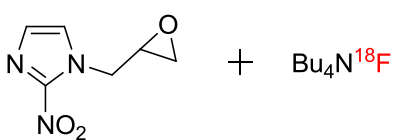
This labelling reaction was intended to be a one-pot process that did not also rely on the additional removal of protecting groups to finish the synthesis, although the synthesis time was reasonable (1h) but the yield was too low (less than 1%) to develop the process for potential routine studies/production. The specific activity was limited to 100 GBq/mmol.

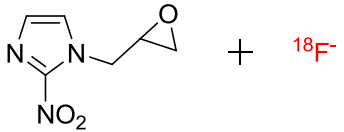
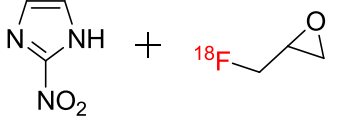
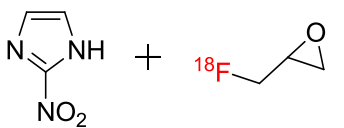
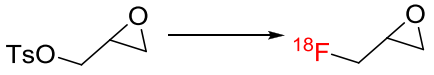
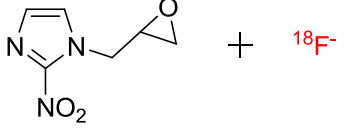
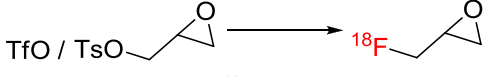
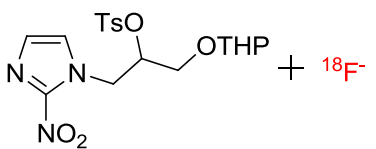
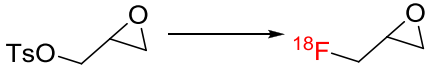
The failure of the synthesis likely stems from the lack of a suitable activator (Lewis acid, e.g. H⁺ or metal cation) coordinated to the epoxide oxygen atom during nucleophilic fluoride displacement of the terminal C-O epoxide bond



Scheme 51.

The first useful two-step alternative synthesis of [¹⁸F]FMISO was developed¹²⁷ demonstrating a high yield (RCY 40% from end of bombardment (EOB)) and purity with SA of 37 TBq mmol⁻¹. The first step involves the synthesis of fluoroalkylating agent [¹⁸F]epifluorohydrin, which subsequently reacts with 2-nitroimidazole to yield [¹⁸F]FMISO (Scheme 51). HPLC purification is needed to obtain high radiochemical purity. Further modifications have been reported with increasing labeling yields¹²⁸, microwave heating¹²⁹, SepPack cartridges¹³⁰.

Entry	Reaction procedure	RCY	Overall synthesis time	SA (if available)	Reference/author
1	 Nucleophilic attack of CA fluoride as TBAF on the epoxide ring of MISO-epoxide	< 1%	-	-	Jerabek ¹²⁶

2	 <p>Nucleophilic attack of CA fluoride on the epoxide ring of MISO-epoxide</p>	< 1%	60 min	2.75 Ci/mmol	Jerabek ⁷⁷
3	 <p>Preparation of Epi-¹⁸F, distillation, coupling to 2-nitroimidazole under basic conditions (proton sponge)</p>	5%	>40 min	-	Grierson ¹³¹
4	 <p>Preparation of Epi-¹⁸F, distillation, coupling to 2-nitroimidazole under basic conditions</p>	40%	133 min	670 Ci/mmol	Grierson ¹³¹
5	 <p>Preparation of Epi-¹⁸F from glycidyltosylate</p>	15-26%	120 min	-	Hwang ¹³²
6	 <p>Nucleophilic attack of CA fluoride on the epoxide ring of MISO-epoxide</p>	< 1%	90 min		Hwang ¹³³
	 <p>Preparation of Epi-¹⁸F from glycidyltosylate and glycidyltriflate, silica column purification, coupling to 2-nitroimidazole under basic conditions</p>	12-21%	90 min	>400 Ci/mmol	
7	 <p>¹⁸F-fluoride nucleophilic substitution of tosylate on the THP protected precursor, hydrolysis</p>	45%	50 min	-	Lim ¹³⁴
8	 <p>Preparation of Epi-¹⁸F from glycidyltosylate, coupling to 2-nitroimidazole under basic</p>	62%	70 min	-	McCarthy ¹²⁹

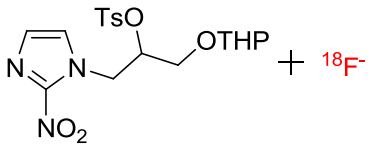
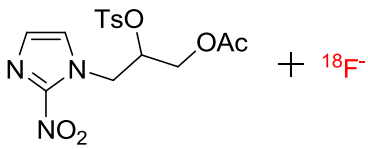
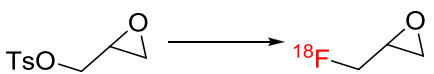
conditions, microwave heating					
9	 ^{18}F -fluoride nucleophilic substitution of tosylate on the THP-protected precursor, hydrolysis	55-89%	15-50 min	>600 Ci/mmol	Lim ¹³⁵
10	 ^{18}F -fluoride nucleophilic substitution of tosylate on the acetyl protected precursor	12-18%	60-70 min	-	Cherif ¹³⁶
11	 Preparation of Epi- ^{18}F from glycidyltosylate in a one-pot reaction procedure	20%	80 min	-	Tada ¹³⁷

Table 16. Synthetic approaches to [^{18}F]FMISO¹²⁵.

Nucleophilic opening of MISO-epoxides could be performed as enantioselective reaction (table 16, entries 1, 2 and 6), but because of low yields this route was abandoned. [^{18}F]-epifluorohydrine two step labelling strategy can be used for the synthesis of enantiopure [^{18}F]FMISO (Table 16, entries 3, 4, 5, 8, 11), however this method was too complicated for routine production and is no longer in use.

The most practical method is based on the nucleophilic substitution of the tosylate leaving group by ^{18}F -fluoride on the tetrahydropyranyl protected precursor 1-(2'-nitro-1'-imidazolyl)-2-O-tetrahydropyranyl-3-O-toluenesulfonylpropanediol (NITTP), followed by the hydrolysis of the protecting group (entries 7, 9). An automated synthesis of [^{18}F]FMISO by this method using either HPLC or SepPaks for the purification of the radiotracer was also reported¹³⁸. The radiochemical yield obtained when using NITTP was found to be higher than 40%, and reproducible, with a radiochemical purity > 97% and SA 34TBq mmol⁻¹. The total synthesis time was 50 min.

MISO-diol with leaving group (OTs, OTf, OMs) and hydroxyl protecting group (Ac or THP) usually gave high yields, but on the other hand stretches the time of synthesis (entries 7, 9, 10). Complicated multistep precursor synthetic route makes the synthesis more expensive. Enantiopure product cannot be obtained from this methodology.

The question if *R* and *S* isomers give equal or different biodistribution in the organism – still needs to be answered. Our studies on the chiral synthesis of [^{18}F]FMISO and in vivo studies of enantiopure samples of [^{18}F]FMISO provide the answer to this question.

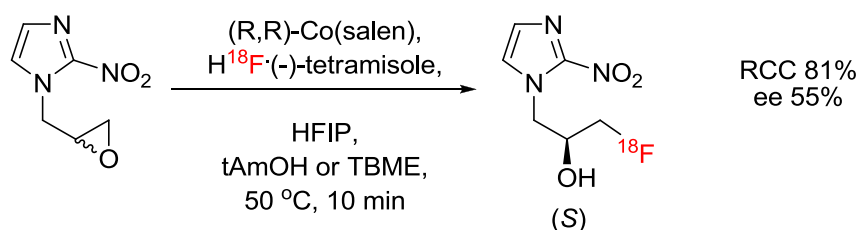
3.2 Results and discussion

3.2.1 Discussions of [¹⁸F]FMISO synthesis

Encouraged by the good results from radiofluorination of meso-epoxides (RCY up to 93% and ee 45% for cyclohexylfluorohydrine) we turned our attention to radiosynthesis of [¹⁸F]FMISO.

[¹⁸F]FMISO, a 2-nitroimidazole ¹⁸F-fluorohydrine, is currently the most widely used tumor hypoxia PET imaging agent¹³⁹. The direct ¹⁸F-hydrofluorination of epoxides is a particularly attractive approach. The one step enantioselective synthesis of non-radioactive FMISO was showcased by Doyle⁹⁷.

In our hands, the radiofluorination of the racemic F-MISO epoxide, obtained from 2-nitroimidazole and the racemic epichlorohydrin yielded [¹⁸F]FMISO in 17% RCY at room temperature. At 75 °C the RCY increased to 81% and the product was obtained in 38% ee. Lowering the reaction temperature to 50 °C proved to be a compromise reaction temperature: [¹⁸F]FMISO was obtained in 81% RCY and 55% enantiomeric excess (Scheme 52).



Scheme 52.

High boiling point of tAmOH gave us an opportunity to use a standard 10 ml disposable glass vial instead of a high pressure glass test tubes. Reaction time was reduced from 1 h (used in radiofluorination of meso-epoxides) to 10 min. MISO-epoxide seems to be more reactive than the meso-epoxides described above. Even heating to 50 °C is enough to get a high yield.

Entry	t, °C	RCC, %	ee, %
1	25	17	
2	50	81	55
3	75	81	38
4	100	87	33

Table 17. RCC and ee for [¹⁸F]FMISO at different temperatures.

The reaction mixture volume should be minimized to achieve high conversion and simplify the purification procedure. We found the optimal volume is in the range of 1 ml.

The decrease in catalyst loading (from 0.1 to 0.25 eq.) was effective; the same time was required to achieve the equal level of product formation. Surprisingly, further decrease of the catalyst amount (1:1 and 2:1 catalyst – epoxide ratio) gave less conversion of ¹⁸F (Figure 21).

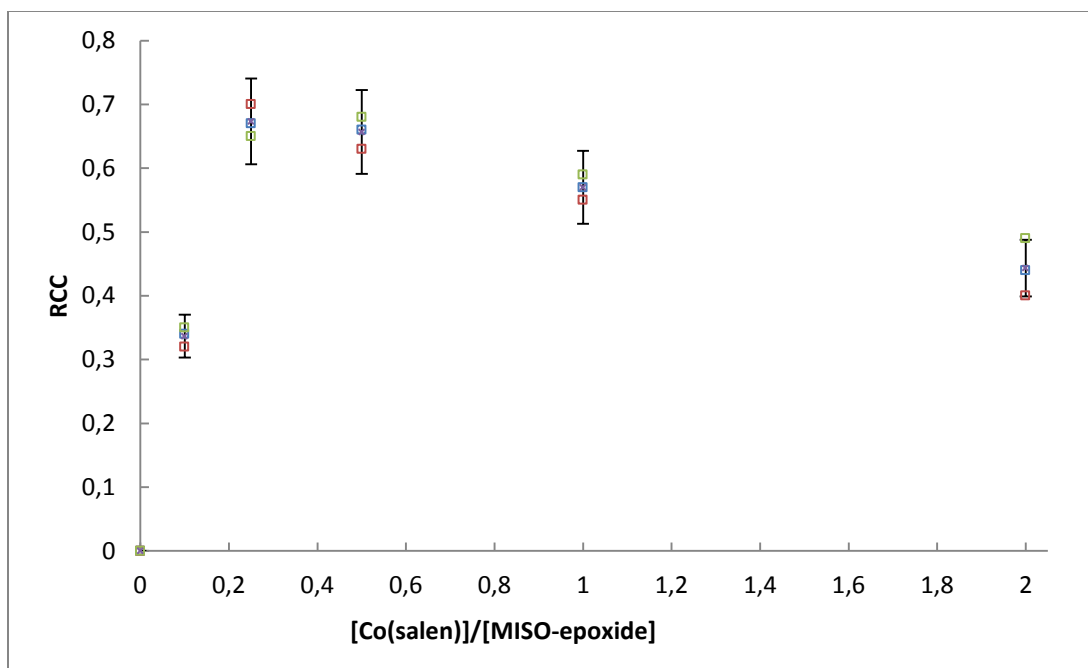
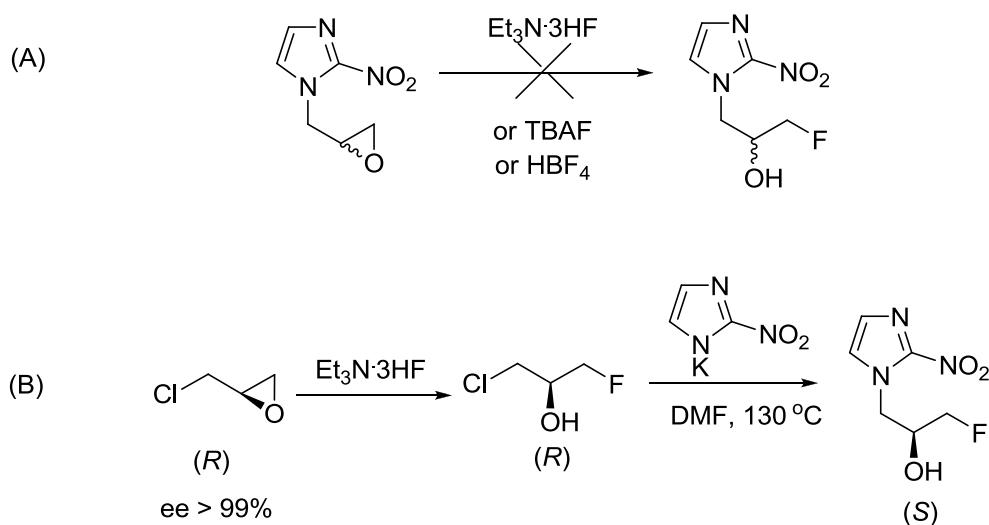


Figure 21. RCC to the Co(Salen)/MISO-epoxide ratio plot (10 min at 50 °C, 1 mL of tAmOH, conversion was determined by radio TLC).

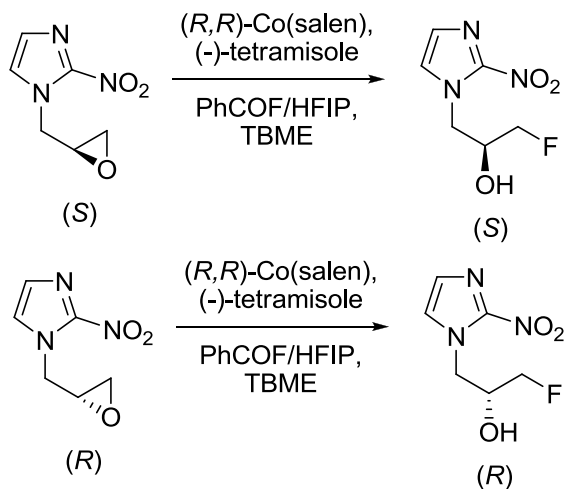
3.2.2 [¹⁸F]FMISO stereochemistry

To determine the stereochemistry of [¹⁸F]FMISO we have also synthesized the enantiomerically pure cold FMISO to be used as a reference material. Our attempts to make direct fluorination (described above for *meso*-epoxides) were inefficient (Scheme 53, A). We used different route – first opening the epoxide in epichlorohydrin followed by alkylation of 2-nitroimidazole (Scheme 53, B):



Scheme 53.

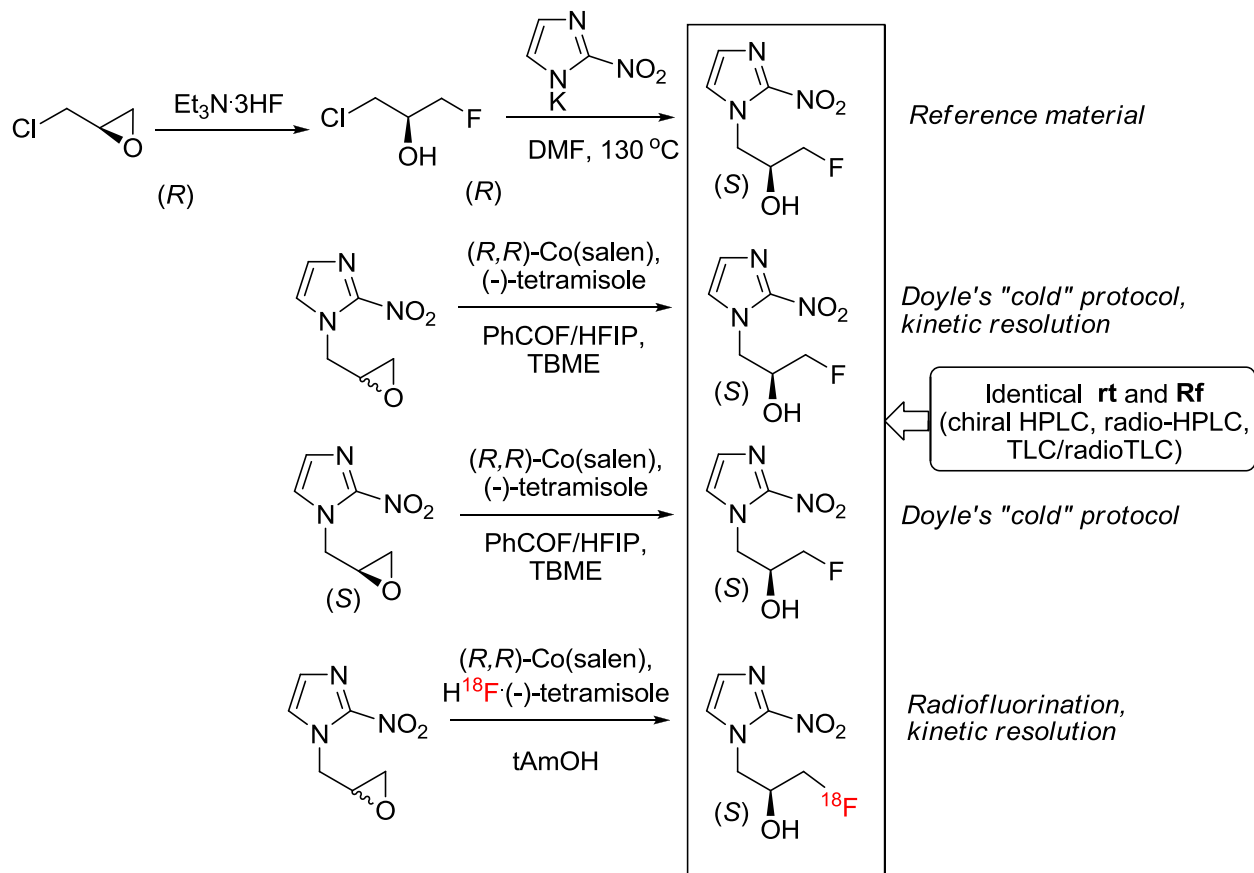
(*S*)-FMISO and (*R*)-FMISO isomers were also synthesized independently applying Doyle's protocol to enantiopure substrates:



Scheme 54.

The comparison of chiral HPLC traces/radiotracers and TLC/radioTLC traces was done. The stereochemistry of these traces was in agreement with chiral traces of (*S*) and (*R*)-FMISO, synthesized from enantiomerically pure (*R*) and (*S*)- epichlorohydrines.

The major enantiomer of [^{18}F]FMISO from the reaction mediated with (*R,R*)-catalyst (Scheme 52, Scheme 55) was identified as the (*S*)-stereoisomer - this result is in line with the (*S*)-stereochemistry for FMISO reported by Doyle:



Scheme 55.

3.2.3 New strategy

Unfortunately this approach (kinetic resolution) gave too low enantiomeric purity of [^{18}F]FMISO for *in vivo* experiments (ee 55% at 50 °C). In the drug studies it is preferable to use pure compounds with as few impurities as possible. To gain information about an interaction of enantiomers, mixtures should be avoided. Often only one isomer is therapeutically active, but this does not mean that the other is really inactive. It may also contribute to the side-effect. The presence of a 50% impurity of isomeric ballast in drug, even if found to be innocent, should be avoided if it is possible¹⁴⁰.

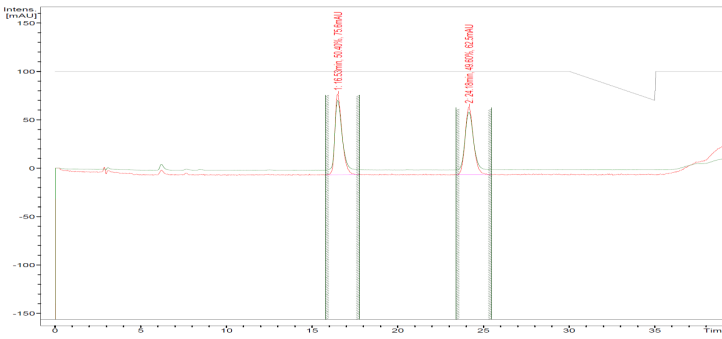
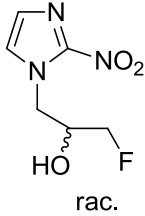
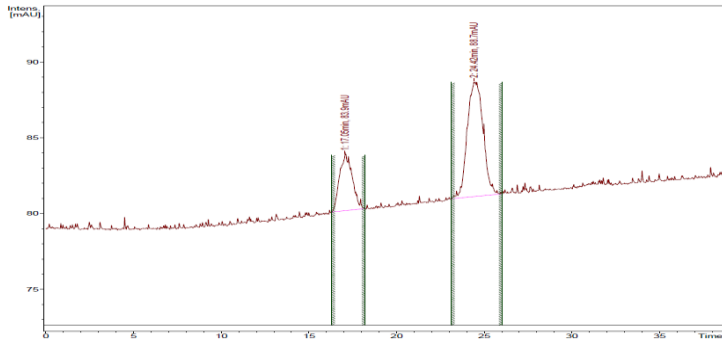
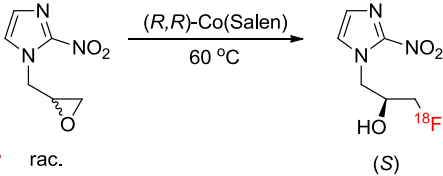
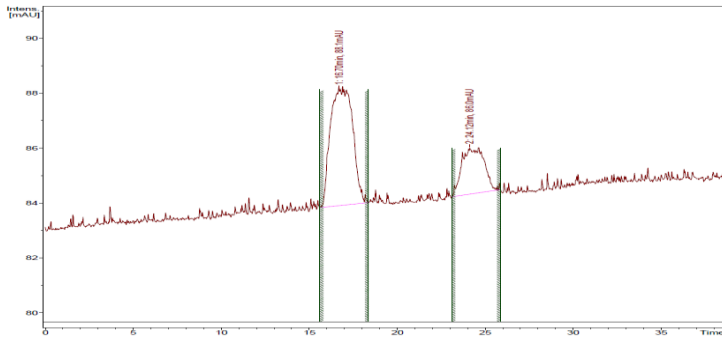
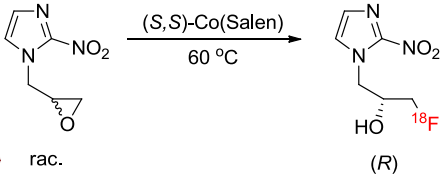
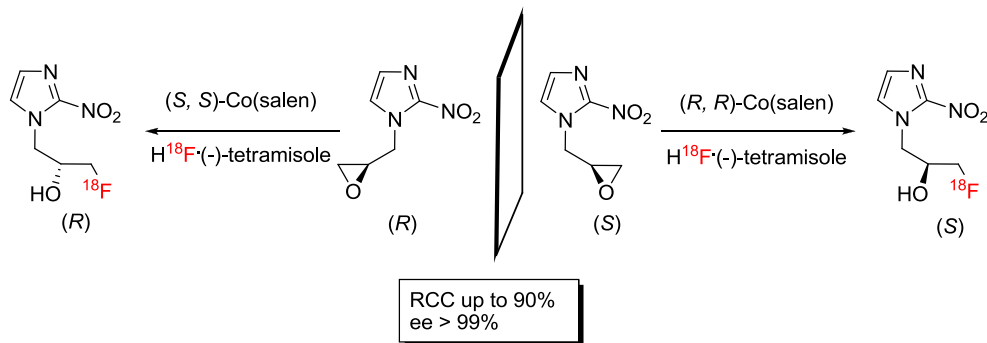
Entry	Chiral HPLC trace	Description
1		<p>Racemic FMISO</p>  <p>rac.</p>
		(UV trace (254 nm, 220-600 nm))
2		 <p>rac.</p> <p>(S)</p>
		(radiotracer)
3		 <p>rac.</p> <p>(R)</p>
		(radiotracer)

Table 18. Chiral HPLC trace and radiotracers from [¹⁸F]FMISO kinetic resolution.

Therefore, another strategy to synthesize enantiomerically pure FMISO was chosen - we decided to use enantiopure substrates (>99% ee) for further radiofluorination, instead of performing kinetic resolution of racemic substrates – MISO-epoxides.



Scheme 56.

Synthesis of enantiopure substrates was done according to the procedure described below. The *S* and *R* epichlorohydrines (>99% ee) are commercially available compounds, what makes the chiral MISO-epoxides more accessible.

Due to the high activity, the radio synthesis was automated, using the LabVIEW controlled platform, equipped with the standard blocks and parts for a radiosynthesis (syringe pumps, valves, heaters/coolers, argon, helium and vacuum supply, and Geiger Muller counters).

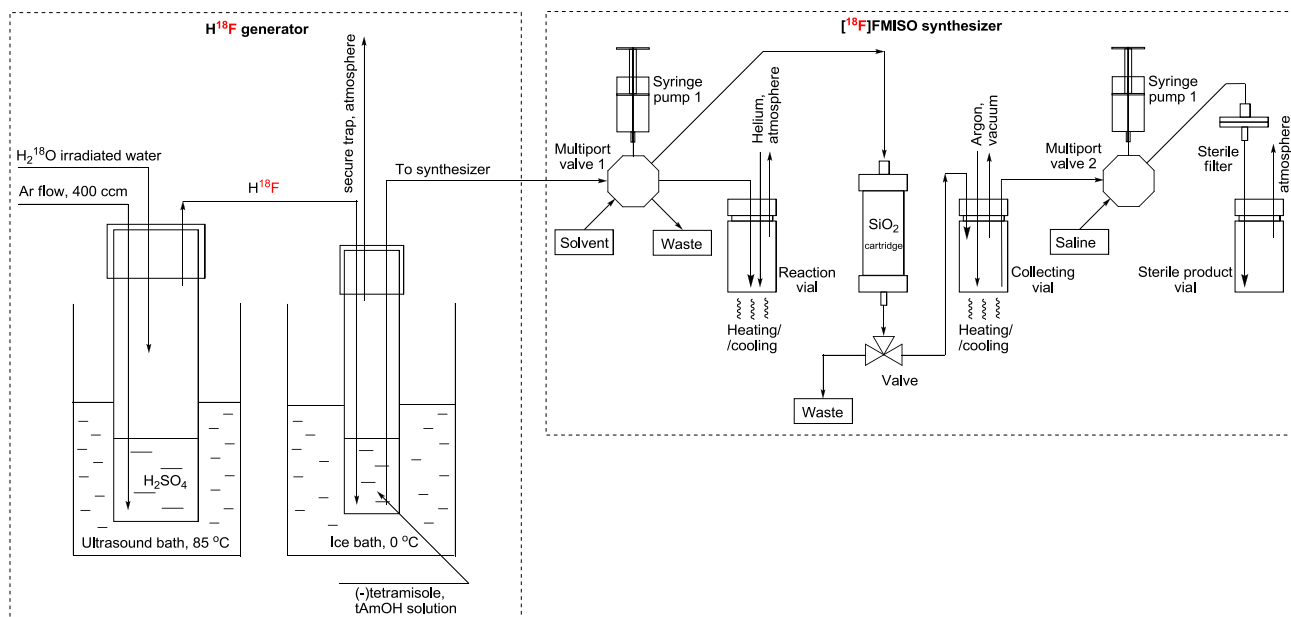


Figure 22. Automated radiosynthesizer.

Overall, the radiosynthesis went as planned, producing the corresponding [^{18}F]FMISO enantiomers in 90% RCC and > 99% enantiopurity (Table 19).

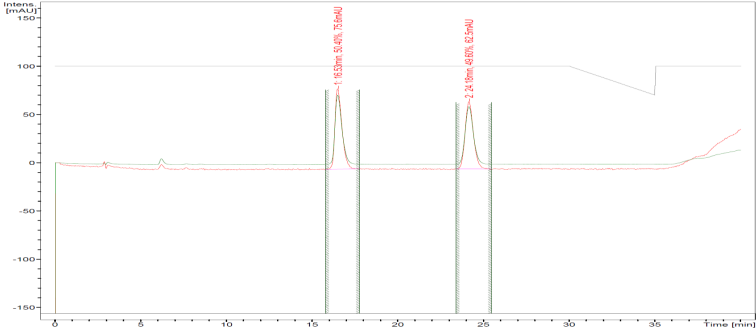
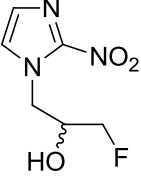
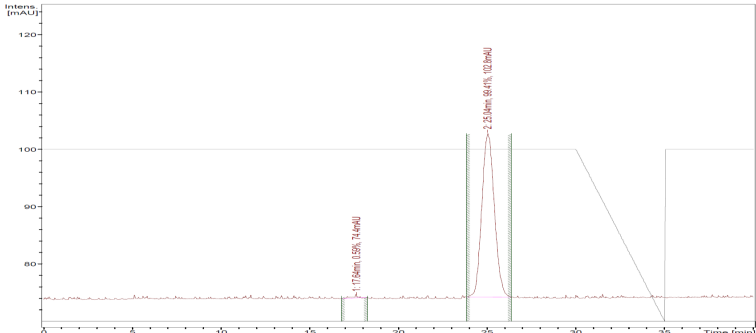
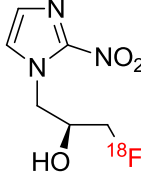
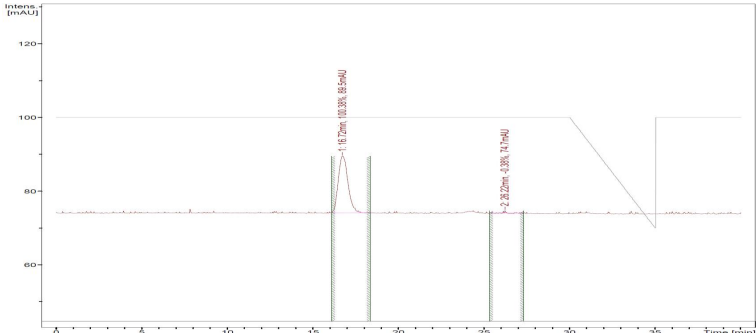
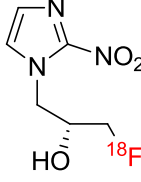
Entry	Chiral HPLC trace	Description
1		<p>Racemic FMISO</p>  <p>rac.</p>
2		 <p>(S)</p> <p>>99% ee, radiotracer</p>
3		 <p>(R)</p> <p>>99% ee, radiotracer</p>

Table 19. Chiral HPLC – radio-HPLC traces of [¹⁸F]FMISO.

3.2.4 Purification

[¹⁸F]FMISO as any radiopharmaceutical requires careful purification before it can be released for biological studies or to a patient¹⁴¹. The main disadvantage of most modern methods for [¹⁸F]FMISO synthesis is purification using HPLC systems. This also affects the total synthesis time¹⁴². We have developed a new and efficient purification method which uses a simple solid phase extraction (SPE) methodology which does not require HPLC.

According to the developed protocol[†], the reaction mixture was loaded onto the Supelco silica cartridge and sequentially washed with hexane and CH₂Cl₂ (Figure 23). This step removed tAmOH, HFIP and the Co(salen) catalyst, while the product, unreacted epoxide and unreacted ¹⁸F-fluoride remained on the cartridge. The cartridge was then gradient-eluted with CH₂Cl₂-MeCN mixture (0 - 33 % MeCN), which removed the unreacted epoxide and finally elutes [¹⁸F]FMISO into the collecting vial. The enantiomerically pure [¹⁸F]FMISO, which was >99% radiopure (from radio-TLC and radio-HPLC traces) and contained no cold impurities (HPLC and GC control) after removing of solvents (evaporation under 100 mbar vacuum and low argon flow) was dissolved in saline and was filtered through a sterile filter to make the final [¹⁸F]FMISO formulation.

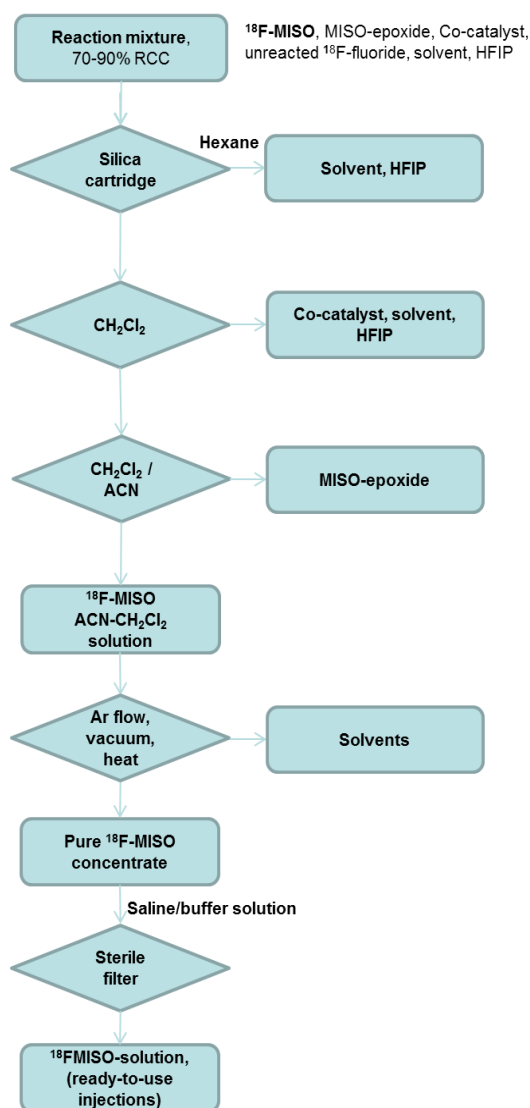


Figure 23. [¹⁸F]FMISO purification scheme.

[†]The protocol was made by F. Zhuravlev

The specific activity of [^{18}F]FMISO was measured to be higher than 100 Gb/mmol. The purification takes 40 min and the overall radiosynthesis time, including [^{18}F]HF generation and transfer, is one hour.

This [^{18}F]FMISO purification scheme was adopted for the automated radiosynthesizer installed in our laboratory and rebuilt according to our needs.

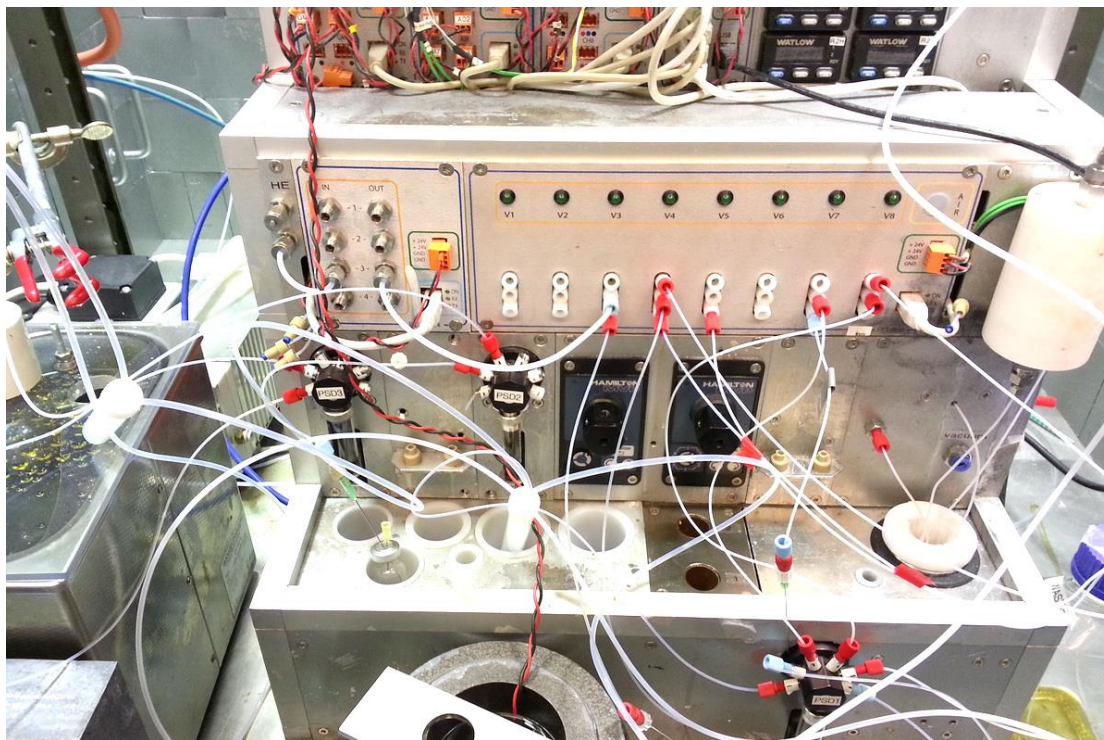


Figure 24. Radiosynthesizer adopted for [^{18}F]FMISO synthesis.

A program for handling the synthesis was written (LabVIEW platform):

Step #	Flow 1	Flop.2	Temp 1	Temp 2	MPV 1	MPV 2	Pump	LV	Valves	Message	Time (s)	Step #	PSD #	Vol (mul)	Valve p.u.	Valve dsp	Speed p.u.	Speed dsp
0	0	0	20	20	1	1	0	0	00000000	init	2	0	0	1	1	0	0	0
1	40	0	20	20	1	1	0	0	00000000	prime psd1	2	1	1	1000	1	1	20000000	20000000
2	40	0	20	20	1	1	0	0	00000000	transfer TM RV1	2	2	1	1500	1	3	20000000	20000000
3	40	0	20	20	1	1	0	0	00000010	transfer TM RV2	2	3	1	1500	1	3	20000000	20000000
4	40	0	65	65	1	1	0	0	00100000	He and heat	600	4	1	0	1	1	0	0
5	40	0	0	0	1	1	0	0	00100000	cool to RT	420	5	1	0	1	1	0	0
6	40	0	20	20	1	1	0	0	00000001	load RV1 SiO2-1	2	6	1	1500	3	4	20000000	60000000
7	40	0	20	20	1	1	0	0	00000001	wash SiO2-1 hex	2	7	1	15000	6	4	20000000	60000000
8	40	0	20	20	1	1	0	0	00000001	rinse RV1	2	8	1	1500	2	3	60000000	200000000
9	40	0	20	20	1	1	0	0	00000001	load wash SiO2-1	2	9	1	1700	3	4	60000000	60000000
10	40	0	20	20	1	1	0	0	00000001	wash SiO2-1 hex	2	10	1	25000	2	4	60000000	60000000
11	40	0	20	20	1	1	0	0	00000001	wash SiO2-1 3-1	2	11	1	22000	5	4	20000000	60000000
12	40	0	20	20	1	1	0	0	00010001	elute SiO2-1	2	12	1	25000	5	4	20000000	60000000
13	40	0	20	20	1	1	0	0	00000010		2	13	1	1500	3	4	20000000	60000000
14	40	0	20	20	1	1	0	0	00000000		2	14	1	15000	6	4	20000000	60000000
15	40	0	20	20	1	1	0	0	00000010		2	15	1	1500	2	3	60000000	60000000
16	40	0	20	20	1	1	0	0	00000010		2	16	1	1700	3	4	60000000	60000000
17	40	0	20	20	1	1	0	0	00000000		2	17	1	25000	2	4	60000000	60000000
18	40	0	20	20	1	1	0	0	00000000		2	18	1	22000	5	4	20000000	60000000
19	40	0	20	20	1	1	0	0	00001000		2	19	1	25000	5	4	20000000	60000000

Figure 25. [^{18}F]FMISO synthesizer program.

3.2.5 QC control

The radiochemical identity was confirmed by HPLC/radio-HPLC and TLC/radioTLC methods. HPLC traces of the reference material and test solution were identical. TLC plates also showed same R_f for the reference and test samples.

Table 20. C18 HPLC traces.

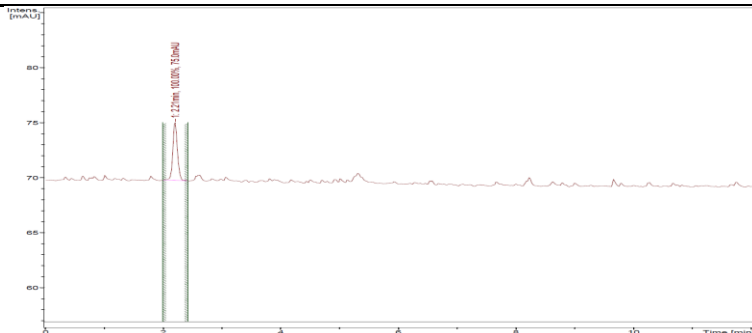
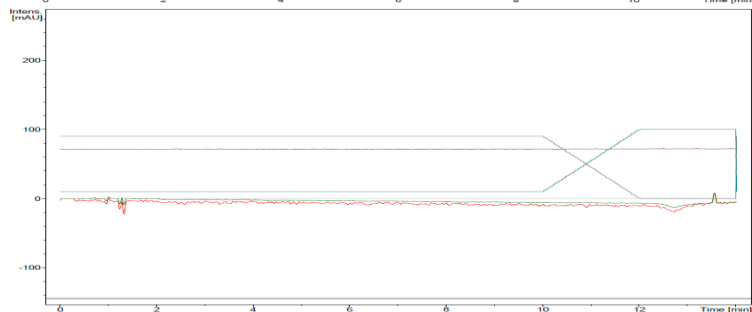
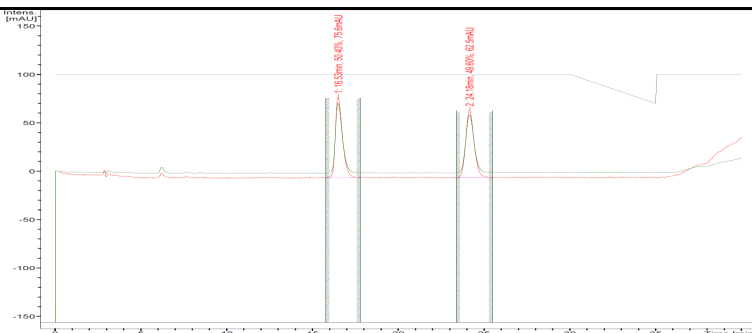
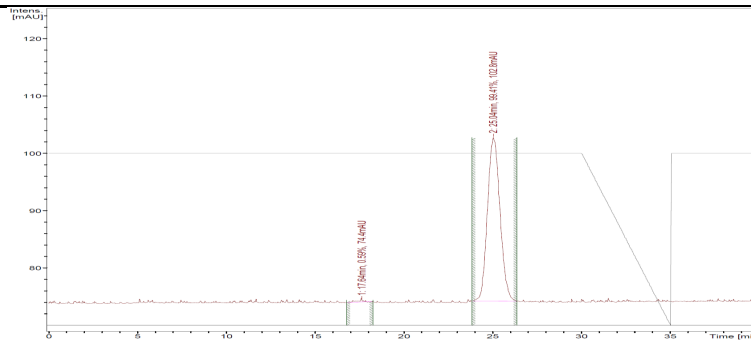
Entry	HPLC trace	Description
1	 <p>The figure shows a radio HPLC trace with a single prominent peak at 1.12 minutes. The y-axis is labeled 'Intensity (mAU)' and ranges from 60 to 80. The x-axis is labeled 'Time (min)' and ranges from 0 to 10. The peak is labeled with its retention time, '1.12 min, 100.0%, 1.12 mAU'.</p>	Radio HPLC trace of a final product
2	 <p>The figure shows a UV HPLC trace with a single prominent peak at 1.12 minutes. The y-axis is labeled 'Intensity (mAU)' and ranges from -100 to 200. The x-axis is labeled 'Time (min)' and ranges from 0 to 12. The peak is labeled with its retention time, '1.12 min, 100.0%, 1.12 mAU'.</p>	UV HPLC trace of a final product

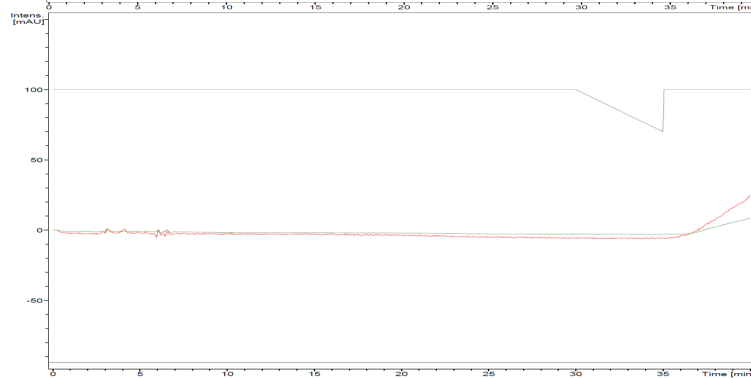
Table 21. Chiral traces normal phase column.

Entry	Chiral HPLC trace	Description
1	 <p>The figure shows a chiral HPLC trace for a racemic FMISO standard. The y-axis is labeled 'Intensity (mAU)' and ranges from -150 to 150. The x-axis is labeled 'Time (min)' and ranges from 0 to 35. There are two distinct peaks: one at 15.53 minutes and another at 24.98 minutes. Both peaks are labeled with their retention times and '100.0%' purity. The peak at 15.53 min is labeled '15.53 min, 100.0%, 135.6 mAU' and the peak at 24.98 min is labeled '24.98 min, 100.0%, 63.3 mAU'.</p>	Racemic FMISO (reference standard from ABX advanced biochemical compounds), 0% ee

2

RadioTRACE of
(S)-[¹⁸F]FMISO

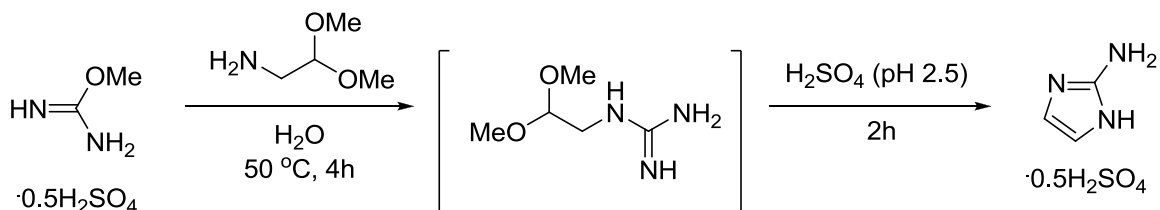
3

UV trace of
(S)-[¹⁸F]FMISO

The content of residual solvents (MeCN and CH₂Cl₂) was checked with GC (under the constant oven temperature, flame ionization detection) and found to be below recommended values for [¹⁸F]FDG. Also, the mass of the vials was measured before and after evaporation of the solvent, the difference was less than 0.1 mg. The pH values were about physiological pH.

3.3 Experimental part

2-Aminoimidazole-hemisulfate

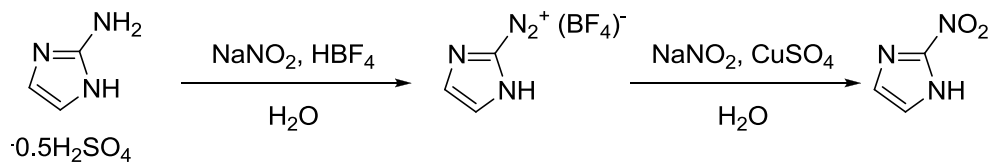


Scheme 57.

2-Aminoimidazole-hemisulfate was prepared from O-methyl-isourea-hemisulfate and 2-amino-acetaldehyde-diethylacetale according to the described procedure¹⁴³. The title compound was isolated as an off-white solid (82%). ¹H NMR data agreed with literature values¹⁴³

2-Nitroimidazole

2-Nitroimidazole was prepared according to the modified method¹⁴⁴ from 2-amino-imidazole-hemisulfate:

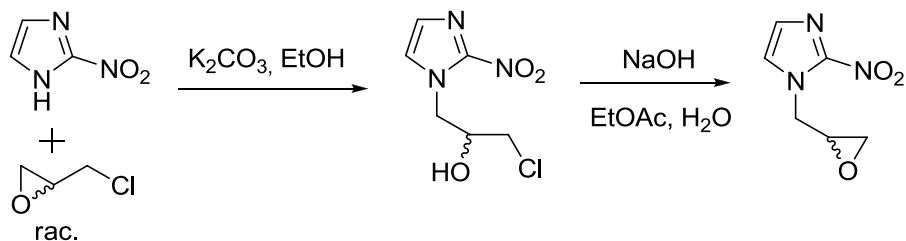


Scheme 58.

2-Aminoimidazole-hemisulfate (1.58 g, 12.0 mmol) was dissolved in water (20 mL) and fluoroboric acid (50% w/v, 14 mL). The solution was cooled to -20 °, and a solution of sodium nitrite (8.28 g, 119.2 mmol) in water (20 mL) was added dropwise. The solution was stirred at -10 °C for 30 min, then poured into a solution of CuSO₄ (40 g, 238 mmol) in water (400 mL). Additional sodium nitrite (8.28 g, 119.2 mmol) was added and the mixture was stirred at room temperature for 2 h. The solution was extracted with EtOAc (400 mL) in a continuous extractor for 2 days. The organic extract was evaporated in vacuo, and the residue was recrystallized from ethanol to afford 2-nitroimidazole as a yellow powder (0.7 g, 52%). NMR data were in agreement with literature values¹⁴⁴.

Racemic 2-nitro-1-(oxiran-2-ylmethyl)-1H-imidazole (MISO-epoxide)

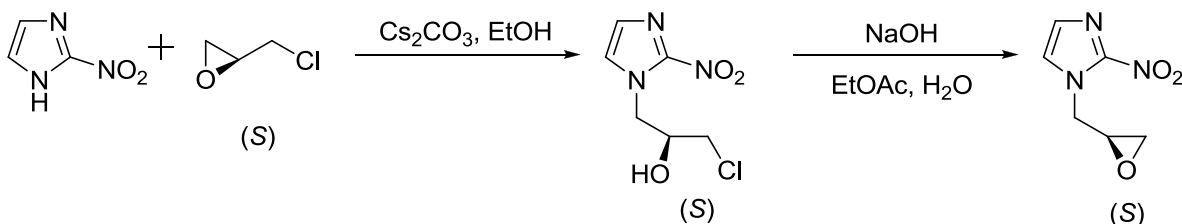
MISO-epoxide was prepared according to the modified procedure¹⁴⁵ as a one pot synthesis:



Scheme 59.

2-Nitroimidazole (1.00 g, 8.8 mmol, 1.0 eq.) and potassium carbonate (122 mg, 0.88 mmol, 0.1 eq.) was treated with (*S*)-epichlorohydrin (10 ml, 0.13 mol, excess), and the resultant mixture was gently heated and refluxed for 1 h under inert atmosphere. The hot solution was filtered through a glass filter; solvent was removed in vacuo and off-white precipitate was dried. EtOAc (20 mL) and 10 % NaOH (20 mL) were added to this precipitate and stirred for 1 h at room temperature. The organic layer was separated and dried over Na₂SO₄. Solvent was removed in vacuo and the remaining brown oil was passed through a silica cartridge with EtOAc (50 ml). Storing this yellow viscous liquid at -20 °C over night gave solid crystalline product (1.37 g, 92% yield, m.p. 50-60 °C). Spectral data agreed with literature values¹⁴⁵.

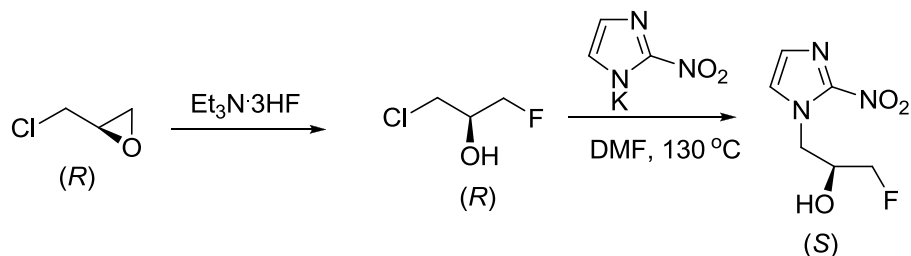
(*S*)-2-nitro-1-(oxiran-2-ylmethyl)-1H-imidazole ((*S*)-MISO-epoxide)



Scheme 60.

A stirred suspension of 2-nitroimidazole (1.00 g, 8.8 mmol, 1.0 eq) and cesium carbonate (145 mg, 0.44 mmol, 0.05 eq.) in 20 mL of dry EtOH was treated with (*S*)-epichlorohydrin (760 μl, 9.6 mmol, 1.1 eq.), and the resultant mixture was gently refluxed for 1 h under argon. The hot solution was filtered through glass wool; solids were washed with hot ethanol (10 mL). Half of the solvent was removed in vacuo, the concentrated solution was stored at -20 °C overnight. Off-white precipitate of 1-(2-Hydroxy-3-chloropropyl)-2-nitroimidazole was filtered and dried in vacuo. A flask with solid chlorohydrine was charged with EtOAc (20 mL) and 10 % NaOH (20 mL) and stirred for 1 h at room temperature. The organic layer was separated and dried over Na₂SO₄. The solvent was removed in vacuo. Yield 88% (1.31 g).

(*R*)-MISO-epoxide was synthesized in analogous manner to (*S*)-MISO-epoxide from (*S*)-epichlorohydrin. Yield 85% (1.26 g)

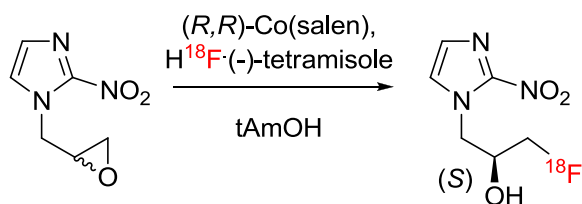


Scheme 61.

1-Chloro-3-fluoropropan-2-ol Epichlorohydrine (1.0 g, 10.8 mmol, 1.0 eq.) was reacted with TREAT HF (1.77 mL, 10.8 mmol, 1.0 eq.) in a sealed test tube for 2 h at 130 °C. After this time the ampule was opened and the reaction mixture was crashed with a mixture of ice (10 g) and ammonia hydroxide solution (30%, 10 mL), then washed with Et₂O (3x15 mL). The organic phase was washed with aqueous HCl (1 N, 10 mL), and dried over Na₂SO₄. Removing of solvent and distillation of residues in kugelrohr (10 mbar, 90 °C) gave the desired chlorofluorohydrine in 88% yield (1.07 g).

FMISO reference material Dry DMF (5 mL) was added to a mixture of 2-nitroimidazole (500 mg 4.4 mmol, 1.0 eq.) and KO^tBu (490 mg 4.4 mmol, 1.0 eq.) with stirring. The reaction mixture was heated to 130 °C for 15 min, after which the mixture was cooled to 80 °C and potassium iodide (1 mg, <0.01 eq.) with 1-chloro-3-fluoropropan-2-ol (680 mg, 5.9 mmol, 1.3 eq.) was added. The mixture was stirred for 1 h at 130 °C. The solvent was then evaporated. The obtained solid was purified by column chromatography, using EtOAc/CHCl₃ gradient(70/30 to 100) to afford pure FMISO as an off-white solid (80%, 505 mg)

Radiofluorination of MISO-epoxide



Scheme 62.

A 10 mL glass reaction vial was charged with (R,R)Co(salen) (4.5 mg, 0.25 equiv., 0.0075 mmol) and HFIP (250 ml). The resulting slurry was stirred for 5 min under air followed by the addition of MISO-epoxide (5.0 mg, 1.0 equiv., 0.030 mmol) and the solution of [¹⁸F]HF(-)-tetramisole (0.6 mg, 0.003 mmol, 0.1 eq.) in tAmOH (3 mL). The reaction vial was heated to 50–65 °C. After 10 min the vial was opened and the reaction mixture was analyzed and purified as described further down.

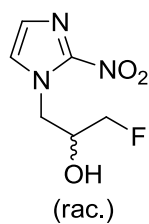
Purification of [¹⁸F]FMISO

The reaction mixture (1 mL solution in tAmOH) was loaded onto Supelco (irreg. SiO₂, 40-60 μm, 4 g) silica cartridge, preconditioned with hexane. The cartridge was washed with hexane (20 ml), CH₂Cl₂ (20 ml),

and CH_2Cl_2 / MeCN 3:1 (20 ml). Another portion of CH_2Cl_2 / MeCN 3:1 (20 ml) was collected and the solvent was removed with a flow of argon under vacuo. The residue was dissolved in 3 ml of sterile saline solution for injections and filtered through a sterile filter (0.22 μm).

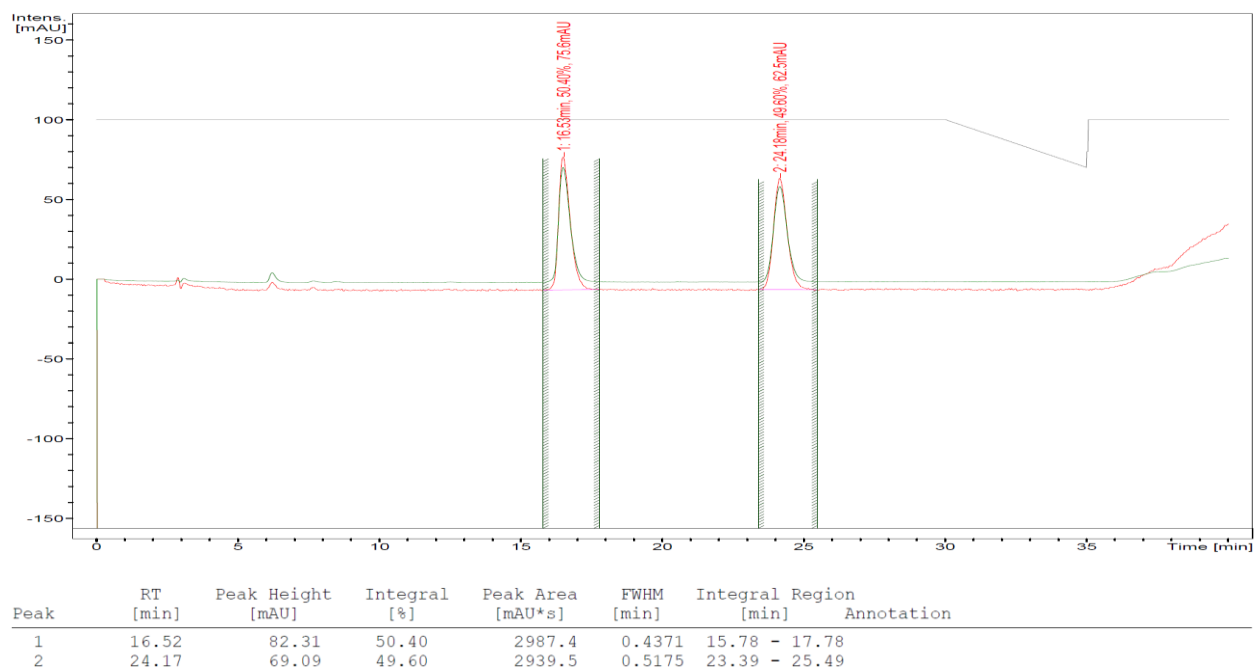
Chiral HPLC traces

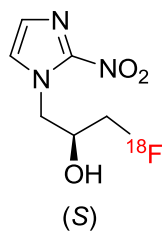
Chiral HPLC/radioHPLC was done using Chiralpak AD-3, 150 mm x 2.1 mm column using hexane-iPrOH (10% iPrOH volume) isocratic elution (flow rate 0.150 ml/min)



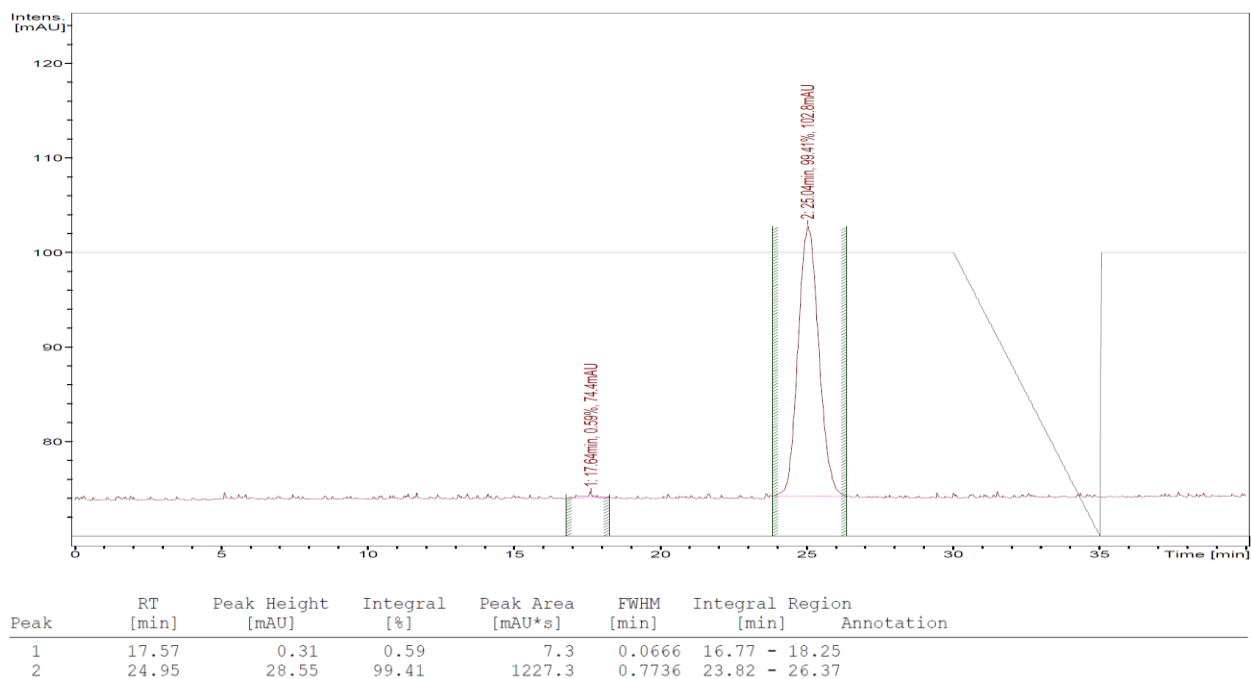
Racemic FMISO (reference standard), 0% ee

HPLC-UV trace (254 nm, 220-600 nm)

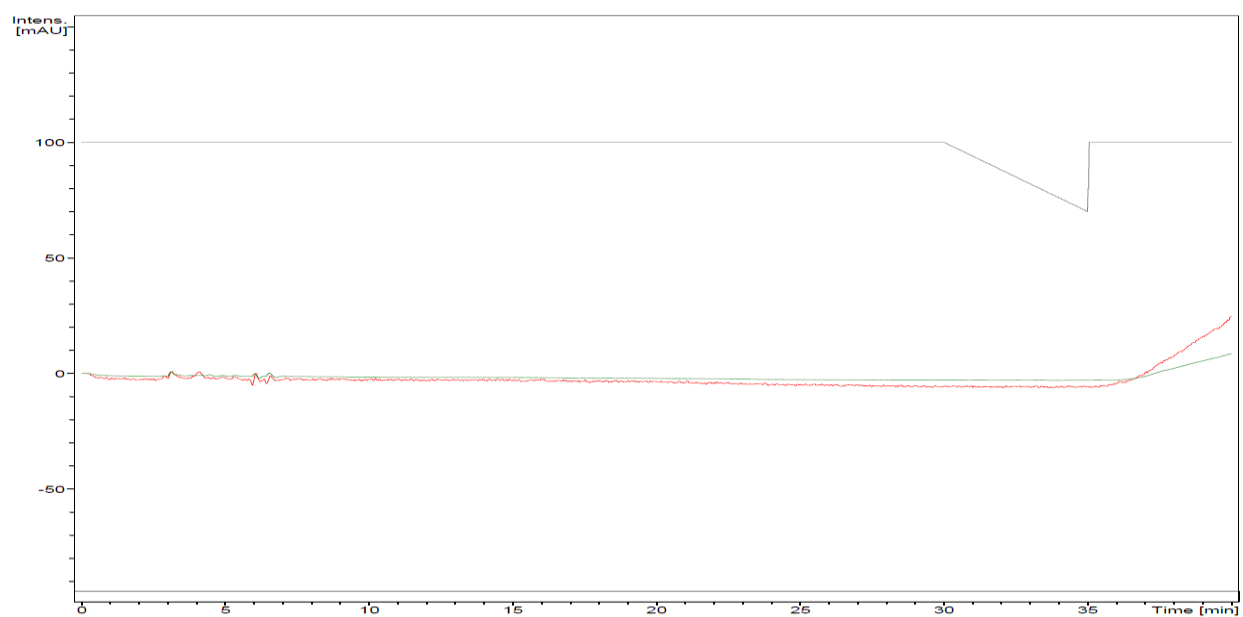


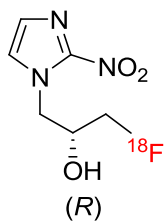


>99% ee, HPLC radiotrace

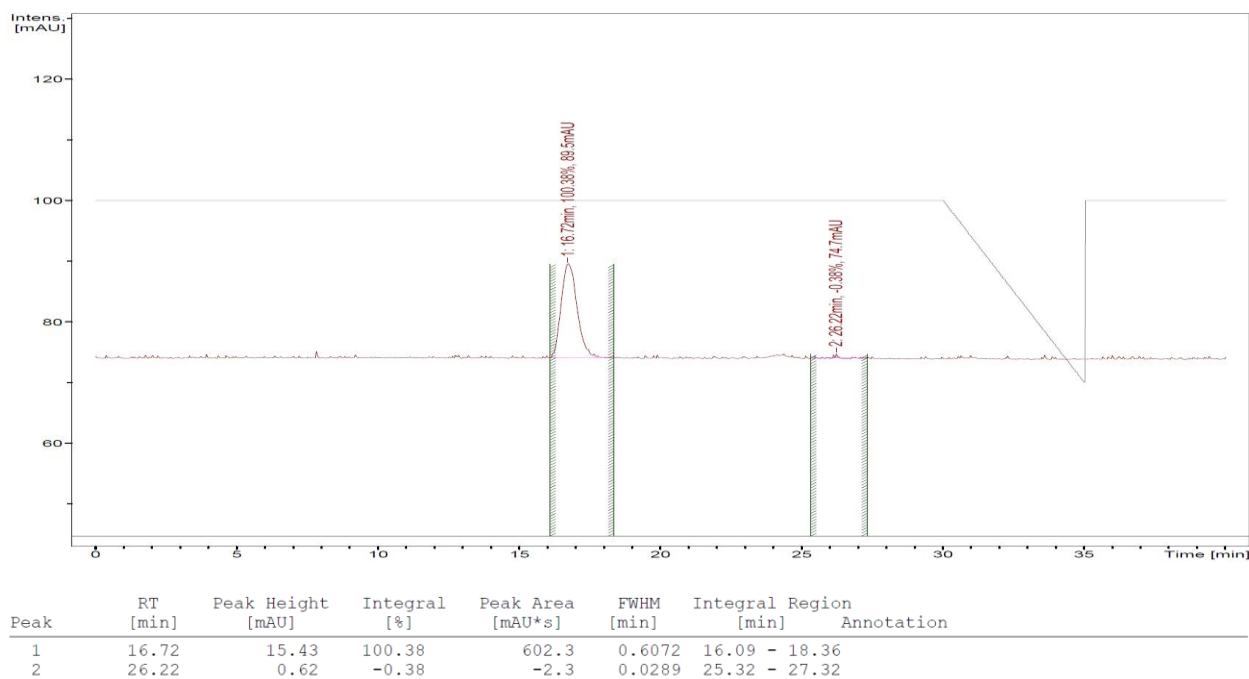


HPLC-UV trace

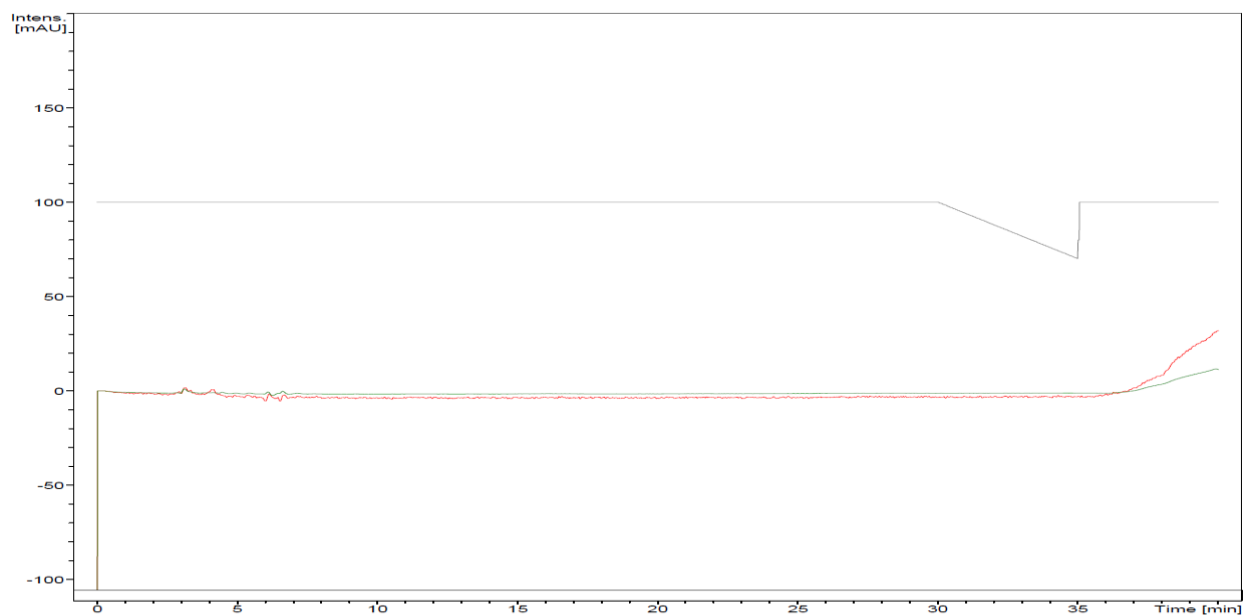




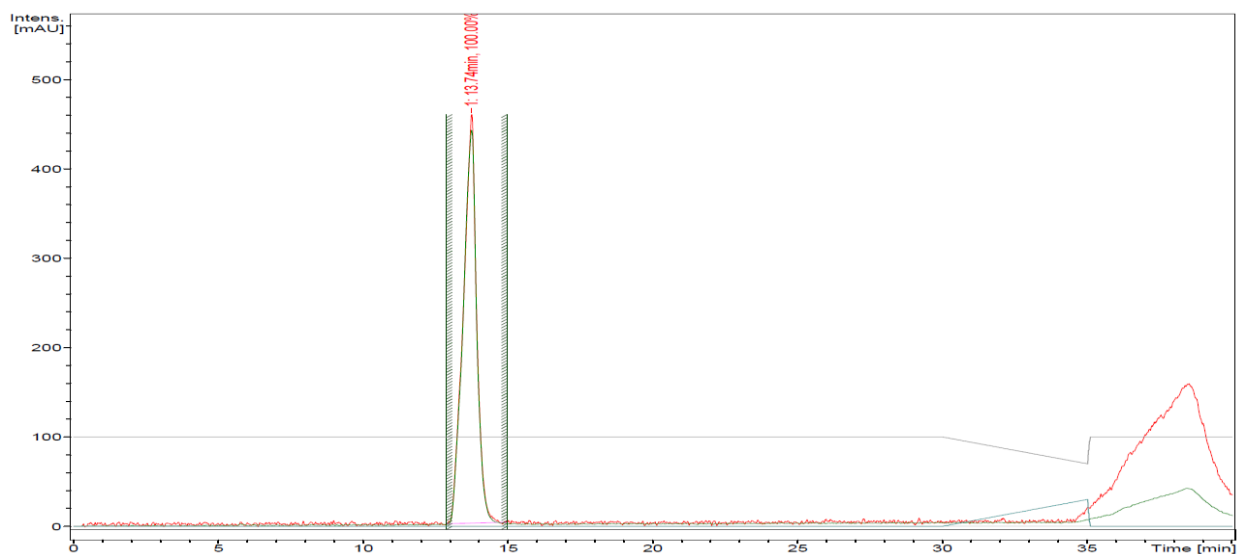
>99% ee, HPLC radiotrace



HPLC-UV trace

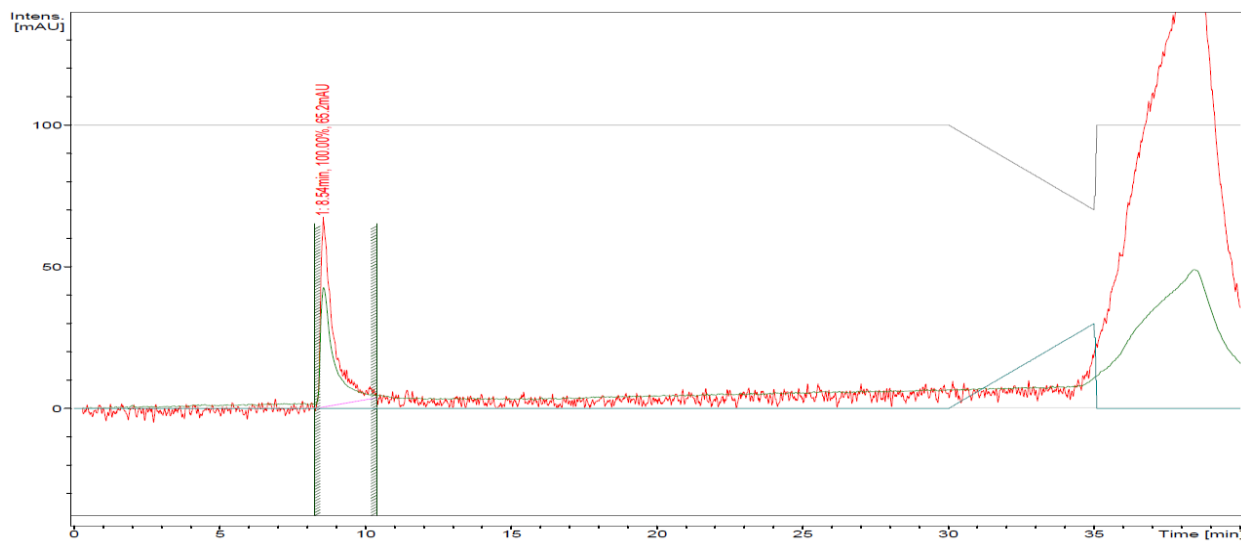


MISO-epoxide (reference)



Peak	RT [min]	Peak Height [mAU]	Integral [%]	Peak Area [mAU*s]	FWHM [min]	Integral Region [min]	Annotation
1	13.71	457.24	100.00	18370.3	0.4687	12.88 - 14.97	

(-)-tetramisole (reference)

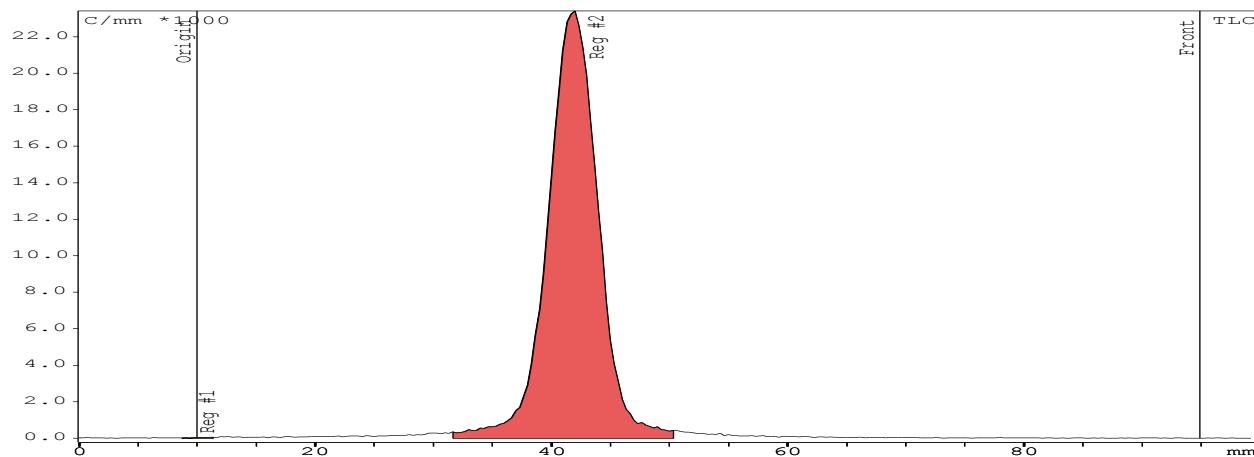


Peak	RT [min]	Peak Height [mAU]	Integral [%]	Peak Area [mAU*s]	FWHM [min]	Integral Region [min]	Annotation
1	8.51	64.76	100.00	2493.0	0.3696	8.25 - 10.38	

Purity tests

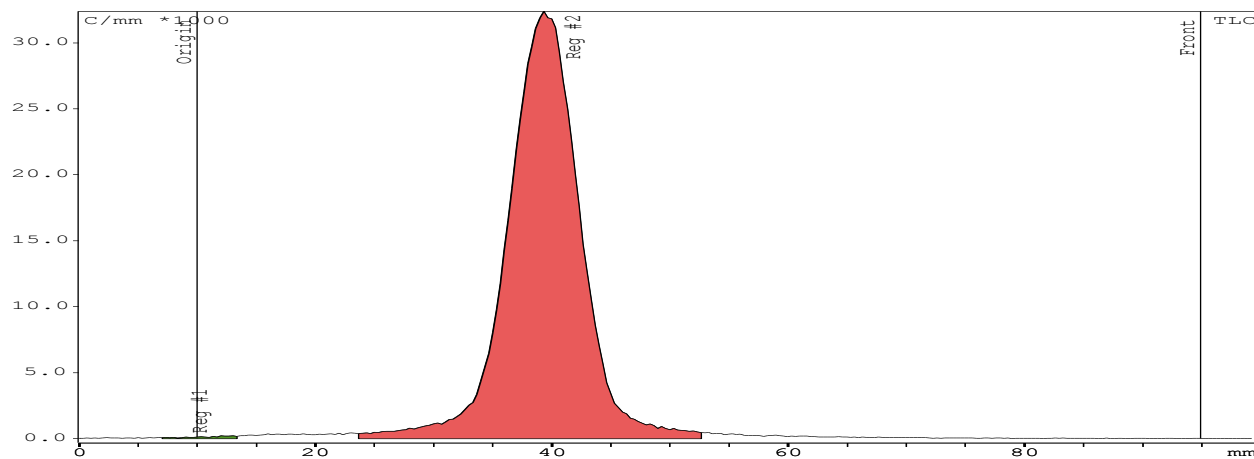
(normal SiO₂ plates, CHCl₃-CH₃CN 3:7)

(*R*)-[¹⁸F]FMISO



Substance	R/F	%Area
Reg #1	0.01	0.08
Reg #2	0.38	99.92

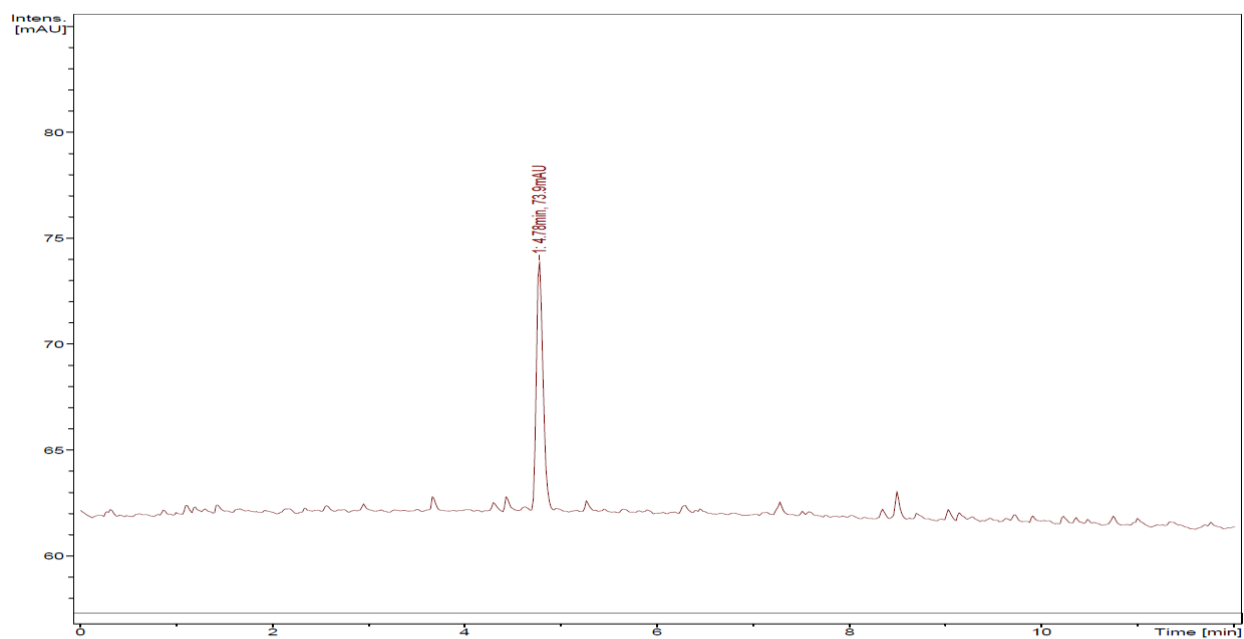
(*S*)-[¹⁸F]FMISO



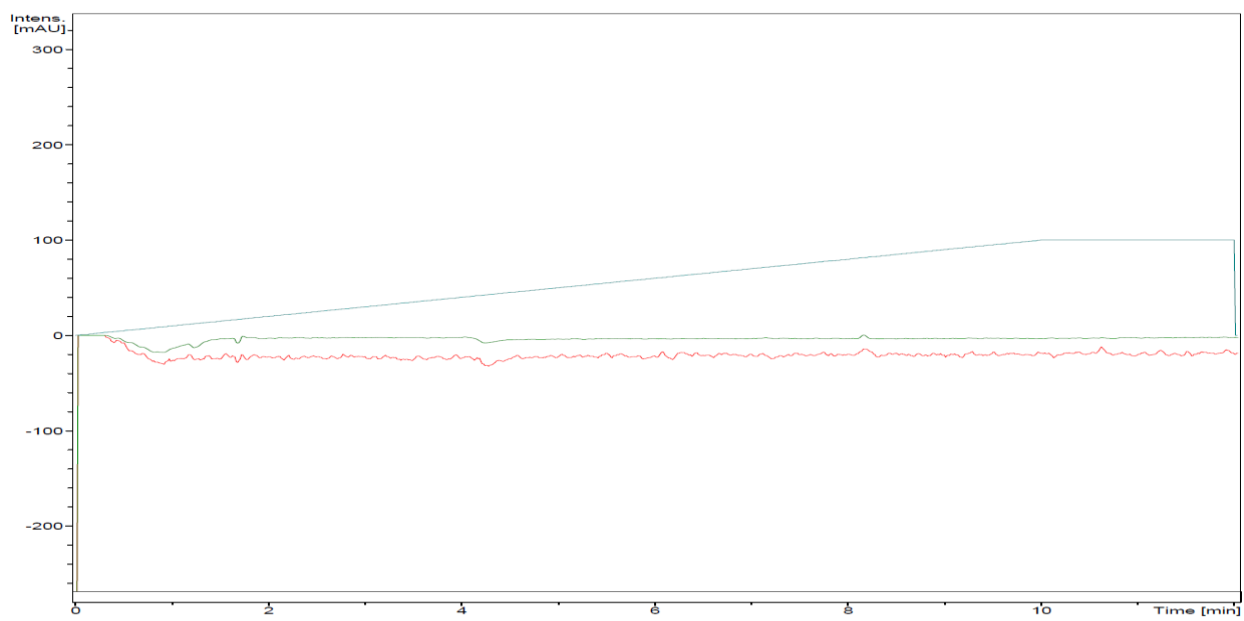
Substance	R/F	%Area
Reg #1	0.00	0.34
Reg #2	0.35	99.66

(R)-[¹⁸F]FMISO

HPLC radiotrace

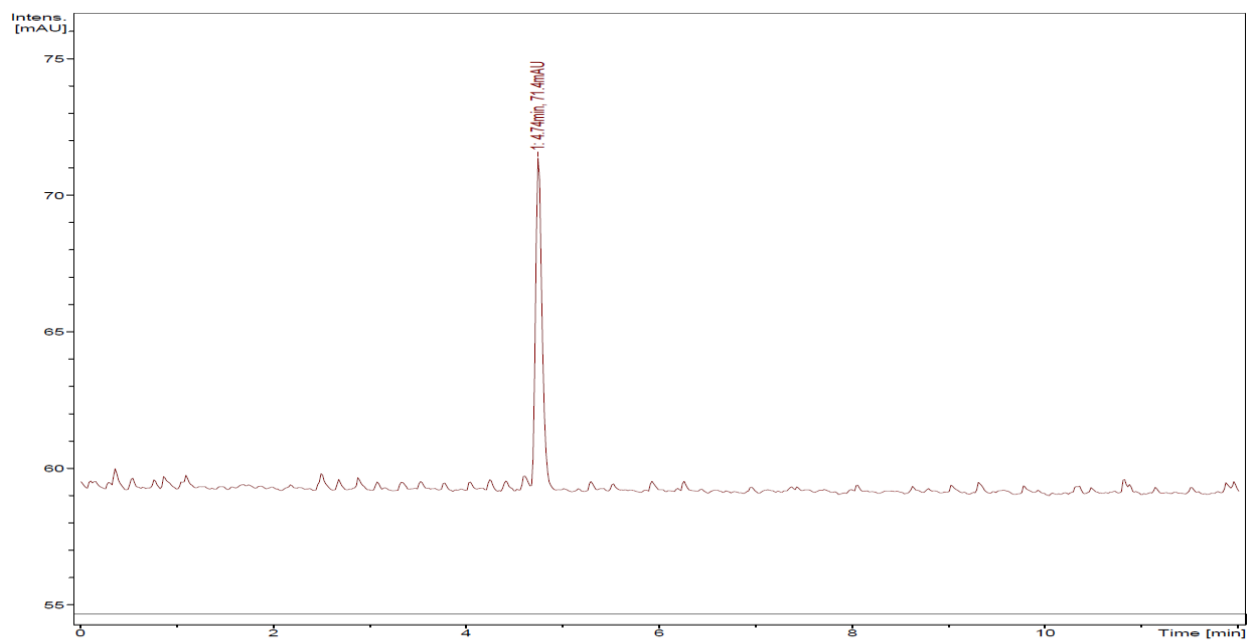


HPLC-UV trace

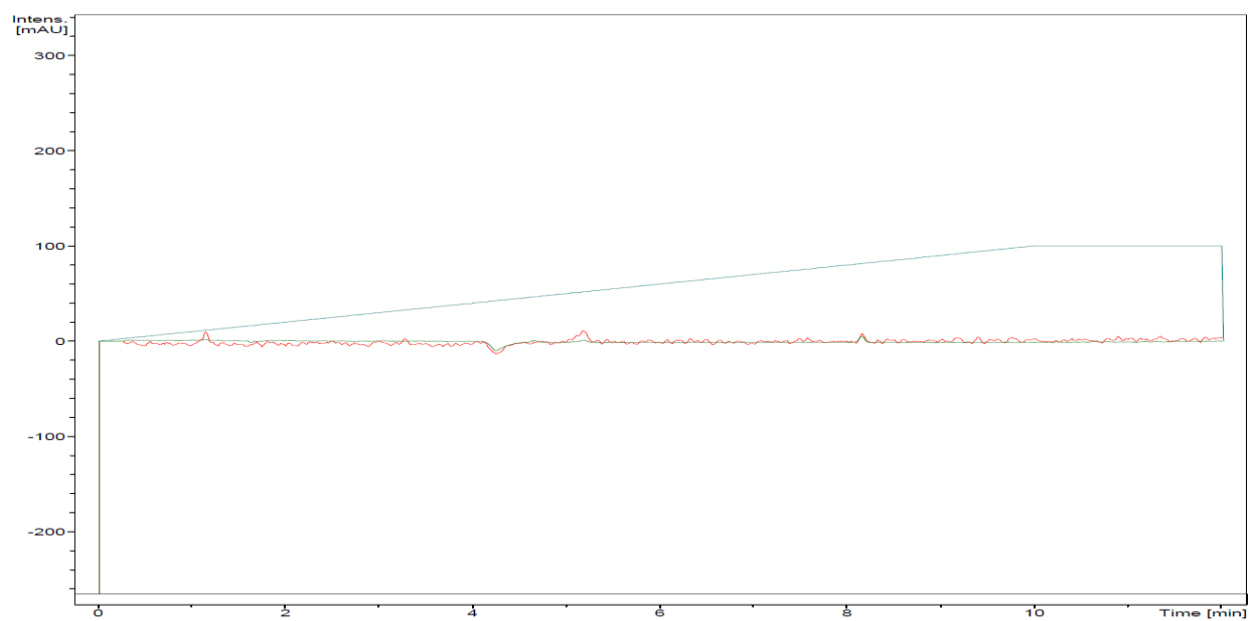


(S)-[¹⁸F]FMISO

HPLC radiotrace



HPLC-UV trace



3.4 In vivo studies

Preliminary studies

The in vivo studies were performed by our collaborators from the Panum institute – Dr. Jesper Tranekjær Jørgensen from the group of Prof. Andreas Kjaer.

Two separate studies were performed in one. The mice were divided into two groups, 5 mice in each group (mouse average mass 26.2 g) with two FaDu tumors (average size 489 mm³, in range from 65 mm³ to 1080 mm³) were injected with *R* and *S* [¹⁸F]FMISO solutions (4.91±0.55 MBq ((*R*)-[¹⁸F]FMISO) and 4.55±0.77 MBq ((*S*)-[¹⁸F]FMISO)) made in our group. After a waiting period (1.5 h and 4 h after injection, instead of preferred 1 h and 3 h) the distribution of [¹⁸F]FMISO in the mice was measured via a PET scanner. This timing is important to ensure that the tracer has equilibrated proportionally to the partition coefficient in blood and tissue¹²¹.

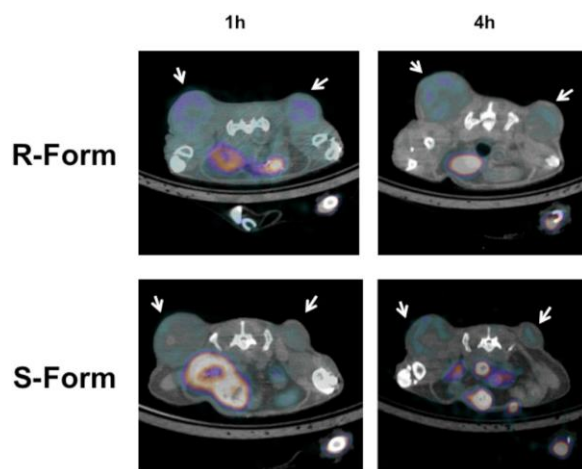


Figure 2613.

The counts were corrected for decay, counting efficiency, tissue weight and injected dose. Regions of interest were drawn on all scans on tumors, sections of muscle and liver tissue and %ID/g, tumor-to-muscle (T/M) and tumor-to-liver (T/L) ratios calculated.





Figure 27.

Due to some technical problems with the PET-CT scanner, the time between injection and scan was different for the *R* and *S* isomer (average time for *S* injected 83.8 min (from 63 to 100 min) and 93.4 for the *R*-injected (from 88 to 99 min))

This scan showed a slightly higher tumor uptake for the *R*-form, also a higher uptake was observed in muscles. Tumor-to-muscle ratio, however, was higher for the *S*-form.

The second scan (*S*-form average time 271.8 min (from 256 to 291 min), the *R*-form average time 286.8 min (from 278 to 293 min)) also showed a higher tumor uptake for *R*-isomer, while almost no difference between liver and muscles uptakes was observed.

Because of the PET-CT instrument problems resulted in scattered time between injection and scans, we used this data set as the preliminary observations. Also, the dispersion in tumor size was immense – from 65 to 1080 mm³. Big tumors showed an absence of [¹⁸F]FMISO in the center of the tumor – this will lead to incorrect %ID/g numbers

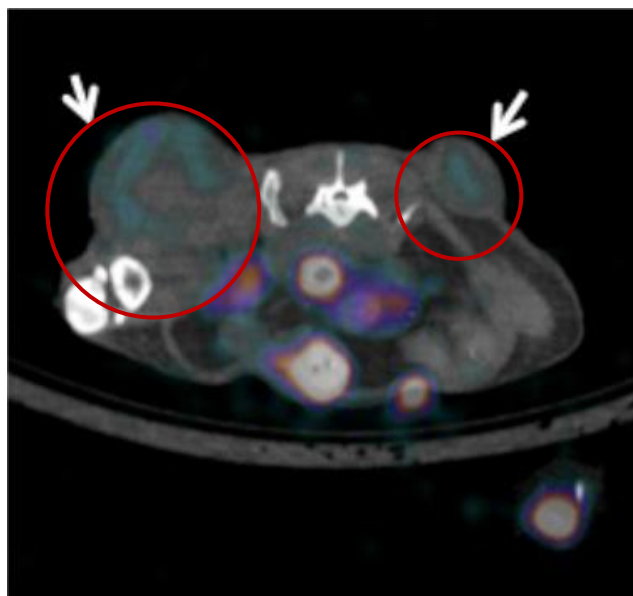


Figure 28. The cross section showing different action of big (left) and small (right) tumors – no radiotracer in the center of the left tumor was observed.

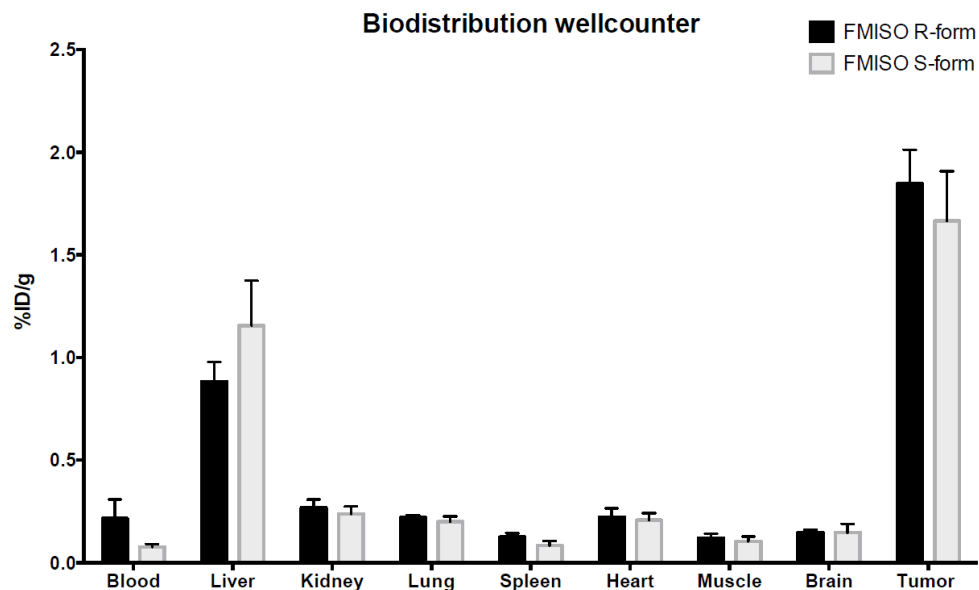


Figure 29.

The well counter data showed more or less the same situation with distribution of [¹⁸F]FMISO in different tissues. As a conclusion we can say that the behavior of these two isomers seems to be almost the same.

Second set

Our second attempt was done more accurately – the difference of periods between injection and scans was minimal (63.0 ± 6.2 min and 183.4 ± 3.8 min), also tumors were more or less equal in size, [¹⁸F]FMISO was distributed evenly in a tumor.

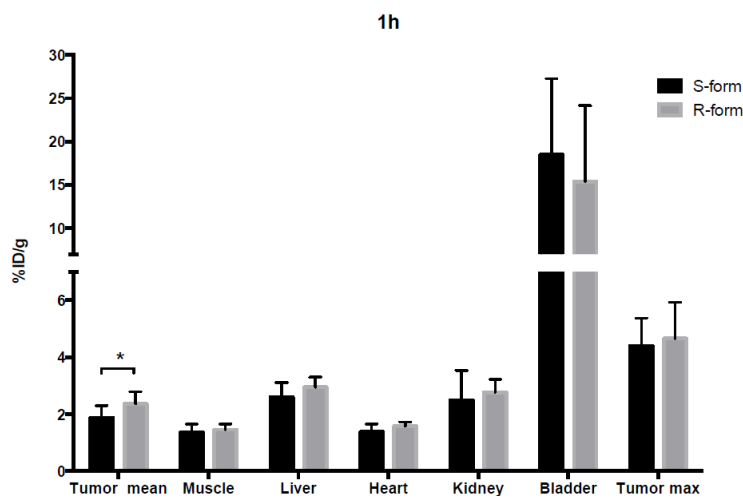


Figure 30.

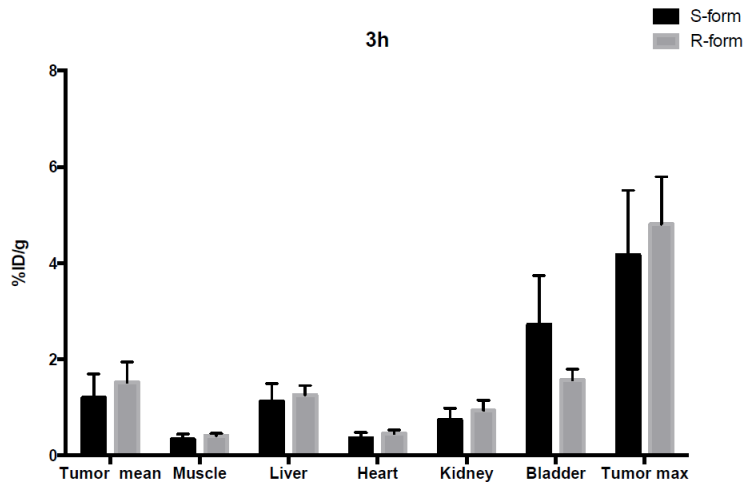


Figure 31.

PET-CT tracer uptake of the two stereoisomers showed no significant difference between the R and the S-form of [^{18}F]FMISO

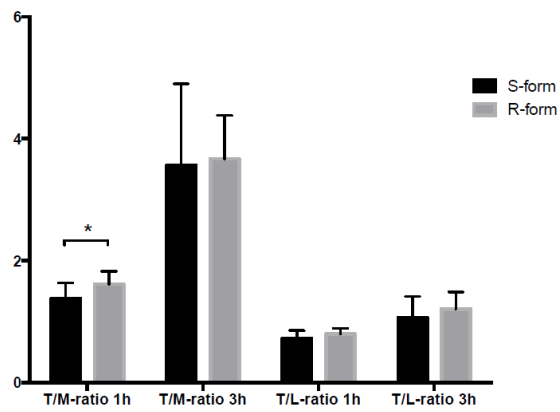


Figure 32.

The well counter data shows more or less the same distribution as the PET-scans data.

Dynamic PET scans

For the dynamic FMISO scans another set of the experiment was performed. Two groups of mice, three in each group were PET scanned for 2 hours; acquisition was started 12-20 seconds before the mice were injected with [^{18}F]FMISO solutions.

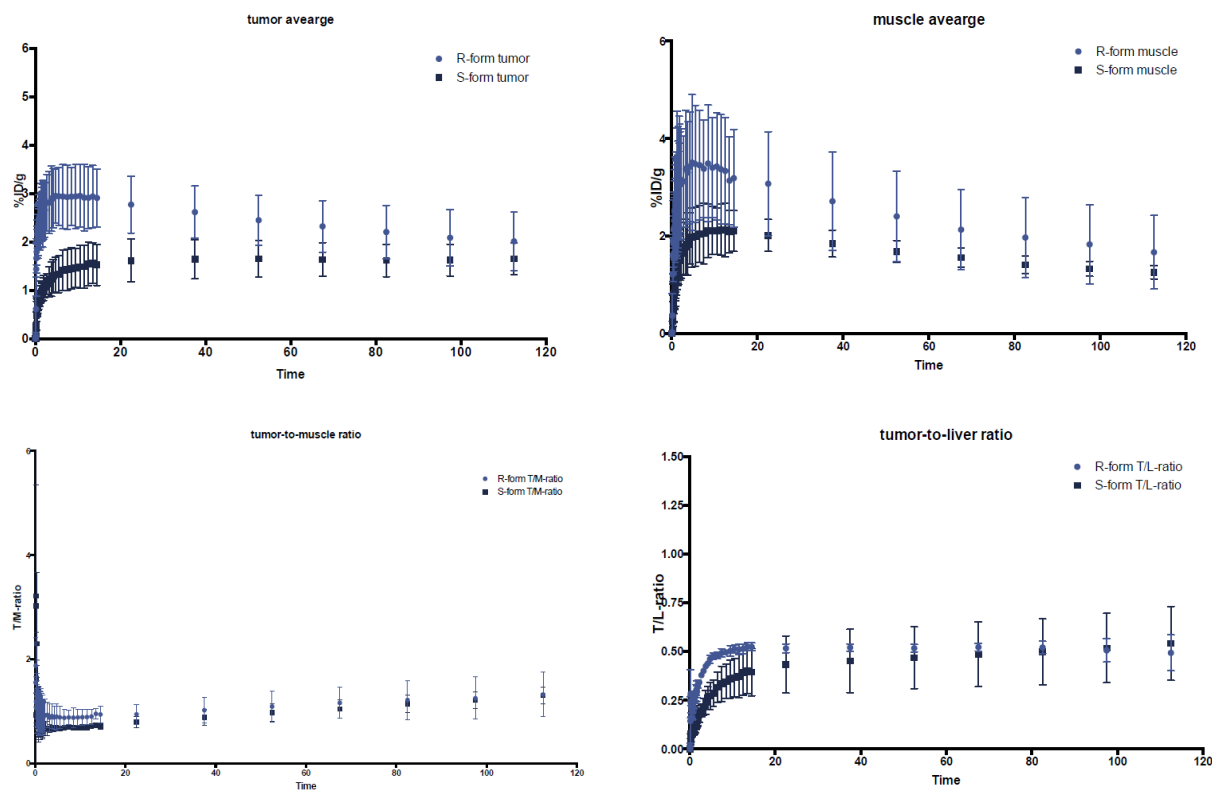


Figure 33.

In most of the tissues there are no differences between the time activity curves (TACs) of the R- and the S-form, but in the tumor and muscle tissues there appears to be a tendency that the early uptake of the R-form is higher than the S-form (Figure 33). The difference decreases over the experiment and as the increased uptake applies for both tumor and muscle tissue there are no difference in tumor-to-muscle ratio. Some kind of difference between the two enantiomers could be observed, but it is negligible.

Conclusions

In the presented work the enantioselective Co(salen)-mediated no-carrier-added radiofluorination of epoxides has been achieved for the first time. The procedure employs [^{18}F]HF_{gas}, as an efficient source of nucleophilic ^{18}F -fluoride.

A number of model *meso*-epoxides were successfully radiofluorinated producing ^{18}F -fluorohidrines in high RCC and RCY, and modest enantioselectivity. The developed procedure is simple, rapid and leads itself to easy automation.

This methodology was adopted for the first automated enantioselective single step radiosynthesis of PET hypoxia radiotracer [^{18}F]FMISO in 81% RCY and 55% enantioselectivity. The use of enantiopure substrates for the synthesis of both enantiomers allowed us to obtain the (S) and (R)-[^{18}F]FMISO enantiomers with > 99% enantiopurity.

Quantitative and pharmacokinetic data were obtained for the first time for the both enantiomers of [^{18}F]FMISO. The *R*-form showed higher uptake in tumor as well as in muscle tissues, thus displaying nearly identical tumor-to muscle ratios and showing very similar imaging properties of both the (S) and (R)-[^{18}F]FMISO.

References

1. Schwaiger, M.; Ziegler, S.; Nekolla, S. G., PET/CT: challenge for nuclear cardiology. *Journal of Nuclear Medicine* **2005**, *46* (10), 1664-1678.
2. Glaser, M.; Luthra, S. K.; Brady, F., Applications of positron-emitting halogens in PET oncology (Review). *International journal of oncology* **2003**, *22* (2), 253-268.
3. Luyten, P.; Marien, A.; Heindel, W.; Van Gerwen, P.; Herholz, K.; Den Hollander, J.; Friedmann, G.; Heiss, W., Metabolic imaging of patients with intracranial tumors: H-1 MR spectroscopic imaging and PET. *Radiology* **1990**, *176* (3), 791-799.
4. Roelcke, U.; Leenders, K. L., PET in neuro-oncology. *Journal of cancer research and clinical oncology* **2001**, *127* (1), 2-8.
5. Morrish, P.; Sawle, G.; Brooks, D., An [18F] dopa-PET and clinical study of the rate of progression in Parkinson's disease. *Brain* **1996**, *119* (2), 585-591.
6. Levin, C. S., Primer on molecular imaging technology. *European journal of nuclear medicine and molecular imaging* **2005**, *32* (2), S325-S345.
7. Schindler, T. H.; Schelbert, H. R.; Quercioli, A.; Dilsizian, V., Cardiac PET imaging for the detection and monitoring of coronary artery disease and microvascular health. *JACC: Cardiovascular Imaging* **2010**, *3* (6), 623-640.
8. Schelbert, H. R.; Beanlands, R.; Bengel, F.; Knuuti, J.; DiCarli, M.; Machac, J.; Patterson, R., PET myocardial perfusion and glucose metabolism imaging: Part 2-Guidelines for interpretation and reporting. *Journal of nuclear cardiology* **2003**, *10* (5), 557-571.
9. Nitzsche, E. U.; Choi, Y.; Czernin, J.; Hoh, C. K.; Huang, S.-C.; Schelbert, H. R., Noninvasive Quantification of Myocardial Blood Flow in Humans A Direct Comparison of the [13N] Ammonia and the [15O] Water Techniques. *Circulation* **1996**, *93* (11), 2000-2006.
10. Read, S.; Hirano, T.; Abbott, D.; Sachinidis, J.; Tochon-Danguy, H.; Chan, J.; Egan, G.; Scott, A.; Bladin, C.; McKay, W., Identifying hypoxic tissue after acute ischemic stroke using PET and 18F-fluoromisonidazole. *Neurology* **1998**, *51* (6), 1617-1621.
11. Nekolla, S. G.; Martinez-Moeller, A.; Saraste, A., PET and MRI in cardiac imaging: from validation studies to integrated applications. *European journal of nuclear medicine and molecular imaging* **2009**, *36* (1), 121-130.
12. Workman Jr, R. B.; Coleman, R. E., *PET/CT*. Springer: 2006.
13. Strauss, L. G.; Conti, P. S., The applications of PET in clinical oncology. *Journal of nuclear medicine: official publication, Society of Nuclear Medicine* **1991**, *32* (4), 623-48; discussion 649-50.
14. Chen, W., Clinical applications of PET in brain tumors. *Journal of nuclear medicine* **2007**, *48* (9), 1468-1481.
15. Tai, Y. F.; Piccini, P., PET in Clinical Neurology. In *Positron Emission Tomography*, Springer: 2006; pp 453-461.
16. Kuhl, D. E.; Minoshima, S.; Fessler, J. A.; Ficaro, E.; Wieland, D.; Koeppe, R. A.; Frey, K. A.; Foster, N. L., In vivo mapping of cholinergic terminals in normal aging, Alzheimer's disease, and Parkinson's disease. *Annals of neurology* **1996**, *40* (3), 399-410.
17. Tai, Y.; Piccini, P., Applications of positron emission tomography (PET) in neurology. *Journal of Neurology, Neurosurgery & Psychiatry* **2004**, *75* (5), 669-676.
18. Gould, M. K.; Maclean, C. C.; Kuschner, W. G.; Rydzak, C. E.; Owens, D. K., Accuracy of positron emission tomography for diagnosis of pulmonary nodules and mass lesions: a meta-analysis. *Jama* **2001**, *285* (7), 914-924.

19. Moog, F.; Bangerter, M.; Diederichs, C. G.; Guhlmann, A.; Kotzerke, J.; Merkle, E.; Kolokythas, O.; Herrmann, F.; Reske, S. N., Lymphoma: role of whole-body 2-deoxy-2-[F-18] fluoro-D-glucose (FDG) PET in nodal staging. *Radiology* **1997**, *203* (3), 795-800.
20. Kostakoglu, L.; Leonard, J. P.; Kuji, I.; Coleman, M.; Vallabhajosula, S.; Goldsmith, S. J., Comparison of fluorine-18 fluorodeoxyglucose positron emission tomography and Ga-67 scintigraphy in evaluation of lymphoma. *Cancer* **2002**, *94* (4), 879-888.
21. Shen, Y.-Y.; Kao, A.; Yen, R.-F., Comparison of 18F-fluoro-2-deoxyglucose positron emission tomography and gallium-67 citrate scintigraphy for detecting malignant lymphoma. *Oncology reports* **2002**, *9* (2), 321-325.
22. Spaepen, K.; Stroobants, S.; Verhoef, G.; Mortelmans, L., Positron emission tomography with [18F] FDG for therapy response monitoring in lymphoma patients. *European journal of nuclear medicine and molecular imaging* **2003**, *30* (1), S97-S105.
23. Friedman, K. P.; Wahl, R. L. In *Clinical use of positron emission tomography in the management of cutaneous melanoma*, Seminars in nuclear medicine, Elsevier: 2004; pp 242-253.
24. Yap, C. S.; Seltzer, M. A.; Schiepers, C.; Gambhir, S. S.; Rao, J.; Phelps, M. E.; Valk, P. E.; Czernin, J., Impact of whole-body 18F-FDG PET on staging and managing patients with breast cancer: the referring physician's perspective. *Journal of Nuclear Medicine* **2001**, *42* (9), 1334-1337.
25. Kau, R. J.; Alexiou, C.; Laubenbacher, C.; Werner, M.; Schwaiger, M.; Arnold, W., Lymph node detection of head and neck squamous cell carcinomas by positron emission tomography with fluorodeoxyglucose F 18 in a routine clinical setting. *Archives of Otolaryngology-Head & Neck Surgery* **1999**, *125* (12), 1322-1328.
26. Hannah, A.; Scott, A. M.; Tochon-Danguy, H.; Chan, J. G.; Akhurst, T.; Berlangieri, S.; Price, D.; Smith, G. J.; Schelleman, T.; McKay, W., Evaluation of 18F-fluorodeoxyglucose positron emission tomography and computed tomography with histopathologic correlation in the initial staging of head and neck cancer. *Annals of surgery* **2002**, *236* (2), 208.
27. Cohade, C.; Osman, M.; Leal, J.; Wahl, R. L., Direct comparison of 18F-FDG PET and PET/CT in patients with colorectal carcinoma. *Journal of Nuclear Medicine* **2003**, *44* (11), 1797-1803.
28. Diehl, M.; Risse, J. H.; Brandt-Mainz, K.; Dietlein, M.; Bohuslavizki, K. H.; Matheja, P.; Lange, H.; Bredow, J.; Körber, C.; Grünwald, F., Fluorine-18 fluorodeoxyglucose positron emission tomography in medullary thyroid cancer: results of a multicentre study. *European journal of nuclear medicine* **2001**, *28* (11), 1671-1676.
29. Eschmann, S.-M.; Paulsen, F.; Reimold, M.; Dittmann, H.; Welz, S.; Reischl, G.; Machulla, H.-J.; Bares, R., Prognostic impact of hypoxia imaging with 18F-misonidazole PET in non-small cell lung cancer and head and neck cancer before radiotherapy. *Journal of Nuclear Medicine* **2005**, *46* (2), 253-260.
30. Estrada, K., *Notes on Nuclear Medicine Imaging*. Lulu. com.
31. von Schulthess, G. K., *Molecular Anatomic Imaging: PET-CT and SPECT-CT Integrated Modality Imaging*. Lippincott Williams & Wilkins: 2007.
32. Gemmell, H. G.; Sharp, P. F.; Besson, J. A.; Ebmeier, K. P.; Smith, F. W., A comparison of Tc-99m HM-PAO and I-123 IMP cerebral SPECT images in Alzheimer's disease and multi-infarct dementia. *European journal of nuclear medicine* **1988**, *14* (9-10), 463-466.
33. Perret, J.; Prasher, S.; Kantzas, A.; Hamilton, K.; Langford, C., Preferential solute flow in intact soil columns measured by SPECT scanning. *Soil Science Society of America Journal* **2000**, *64* (2), 469-477.
34. McElroy, D.; Hoffman, E.; MacDonald, L.; Patt, B.; Iwanczyk, J.; Yamaguchi, Y.; Levin, C., Evaluation of breast tumor detectability with two dedicated, compact scintillation cameras. *Nuclear Science, IEEE Transactions on* **2002**, *49* (3), 794-802.
35. Bateman, T. M., Advantages and disadvantages of PET and SPECT in a busy clinical practice. *Journal of Nuclear Cardiology* **2012**, *19* (1), 3-11.
36. Badawi, R. Introduction to PET physics.

37. Ratib, O., PET/MRI: a new era in multimodality molecular imaging. *Clinical and Translational Imaging* **2013**, *1* (1), 5-10.
38. Necchi, M., Positron Emission Tomography: status of the art and future perspectives. *Scientifica Acta*, ISBN, 88-85159.
39. Halperin, E. C.; Brady, L. W.; Wazer, D. E.; Perez, C. A., *Perez & Brady's Principles and Practice of Radiation Oncology*. Lippincott Williams & Wilkins: 2013.
40. Sanchez-Crespo, A.; Andreo, P.; Larsson, S. A., Positron flight in human tissues and its influence on PET image spatial resolution. *European journal of nuclear medicine and molecular imaging* **2004**, *31* (1), 44-51.
41. Brownell, G. L.; Sweet, W. H., Localization of brain tumors with positron emitters. *Nucleonics* **1953**, *11* (11), 40-45.
42. Troyer, G.; Schenter, R., Medical isotope development and supply opportunities in the 21st century. *Journal of radioanalytical and nuclear chemistry* **2009**, *282* (1), 243-246.
43. Mohnike, W.; Hör, G.; Schelbert, H. R., *Oncologic and Cardiac PET/CT-Diagnosis: An Interdisciplinary Atlas and Manual*. Springer: 2008.
44. Keur, H. v. d., Medical Radioisotopes Production Without A Nuclear Reactor. *Laka Foundation* **2010**.
45. Chao, A., *Reviews of Accelerator Science and Technology: Medical Applications of Accelerators*. World Scientific Publishing Company, Incorporated: 2009.
46. IAEA, Cyclotron produced Radionuclides: principle and practice. .
47. Paans, A. M.; van Waarde, A.; Elsinga, P. H.; Willemsen, A.; Vaalburg, W., Positron emission tomography: the conceptual idea using a multidisciplinary approach. *Methods* **2002**, *27* (3), 195-207.
48. Vaalburg, W.; Kamphuis, J.; Beerling-Van Der Molen, H.; Reiffers, S.; Rijskamp, A.; Woldring, M., An improved method for the cyclotron production of ^{13}N -labelled ammonia. *The International journal of applied radiation and isotopes* **1975**, *26* (5), 316-318.
49. Wieland, B.; Bida, G.; Padgett, H.; Hendry, G.; Zippi, E.; Kabalka, G.; Morelle, J.-L.; Verbruggen, R.; Ghyoot, M., In-target production of ^{13}N ammonia via proton irradiation of dilute aqueous ethanol and acetic acid mixtures. *International journal of radiation applications and instrumentation. Part A. Applied radiation and isotopes* **1991**, *42* (11), 1095-1098.
50. Ter-Pogossian, M.; Powers, W., The use of radioactive oxygen-15 in the determination of oxygen content in malignant neoplasms. *Radioisotopes in scientific research. Londres: Pergamon* **1958**.
51. Ter-Pogossian, M.; Spratt, J. S.; Rudman, S.; Spencer, A., Radioactive oxygen 15 in study of kinetics of oxygen of respiration. *American Journal of Physiology--Legacy Content* **1961**, *201* (3), 582-586.
52. Diksic, M.; Reba, R. C., *Radiopharmaceuticals and Brain Pathophysiology Studied with Pet and Spect*. CRC Press: 1990.
53. Lambrecht, R. M.; Neirinckx, R.; Wolf, A., Cyclotron isotopes and radiopharmaceuticals—XXIII: Novel anhydrous ^{18}F -fluorinating intermediates. *The International Journal of Applied Radiation and Isotopes* **1978**, *29* (3), 175-183.
54. Casella, V.; Ido, T.; Wolf, A.; Fowler, J.; MacGregor, R.; Ruth, T., Anhydrous F-18 labeled elemental fluorine for radiopharmaceutical preparation. *Journal of nuclear medicine: official publication, Society of Nuclear Medicine* **1980**, *21* (8), 750.
55. Roberts, A.; Daniel, L.; Nickles, R., A high power target for the production of ^{18}F fluoride. *Nuclear Instruments and Methods in Physics Research Section B: Beam Interactions with Materials and Atoms* **1995**, *99* (1), 797-799.
56. Lewis, J. S.; Laforest, R.; Buettner, T. L.; Song, S.-K.; Fujibayashi, Y.; Connett, J. M.; Welch, M. J., Copper-64-diacetyl-bis (N4-methylthiosemicarbazone): An agent for radiotherapy. *Proceedings of the National Academy of Sciences* **2001**, *98* (3), 1206-1211.

57. Welch, M. J.; Redvanly, C. S., Handbook of radiopharmaceuticals. *Radiochemistry and Applications*. Wiley **2003**, 3.
58. García-Sosa, I.; Ramírez, F. D. M., Preliminary synthesis of 2-[¹⁸F]-FDG using ¹⁸F produced in the TRIGA MARK III nuclear reactor of Mexico. *Journal of radioanalytical and nuclear chemistry* **1993**, 173 (2), 239-247.
59. Gatley, S.; Hichwa, R.; Shaughnessy, W.; Nickles, R., ¹⁸F-labeled lower fluoroalkanes; Reactor-produced gaseous physiological tracers. *The International journal of applied radiation and isotopes* **1981**, 32 (4), 211-214.
60. Stöcklin, G.; Pike, V. W., *Radiopharmaceuticals for Positron Emission Tomography-Methodological Aspects*. Springer: 1993; Vol. 24.
61. Brodack, J. W.; Kilbourn, M. R.; Welch, M. J.; Katzenellenbogen, J. A., NCA 16α-[¹⁸F] fluoroestradiol-17β: The effect of reaction vessel on fluorine-18 resolubilization, product yield, and effective specific activity. *International Journal of Radiation Applications and Instrumentation. Part A. Applied Radiation and Isotopes* **1986**, 37 (3), 217-221.
62. Lee, Y.-S., Radiopharmaceuticals for Molecular Imaging. *Open Nuclear Medicine Journal* **2010**.
63. Reivich, M.; Kuhl, D.; Wolf, A.; Greenberg, J.; Phelps, M. a.; Ido, T.; Casella, V.; Fowler, J.; Hoffman, E.; Alavi, A., The [¹⁸F] fluorodeoxyglucose method for the measurement of local cerebral glucose utilization in man. *Circulation research* **1979**, 44 (1), 127-137.
64. Yu, S., Review of ¹⁸F-FDG synthesis and quality control. *Biomed Imaging Interv J* **2006**, 2 (4), 1-11.
65. Di Chiro, G.; Oldfield, E.; Wright, D. C.; De Michele, D.; Katz, D. A.; Patronas, N. J.; Doppman, J.; Larson, S.; Ito, M.; Kufta, C., Cerebral necrosis after radiotherapy and/or intraarterial chemotherapy for brain tumors: PET and neuropathologic studies. *American journal of roentgenology* **1988**, 150 (1), 189-197.
66. Doyle, W. K.; Budinger, T. F.; Valk, P. E.; Levin, V. A.; Gutin, P. H., Differentiation of cerebral radiation necrosis from tumor recurrence by [¹⁸F] FDG and ⁸²Rb positron emission tomography. *Journal of computer assisted tomography* **1987**, 11 (4), 563-570.
67. Patronas, N.; Di Chiro, G.; Brooks, R.; DeLaPaz, R.; Kornblith, P.; Smith, B.; Rizzoli, H.; Kessler, R.; Manning, R.; Channing, M., Work in progress:[¹⁸F] fluorodeoxyglucose and positron emission tomography in the evaluation of radiation necrosis of the brain. *Radiology* **1982**, 144 (4), 885-889.
68. Czernin, J.; Satyamurthy, N.; Schiepers, C., Molecular mechanisms of bone ¹⁸F-NaF deposition. *Journal of Nuclear Medicine* **2010**, 51 (12), 1826-1829.
69. Eidelberg, D.; Moeller, J.; Dhawan, V.; Sidtis, J.; Ginos, J.; Strother, S.; Cedarbaum, J.; Greene, P.; Fahn, S.; Rottenberg, D., The metabolic anatomy of Parkinson's disease: complementary [¹⁸F] fluorodeoxyglucose and [¹⁸F] fluorodopa positron emission tomographic studies. *Movement Disorders* **1990**, 5 (3), 203-213.
70. Namavari, M.; Bishop, A.; Satyamurthy, N.; Bida, G.; Barrio, J. R., Regioselective radiofluorodestannylation with [¹⁸F] F₂ and [¹⁸F] CH₃COOF: a high yield synthesis of 6-[¹⁸F] Fluoro-L-dopa. *International journal of radiation applications and instrumentation. Part A, Applied radiation and isotopes* **1992**, 43 (8), 989-996.
71. Been, L. B.; Suurmeijer, A. J.; Cobben, D. C.; Jager, P. L.; Hoekstra, H. J.; Elsinga, P. H., [¹⁸F] FLT-PET in oncology: current status and opportunities. *European journal of nuclear medicine and molecular imaging* **2004**, 31 (12), 1659-1672.
72. Lee, S. J.; Oh, S. J.; Chi, D. Y.; Kil, H. S.; Kim, E. N.; Ryu, J. S.; Moon, D. H., Simple and highly efficient synthesis of 3'-deoxy-3'-[¹⁸F] fluorothymidine using nucleophilic fluorination catalyzed by protic solvent. *European journal of nuclear medicine and molecular imaging* **2007**, 34 (9), 1406-1409.

73. Reischl, G.; Blocher, A.; Wei, R.; Ehrlichmann, W.; Kuntzsch, M.; Solbach, C.; Dohmen, B. M.; Machulla, H.-J., Simplified, automated synthesis of 3'[^18F] fluoro-3'-deoxy-thymidine ([^18F] FLT) and simple method for metabolite analysis in plasma. *Radiochimica Acta* **2006**, *94* (8), 447-452.
74. Nordberg, A.; Rinne, J. O.; Kadir, A.; Långström, B., The use of PET in Alzheimer disease. *Nature Reviews Neurology* **2010**, *6* (2), 78-87.
75. Hara, T.; Kondo, T.; Hara, T.; Kosaka, N., Use of 18F-choline and 11C-choline as contrast agents in positron emission tomography imaging-guided stereotactic biopsy sampling of gliomas. *Journal of neurosurgery* **2003**, *99* (3), 474-479.
76. Wester, H. J.; Herz, M.; Weber, W.; Heiss, P.; Senekowitsch-Schmidtke, R.; Schwaiger, M.; Stöcklin, G., Synthesis and radiopharmacology of O-(2-[18F] fluoroethyl)-L-tyrosine for tumor imaging. *Journal of nuclear medicine: official publication, Society of Nuclear Medicine* **1999**, *40* (1), 205-212.
77. Jerabek, P. A.; Patrick, T. B.; Kilbourn, M. R.; Dischino, D. D.; Welch, M. J., Synthesis and biodistribution of ¹⁸F-labeled fluoronitroimidazoles: Potential in vivo markers of hypoxic tissue. *International Journal of Radiation Applications and Instrumentation. Part A. Applied Radiation and Isotopes* **1986**, *37* (7), 599-605.
78. Piert, M.; Machulla, H.-J.; Picchio, M.; Reischl, G.; Ziegler, S.; Kumar, P.; Wester, H.-J.; Beck, R.; McEwan, A. J.; Wiebe, L. I., Hypoxia-specific tumor imaging with 18F-fluoroazomycin arabinoside. *Journal of Nuclear Medicine* **2005**, *46* (1), 106-113.
79. Lewis, J. S.; McCarthy, D. W.; McCarthy, T. J.; Fujibayashi, Y.; Welch, M. J., Evaluation of 64Cu-ATSM in vitro and in vivo in a hypoxic tumor model. *Journal of nuclear medicine: official publication, Society of Nuclear Medicine* **1999**, *40* (1), 177-183.
80. Kamlet, A. S.; Neumann, C. N.; Lee, E.; Carlin, S. M.; Moseley, C. K.; Stephenson, N.; Hooker, J. M.; Ritter, T., Application of Palladium-Mediated 18F-Fluorination to PET Radiotracer Development: Overcoming Hurdles to Translation. *PloS one* **2013**, *8* (3), e59187.
81. Tressaud, A.; Haufe, G., *Fluorine and Health: Molecular Imaging, Biomedical Materials and Pharmaceuticals*. Elsevier Science: 2008.
82. Mathiessen, B.; Jensen, M.; Zhuravlev, F., [18F] Fluoride recovery via gaseous [18F] HF. *Journal of Labelled Compounds and Radiopharmaceuticals* **2011**, *54* (13), 816-818.
83. Mathiessen, B.; Jensen, A. T.; Zhuravlev, F., Homogeneous nucleophilic radiofluorination and fluorination with phosphazene hydrofluorides. *Chemistry-A European Journal* **2011**, *17* (28), 7796-7805.
84. Kim, D. W.; Choe, Y. S.; Chi, D. Y., A new nucleophilic fluorine-18 labeling method for aliphatic mesylates: reaction in ionic liquids shows tolerance for water. *Nuclear medicine and biology* **2003**, *30* (4), 345-350.
85. Mulholland, G.; Mangner, T.; Jewett, D.; Kilbourn, M., Polymer-supported nucleophilic radiolabeling reactions with [18F] fluoride and [11C] cyanide ion on quaternary ammonium resins. *Journal of Labelled Compounds and Radiopharmaceuticals* **1989**, *26* (1-12), 378-380.
86. Toorongian, S. A.; Mulholland, G. K.; Jewett, D. M.; Bachelor, M. A.; Kilbourn, M. R., Routine production of 2-deoxy-2-[^18F] fluoro-d-glucose by direct nucleophilic exchange on a quaternary 4-aminopyridinium resin. *International journal of radiation applications and instrumentation. Part B. Nuclear medicine and biology* **1990**, *17* (3), 273-279.
87. Mathiessen, B.; Zhuravlev, F., Automated Solid-Phase Radiofluorination Using Polymer-Supported Phosphazenes. *Molecules* **2013**, *18* (9), 10531-10547.
88. Brandt, J. R.; Lee, E.; Boursalian, G. B.; Ritter, T., Mechanism of electrophilic fluorination with Pd (IV): fluoride capture and subsequent oxidative fluoride transfer. *Chemical Science* **2014**, *5* (1), 169-179.
89. Hollingworth, C.; Hazari, A.; Hopkinson, M. N.; Tredwell, M.; Benedetto, E.; Huiban, M.; Gee, A. D.; Brown, J. M.; Gouverneur, V., Palladium-Catalyzed Allylic Fluorination. *Angewandte Chemie International Edition* **2011**, *50* (11), 2613-2617.

90. Lee, E.; Kamlet, A. S.; Powers, D. C.; Neumann, C. N.; Boursalian, G. B.; Furuya, T.; Choi, D. C.; Hooker, J. M.; Ritter, T., A fluoride-derived electrophilic late-stage fluorination reagent for PET imaging. *Science* **2011**, *334* (6056), 639-642.
91. Barthazy, P.; Hintermann, L.; Stoop, R. M.; Wörle, M.; Mezzetti, A.; Togni, A., Carbon– Fluorine Bond Formation via a Five-Coordinate Fluoro Complex of Ruthenium (II), Preliminary Communication. *Helvetica Chimica Acta* **1999**, *82* (12), 2448-2453.
92. Barthazy, P.; Stoop, R. M.; Wörle, M.; Togni, A.; Mezzetti, A., Toward Metal-Mediated CF Bond Formation. Synthesis and Reactivity of the 16-Electron Fluoro Complex [RuF (dppp) 2] PF₆ (dppp= 1, 3-Bis (diphenylphosphino) propane). *Organometallics* **2000**, *19* (15), 2844-2852.
93. Hintermann, L.; Läng, F.; Maire, P.; Togni, A., Interactions of Cationic Palladium (II)-and Platinum (II)- η^3 -Allyl Complexes with Fluoride: Is Asymmetric Allylic Fluorination a Viable Reaction? *European journal of inorganic chemistry* **2006**, *2006* (7), 1397-1412.
94. Amatore, C.; Jutand, A.; Mensah, L.; Meyer, G.; Fiaud, J. C.; Legros, J. Y., Effect of the Leaving Group on the Rate and Mechanism of the Palladium-Catalyzed Isomerization of Cyclic Allylic Benzoates in Allylic Substitutions. *European journal of organic chemistry* **2006**, *2006* (5), 1185-1192.
95. Topczewski, J. J.; Tewson, T. J.; Nguyen, H. M., Iridium-Catalyzed Allylic Fluorination of Trichloroacetimidates. *Journal of the American Chemical Society* **2011**, *133* (48), 19318-19321.
96. Lee, E.; Hooker, J. M.; Ritter, T., Nickel-mediated oxidative fluorination for PET with aqueous [18F] fluoride. *Journal of the American Chemical Society* **2012**, *134* (42), 17456-17458.
97. Kalow, J. A.; Doyle, A. G., Mechanistic Investigations of Cooperative Catalysis in the Enantioselective Fluorination of Epoxides. *Journal of the American Chemical Society* **2011**, *133* (40), 16001-16012.
98. Bruns, S.; Haufe, G., Enantioselective introduction of fluoride into organic compounds: First asymmetric ring opening of epoxides by hydrofluorinating reagents. *Journal of Fluorine Chemistry* **2000**, *104* (2), 247-254.
99. Haufe, G.; Bruns, S.; Runge, M., Enantioselective ring-opening of epoxides by HF-reagents: Asymmetric synthesis of fluoro lactones. *Journal of Fluorine Chemistry* **2001**, *112* (1), 55-61.
100. Haufe, G.; Bruns, S., (Salen) chromium Complex Mediated Asymmetric Ring Opening of meso- and Racemic Epoxides with Different Fluoride Sources. *Advanced Synthesis & Catalysis* **2002**, *344* (2), 165-171.
101. Kalow, J. A.; Doyle, A. G., Enantioselective ring opening of epoxides by fluoride anion promoted by a cooperative dual-catalyst system. *Journal of the American Chemical Society* **2010**, *132* (10), 3268-3269.
102. Blackmond, D. G., Reaction progress kinetic analysis: a powerful methodology for mechanistic studies of complex catalytic reactions. *Angewandte Chemie International Edition* **2005**, *44* (28), 4302-4320.
103. Liang, T.; Neumann, C. N.; Ritter, T., Introduction of Fluorine and Fluorine-Containing Functional Groups. *Angewandte Chemie International Edition* **2013**, *52* (32), 8214-8264.
104. Hollingworth, C.; Gouverneur, V., Transition metal catalysis and nucleophilic fluorination. *Chemical Communications* **2012**, *48* (24), 2929-2942.
105. De Kleijn, J. P.; Seetz, J. W.; Zawierko, J. F.; Van Zanten, B., Labelling with reactor produced 18F—III.(1) Polymer supported 18F as a fluorinating agent. *The International Journal of Applied Radiation and Isotopes* **1977**, *28* (6), 591-594.
106. Olah, G. A.; Meidar, D., Synthetic Methods and Reactions. 43. Preparation of Fluorohydrins from Epoxides with Pyridinium Poly-hydrogen Fluoride. *Israel Journal of Chemistry* **1978**, *17* (1-2), 148-149.
107. Stevenson, C. P.; Nielsen, L. P.; Jacobsen, E. N., Preparation of (S)-Methyl Glycidate via Hydrolytic Kinetic Resolution. *Organic Syntheses* **2006**, 162-169.

108. Kim, D. W.; Ahn, D.-S.; Oh, Y.-H.; Lee, S.; Kil, H. S.; Oh, S. J.; Lee, S. J.; Kim, J. S.; Ryu, J. S.; Moon, D. H., A new class of SN2 reactions catalyzed by protic solvents: facile fluorination for isotopic labeling of diagnostic molecules. *Journal of the American Chemical Society* **2006**, *128* (50), 16394-16397.
109. Seco, J. M.; Quinoa, E.; Riguera, R., The assignment of absolute configuration by NMR. *Chemical reviews* **2004**, *104* (1), 17-118.
110. Seco, J. M.; Quiñoá, E.; Riguera, R., A practical guide for the assignment of the absolute configuration of alcohols, amines and carboxylic acids by NMR. *Tetrahedron: Asymmetry* **2001**, *12* (21), 2915-2925.
111. Wölker, D.; Haufe, G., Synthesis of optically active vicinal fluorohydrins by lipase-catalyzed deracemization. *The Journal of organic chemistry* **2002**, *67* (9), 3015-3021.
112. Zhao, H.; Pendri, A.; Greenwald, R. B., General procedure for acylation of 3 alcohols: Scandium triflate/DMAP reagent. *The Journal of organic chemistry* **1998**, *63* (21), 7559-7562.
113. Greenwald, R. B.; Pendri, A.; Zhao, H., High yield method for stereoselective acylation of tertiary alcohols. Google Patents: 2000.
114. Ciaccio, J. A.; Drahus, A. L.; Meis, R. M.; Tingle, C. T.; Smrtka, M.; Geneste, R., "Instant Methylide" Modification of the Corey-Chaykovsky Epoxide Synthesis. *Synthetic communications* **2003**, *33* (12), 2135-2143.
115. Ebner, C.; Müller, C. A.; Markert, C.; Pfaltz, A., Determining the enantioselectivity of chiral catalysts by mass spectrometric screening of their racemic forms. *Journal of the American Chemical Society* **2011**, *133* (13), 4710-4713.
116. Miller, P. W.; Long, N. J.; Vilar, R.; Gee, A. D., Synthesis of ¹¹C, ¹⁸F, ¹⁵O, and ¹³N radiolabels for positron emission tomography. *Angewandte Chemie International Edition* **2008**, *47* (47), 8998-9033.
117. Parker, C. A.; Matthews, J. C.; Gunn, R. N.; Martarello, L.; Cunningham, V. J.; Domett, D.; Knibb, S. T.; Bender, D.; Jakobsen, S.; Brown, J., Behaviour of [¹¹C] R (-)- and [¹¹C] S (+)-rolipram in vitro and in vivo, and their use as PET radiotracers for the quantitative assay of PDE4. *Synapse* **2005**, *55* (4), 270-279.
118. Smith, T. G.; Robbins, P. A.; Ratcliffe, P. J., The human side of hypoxia-inducible factor. *British journal of haematology* **2008**, *141* (3), 325-334.
119. Mees, G.; Dierckx, R.; Vangestel, C.; Van de Wiele, C., Molecular imaging of hypoxia with radiolabelled agents. *European journal of nuclear medicine and molecular imaging* **2009**, *36* (10), 1674-1686.
120. Archer, C. M.; Edwards, B.; Powell, N. A., Radiopharmaceuticals for imaging hypoxia. In *Current Directions in Radiopharmaceutical Research and Development*, Springer: 1996; pp 81-88.
121. Krohn, K. A.; Link, J. M.; Mason, R. P., Molecular imaging of hypoxia. *Journal of Nuclear Medicine* **2008**, *49* (Suppl 2), 129S-148S.
122. Lee, S. T.; Scott, A. M. In *Hypoxia Positron Emission Tomography Imaging With ¹⁸F-Fluoromisonidazole*, Seminars in nuclear medicine, Elsevier: 2007; pp 451-461.
123. Casciari, J.; Graham, M.; Rasey, J., A modeling approach for quantifying tumor hypoxia with [¹⁸F] fluoromisonidazole PET time-activity data. *Medical physics* **1995**, *22* (7), 1127-1139.
124. PET, A. I. P. E. T., Investigator's Brochure.
125. Machulla, H. J., *Imaging of Hypoxia: Tracer Developments*. Springer: 1999.
126. Jerabek, P.; Dischino, D.; Kilbourn, M.; Welch, M. In *SYNTHESIS OF F-18 LABELED 1-(2-NITRO-1-IMIDAZOYL)-3-FLUORO-2-PROPANOL, A HYPOXIC CELL RADIOSENSITIZER*, JOURNAL OF LABELLED COMPOUNDS & RADIOPHARMACEUTICALS, JOHN WILEY & SONS LTD BAFFINS LANE CHICHESTER, W SUSSEX, ENGLAND PO19 1UD: 1984; pp 1234-1235.
127. Koh, W.-j.; Rasey, J. S.; Grierson, J. R.; Graham, M. M.; Modell, H. I.; Russell, K. J.; Griffin, T. W.; Krohn, K. A., Imaging tumor hypoxia using positron emission tomography imaging of [¹⁸F]

- fluoromisonidazole: A report of work during the astro research year. *International Journal of Radiation Oncology* Biology* Physics* **1989**, *17*, 198.
128. Kämäräinen, E. L.; Kyllönen, T.; Nihtilä, O.; Björk, H.; Solin, O., Preparation of fluorine-18-labelled fluoromisonidazole using two different synthesis methods. *Journal of Labelled Compounds and Radiopharmaceuticals* **2004**, *47* (1), 37-45.
129. McCarthy, T. J.; Dence, C. S.; Welch, M. J., Application of microwave heating to the synthesis of [¹⁸F] fluoromisonidazole. *Applied radiation and isotopes* **1993**, *44* (8), 1129-1132.
130. Patt, M.; Kuntzsch, M.; Machulla, H.-J., Preparation of [18 F] fluoromisonidazole by nucleophilic substitution on THP-protected precursor: yield dependence on reaction parameters. *Journal of radioanalytical and nuclear chemistry* **1999**, *240* (3), 925-927.
131. Grierson, J. R.; Link, J. M.; Mathis, C. A.; Rasey, J. S.; Krohn, K. A., A radiosynthesis of fluorine-18 fluoromisonidazole. *Journal of nuclear medicine : official publication, Society of Nuclear Medicine* **1989**, *30* (3), 343-50.
132. Hwang, D. R.; Pence, C.; Welch, M.; Shelton, M.; Bergmann, S., An improved synthesis of no-carrier-added 3-[18F]-fluoro-1-(2-nitro-1-imidazolyl)-2-propanol. *Journal of Labelled Compounds and Radiopharmaceuticals* **1989**, *26* (1-12), 442-444.
133. Hwang, D.-R.; Dence, C.; Bonasera, T.; Welch, M., No-carrier-added synthesis of 3-[¹⁸F] fluoro-1-(2-nitro-1-imidazolyl)-2-propanol. A potential PET agent for detecting hypoxic but viable tissues. *International Journal of Radiation Applications and Instrumentation. Part A. Applied Radiation and Isotopes* **1989**, *40* (2), 117-126.
134. Lim, J.; Berridge, M., Efficient radiosynthesis of [18 F] fluoromisonidazole suitable for routine PET. *J. Label. Compds. Radiopharm* **1993**, *22*, 541-543.
135. Lim, J.-L.; Berridge, M. S., An efficient radiosynthesis of [¹⁸F] fluoromisonidazole. *Applied radiation and isotopes* **1993**, *44* (8), 1085-1091.
136. Cherif, A.; Yang, D. J.; Tansey, W.; Kim, E. E.; Wallace, S., Rapid Synthesis of 3-[18 F] Fluoro-1-(2'-Nitro-1'-Imidazolyl)-2-Propanol ([18 F] Fluoromisonidazole). *Pharmaceutical research* **1994**, *11* (3), 466-469.
137. Tada, M.; Iwata, R.; Sugiyama, H.; Sato, K.; Kubota, K.; Kubota, R.; Takahashi, H.; Fukuda, H.; Ido, T., A concise one-pot synthesis of [18F] fluoromisonidazole from (2R)-(-)-glycidyl tosylate. *Journal of Labelled Compounds and Radiopharmaceuticals* **1996**, *38* (8), 771-774.
138. Tang, G.; Wang, M.; Tang, X.; Gan, M.; Luo, L., Fully automated one-pot synthesis of [¹⁸F] fluoromisonidazole. *Nuclear medicine and biology* **2005**, *32* (5), 553-558.
139. Padhani, A. R.; Krohn, K. A.; Lewis, J. S.; Alber, M., Imaging oxygenation of human tumours. *European radiology* **2007**, *17* (4), 861-872.
140. Ariens, E., Stereochemistry, a basis for sophisticated nonsense in pharmacokinetics and clinical pharmacology. *European journal of clinical pharmacology* **1984**, *26* (6), 663-668.
141. Dunphy, M. P.; Lewis, J. S., Radiopharmaceuticals in preclinical and clinical development for monitoring of therapy with PET. *Journal of Nuclear Medicine* **2009**, *50* (Suppl 1), 106S-121S.
142. Kilbourn, M. R.; Scott, P. J.; Hockley, B. G., *Radiochemical Syntheses, Radiopharmaceuticals for Positron Emission Tomography*. John Wiley & Sons: 2011; Vol. 1.
143. Weinmann, H.; Harre, M.; Koenig, K.; Merten, E.; Tilstam, U., Efficient and environmentally friendly synthesis of 2-amino-imidazole. *Tetrahedron letters* **2002**, *43* (4), 593-595.
144. Yap, S.; Woodman, O. L.; Crack, P. J.; Williams, S. J., Synthesis of a hypoxia-targeted conjugate of the cardioprotective agent 3', 4'-dihydroxyflavonol and evaluation of its ability to reduce ischaemia/reperfusion injury. *Bioorganic & medicinal chemistry letters* **2011**, *21* (17), 5102-5106.
145. SERCEL, A. D.; BEYLIN, V. G.; MARLATT, M. E.; LEJA, B.; HOLLIS SHOWALTER, H.; MICHEL, A., Synthesis of the enantiomers of the dual function 2-nitroimidazole radiation sensitizer RB 6145. *Journal of heterocyclic chemistry* **2006**, *43* (6), 1597-1604.

Appendix



Co(salen)-mediated enantioselective radiofluorination of epoxides. Radiosynthesis of enantiomerically enriched [^{18}F]F-MISO via kinetic resolution



Evgeny Revunov, Fedor Zhuravlev*

Hevesy Laboratory, Center for Nuclear Technologies, Technical University of Denmark, Frederiksborgvej 399, Building 202, Roskilde, Denmark

ARTICLE INFO

Article history:

Received 24 July 2013

Received in revised form 30 August 2013

Accepted 11 September 2013

Available online 20 September 2013

Keywords:

Radiofluorination

Metal mediated

F-MISO

PET

[^{18}F]

ABSTRACT

The first example of transition metal mediated enantioselective radiofluorination of epoxides is reported. The procedure utilizes gaseous [^{18}F]HF in a combination with (–)tetramisole and (R,R)-Co(salen), giving the corresponding (S,S)- ^{18}F -fluorohydrines in 78–93% radiochemical yield (RCY) and 20–46% enantioselectivities (ee). The use of this methodology allowed for a single step radiosynthesis of [^{18}F]F-MISO, which took 1.5 h and after solid phase-based purification delivered [^{18}F]F-MISO in 81%/45% analytical/preparative RCY and 55% ee.

© 2013 Elsevier B.V. All rights reserved.

1. Introduction

The radioisotope fluorine-18, produced by the $^{18}\text{O}(p,n)^{18}\text{F}$ reaction, undergoes positron decay (97% β^+ , 649 keV) with a half-life of 109.7 min, making it possible to incorporate fluorine-18 into organic molecules via short radiosynthesis. Due to its low positron energy the resulting ^{18}F -labeled radiotracers typically yield excellent PET (positron emission tomography) images with the spatial resolution as high as 2 mm [1]. The favorable radioimaging properties of fluorine-18 are offset by its multi-step recovery and activation process. The high specific activity radionuclide is typically produced and extracted from water solution as potassium [^{18}F]fluoride-cryptand complex. As a result, radiofluorination is dominated by nucleophilic substitution chemistry of [^{18}F]fluoride [2,3]. In contrast, recent advances in transition metal mediated fluorination utilized a variety of fluoride sources and metal systems [4]. The substrate scope includes alkynes [5,6], alkyl- and allyl halides [7–9], trichloroacetimidates [10], carbonates, *p*-nitrobenzoates [9,11], aryl triflate [12], functionalized aryls [13–15], and epoxides. In particular, transition metal-mediated asymmetric hydrofluorination of epoxides, pioneered by Haufe [16–18] has been recently developed into a highly efficient catalytic system by Doyle and co-workers [19,20]. However with few notable exceptions

[9,10,21], the translation of transition metal mediated ^{19}F -chemistry into non carrier added (n.c.a.) ^{18}F -radiofluorination so far has been limited. Although the nucleophilic epoxide opening with [^{18}F]fluoride has received attention over the years the efficient reaction remains challenging and the yields vary significantly [22–25].

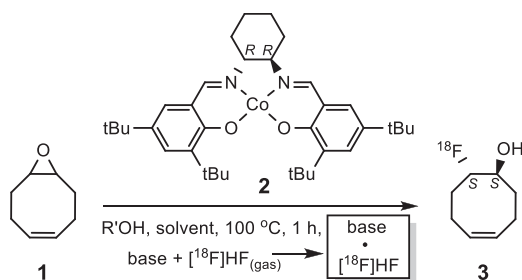
Recently reported entry into efficient production of [^{18}F]HF [26] and the use of [^{18}F]HF-base for radiofluorination [27] prompted us to investigate the extension of Co(salen)-mediated enantioselective hydrofluorination of epoxides [19,20] to the corresponding ^{18}F -hydrofluorination. Herein, we disclose the first example of n.c.a. enantioselective radiofluorination of epoxides and the kinetic resolution of important PET tracer [^{18}F]F-MISO using [^{18}F]HF and Co(salen)/chiral thiourea system under the n.c.a. radiofluorination conditions.

2. Results and discussion

In a preliminary experiment, [^{18}F]HF, produced by acidification of cyclotron-irradiated [^{18}O]water and trapped as [^{18}F](–)tetramisole hydrofluoride, was reacted with 9-oxabicyclo[6.1.0]non-4-ene **1** in the presence of chiral (R,R)-Co(salen) **2** and hexafluoroisopropanol (HFIP) in *tert*-butyl methyl ether (TBME) (Scheme 1).

After 1 h at 100 °C radio-TLC analysis indicated that the corresponding ^{18}F -fluorohydrin **3** was obtained in 78% RCY. The enantioselectivity was only 32%, as measured by the normal phase chiral radio-HPLC performed on a Chiralpak AD-3 column.

* Corresponding author. Tel.: +45 51529763.
E-mail address: fezh@dtu.dk (F. Zhuravlev).

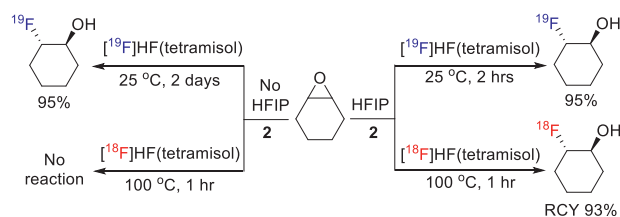


Scheme 1. Enantioselective ^{18}F -hydrofluorination of 9-oxabicyclo[6.1.0]non-4-ene using $[^{18}\text{F}]\text{HF}/(-)\text{-tetramisol-(R,R)-Co(salen)}$.

Lowering the reaction temperature to 75 °C led to an increase in enantioselectivity to 48% but the RCY of **3** dropped to 25%. No reaction was observed at room temperature. We have also noticed that HFIP, used in the earlier work to facilitate the release of HF from benzoyl fluoride [19,20], was essential for successful radiofluorination. A control experiment where $[^{18}\text{F}]\text{HF}$ was introduced into the reaction mixture *without* HFIP yielded no ^{18}F -fluorohydrin **3** (Table 1, entry 2).

Other alcohols and phenols, varying in acidity and steric bulk were markedly less effective than HFIP (Table 1, entries 3–7). Although the role of hydroxylic additives is unclear at the moment, there seemed to be a pronounced “fluorous” effect, as the RCY increased to various degrees when the fluorinated analogs were used (Table 1, entries 3 vs. 1, 4 vs. 5, and 6 vs. 7). To rule out the carrier effect due to possible traces of cold fluoride or HF in HFIP, the latter was carefully purified by a sequential passing through basic alumina and silica, followed by vacuum distillation. This purification had no discernible effect on either the RCY or the specific activity of the product (Table 1, entry 10). The pK_a of the protic additives did not seem to play the major role in the “fluorous” effect as phenol ($\text{pK}_a = 10$) remained inferior to HFIP ($\text{pK}_a = 9.3$, Table 1, entries 1 and 6.) In our hands, the pre-oxidized forms of the catalyst obtained either by using (salen)Co(III)OTs or by $t\text{BuOOH}$ oxidation of (salen)Co(II) [19] were ineffective in the absence of HFIP. The effect of HFIP was also prominent under the cold conditions: the freshly prepared (tetramisole)- $[^{19}\text{F}]\text{HF}$ used in combination with **2** gave the desired fluorocyclohexanol in 95% yield within 2 h. Without HFIP the reaction took two days to reach the same level of conversion (Scheme 2). Based on these observations we believe that HFIP kinetically facilitates hydrofluorination by acting on one or more catalytic Co(salen) species.

Screening of a few nitrogen bases revealed that $(-)\text{-tetramisol}$ was the only effective base as other bases yielded no ^{18}F -hydrofluorination products (Table 1, entry 8). We have also



Scheme 2. The effect of HFIP on enantioselective $^{19/18}\text{F}$ -hydrofluorination of cyclohexene oxide using the $[^{19/18}\text{F}]\text{HF}/(-)\text{-tetramisol-(R,R)-Co(salen)}$ system.

confirmed the strong cooperative effect of Co(salen)/base on RCY and enantioselectivity observed earlier [19,20]. The mismatched enantiomer *ent*-(*S,S*)-**2** gave the *ent*-**3** in only 36% RCY and 27% ee. Changing the solvent from TBME to 2-methyl-2-butanol (*t*AmOH) resulted in lower yield but higher enantioselectivity (Table 1, entry 9).

The substrate scope of ^{18}F -hydrofluorination was investigated by reacting a substrate with a mixture of $[^{18}\text{F}](-)\text{-tetramisole}$ hydrofluoride, (*R,R*)-Co(salen) **2**, and HFIP in TBME at 100 °C (Table 2). The RCYs for desymmetrization of the meso epoxides were uniformly high (entries 1–3). However, the enantioselectivities were only moderate-to-low, most likely due to high reaction temperatures required for opening of cyclic epoxides. This was consistent with the moderate 52% ee obtained after applying the cold protocol to cyclopentane oxide. Surprisingly, terminal polycyclic aromatic epoxides proved to be challenging substrates: the 1-naphthalenyloxirane (entry 4) was unreactive, and 9-anthryloxirane gave unidentified products.

Recognizing the general limitations imposed by the use of normal phase chiral radio-HPLC (column availability/price, solvent system), we sought a more practical alternative to measuring RCY and ee. Gratifyingly, the diastereomeric derivatization of fluorohydrins as Boc-Ala or Boc-Val esters with the subsequent use of radio-TLC provided for an inexpensive and expeditious quantification of RCY and *de* for all fluorohydrins in this study. Interestingly, the separation of diastereomeric esters was consistently better on the C18-modified silica than on the regular silica, chiral silica, or alumina oxide. In all cases the RCY and *de* obtained with the radio-TLC were consistent with those obtained by the radio-HPLC (Fig. 1, see the Supporting Information for more details).

One important question which needed to be answered was whether the fluoro- and radiofluorohydrins resulting from the (*R,R*)-Co(salen)-mediated opening of meso epoxides with PhCOF/HFIP and $[^{18}\text{F}]\text{HF}$ had the same absolute configuration. Because the direct determination of absolute stereochemistry of radiolabeled

Table 1
The results of enantioselective ^{18}F -hydrofluorination as shown in Scheme 1.

Entry ^a	Base	R'OH	Solvent	RCY ^b [%]	ee ^c [%]
1	$(-)\text{-Tetramisole}$	HFIP	TBME	78	32
2	$(-)\text{-Tetramisole}$	none	TBME	<1	– ^d
3	$(-)\text{-Tetramisole}$	<i>i</i> PrOH	TBME	3	–
4	$(-)\text{-Tetramisole}$	<i>t</i> BuOH	TBME	5	–
5	$(-)\text{-Tetramisole}$	(CF_3) ₃ COH	TBME	26	–
6	$(-)\text{-Tetramisole}$	PhOH	TBME	5	–
7	$(-)\text{-Tetramisole}$	$\text{C}_6\text{F}_5\text{OH}$	TBME	16	–
8	DBU, DBN, Et_3N , Py	HFIP	TBME	<1	–
9	$(-)\text{-Tetramisole}$	HFIP	<i>t</i> AmOH	50	68
10	$(-)\text{-Tetramisole}$	HFIP ^e	<i>t</i> AmOH	53	–

^a All reactions were performed in duplicate, average values are given.




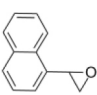
^b RCY: analytical decay-corrected RCY were measured by radio-HPLC or radio-TLC and based on $[^{18}\text{F}]\text{HF}$.

^c Determined using radio-HPLC on a Chiralpak AD-3 column.

^d Not measured.

^e Purified (see text), SA > 100 Gb/ μmol .

Table 2
The results of enantioselective ^{18}F -hydrofluorination as shown in Scheme 2.^a

Entry ^a	Epoxide	Solvent	RCY ^b [%]	ee ^c [%]
1		TBME or <i>t</i> -AmOH	93	45
2		TBME	73	20
3		TBME	78	33
4		TBME	<1	–

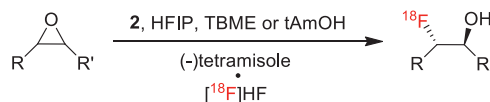
^a **2**, [^{18}F]HF/(–)-tetramisole, HFIP, 100 °C, 1 h, average of 3 experiments.

^b RCY: analytical decay-corrected RCY were measured by radio-HPLC or radio-TLC and based on [^{18}F]HF.

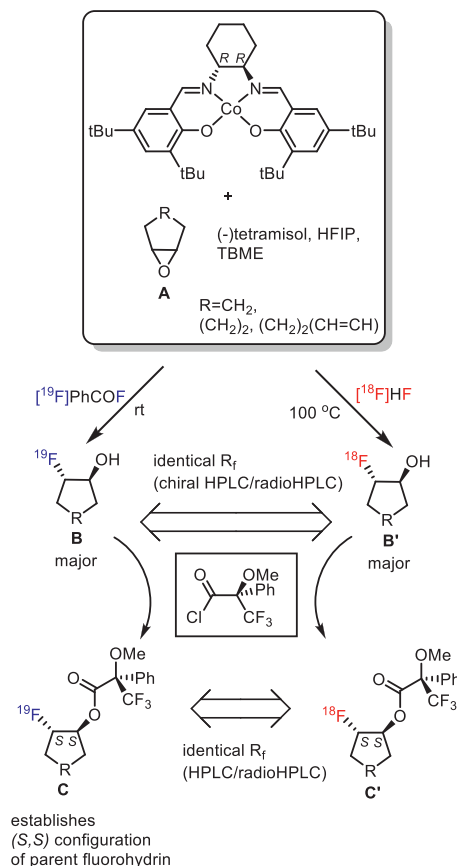
^c Determined using radio-HPLC on a Chiralpak AD-3.

substrates was not possible due to their subnanomolar concentrations, we developed an indirect method, based on comparison of ^{18}F -radiofluorohydrin derivatives with their ^{19}F -isotopomers, for which absolute configuration could be reliably established. The workflow is illustrated in Scheme 4. The (*R,R*)Co(salen)-mediated fluorination and radiofluorination of meso epoxides (A) yielded the corresponding isotopomeric fluorohydrins (B) and radiofluorohydrins (B') having identical R_f values as measured by normal phase chiral HPLC/radioHPLC. The reaction of (B) with (*R*)-(–)- α -methoxy- α -(trifluoromethyl)phenylacetyl chloride was fast and complete within minutes giving the corresponding Mosher esters (C) in high diastereoselectivity (*de* > 95%). The ^1H NMR based Mosher analysis established the (*S,S*) configuration of the major diastereomer C (Table 3). The diastereomers C were resolvable by the standard reverse-phase HPLC. The same Mosher derivatization of the corresponding radiofluorohydrins (B') resulted in radio-HPLC-resolvable diastereomeric ^{18}F -isotopomers C'. The C and C' had identical HPLC/radioHPLC retention times, thus establishing the (*S,S*) configuration of [^{18}F]2-fluorocyclohexanol, [^{18}F]8-fluorocyclooct-4-enol, and [^{18}F]2-fluoropentanol (Table 3).

Encouraged by good RCY and promising enantioselectivities of the resulting ^{18}F -fluorohydrins we turned to radiosynthesis of [^{18}F]F-MISO. [^{18}F]F-MISO, a 2-nitroimidazole ^{18}F -fluorohydrine, is currently the most widely used tumor hypoxia PET imaging agent [28]. Although alternative nitroimidazole radiofluorination procedures based on Si- ^{18}F and Al- ^{18}F chemistries were recently reported [29,30], the direct ^{18}F -hydrofluorination of epoxides is a particularly attractive approach. The one step enantioselective synthesis of non-radioactive F-MISO was recently showcased by Doyle and Kalow [19]. In our hands, the radiofluorination of the racemic F-MISO epoxide [31], obtained from 2-nitroimidazole and the racemic epichlorohydrin yielded [^{18}F]F-MISO in 17% RCY at room temperature (Scheme 3). At 75 °C the RCY increased to 81%



Scheme 3. Enantioselective ^{18}F -hydrofluorination of meso and terminal epoxides (see Table 2).



Scheme 4. Determination of absolute stereochemistry using Mosher esters.

and the product was obtained in 38% ee. Finally, 50 °C proved to be the optimal reaction temperature: [^{18}F]F-MISO was obtained in 81% RCY and 55% enantiomeric excess. To determine the absolute configuration of the major enantiomer the independent syntheses of both the (*S*) and the (*R*)-F-MISO were undertaken (Scheme 5).

HPLC/radio-HPLC showed that the R_f value of the major radioactive product was identical to that of the authentic (*S*)-F-MISO establishing the configuration of the major enantiomer of [^{18}F]F-MISO as the (*S*) stereoisomer. This result is in line with the (*S*) stereochemistry reported by Kalow and Doyle [19].

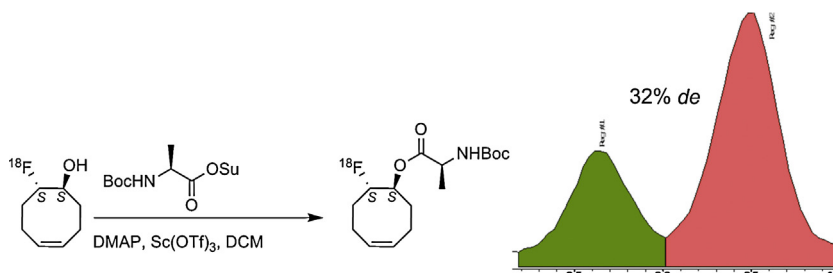


Fig. 1. The diastereomeric derivatization of 3 and the corresponding radio-TLC trace.

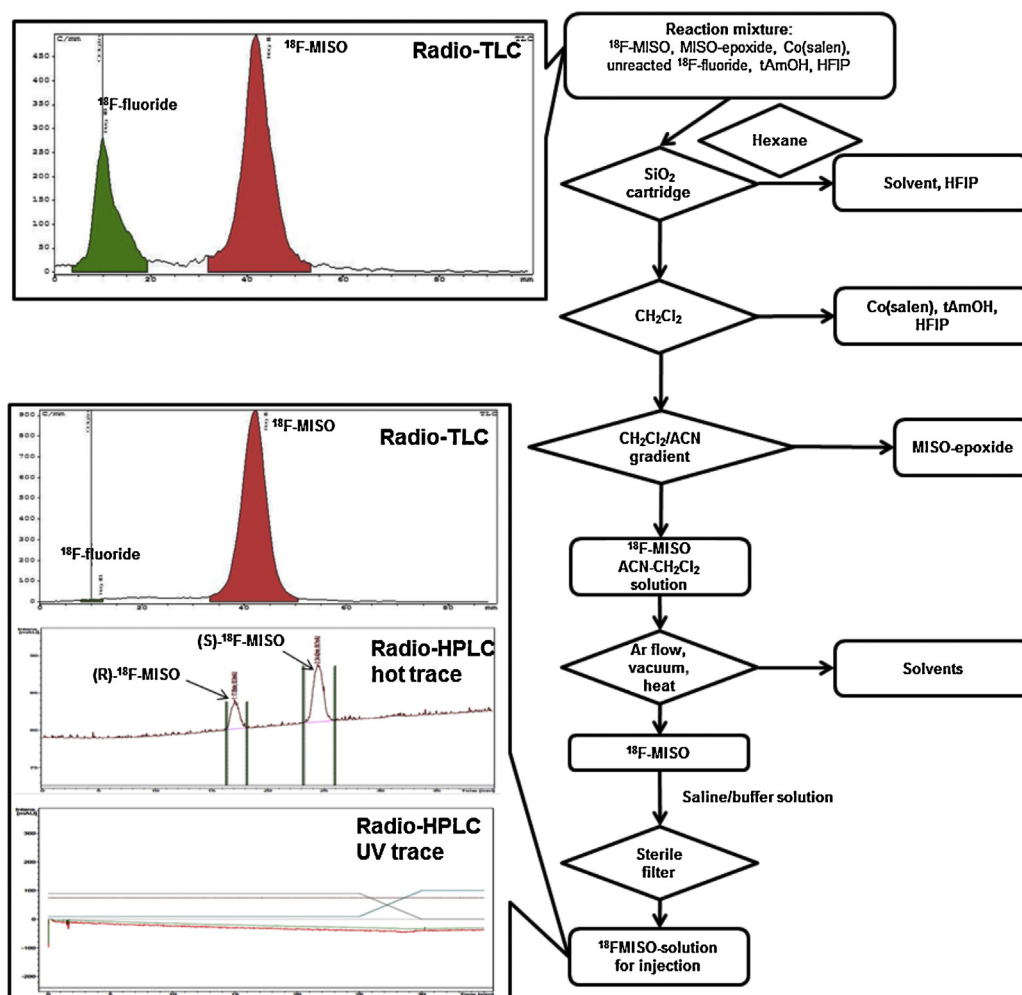
Table 3Determination of absolute stereochemistry by ^1H NMR using Mosher esters as shown in Scheme 4.

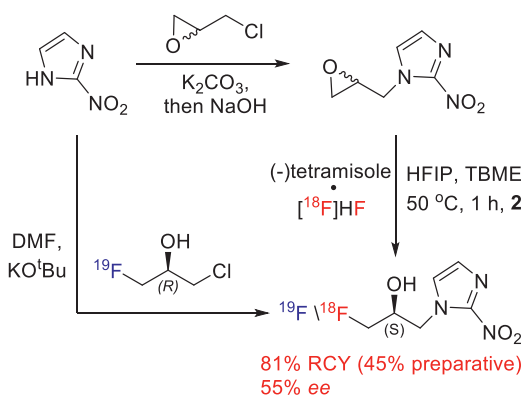
Entry	Fluorohydrin	Proton	$\Delta\delta^{\text{SR}}$	Carbon configuration
1	2-Fluorocyclohexanol	–FCH– –CH ₂ –HCO–	4.48–4.39 = 0.09 (pos.) 1.34–1.48 = –0.14 (neg.)	S
2	8-Fluorocyclooct-4-enol	–FCH– –CH ₂ –HCO–	4.78–4.70 = 0.08 (pos.) 2.10–2.17 = –0.07 (neg.) 1.72–1.86 = –0.14 (neg.)	S
3	2-Fluoropentanol	–FCH– –CH ₂ –HCO–	5.06–4.96 = 0.10 (pos.) 2.18–2.21 = –0.03 (neg.) 1.63–1.79 = –0.13 (neg.)	S

^{18}F]F-MISO is a radiopharmaceutical which requires careful purification before it can be released to the patient [32]. Currently, ^{18}F]F-MISO is purified using HPLC [33]. We have developed a new and efficient purification method which uses a simple solid phase extraction (SPE) methodology and does not require HPLC. According to the developed protocol, the reaction mixture (Fig. 2, top radio-TLC trace) is loaded onto the Supelco silica cartridge and sequentially washed with hexane and CH_2Cl_2 . This removes tAmOH, HFIP and the Co(salen) catalyst, while the unreacted ^{18}F]fluoride remains on the cartridge. The cartridge is then gradient-eluted with CH_2Cl_2 :MeCN, which removes the epoxide and finally elutes ^{18}F]F-MISO. The enantiomerically enriched ^{18}F]F-MISO, which is 99% radiopure and contains no cold impurities is dissolved in a saline solution and is filtered through a sterile filter to make the final ^{18}F]F-MISO formulation.

The specific activity of ^{18}F]F-MISO was measured to be higher than $100\text{ Gb}/\mu\text{mol}$. The purification takes 40 min and the overall radiosynthesis time, including ^{18}F]HF generation and transfer, is 1.5 h.

Akin to the recently reviewed metal-mediated radiofluorinations, [4] the Co(salen)-mediated radiofluorination does not require a carrier nor does it form any other ^{18}F -containing byproducts. Given the same sense of enantiomeric induction and generally comparable, albeit attenuated rates, it is tempting to assume that radiofluorination and the parent fluorination follow the same mechanism [19]. However, different reactivity toward terminal epoxides, different behavior with respect to the bases (Table 1, entry 8) and the concentration argument (the sub-nanomolar concentration of ^{18}F]fluoride should preclude the formation of any dimeric metal-fluorides), suggest that the

**Fig. 2.** Purification of ^{18}F]F-MISO flowchart.



Scheme 5. Enantioselective radiosynthesis of $[^{18}\text{F}]$ -MISO via kinetic resolution and the proof of absolute stereochemistry of the major enantiomer.

mechanistic differences between the tracer ^{18}F and the bulk ^{19}F chemistries might be larger than initially expected.

3. Conclusions

In conclusion, we report here the first example of transition metal mediated enantioselective n.c.a. radiofluorination of epoxides. The procedure utilizes gaseous $[^{18}\text{F}]\text{HF}$ and requires elevated temperature producing the ^{18}F -fluorohydrins in high RCY and modest enantioselectivities. The use of this methodology allowed us to accomplish the first enantioselective, single step radiosynthesis of $[^{18}\text{F}]$ -MISO in 81% RCY and 55% enantioselectivity. Animal studies directed at elucidating the impact of absolute stereochemistry of $[^{18}\text{F}]$ -MISO on hypoxic tumor PET imaging are in progress.

4. Experimental

The epoxides (9-oxabicyclo[6.1.0]non-4-ene, cyclohexene oxide and cyclopentene oxide), epichlorohydrins ((S), (R) and racemic), 2-nitroimidazole, (-)-tetramisole hydrochloride were purchased from Sigma–Aldrich and used as received without further purification. The solvents (*tert*-butyl methyl ether (TBME, anhydrous), and 2-methyl-2-butanol (*t*AmOH), anhydrous) were purchased from Sigma–Aldrich and used as received without further purification. 1,1,1,3,3,3-Hexafluoro-2-propanol (HFIP) was purchased from Sigma–Aldrich and purified by sequential passing through silica, activated alumina followed by vacuum distillation. The reported RCYs refer to analytical radio-HPLC or radio-TLC yields for meso-epoxides, and isolated yields for $[^{18}\text{F}]$ -MISO; all yields were based on $[^{18}\text{F}]\text{HF}/(-)$ -tetramisole and decay corrected. The specific activity was estimated from a 5 point-calibration curve using UV-VIS spectroscopy. All reactions were performed without exclusion of moisture and air. The radiofluorinations were performed in the pressure glass tubes (ACE GLASS Inc.) equipped with PTFE screw caps. The reaction vials used for radiofluorination were washed with piranha solution (3:1 mixture of conc. H_2SO_4 and 30% H_2O_2) and oven-dried at 150 °C overnight. Radio-TLC was performed using a Raytest MiniGita TLC scanner. Thin-layer chromatography (TLC) was run on precoated plates of silica gel 60 F254 (Merck), chiral modified, impregnated with Cu^{2+} reagent, chiral-silica gel matrix silica gel C18 on TLC Plates (Fluka) or reverse phase C18-silica gel matrix TLC UniplatesTM (Analtech). The Supelco silica cartridges (4 g) were purchased from Aldrich. The HPLC and radio-HPLC measurements were performed on Hitachi EliteChrom equipped with Carrol&Ramsey 105-S radio-detector. The normal phase chiral HPLC/radio-HPLC was done using Chiralpak AD-3, 150 mm \times 2.1 mm column using hexane-

*i*PrOH isocratic elution. The reverse phase HPLC was performed on a Phenomenex Luna 3u C18(2) column (100 Å, 100 mm \times 2.00 mm) using flow rate at 0.200 mL/min and isocratic elution with 9/1 (5% ACN in H_2O)/(100% ACN). The radiochemical purity was determined by radio-TLC or radio-HPLC and calculated as: $\text{RCP} = (\text{Area}^{\text{product}}/\text{Total area}) \times 100\%$. The RCY (analytical) was determined by the dose calibrator and calculated as $\text{RCY} = \text{Activity}^{\text{product}} \times \text{RCP} / \text{Activity}^{[^{18}\text{F}]\text{HF}}$. The preparative RCY of $[^{18}\text{F}]$ -MISO was determined analogously on the cartridge-purified sterile formulation of the product.

4.1. $[^{18}\text{F}]$ Fluoride

The aqueous solutions of $[^{18}\text{F}]$ fluoride were prepared by the $^{18}\text{O}(\text{p},\text{n})^{18}\text{F}$ reaction in a GE PETtrace cyclotron using a 1.8-mL of 95% enriched $[^{18}\text{O}]\text{water}$ irradiated by a 14.1-MeV beam at 20–25 mA for 60–90 min.

4.2. $[^{18}\text{F}]\text{HF}$ generation and transfer

$[^{18}\text{F}]$ Fluoride (cyclotron target wash, 1 mL, 150–7000 MBq) was added to a polyethylene (PE) reaction vial containing H_2SO_4 (98%, 5 mL). The reaction vial was heated for 30 min at 80 °C in an ultrasound bath while being irradiated at 35 kHz. $[^{18}\text{F}]\text{HF}$ was carried through the PE tubing (ID = 3.0 mm, OD = 4.5 mm, Buch&Holm, Denmark) by argon flow (300–400 scc/min) into a PE receiving vial containing (-)-tetramisole (0.02 mmol) in TBME or *t*AmOH (3 mL) at 0 °C. The $[^{18}\text{F}]\text{HF}$ yield was about 80% as measured by the dose calibrator.

4.3. Radiofluorination of the meso- and terminal polycyclic aromatic epoxides

An oven-dried high pressure glass tube equipped with a stir bar was charged with Co(salen) **2** (or **ent-2**) (12.0 mg, 0.020 mmol) and HFIP (112 μL , 0.80 mmol). The resulting slurry was then stirred for 5 min under air; an epoxide (0.20 mmol) was added neat followed by the solution of $[^{18}\text{F}]\text{HF}/(-)$ -tetramisole (4.1 mg, 0.020 mmol) in TBME (3 mL). The reaction mixture was then heated at 100 °C for 1 h. The reaction conversion was monitored by radio-TLC. No loss of activity due to volatilization was observed.

4.4. Derivatization of $[^{18}\text{F}]$ -fluorohydrins with the hydroxysuccinimide esters of Boc-protected amino acids

1 mL of the reaction mixture containing the corresponding ^{18}F -fluorohydrin was placed into a 10 mL vial and the solvent was evaporated with a flow of argon. 1 mL of CH_2Cl_2 was then added and the solution was evaporated to dryness again. The resulting residues were dissolved in 1 mL of CH_2Cl_2 . The second glass vial was charged with $\text{Sc}(\text{OTf})_3$ (1 equiv., 0.04 mmol, 21 mg), DMAP (5 equiv., 0.20 mmol, 26 mg) and 0.5 mL of CH_2Cl_2 , this mixture was stirred for 5 min at rt. Then, the solutions were combined and the resulting mixture was stirred for additional 2 min at room temperature, followed by the addition of Boc-Ala-OSu (5 equiv., 0.21 mmol, 60 mg) in one portion, and the mixture was stirred 2 more minutes, providing the diastereomeric material for radio-TLC.

4.5. Radiosynthesis of $[^{18}\text{F}]$ -MISO

A glass reaction vial was charged with (R,R)Co(salen) (4.5 mg) and HFIP (250 μL). The resulting slurry was stirred for 5 min under air followed by the addition of MISO-epoxide (5.0 mg, 1.0 equiv., 0.030 mmol) and the solution of $[^{18}\text{F}]\text{HF}$ -levamisole (0.6 mg, 0.1 equiv., 0.003 mmol) in *t*-AmOH (3 mL). The reaction vial was

heated at 50–65 °C. After 15 min the pressure tube was opened and the reaction mixture was loaded onto a Supelco silica cartridge preconditioned with hexane. The cartridge was washed with hexane (20 mL), CH₂Cl₂ (20 mL), and eluted with CH₂Cl₂: MeCN (3:1, 4 × 10 mL). The product was collected in two last fractions. The solvent was removed with a flow of Ar; the residue was dissolved in 3 mL of DPBS buffer and filtered through a 0.22 μm sterile filter. The total time of the synthesis was 1 h. The radiochemical purity of [¹⁸F]F-MISO was higher than 99%, and the specific activity was found to be greater than 100 GBq/μmol.

Appendix A. Supplementary data

Supplementary data associated with this article can be found, in the online version, at <http://dx.doi.org/10.1016/j.jfluchem.2013.09.006>.

References

- [1] L. Cai, S. Lu, V.W. Pike, *Eur. J. Org. Chem.* 2008 (2008) 2853–2873.
- [2] D. Roeda, F. Dollé, *Curr. Radiopharm.* 3 (2010) 81–108.
- [3] S.M. Ametamey, M. Honer, P.A. Schubiger, *Chem. Rev.* 108 (2008) 1501–1516.
- [4] C. Hollingworth, V. Gouverneur, *Chem. Commun.* 48 (2012) 2929–2942.
- [5] J.A. Akana, K.X. Bhattacharyya, P. Müller, J.P. Sadighi, *J. Am. Chem. Soc.* 129 (2007) 7736–7737.
- [6] B.C. Gorske, C.T. Mbofana, S.J. Miller, *Org. Lett.* 11 (2009) 4318–4321.
- [7] P. Barthazy, R.M. Stoop, M. Wörle, A. Togni, A. Mezzetti, *Organometallics* 19 (2000) 2844–2852.
- [8] M.H. Katcher, A.G. Doyle, *J. Am. Chem. Soc.* 132 (2010) 17402–17404.
- [9] C. Hollingworth, A. Hazari, M.N. Hopkinson, M. Tredwell, E. Benedetto, M. Huiban, A.D. Gee, J.M. Brown, V. Gouverneur, *Angew. Chem. Int. Ed.* 50 (2011) 2613–2617.
- [10] J.J. Topczewski, T.J. Tewson, H.M. Nguyen, *J. Am. Chem. Soc.* 133 (2011) 19318–19321.
- [11] E. Benedetto, M. Tredwell, C. Hollingworth, T. Khotavivattana, J.M. Brown, V. Gouverneur, *Chem. Sci.* 4 (2013) 89–96.
- [12] D.A. Watson, M. Su, G. Teverovskiy, Y. Zhang, J. García-Fortanet, T. Kinzel, S.L. Buchwald, *Science* 325 (2009) 1661–1664.
- [13] T. Furuya, A.E. Strom, T. Ritter, *J. Am. Chem. Soc.* 131 (2009) 1662–1663.
- [14] P. Tang, T. Ritter, *Tetrahedron* 67 (2011) 4449–4454.
- [15] T. Furuya, T. Ritter, *Org. Lett.* 11 (2009) 2860–2863.
- [16] S. Bruns, G. Haufe, *J. Fluorine Chem.* 104 (2000) 247–254.
- [17] G. Haufe, S. Bruns, M. Runge, *Adv. Synth. Catal.* 344 (2002) 165–171.
- [18] G. Haufe, S. Bruns, M. Runge, *J. Fluorine Chem.* 112 (2001) 55–61.
- [19] J.A. Kalow, A.G. Doyle, *J. Am. Chem. Soc.* 133 (2011) 16001–16012.
- [20] J.A. Kalow, A.G. Doyle, *J. Am. Chem. Soc.* 132 (2010) 3268–3269.
- [21] E. Lee, J.M. Hooker, T. Ritter, *J. Am. Chem. Soc.* 134 (2012) 17456–17458.
- [22] D.-R. Hwang, C.S. Dence, T.A. Bonasera, M.J. Welch, *Int. J. Radiat. Appl. Instrum. Appl. Radiat. Isot.* 40 (1989) 117–126.
- [23] S.A. Park, C.H. Lim, K.-H. Chung, *Bull. Korean Chem. Soc.* 28 (2007) 1835.
- [24] R. Schirmmayer, P. Lucas, E. Schirmmayer, B. Wängler, C. Wängler, *Tetrahedron Lett.* 52 (2011) 1973–1976.
- [25] D.Y. Chi, D.W. Kim, D.H. Moon, S.J. Oh, J.-S. Ryu, *WO 2006/065038 A1*.
- [26] B. Mathiessen, M. Jensen, F. Zhuravlev, *J. Labelled Compd. Radiopharm.* 54 (2011) 816–818.
- [27] B. Mathiessen, A.T.I. Jensen, F. Zhuravlev, *Chem. Eur. J.* 17 (2011) 7796–7805.
- [28] A.R. Padhani, K.A. Krohn, J.S. Lewis, M. Alber, *Eur. Radiol.* 17 (2007) 861–872.
- [29] C. Wängler, A. Kostikov, J. Zhu, J. Chin, B. Wängler, R. Schirmmayer, *Appl. Sci.* 2 (2012) 277–302.
- [30] L. Hoigebazar, J.M. Jeong, J.-Y. Lee, D. Shetty, B.Y. Yang, Y.-S. Lee, D.S. Lee, M.C. Lee, *J. Med. Chem.* 55 (2012) 3155–3162.
- [31] D.Y.-W. Lee, X.-S. Ji, J.A. Raleigh *WO/2008/070336*.
- [32] M.P.S. Dunphy, J.S. Lewis, *J. Nucl. Med.* 50 (2009) 106S–121S.
- [33] P.J. Riss, V. Ferrari, R. Bielik, R. Canales-Candela, Roberto, R. Smith, F. Aigbirhio, *Radiochemical Syntheses: Radiopharmaceuticals for Positron Emission Tomography*, 2012.

Supporting Information

for:

Co(salen)-Mediated Enantioselective Radiofluorination of Epoxides. Radiosynthesis of Enantiomerically Enriched [¹⁸F]F-MISO via Kinetic Resolution

Evgeny Revunov and Fedor Zhuravlev*

Hevesy Laboratory, Center for Nuclear Technologies

Technical University of Denmark

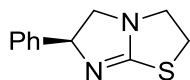
Frederiksborgvej 399, Building 202

E-mail: fezh@dtu.dk

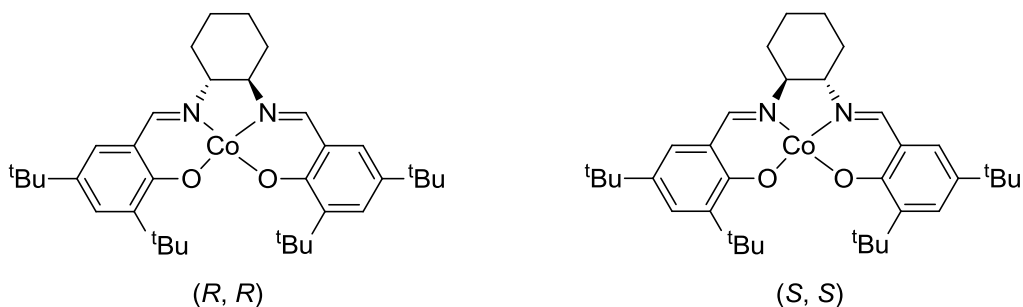
Contents

Materials	2
Selected procedures	4
Radio TLC traces	7
Radio TLC traces of [¹⁸ F]F-MISO	10
Chiral Radio HPLC traces of cyclic fluorohydrins	14
Chiral GC traces of of cyclic fluorohydrins	16
HPLC traces of [¹⁸ F]F-MISO	19
HPLC traces of [¹⁸ F]F-MISO after the purification procedure	22
Chiral HPLC traces of [¹⁸ F]F-MISO	24
The Mosher esters experiments	27
HPLC traces of Mosher esters	28

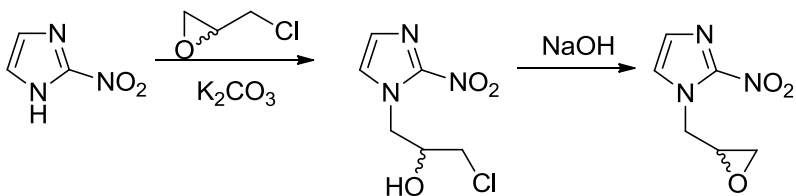
Materials



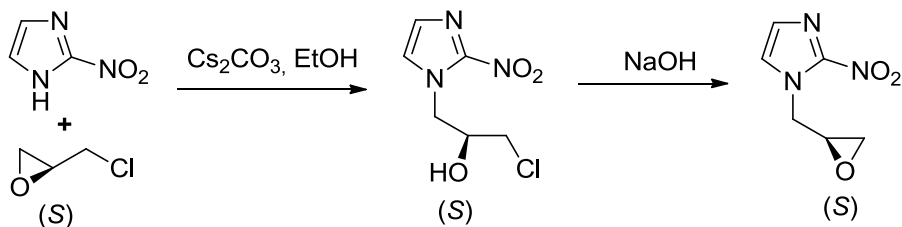
(-)-Tetramisole was prepared from (-)-tetramisole hydrochloride according to the described method¹ and recrystallized from Et₂O.



(R,R)-Co(salen) and **(S,S)-Co(salen)** were purchased from Strem Chemicals and recrystallized from hot TBME under argon.



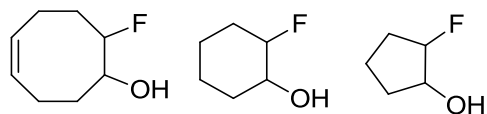
The racemic **1-(2,3-epoxypropyl)-2-nitroimidazole** or **MISO-epoxide** were synthesized according to the literature procedure².



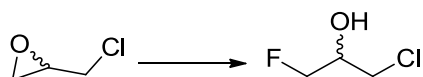
¹ V. B. Birman, X. Li, *Org. Lett.* **2006**, 8, 1351.

² U.S. Pat. Appl. Publ. 20080102026, 01 May 2008.

(S)-MISO-epoxide and (R)-MISO-epoxide were prepared according to the literature procedure³.



The racemic fluorohydrins (8-fluorocyclooct-4-enol, 2-fluorocyclohexanol and 2-fluorocyclopentanol) were synthesized in the same manner: a glass ampule was charged with an epoxide (18.4 mmol, 1.0 eq.) and TREAT HF (3.0 mL, 18.4 mmol, 1.0 eq.). The ampule was flame-sealed and heated overnight at 80 °C. The product was precipitated with a mixture of ice (10 g) and ammonia hydroxide (30%, 10 mL), and washed with Et₂O (3x20 mL). The organic phase was washed with HCl (1N, 10 mL) and dried over Na₂SO₄. The solvent was removed *in vacuo*, and the oily residues were passed through a short SiO₂ column (EtOAc/Hexane, 1/5 to 1/1) giving 80-90% of fluorohydrin as a single product⁴.

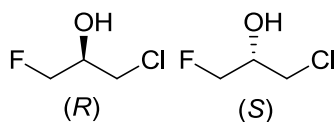


The racemic 1-chloro-3-fluoropropan-2-ol was synthesized from the corresponding racemic epichlorohydrin using the method described above for the *meso*-epoxides. Epichlorohydrin (1.0 g, 10.8 mmol, 1.0 eq.) was reacted with TREAT HF (1.77 mL, 10.8 mmol, 1.0 eq.) in a sealed ampule for 2 h at 130 °C. The ampule was opened and the product was precipitated with a mixture of ice (10 g) and ammonia hydroxide solution (30%, 10 mL), washed with Et₂O (3x15 mL). The organic phase was washed with HCl solution (1 N, 10 mL), and dried over Na₂SO₄. The reaction mixture was concentrated on a Rotovap and distilled using Kugelrohr apparatus (10 mbar, 90 °C) giving the desired chlorofluorohydrin in 88% yield (1.07 g). The spectral data were in agreement with the literature⁵.

³ H. Weinmann, M. Harre, K. Koenig, E. Merten, U. Tilstam, *Tetrahedron Letters* **2002**, *43*, 593–595.

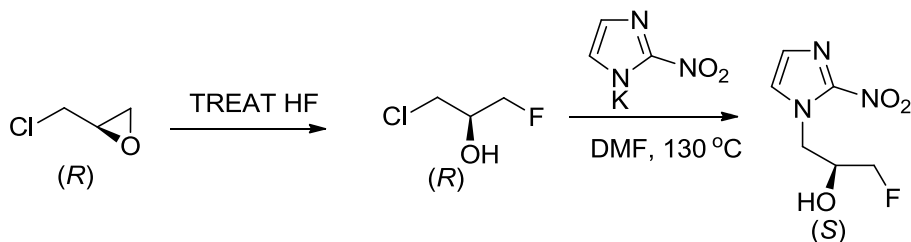
⁴ G. Alvernhe, A. Laurent, G. Haufe, J. Fluorine Chem. **1986**, *34*, 147-156.

⁵ Patent: WO2012/98461 A1, 2012; Patent Family: WO2012/98461 A1.



(R)- and (S)-1-chloro-3-fluoropropan-2-ols were synthesized in a same manner from the (R)- and (S)-epichlorohydrins respectively, in 86% (1.03 g) and 83% (1.01 g) yields, respectively.

F-MISO. Dry DMF (5 mL) was added to a mixture of 2-nitroimidazole (500 mg 4.4 mmol, 1.0 eq.) and KO^tBu (490 mg 4.4 mmol, 1.0 eq.) with stirring. The reaction mixture was heated at 130 °C for 15 min, the mixture was cooled to 80 °C, and potassium iodide (1 mg, <0.01 eq.) and 1-chloro-3-fluoropropan-2-ol (680mg, 5.9 mmol, 1.3 eq.) were added. The mixture was stirred for 1 h at 130 °C. The solvent was evaporated off, and the product was purified by column chromatography, using EtOAc/ CHCl_3 (70/30 to 100), to afford pure F-MISO as off-white solid (80%, 505 mg). The ^1H NMR was in agreement with the literature⁶.



The (S) and (R)-F-MISO were synthesized in a similar manner from (R) and (S)-epichlorohydrins and used as “cold” standards for radio-TLC.

HF-(-)tetramisole was prepared analogously to [^{18}F]HF-(-)tetramisole using 2 mL of HF (48 wt. % in H_2O) and 8 mL of conc. H_2SO_4 .

Selected procedures

Derivatization of [^{18}F]-fluorohydrins with hydroxysuccinimide esters of Boc-protected amino acids. 1 mL of radiofluorination reaction mixture was placed into a 10 mL vial and the solvent

⁶ J. A. Kalow, A. G. Doyle, *J. Am. Chem. Soc.* **2011**, *133*, 16001–16012.

was evaporated with a flow of argon. 1 mL of CH₂Cl₂ was then added and evaporated again to dryness. The resulting residue was redissolved in 1 mL of CH₂Cl₂. The second glass vial (4 mL vial with a screw top) was charged with Sc(OTf)₃ (1 eq., 0.04 mmol, 21 mg), DMAP (5 eq., 0.20 mmol, 26 mg) and 0.5 mL of CH₂Cl₂ and the mixture was stirred 5 min at rt. The solutions from the two vials were combined and the resulting mixture was stirred for additional 2 minutes at room temperature, followed by the addition of Boc-Ala-OSu (5 eq., 0.21 mmol, 60 mg) in one portion, and the mixture was stirred 2 more minutes, providing the diastereomeric material for radio-TLC.

Table 1.

R_F values for enantiomers, ratio of the R_F values, solvent and type of silica TLC plates

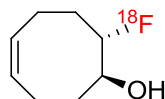
Fluorohydrin	Amino acid derivative	TLC plate	Solvent (v/v)	R _{F1}	R _{F2}	R _{F2} /R _{F1}
8-fluorocyclooct-4-enol	Boc-Ala-OSu	regular	40/60 EtOAc/Hept	0.60	0.66	1.10
8-fluorocyclooct-4-enol	Boc-Ala-OSu	chiral	40/60 EtOAc/Hept	0.70	0.72	1.03
8-fluorocyclooct-4-enol	Boc-Ala-OSu	C18	40/60 EtOAc/Hept	0.79	0.85	1.08
8-fluorocyclooct-4-enol	Boc-Ala-OSu	C18	20/80 EtOAc/Hept	0.53	0.60	1.13
8-fluorocyclooct-4-enol	Boc-Phe-OSu	regular	20/80 EtOAc/Hept	0.37	0.39	1.06
8-fluorocyclooct-4-enol	Boc-Phe-OSu	C18	20/80 EtOAc/Hept	0.50	0.55	1.09
2-fluorocyclohexanol	Boc-Ala-OSu	C18	10/1 Tol/EtOAc	0.569	0.639	1.12
2-fluorocyclopentanol	Boc-Ala-OSu	regular, C18 and chiral	10/1 Tol/EtOAc	no separation		

2-fluorocyclopentanol	Boc-Phe-OSu					
2-fluorocyclopentanol	Boc-Pro-OSu	C18	5/1 Tol/EtOAc	0.52	0.55	1.07
2-fluorocyclopentanol	Boc-Ala-OSu,	regular, C18 and chiral	Tol/EtOAc, CHCl ₃ /CH ₃ CN	no separation		
F-MISO	Boc-Phe-OSu					
F-MISO	Boc-Val-OSu	C18	1/1 Tol/EtOAc	0.41	0.46	1.12
F-MISO	Boc-Val-OSu	C18	5/1 Tol/EtOAc	0.28	0.33	1.17

Radio TLC traces

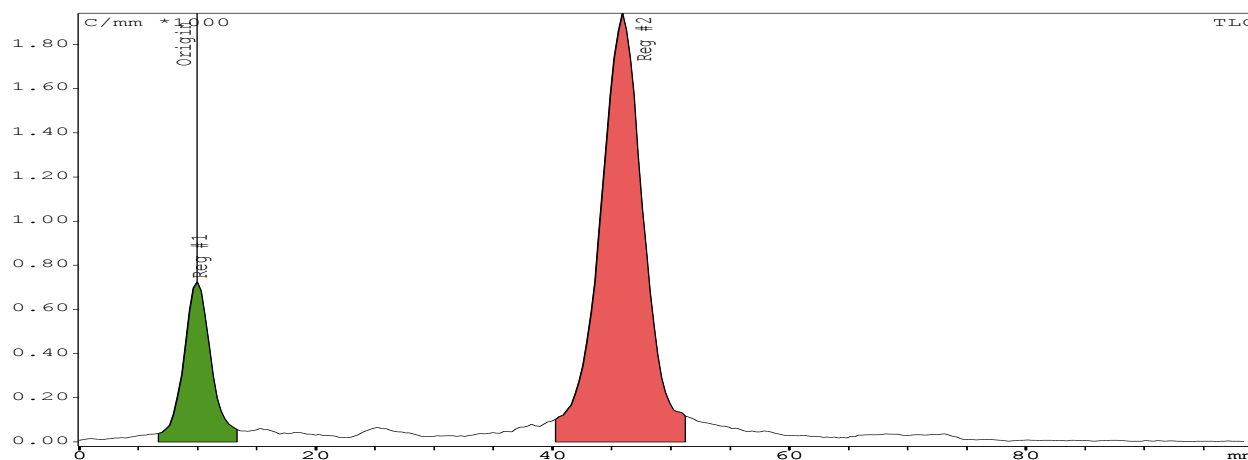
Table 2. Radiofluorination of *meso*-epoxides

Fluorohydrin	t, °C	RCY, %	ee, %	Solvent
2-fluorocyclopentanol	100	73	20	Tol/EtOAc 5/1
2-fluorocyclohexanol	100	93	48	Tol/EtOAc 5/1
8-fluorocyclooct-4-enol	100	78	33	Hept/EtOAc 4/1
8-fluorocyclooct-4-enol	75	25	48	Hept/EtOAc 4/1
8-fluorocyclooct-4-enol	50	5		Hept/EtOAc 4/1
8-fluorocyclooct-4-enol	25	0		Hept/EtOAc 4/1



[¹⁸F]8-fluorocyclooct-4-enol (1 h at 100 °C). C18-silica plate, Hept/EtOAc 4/1, R_F=0.40

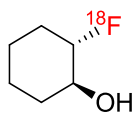
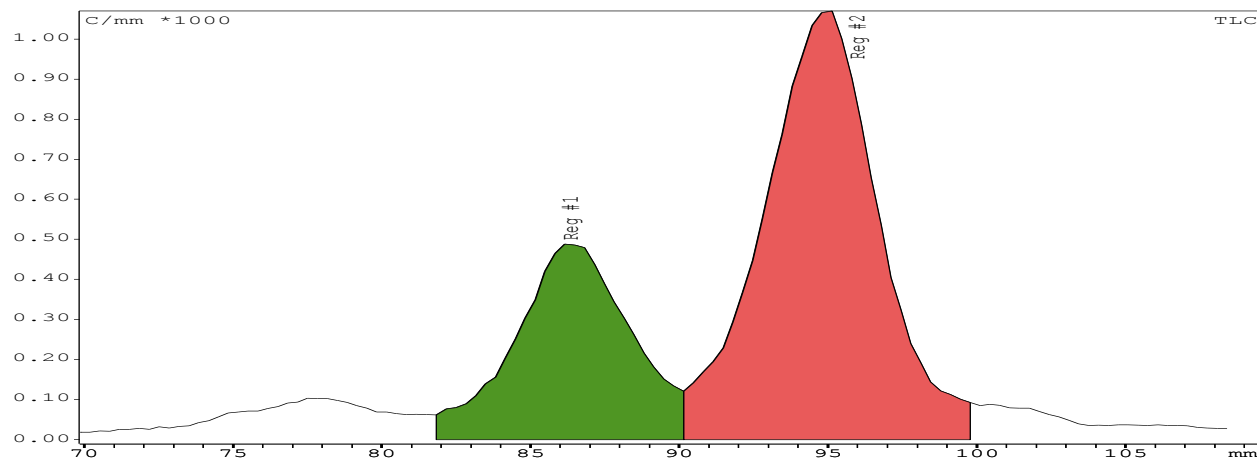
78% RCY (average, 81% (max))



[¹⁸F]8-fluorocyclooct-4-enol, derivatized with Boc-Ala-OSu, C18-silica plate, Tol/EtOAc 5/1

R_{F1}=0.51, R_{F2}=0.56

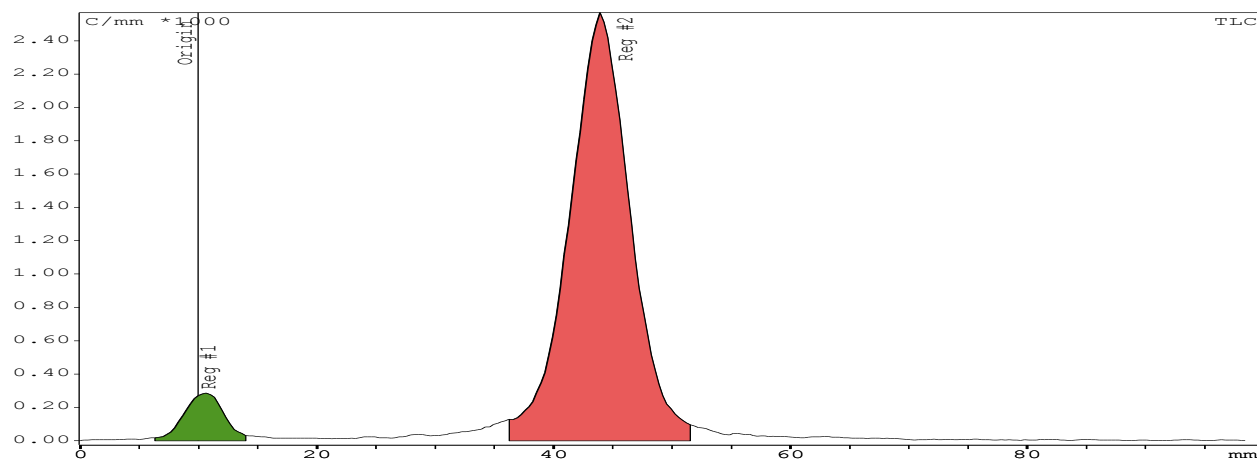
33% ee (average, the R_fs were compared with the “cold” standard)

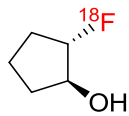


[¹⁸F]2-fluorocyclohexanol. C18-silica plate, Tol/EtOAc 5/1

R_F=0.38

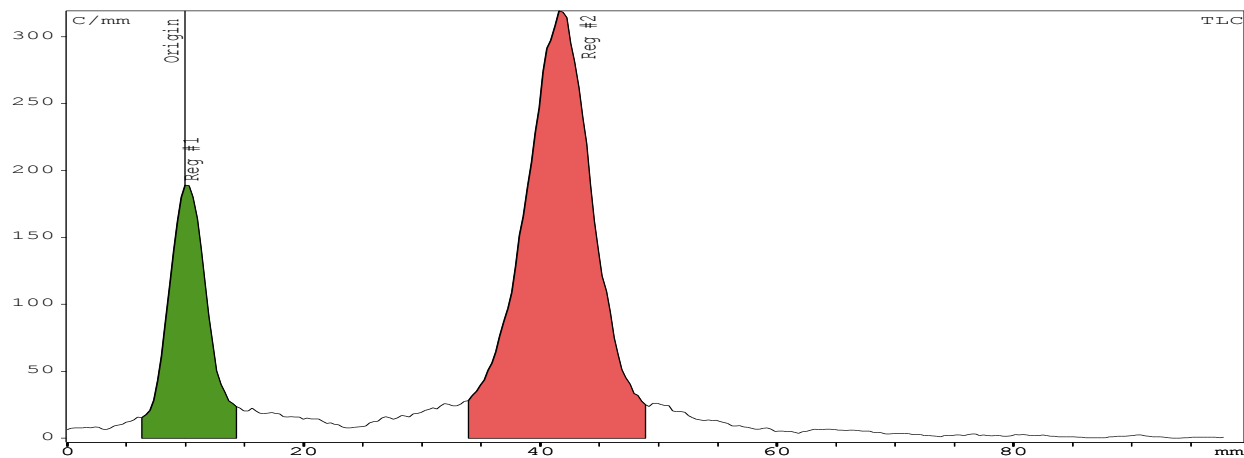
93% RCY (average, max 93%)





2-fluorocyclopentanol. C18-silica plate, Tol/EtOAc 5/1

$R_F=0.36$, **73% RCY** (average, 75% max)



Radio TLC traces of [¹⁸F]F-MISO

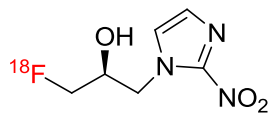
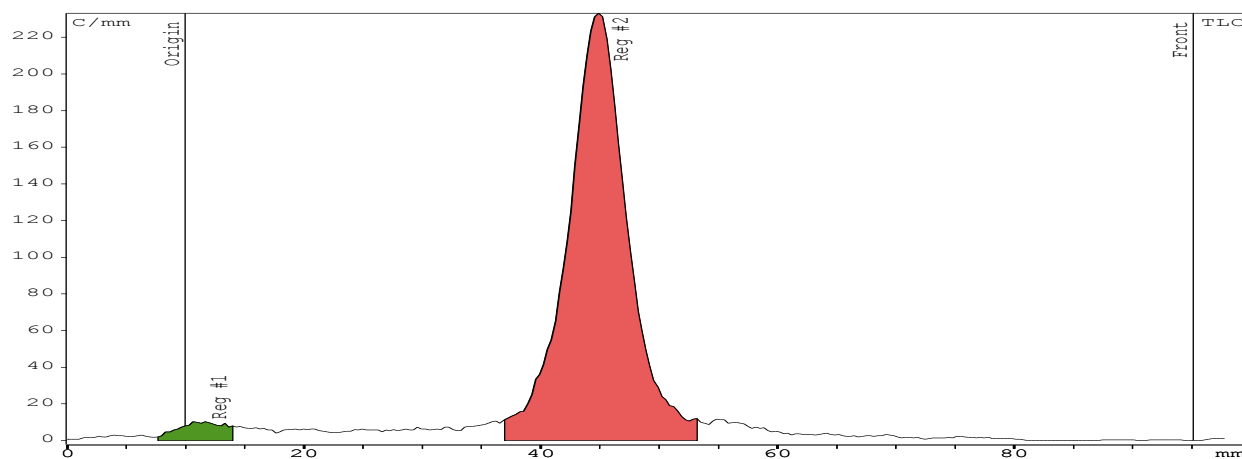


Table 3.

RCY and ee for [¹⁸F]F-MISO at different temperatures

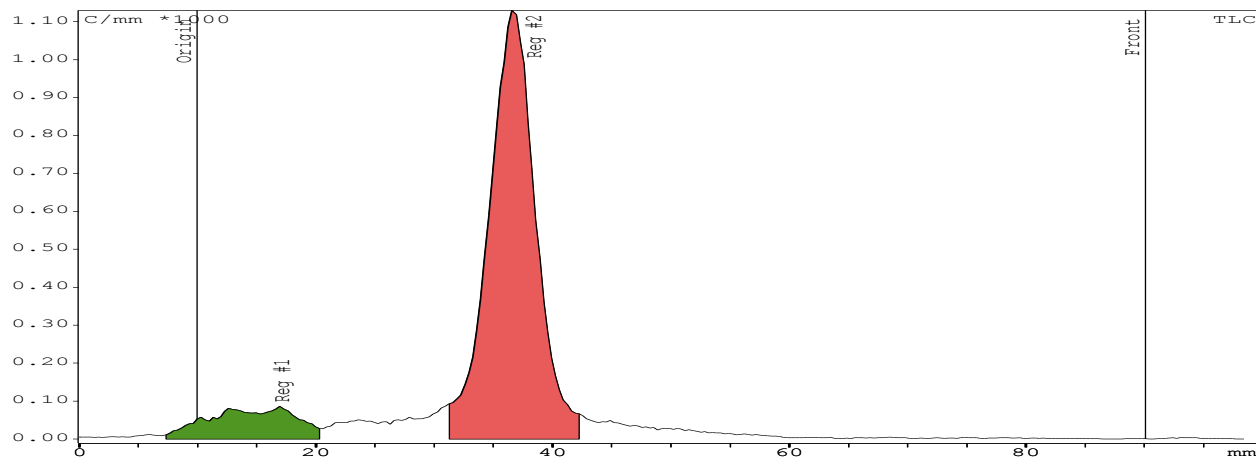
t, °C	RCY, %	ee, %
25	17	
50	81	55
75	81	38
100	87	33

[¹⁸F]F-MISO, 97 % radiopurity



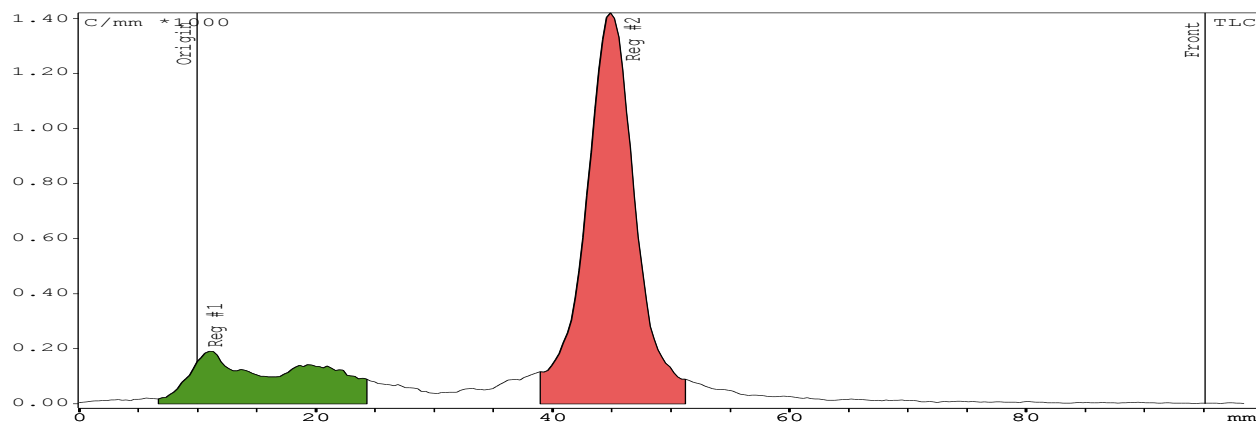
[¹⁸F]F-MISO, 1 h at 100 °C, regular silica

87% RCY



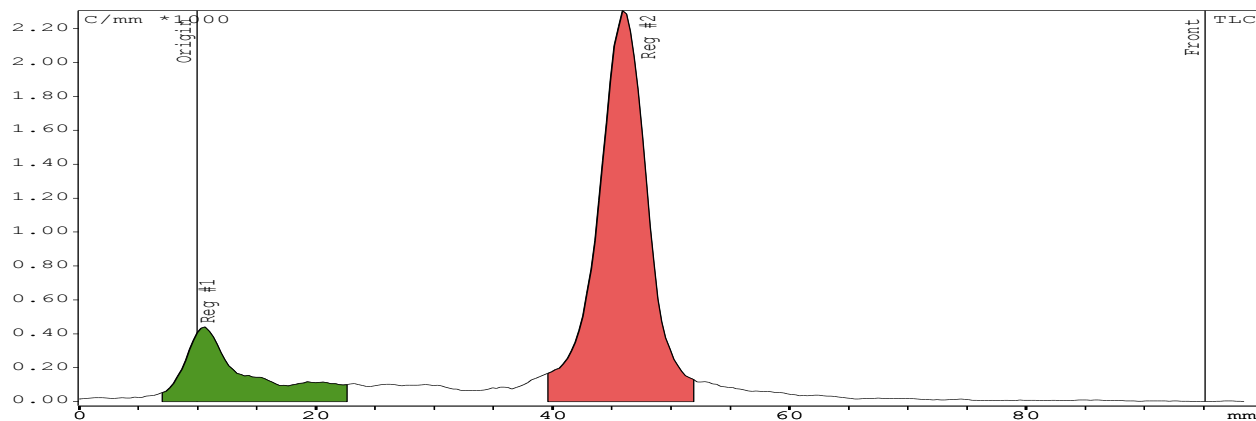
[¹⁸F]F-MISO, 1 h at 75 °C, regular silica

81% RCY



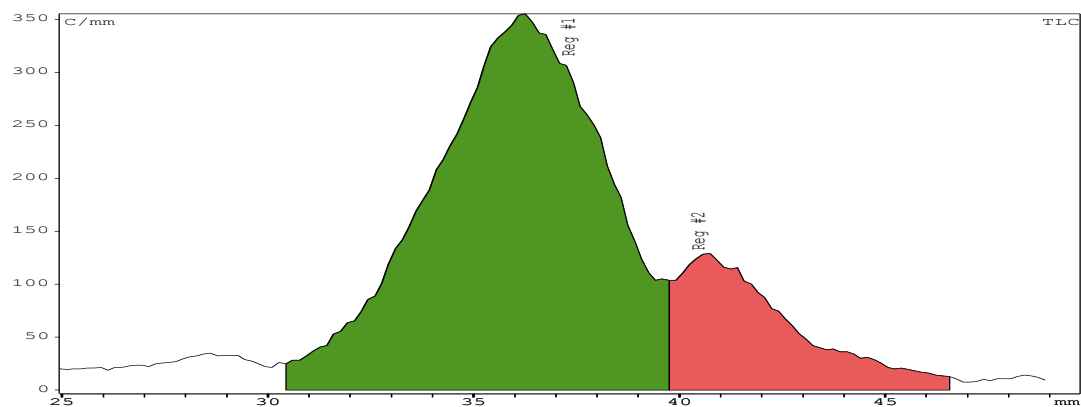
[¹⁸F]F-MISO, 1 h at 50 °C, regular silica

81% RCY



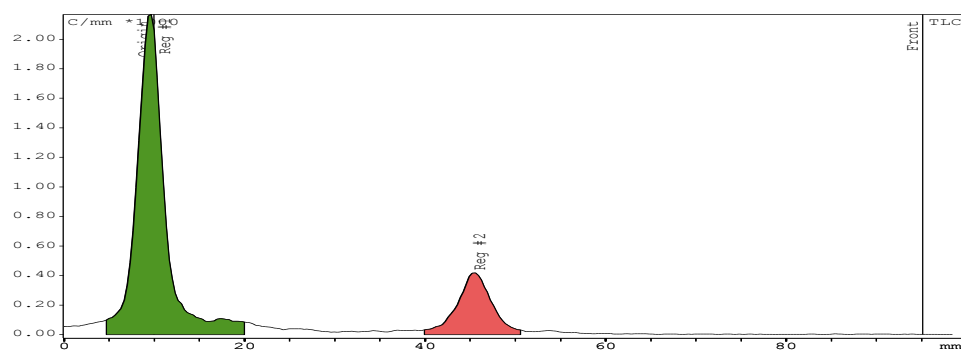
Derivatized with Boc-Val-OSu, C18-silica plate, Tol/EtOAc 5/1

55% ee



[¹⁸F]F-MISO, 1 h at 25 °C, regular silica

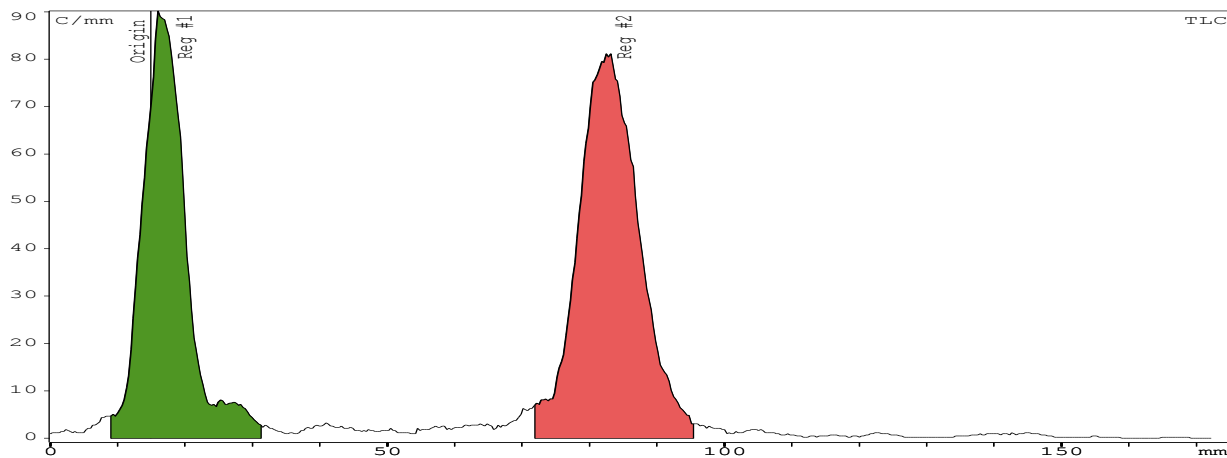
17% RCY



Radiotracers of (R) and (S)-[¹⁸F]-MISO-Val-Boc

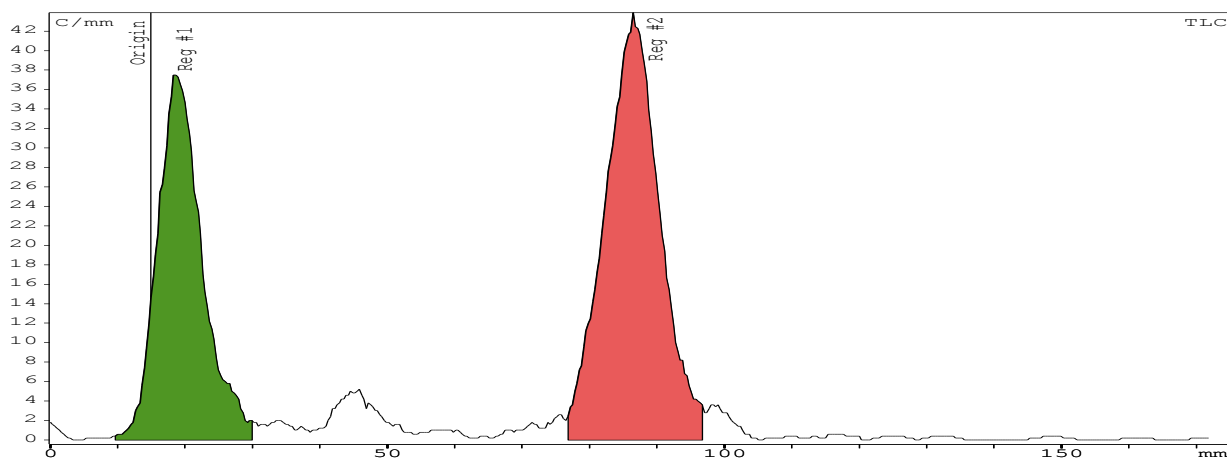
(S)-[¹⁸F]-MISO-Val-Boc

R_F=0.42, C18-silica plate, Tol/EtOAc 1/1



(R)-[¹⁸F]-MISO-Val-Boc

R_F=0.45, C18-silica plate, Tol/EtOAc 1/1

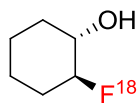


Chiral Radio HPLC traces of cyclic fluorohydrins

Column: Chiralpak AD-3 (AD30CT-QK002)

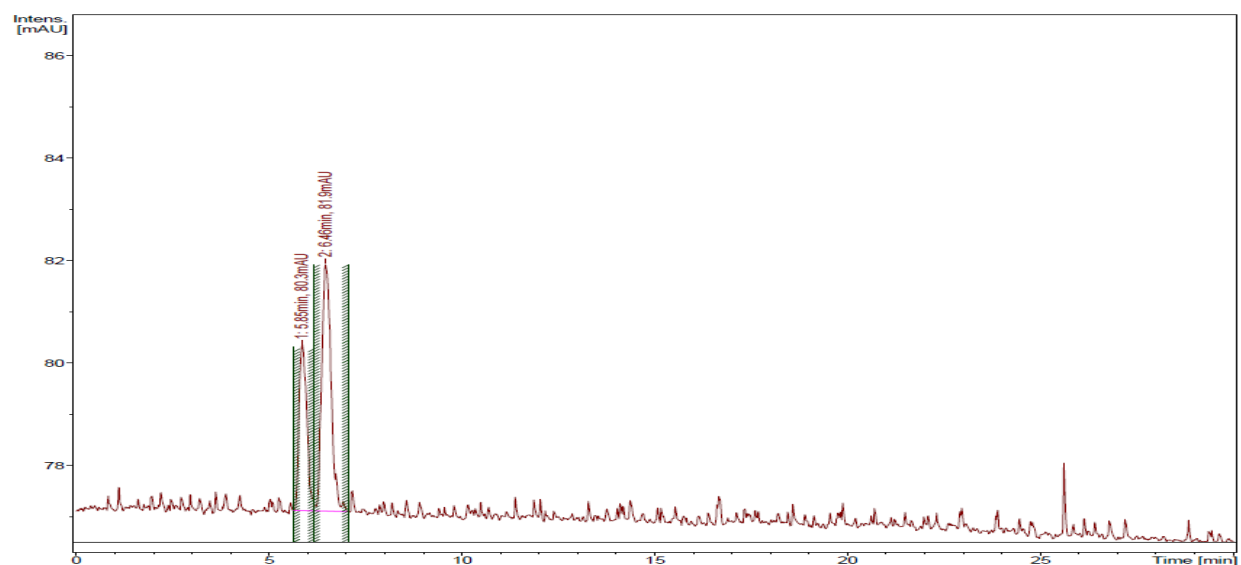
Flow Rate: 0.150 mL/min

Isocratic conditions, 10% ⁱPrOH in Hex

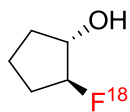


[¹⁸F]2-fluorocyclohexanol

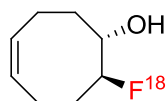
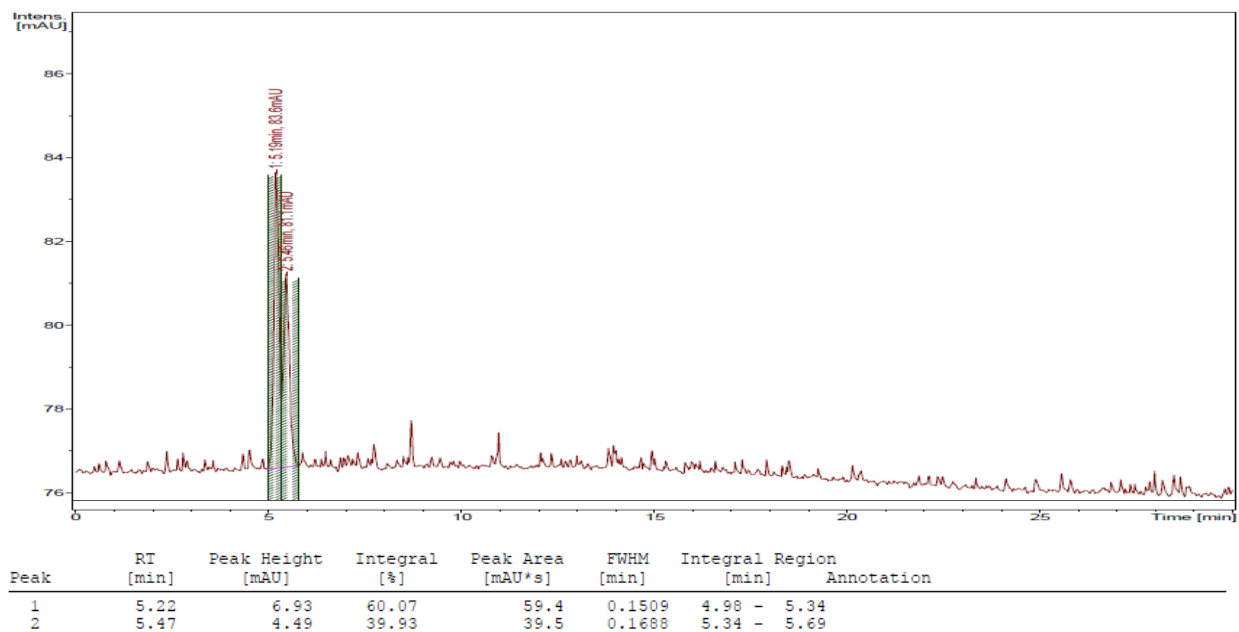
ee 45% (from 3 experiments)



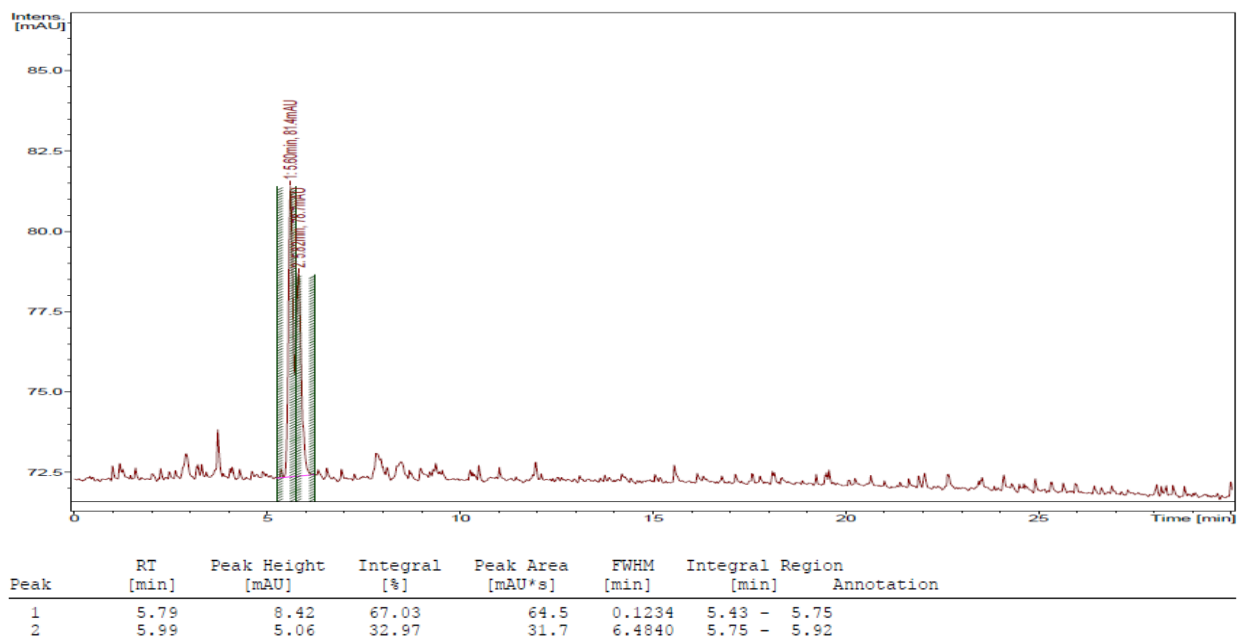
Peak	RT [min]	Peak Height [mAU]	Integral [%]	Peak Area [mAU*s]	FWHM [min]	Integral Region [min]	Annotation
1	5.76	3.16	27.69	30.8	279.5495	5.66 - 5.96	
2	6.33	4.81	72.31	80.3	0.2584	5.96 - 7.06	



[¹⁸F]2-fluorocyclopentanol ee 20% (from 3 experiments)



[¹⁸F]8-fluorocyclooct-4-enol ee 32% (from 3 experiments)



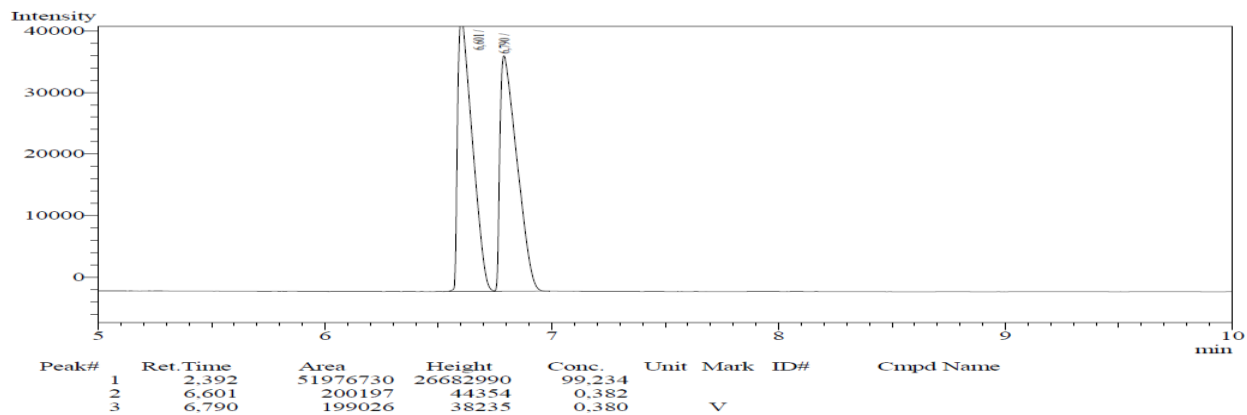
Chiral GC traces of cyclic fluorohydrins

Column: Astec ChiralDEX B-DM 40m x 0.25mm x 0.12um

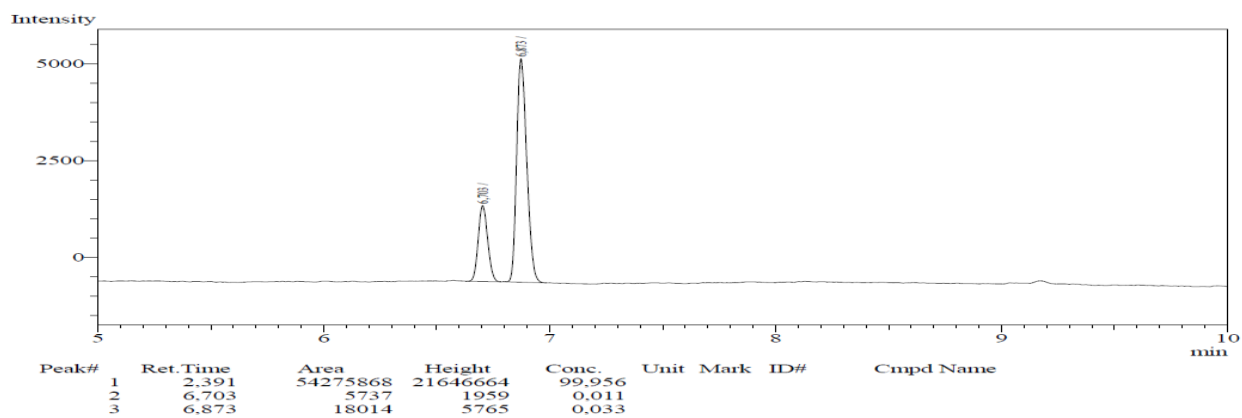
Linear velocity: 36 cm/sec

Isothermal conditions (80 °C)

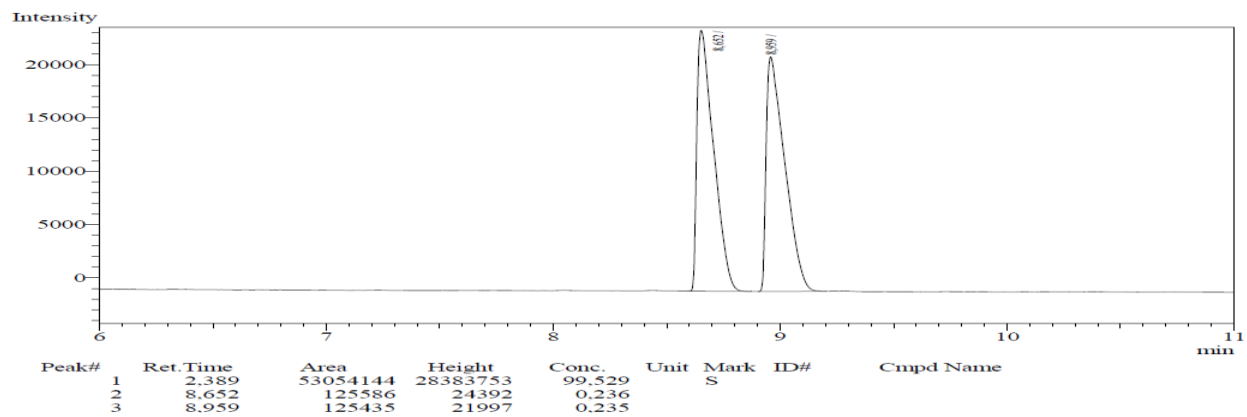
2-fluorocyclopentanol, racemic



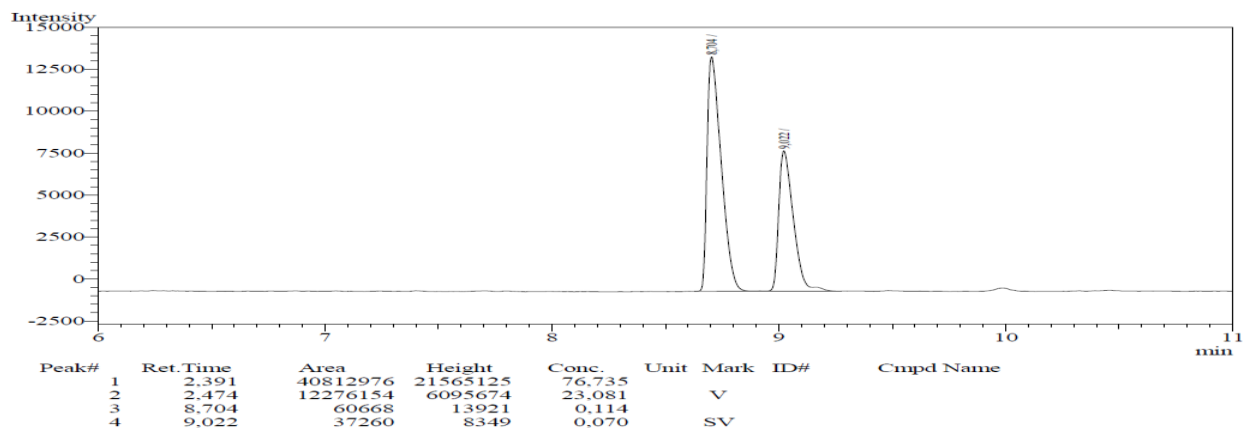
2-fluorocyclopentanol ("cold" experiment, 100 °C), ee 52%



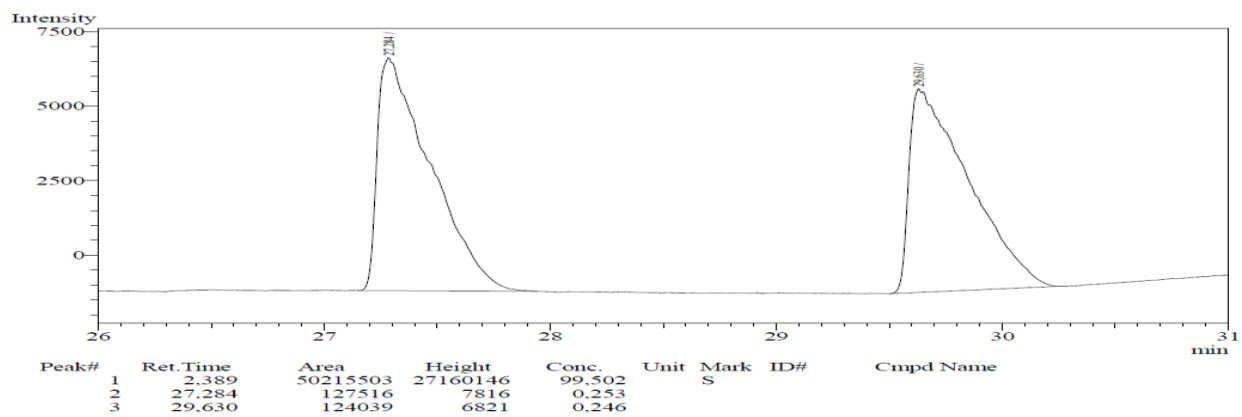
2-fluorocyclohexanol, racemic



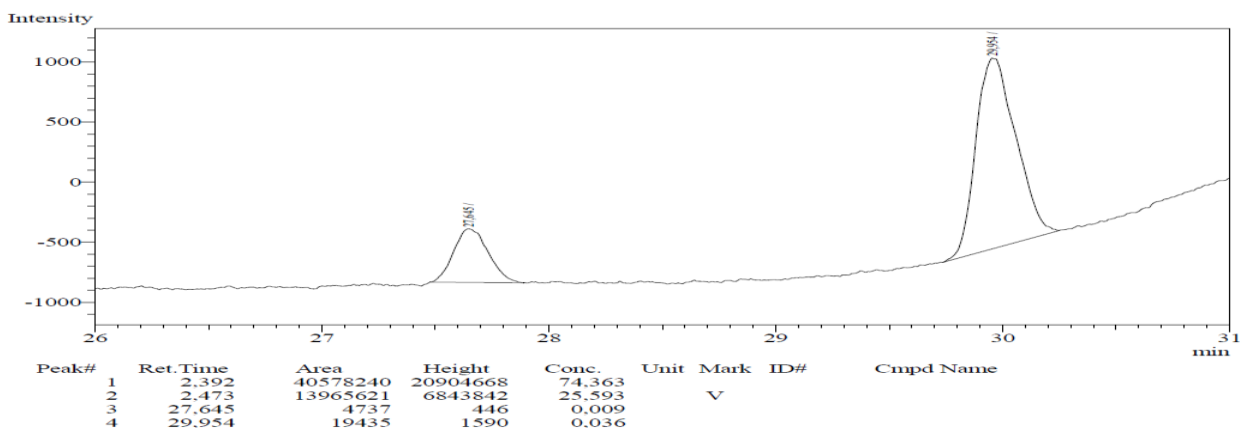
2-fluorocyclohexanol ("cold" experiment, 100 °C), ee 24%



8-fluorocyclooct-4-enol, racemic



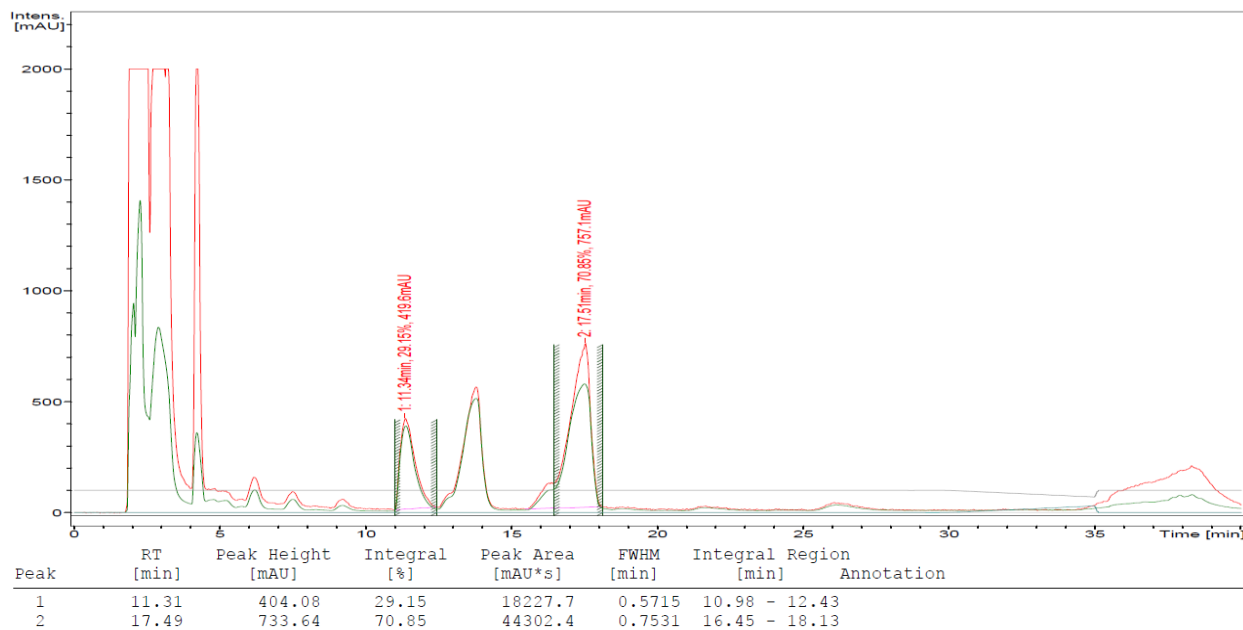
8-fluorocyclooct-4-enol ("cold" experiment, 100 °C), ee 61%



HPLC traces of [¹⁸F]F-MISO

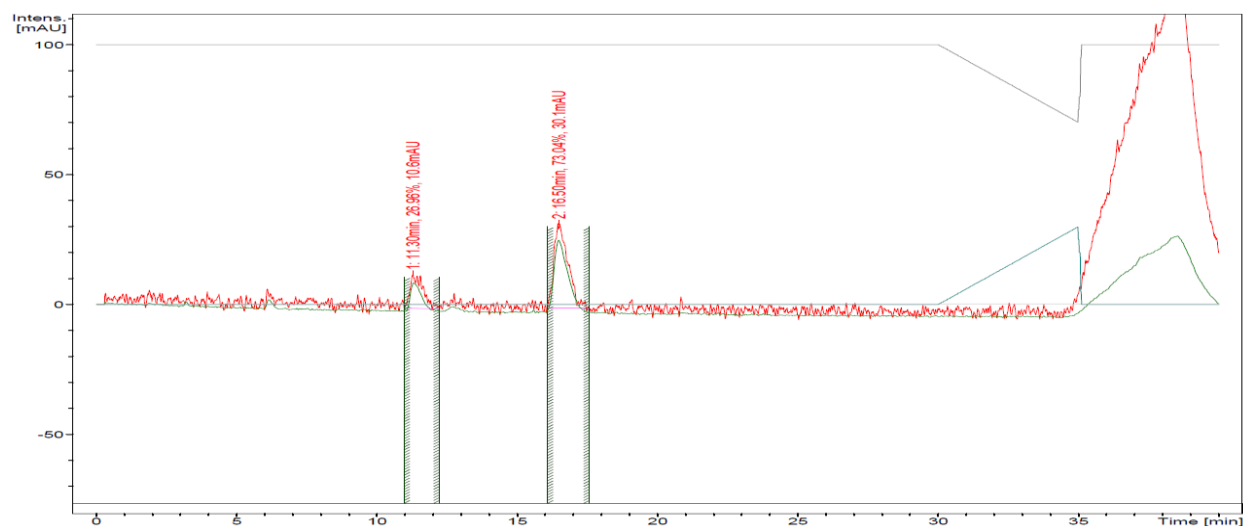
“Cold” reaction mixture (100 °C, 10 min) before the purification procedure

ee 40% (from 2 experiments)



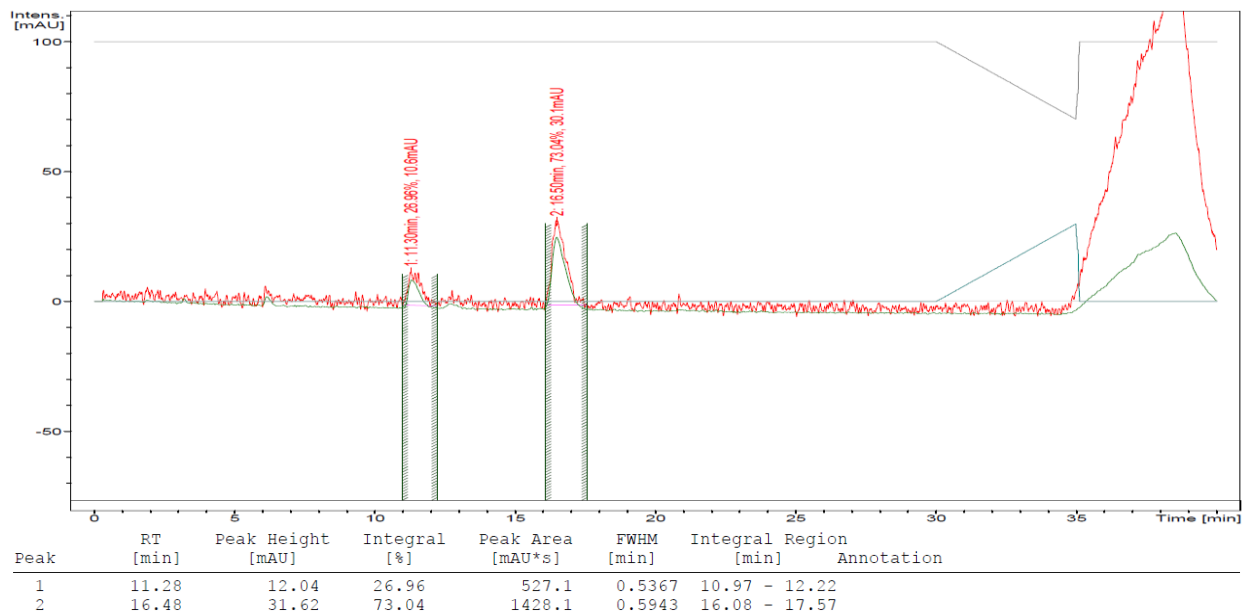
F-MISO (100 °C, 10 min) after the purification procedure

ee 40% (from 2 experiments)



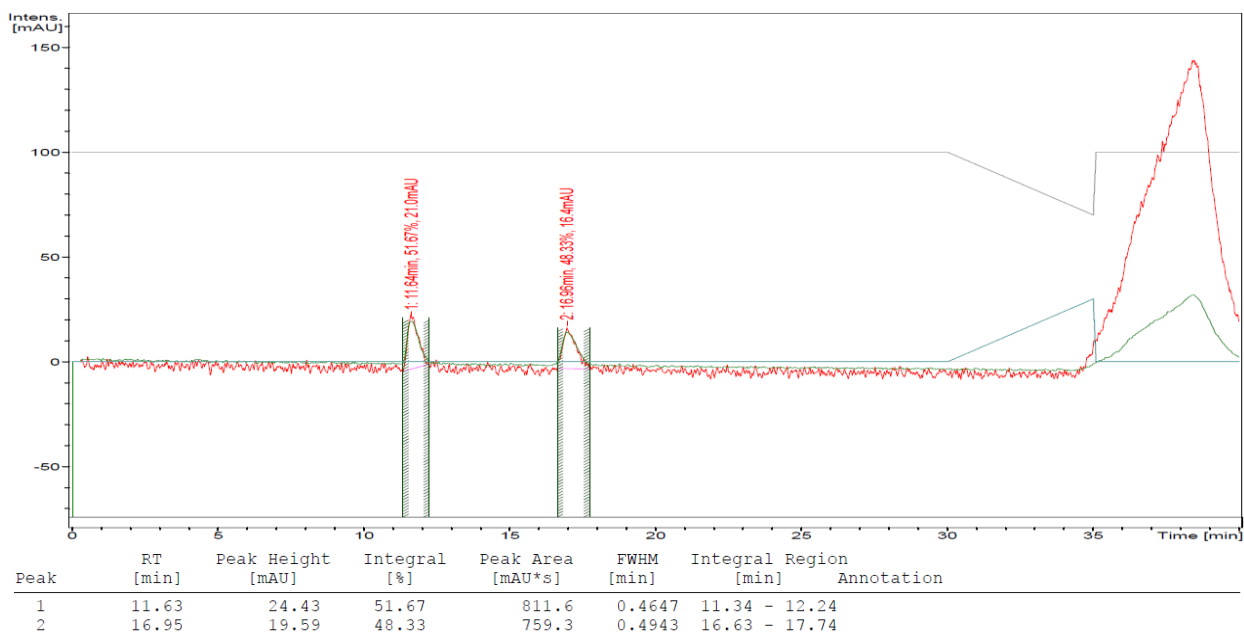
F-MISO (100 °C, 10 min) after the purification procedure

ee 40% (from 2 experiments)

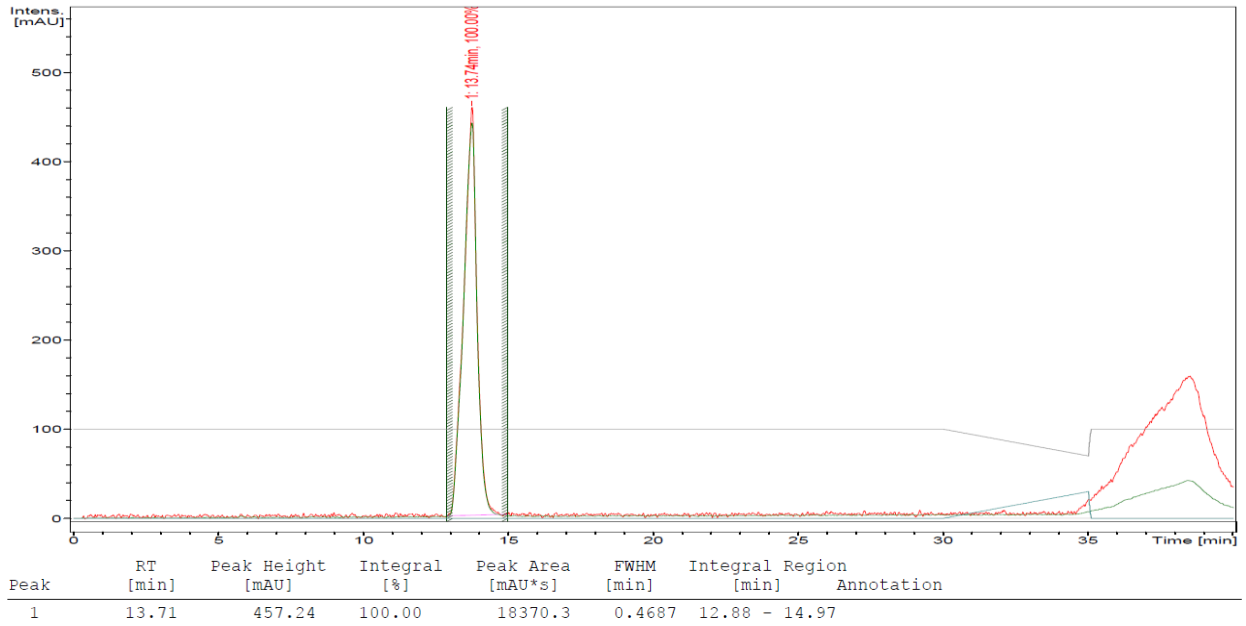


F-MISO (racemic reference material)

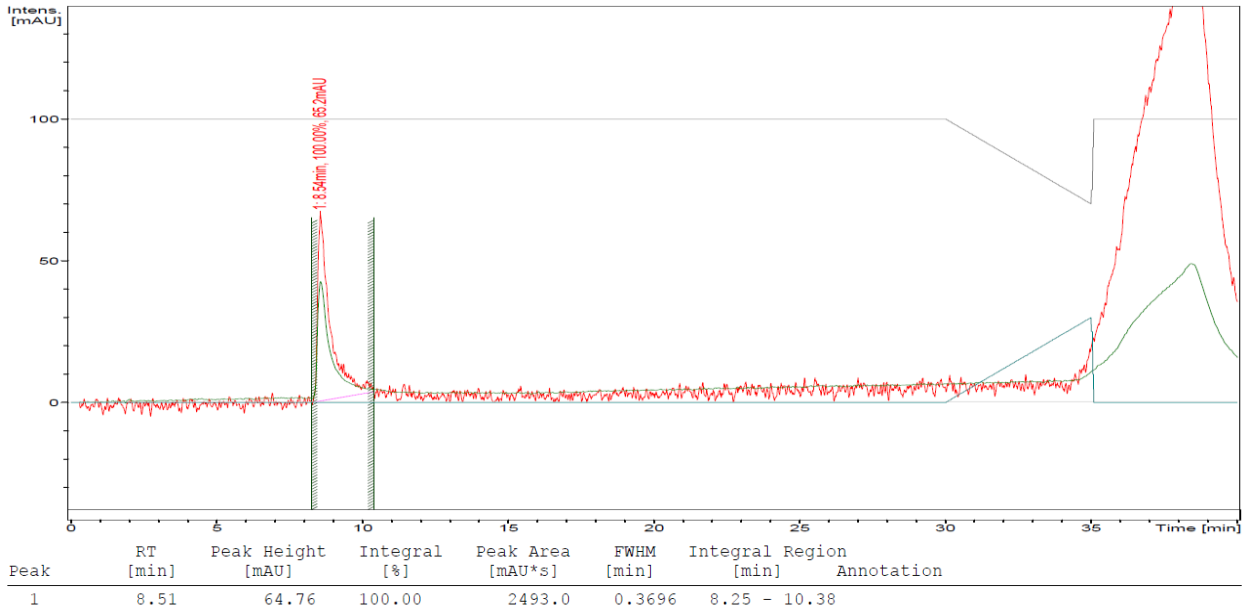
ee 0%



MISO epoxide



(-)-tetramisole



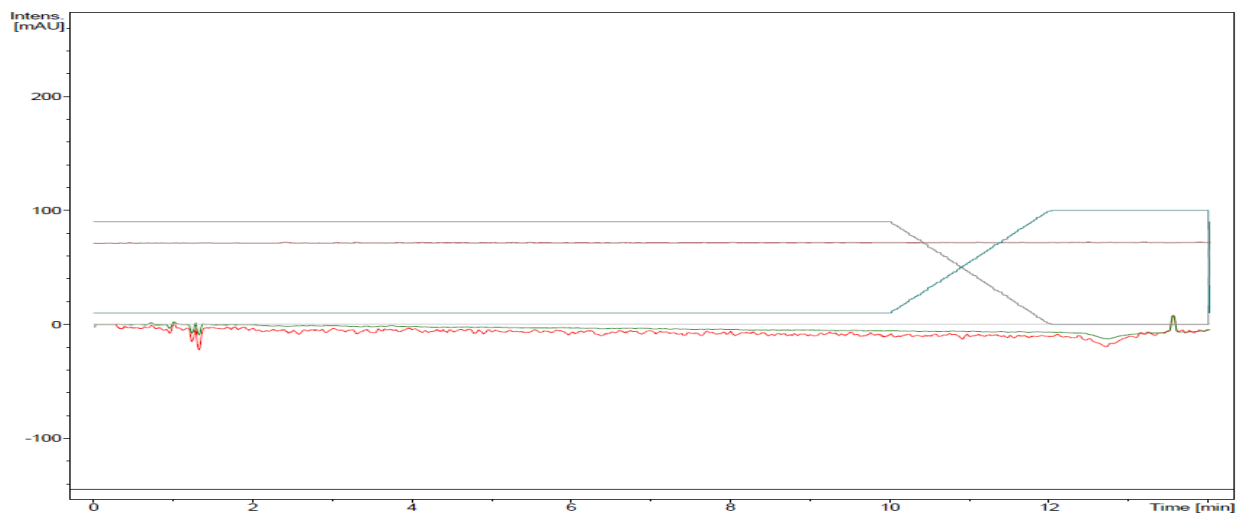
HPLC traces of [¹⁸F]F-MISO after the purification procedure

Column: Phenomenex Luna 3u C18(2) 100A, 100x2.00mm

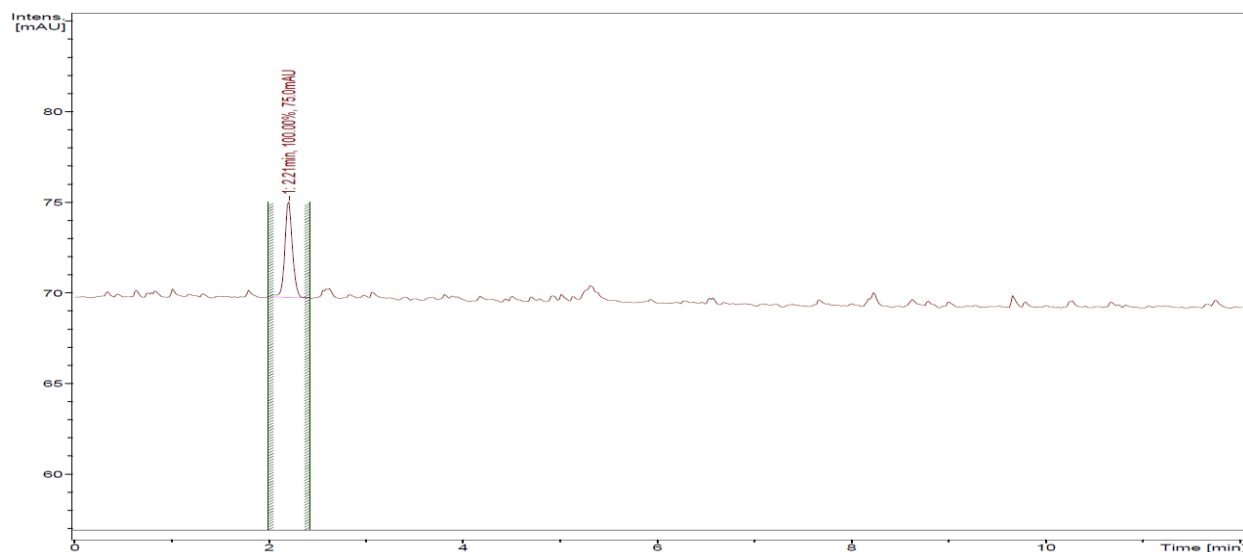
Flow Rate: 0.200 mL/min

Isocratic conditions: 9/1 (5% ACN in H₂O)/(100% ACN)

10 min isocratic conditions – UV trace

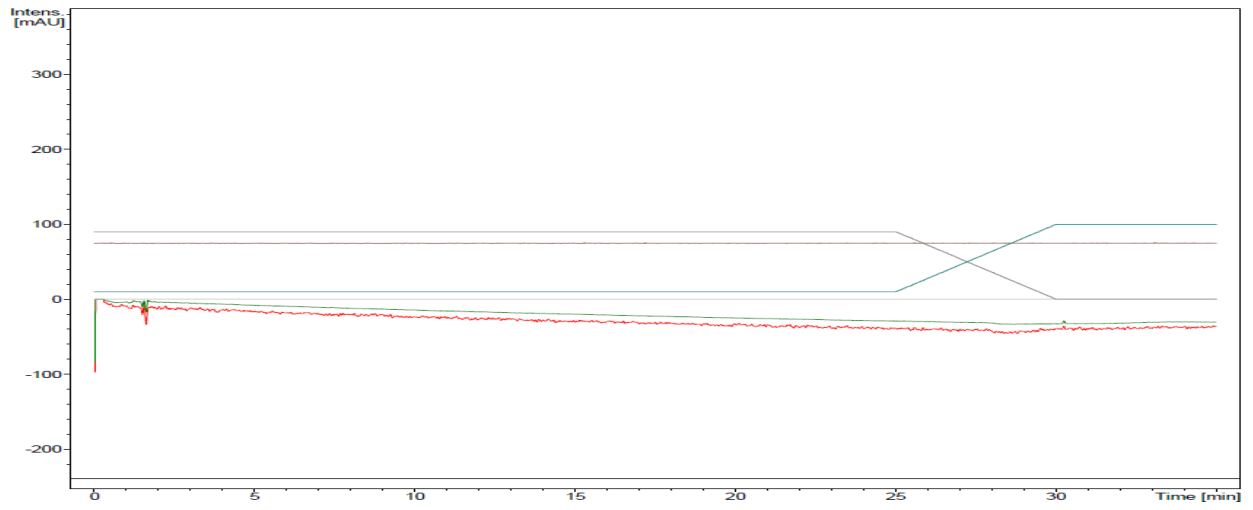


10 min isocratic conditions - radio HPLC trace



Peak	RT [min]	Peak Height [mAU]	Integral [%]	Peak Area [mAU*s]	FWHM [min]	Integral Region [min]	Annotation
1	2.20	5.27	100.00	28.9	0.0808	1.99 - 2.42	

25 min isocratic conditions – UV trace

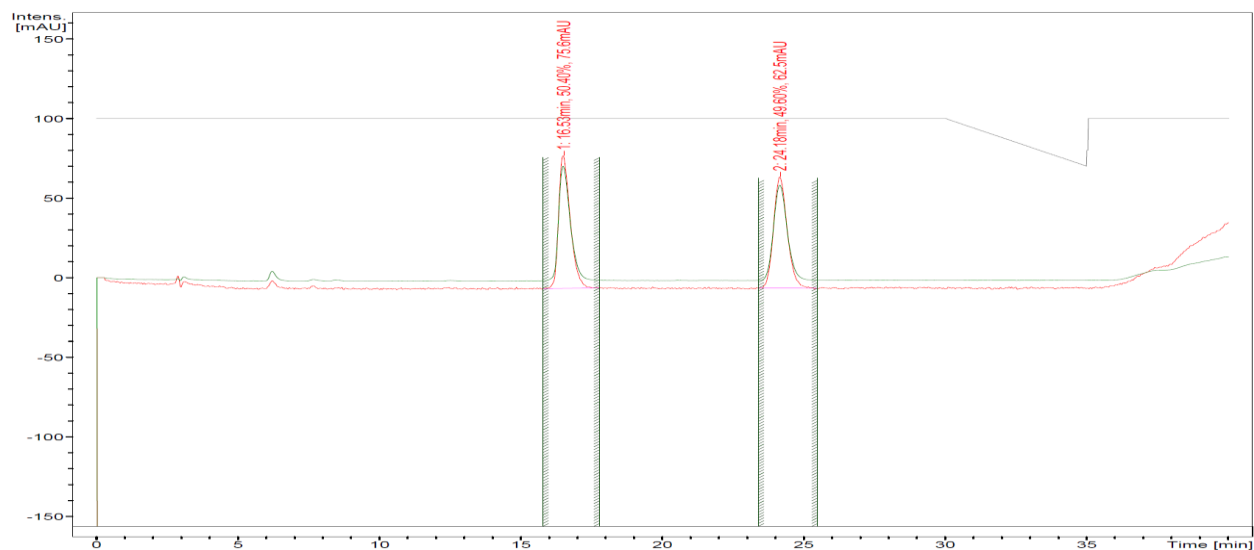
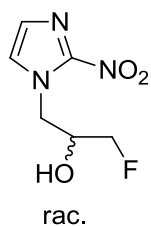


Chiral HPLC traces of [¹⁸F]F-MISO

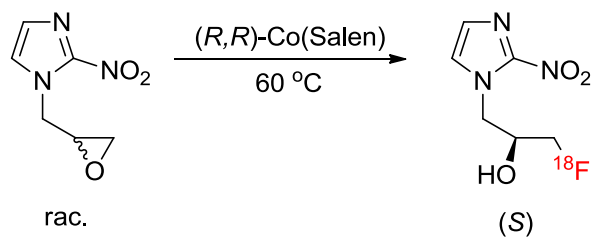
Column: Chiralpak AD-3 (AD30CT-QK002)

Flow Rate: 0.150 mL/min

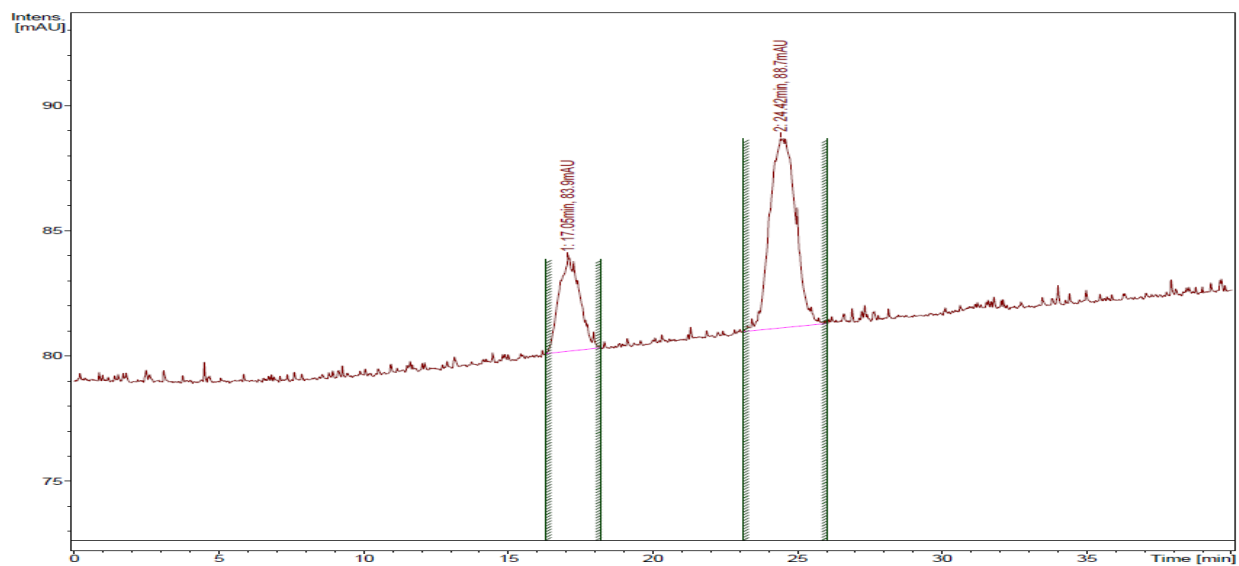
Isocratic conditions, 10% ⁱPrOH in Hex



Peak	RT [min]	Peak Height [mAU]	Integral [%]	Peak Area [mAU*s]	FWHM [min]	Integral Region [min]	Annotation
1	16.52	82.31	50.40	2987.4	0.4371	15.78 - 17.78	
2	24.17	69.09	49.60	2939.5	0.5175	23.39 - 25.49	

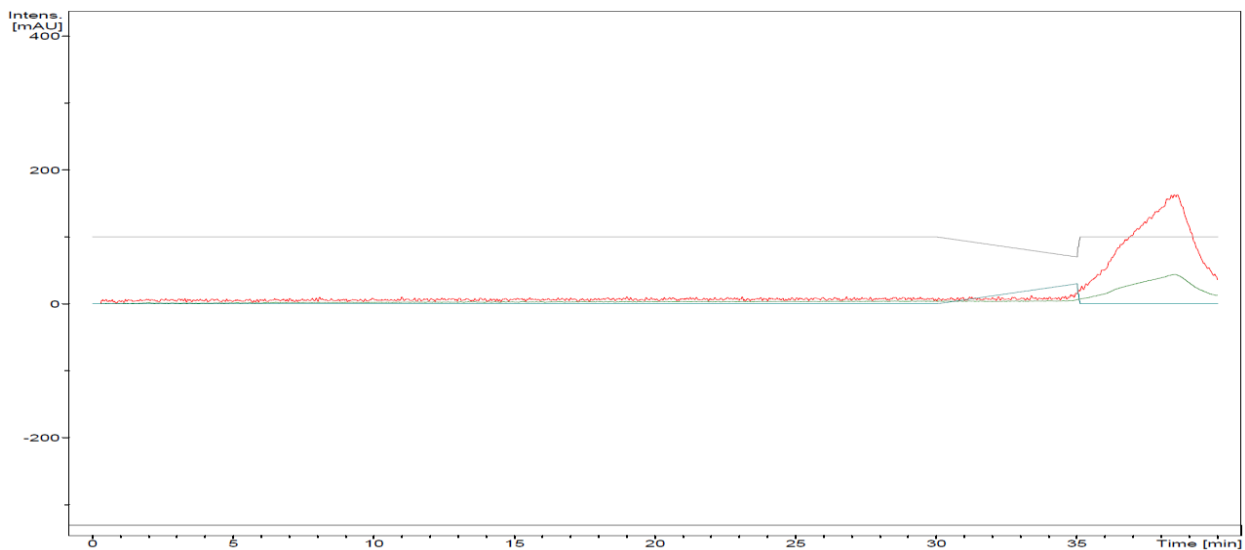


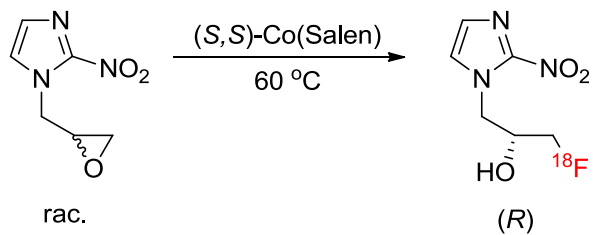
radio trace, ee 44%



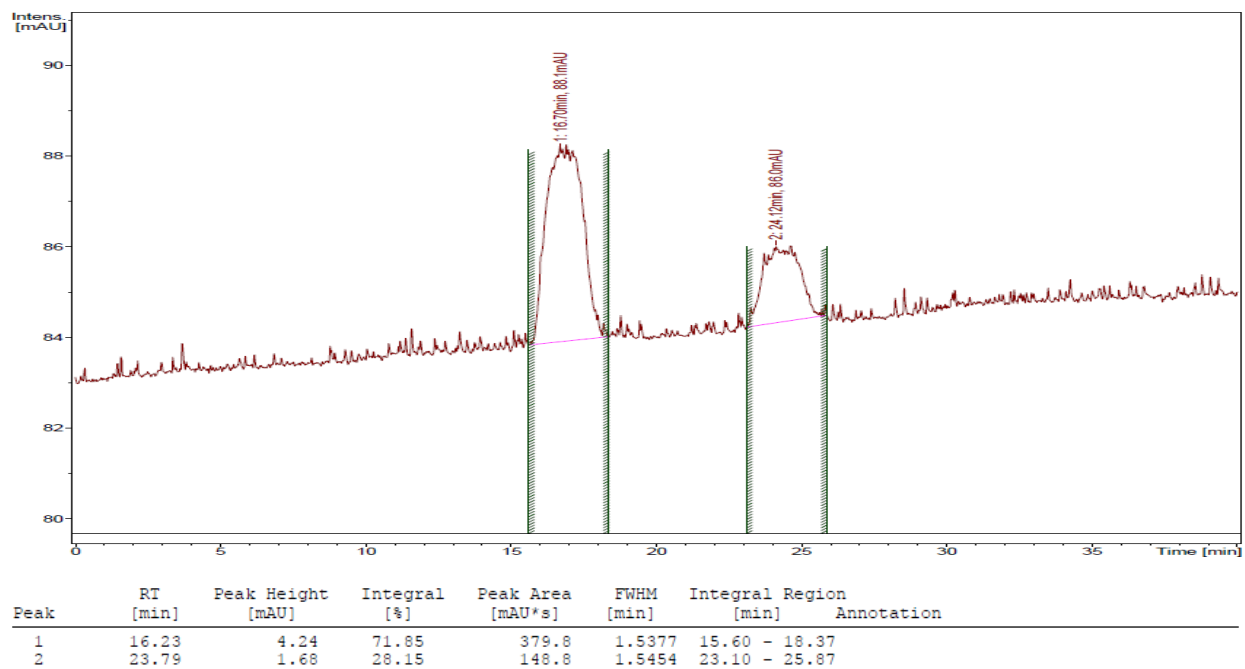
Peak	RT [min]	Peak Height [mAU]	Integral [%]	Peak Area [mAU*s]	FWHM [min]	Integral Region [min]	Annotation
1	17.05	3.68	28.37	189.0	0.8635	16.29 - 18.22	
2	24.42	7.55	71.63	477.3	1.0459	23.12 - 26.04	

UV-trace

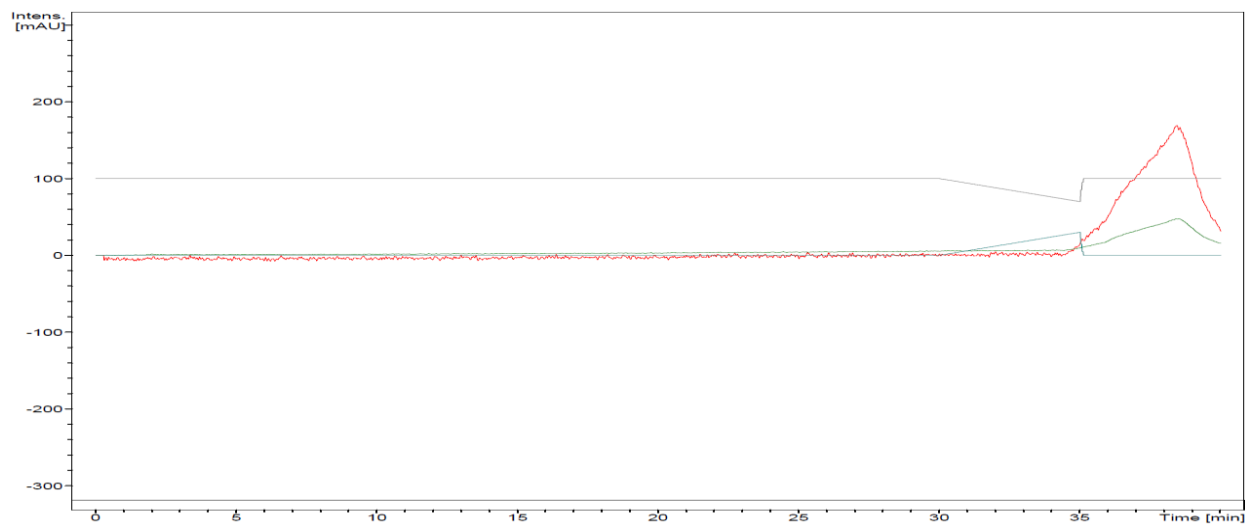




radio trace, ee 44%



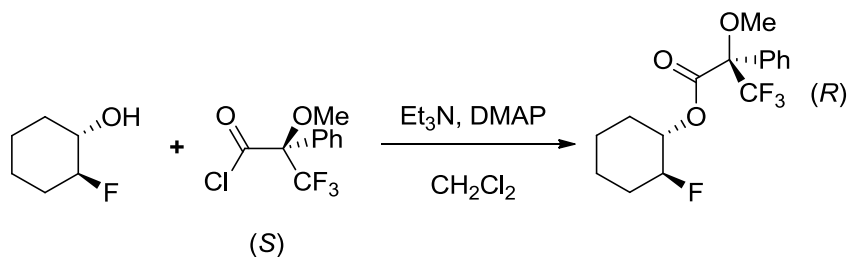
UV-trace



The Mosher esters experiments

The absolute stereochemistry of 8-fluorocyclooct-4-enol and 2-fluorocyclohexanol was assigned by NMR via derivatization of the fluorohydrins with the two enantiomers of α -methoxy- α -trifluoromethylphenylacetyl chloride (MTPACl).

The esters of these fluorohydrines were prepared according to the described method⁷.



A solution of DMAP (<0.1 mg, cat. amount), Et₃N (6.1 μ L, 0.0440 mmol, 10eq.) and fluorohydrin (0.0044 mmol, 1 eq.) in 0.5 mL of dry CH₂Cl₂ was prepared under argon and transferred into the NMR tubes. (S)-MTPACl (1.64 μ L, 0.0088 mmol, 2 eq.) was added. After 15 min the solvent was removed in *vacuo*, CDCl₃ (0.6 ml) was added and the ampule was sealed under *vacuo*, providing a sample for NMR studies. The second sample with (R)-MTPACl was prepared similarly.

Table 4.

Fluorohydrin	Proton	$\Delta\delta^{\text{SR}}$	Carbon configuration
2-fluorocyclohexanol	-FCH-	4.48-4.39=0.09 (pos.)	S
	-CH ₂ -HCO-	1.34-1.48= - 0.14 (neg.)	
8-fluorocyclooct-4-enol	-FCH-	4.78-4.70=0.08 (pos.)	S
	-CH ₂ -HCO-	2.10-2.17= - 0.07 (neg.)	
		1.72-1.86= - 0.14 (neg.)	

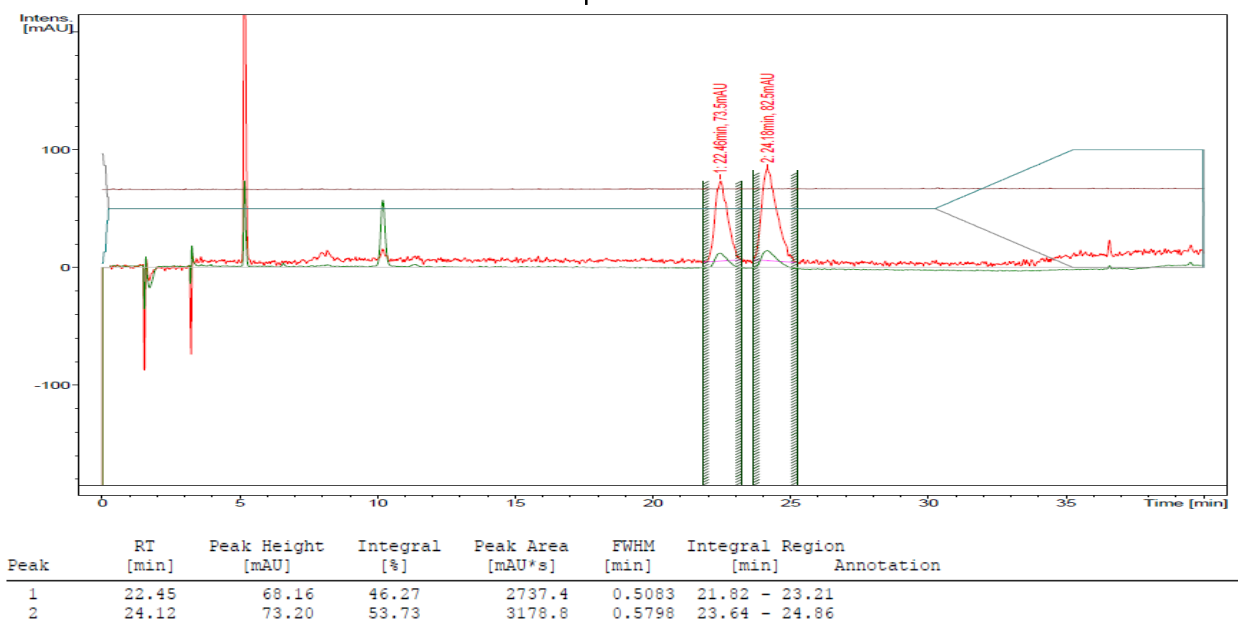
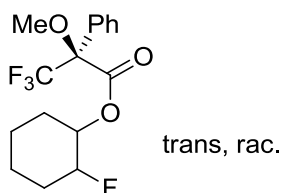
⁷ M. Seco, E. Quin, R. Riguera, *Tetrahedron: Asymmetry* **2002**, *12*, 2915–2925.

HPLC traces of Mosher esters

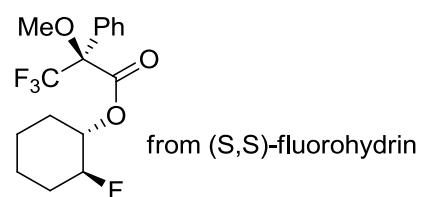
Column: Phenomenex Luna 3u C18(2) 100A, 100x2.00mm

Flow Rate: 0.200 mL/min

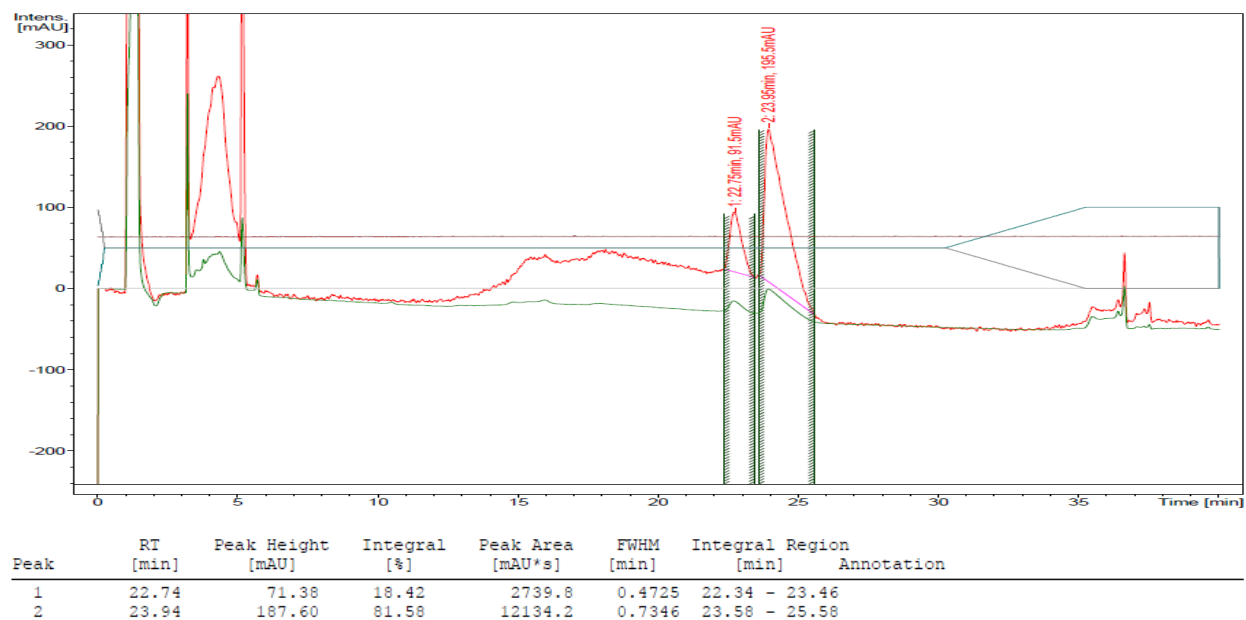
Isocratic conditions 1:1 (5% ACN in H₂O):(100% ACN)

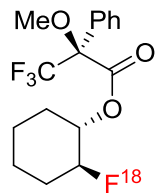


Enantiomerically enriched, from (R,R) Co(Salen), ¹⁹F



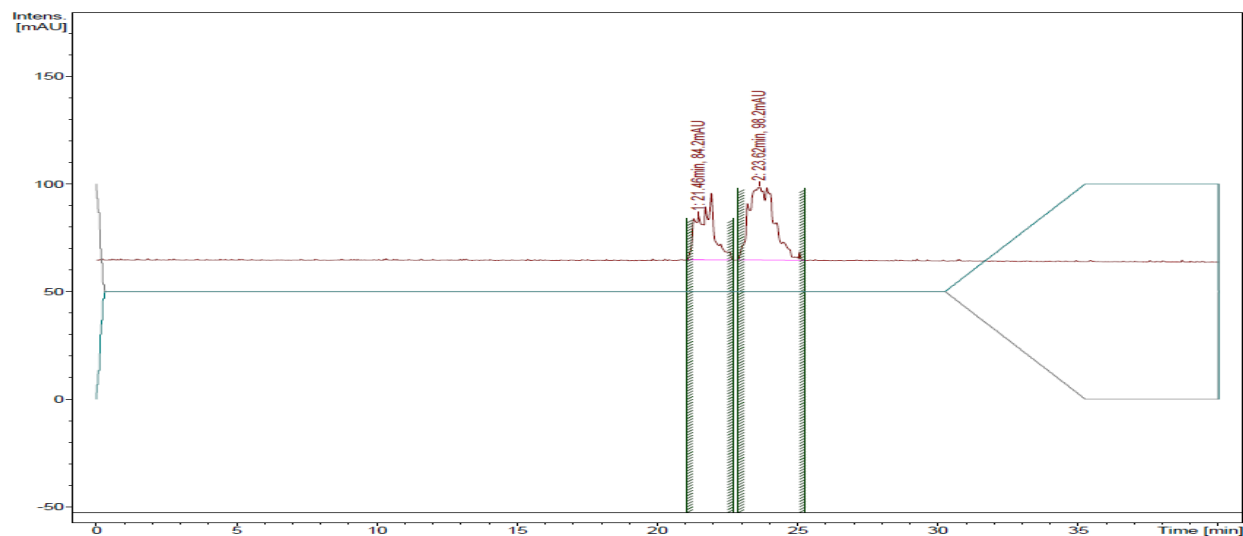
ee 64%





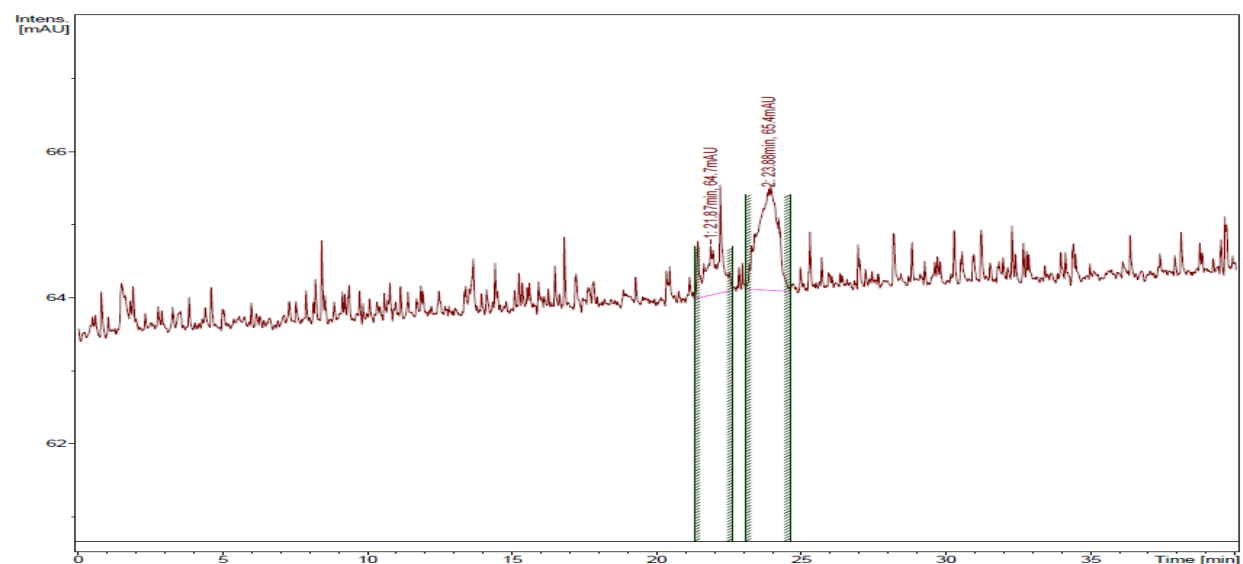
from (S,S)-fluorohydrin

Enantiomerically enriched, obtained from the reaction with (R,R) Co(Salen), ee 40%



Peak	RT [min]	Peak Height [mAU]	Integral [%]	Peak Area [mAU*s]	FWHM [min]	Integral Region [min]	Annotation
1	21.40	19.10	29.60	927.8	0.7837	21.02 - 22.37	
2	23.46	32.73	70.40	2206.9	1.1104	22.79 - 25.24	

ee 38%



Peak	RT [min]	Peak Height [mAU]	Integral [%]	Peak Area [mAU*s]	FWHM [min]	Integral Region [min]	Annotation
1	21.85	0.67	31.44	30.7	0.0803	21.30 - 22.63	
2	23.87	1.31	68.56	66.9	0.9200	23.07 - 24.62	

Feci quod potui, faciant meliora potentes